

A Thesis Submitted for the Degree of PhD at the University of Warwick

Permanent WRAP URL:

<http://wrap.warwick.ac.uk/78601>

Copyright and reuse:

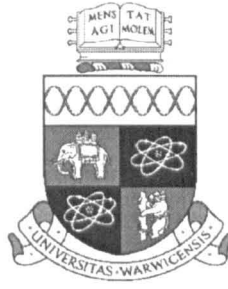
This thesis is made available online and is protected by original copyright.

Please scroll down to view the document itself.

Please refer to the repository record for this item for information to help you to cite it.

Our policy information is available from the repository home page.

For more information, please contact the WRAP Team at: wrap@warwick.ac.uk



Connection Behaviour and Frame Analysis for Structures of Pultruded Profile

Zheng, Youxin

Thesis submitted to the University of Warwick
for the degree of Doctor of Philosophy

Department of Engineering
University of Warwick

May 27, 1998

Dedicated to
my parents,
my wife and son.

Abstract

This thesis concerns a study including testing, analysis and design on beam-to-column connections for the frames of pultruded glass fibre reinforced plastic profiles. The research consists of the two principal aspects of a laboratory test programme to determine connection behaviour and the formulation of a plane frame analytical tool to determine the effect of real connection on frame behaviour.

The laboratory tests involved three different 10 inch beam-to-column connections which can be categorised as having a moment-rotation behaviour that is pinned. These connections had web cleats and the method of connection was by bolting, or bolting combined with adhesive bonding. The test configuration had a central column and two beams in a cruciform arrangement. Loading was applied at the ends of the cantilever beams in such a way that the two identical connections experienced the same moment and shear force. The non-linear moment-rotation characteristics for the connections were determined and the modes of failure established. Another four tests were conducted on different 8 inch beam-to-column connections which can be categorised as being semi-rigid. Two of these connections used steel cleats for the top and bottom seat cleats while the other two had these pieces manufactured of pre-preg glass FRP using a pressure moulding process. The details and the results of these connection tests are presented.

The results of the three tests on pinned connections confirmed conclusions previously reported on similar tests where the beams and column were of the 8 inch wide flange profile. The current practice of recommending that the cleated webs have combined bonding and bolting is shown to provide little additional benefit over that when the connection is bolted.

It is found that a semi-rigid connection with an acceptable moment-rotation behaviour can be obtained using steel angles for the connection pieces. One of the two 'all' FRP connections was also found to have an acceptable moment-rotation characteristic but would be too complicated for real applications. The search therefore continues for the all FRP connection details giving suitable connection behaviour. Combining the results from these experiments and the analysis of the failure modes,

a number of futuristic connection designs are proposed. They include a thin shell cleat piece with curvature to increase its stiffness, six connection details using pieces that connect together by interlock and bonding (this approach reduces the need for bolting) and a radically novel system which does not mimic current steelwork practice.

A new analytical method is presented which predicts the static response of non-linear elastic plane frames of polymeric composite members. Options allow for horizontal and vertical loading, second-order deflections and connections with non-linear moment-rotation characteristics. The matrix stiffness method uses a new approach to cope with the real connection behaviour. The other novel aspects of the analysis are shear deformable members and new stability functions which account for the shear deformation when determining second-order deflections. A number of new (ϕ) functions are derived to group the new stability functions, and these can readily be employed in the computing analysis. The analysis is successfully benchmarked against known semi-rigid frame problems of steelwork and with the limited results from a single experiment on a pultruded single bay frame. A serviceability beam line is presented for beam design and a moment equalized connection stiffness is obtained.

Two unbraced and one braced frame problems are analysed in a parametric study to determine the effect on frame response of having connections with various properties. Live loading is vertical with a horizontal component. Results of overall sway deflection showed how the frames respond when the connection properties are changed from pinned, through semi-rigid, to fully fixed. The sensitivity of the connection stiffness on the overall frame behaviour is demonstrated by the sway and the midspan deflections results, and by the moment distribution in the members. The analysis is shown to provide useful information in our quest for the optimised connection design and their performance when viewed as an integral part of a whole frame.

To establish which connection details are best suited to pultruded frame construction recommendations for further research and development work are given.

Contents

Abstract

Acknowledgement **xviii**

Declaration **xix**

Publications **xx**

Notations **xxi**

1 Introduction **1**

2 Introduction to Polymeric Composite Materials and Their Applications **4**

2.1 Introduction 4

2.2 History of Polymeric Composites 5

2.3 Advantages of Polymeric Composites 8

2.4 FRP Pultruded Composite Profiles 9

2.5 Properties and Design 12

2.6	Applications	13
2.6.1	General Applications of Polymer Composites	14
2.6.2	Structural Engineering Applications	17
2.7	Conclusions	27
3	Literature Review on Connections in Polymer Composite Structures	29
3.1	Introduction	29
3.2	Study of Pultruded Members	31
3.3	Connection Research	32
3.3.1	Adhesively Bonded FRP Connections	33
3.3.2	Bolted Plate-to-plate Connection	35
3.3.3	Review on Pinned Beam-to-column Connection	42
3.3.4	Semi-rigid Beam-to-column Connection	46
3.4	Study of Pultruded Frames	57
3.5	Summary	59
4	Experimental Investigation on Pinned Beam-to-column Connections	61
4.1	Introduction	61
4.2	Description of Connection Specimens	63
4.2.1	Connection Wmj10_bt	63
4.2.2	Connection Wmj10_bt+bd	65
4.2.3	Connection Wmn10_bt	65
4.3	Material Specification and Connection Details	65
4.4	Test Method	67
4.4.1	Test Equipment and Loading Set-up	67

4.4.2	Test Measurement and Data Processing	69
4.4.3	Methods of Testing	70
4.5	Descriptions of Tests	71
4.5.1	Test of Connection Wmj10_bt	71
4.5.2	Test of Connection Wmj10_bt+bd	75
4.5.3	Test of Connection Wmn10_bt	77
4.6	Discussion and Analysis of the Test Results	81
4.7	Conclusions from the Pinned Beam-to-column Connection Tests . . .	88
5	Experimental Investigation on Semi-rigid Beam-to-column Connections	91
5.1	Introduction	91
5.2	Connection Description	93
5.2.1	Connection STmj	94
5.2.2	Connection STmn	95
5.2.3	Connection Tmj	96
5.2.4	Connection Tlmj	98
5.3	Material Specification	100
5.4	Manufacture of Pre-preg Cleats	102
5.5	Testing Techniques	105
5.5.1	Test Equipment and Loading Arrangement	105
5.5.2	Methods and Procedure of Test	105
5.5.3	Test Measurement	106
5.5.4	Data Processing	108
5.6	Descriptions of Tests	109
5.6.1	Test of Connection STmj	109
5.6.2	Test of Connection STmn	115

5.6.3	Test of Connection Tmj	122
5.6.4	Test of Connection TLmj	126
5.7	Discussion and Analysis of the Test Results	132
5.8	Benefits of Semi-rigid Connections	142
5.9	Conclusions	146
6	Conceptual Design of Beam-to-Column Connections for Pultruded Frames	148
6.1	Introduction	148
6.2	Thin Shell Cleat	149
6.3	Beam-to-column Connections	152
6.3.1	Connection No. 1	153
6.3.2	Connection No. 2	154
6.3.3	Connection No. 3	155
6.3.4	Connection No. 4	155
6.3.5	Connection No. 5	156
6.3.6	Connection No. 6	158
6.4	Structural System Concept	158
6.5	Summary	162
7	The Computer Analysis of Plane Frame Structures	165
7.1	Introduction	165
7.2	Sign Conventions and Axes	166
7.3	Matrix Stiffness Method	167
7.4	Semi-rigid Connection	168
7.4.1	Analysis of the Performance of Semi-rigid Connection	169
7.4.2	Model of Element in Semi-rigid Frame	171

7.4.3	Member-end Rotation	172
7.4.4	Member-end Forces	173
7.4.5	Static Equilibrium	176
7.4.6	Solution Method	177
7.4.7	Member End Rotation ϕ	179
7.4.8	Beam Analysis	180
7.5	Effect of Shear deformations	185
7.5.1	Shearing deformations	186
7.5.2	Bending deformations	187
7.5.3	Total Slope of the Beam	188
7.5.4	Total Deflection of the Beam	190
7.5.5	Derivation of Member End Forces	191
7.5.6	Effect of Semi-rigid connection and Member Shear Deformations	193
7.6	Stability Functions Used in the Matrix Displacement Method	197
7.6.1	Stability Functions without Shear	197
7.6.2	Stability Functions with Shear	199
7.7	Sum of Effect of Axial loading, Shearing and Semi-rigid	206
7.7.1	Member without Pinned Connection	206
7.7.2	Member with One End Pinned Connection	208
7.8	Load between Joints	210
7.8.1	Partial Distributed Load	211
7.8.2	Vertical Concentrated Load	212
7.8.3	Axial Concentrated Load	214
7.9	Computer Program	215
7.9.1	Program Procedure	215
7.9.2	Moment-rotation Stiffness k	217
7.9.3	Iteration Process and Convergence Problems	218

7.10	Comparison of Analysis Results with Other Researches	219
7.11	Conclusions	226
8	Frame Analysis and Parametric Studies	227
8.1	Introduction	227
8.2	Effect of Connection Stiffness and Member Shear Deformation	228
8.2.1	Frame Data	229
8.2.2	Determination of Distributed Load ω	231
8.2.3	Lateral Deflection of the Frame	232
8.2.4	Mid-span Deflection of the Beam	235
8.3	Sensitivity of Frame Behaviour to Connection Stiffness	237
8.4	Effect of Connection Flexibility, Member Stiffness and Load	241
8.4.1	Influence of Connection Stiffness and Load	241
8.4.2	Influence of Connection Stiffness and Member Stiffness	243
8.5	Ultimate Connection Moment and Rotation	246
8.6	Analysis of Pultruded Frames with Various Connection Properties	249
8.7	Conclusion	252
9	Conclusions	254
9.1	Conclusions	254
9.1.1	Nominally Pinned Connection	254
9.1.2	Semi-rigid Connections	255
9.1.3	Analytical Modelling	258
9.2	Future Work	260
A	The Detail of Pinned Beam-to-column Connections	261
B	The Detail of Semi-rigid Beam-to-column Connections	268

C	A Guide for Using Frame Structure Analysis Programme sframe	282
C.1	How to Use the Programme	282
C.2	Assumptions and Sign Convention	283
C.3	Units	284
C.4	Preparation of Data File	285
C.4.1	Basic Frame Specification Data	285
C.4.2	Element Properties	286
C.4.3	Boundary Condition	287
C.4.4	Loads	287
C.4.5	Tolerance of Moment and Maximum Number of Iterations	288
C.4.6	Semi-rigid Connection Data	289
C.5	Output Results	291
C.6	Examples	293
C.6.1	Example 1	293
C.6.2	Example 2	295
C.6.3	Example 3	296
C.6.4	Example 4	298
C.6.5	Example 5	299
C.7	Computer Programme of Frame Analysis	300

List of Figures

2.1	GRP dome structure in Benghazi (Hollaway, 1978).	6
2.2	GRP roof structure of Dubai Airport (Hollaway, 1978).	6
2.3	Typical pultrusion process used.	10
2.4	Three EXTREN series: Series 500 (left) Series 525 (center) Series 625 (right).	10
2.5	Exploded view of pultruded composite.	11
2.6	First B-2 aircraft during flight testing. (Courtesy U.S.Air Force.) . .	14
2.7	H.M.S. Wilton, a minehunter whose hull is virtually all glass fabric and polyester resin.	15
2.8	Composite French Renault Espace.	16
2.9	GRP domes at Sharjah International Airport 1977 (Leggatt, 1984). .	17
2.10	Support structure and handrail of this platform surrounding chemical storage tanks are EXTREN.	18
2.11	Pultruded glass fibre EXTREN platform for a petrochemical complex.	19
2.12	FRP supports for FRP pipes, image from MMFG Profile, Fall 1996. .	20
2.13	Miyun highway bridge in China 1982.	21
2.14	GFRP cable-stayed bridge in China 1986.	21
2.15	Composite turret at top of the Sun Bank building in Orlando, Florida (Photo courtesy of MMFG)	22

2.16	Fibreglass pedestrian bridge in Philadelphia 1993.	23
2.17	Glass fibre reinforced plastic motorway message sign gantries.	24
2.18	Advance composite bridge enclosures (Anon, 1997).	25
2.19	Aberfeldy footbridge Scotland, UK 1992.	25
2.20	Bonds Mill lift bridge Gloucestershire, UK 1994.	26
2.21	Fiberline cable-stayed bridge, Denmark 1997.	27
2.22	Longest stress-ribbon footbridge in Japan 1996.	28
3.1	Failure modes of an adhesively bonded joint (Hollaway, 1993).	34
3.2	Failure modes of bolted connections, (a) joint nomenclature; (b) notation; (c) joint failure modes (Hollaway, 1993).	36
3.3	Effect of bolt hole clearance on ultimate load.	40
3.4	Web cleated connections, (a) Bank et al. (1990), (b) Mottram (1994).	43
3.5	Experimental set-up (Bank et al. 1990).	44
3.6	Pultruded FRP beam-to-column connection (Bank et al., 1990).	48
3.7	Pultruded FRP beam-to-column connection (Bank et al., 1992).	50
3.8	Connection details (Bass & Mottram, 1994).	52
3.9	The beam-to-column connections (Bank et al., 1996).	54
3.10	Mosallam's universal connector and beam-to-column connection (Mosallam et al., 1994 a).	55
3.11	The diagonal cracks in the UC connector.	56
3.12	The cruciform plate connection (Turvey and Cooper, 1996 a, 1996 b).	57
3.13	Pultruded GRP frame layout (Turvey, 1996).	59
4.1	Configuration of connections Wmj10_bt and Wmj10_bt+bd	64
4.2	Configuration of connection Wmn10_bt	66
4.3	Test arrangement and loading set-up.	68
4.4	The rotation due to slipping.	71

4.5	Moment-rotation curves of Wmj10_bt	72
4.6	Moment-rotation curves of Wmj10_bt (without slip).	73
4.7	The deformation of connection Wmj10_bt at failure.	74
4.8	Ultimate failure mode of left side connection of test Wmj10_bt	75
4.9	Moment-rotation curves of Wmj10_bt+bd	76
4.10	The deformation of connection Wmj10_bt+bd at failure.	78
4.11	Ultimate failure mode of left side connection of test Wmj10_bt+bd	78
4.12	Moment-rotation curves of Wmn10_bt	79
4.13	Moment-rotation curves of Wmn10_bt (without slip).	80
4.14	The deformation of connection Wmn10_bt at failure.	80
4.15	Ultimate failure mode of right side connection of test Wmn10_bt	81
4.16	Piece-wise moment-rotation curves.	82
4.17	Load and mid-span deflection comparison of the beam with different beam-end connections.	88
5.1	Configuration of connection STmj	94
5.2	Configuration of connection STmn	96
5.3	Configuration of connection Tmj	97
5.4	Bonding in of connection Tmj	98
5.5	Configuration of connection TLmj	99
5.6	Application of the adhesive to cleats for connection TLmj	100
5.7	The detail of steel mould for pre-preg cleat.	103
5.8	The uncured pre-preg cleat in the steel mould.	104
5.9	The transducers arrangement for the tests on connection STmj	107
5.10	The transducers arrangement for the test on connection STmn	107
5.11	The rotation due to slipping.	109
5.12	Moment-rotation curves for connection STmj	110

5.13	The deformation of connection STmj and the deflection of the beams.	111
5.14	Moment-strain curves for the steel cleats in connection STmj .	112
5.15	Strain-rotation curves for the cleats in connections STmj .	113
5.16	Moment-slip curves for connection STmj .	114
5.17	Moment-strain curves for the column bolts in connection STmj .	115
5.18	Moment-rotation curves for connection STmn .	116
5.19	Failure of the right-side beam in connection STmn .	117
5.20	Failure mode of the right-side beam in connection STmn .	118
5.21	Final deflection of the beams in connection STmn .	118
5.22	Moment-strain curves for the cleats of connection STmn .	119
5.23	Strain-rotation curves for the cleats of connection STmn .	120
5.24	Moment-slip curves for connection STmn .	121
5.25	Gap between the top cleat and right-side beam in the test of connection STmn .	121
5.26	Moment-rotation curves for connection Tmj .	122
5.27	Moment-slip curves for connection Tmj .	123
5.28	Moment-rotation curve of connection Tmj (without slip).	124
5.29	Deformation of specimen with connection Tmj .	126
5.30	Moment-rotation curves of TLmj .	127
5.31	Crack on pre-preg cleat.	129
5.32	Deformation of connection TLmj at the end of the test.	130
5.33	Ultimate connection failure due to thread stripping of the composite bolt.	130
5.34	Cracking along the interface of the web and the flange of the column.	131
5.35	Moment-rotation curves for connections STmj and STmn .	132
5.36	Simplified linear piece-wise moment-rotation curves for connections STmj and STmn .	133

5.37	Simplified linear piece-wise moment-rotation curves.	135
5.38	The position of the square composite nuts and the pre-preg cleat of connection Tmj	138
5.39	Comparison of load increase for the beam with different beam-end connections.	144
5.40	Comparison of the middle span deflection for the beam with different beam-end connections.	144
5.41	Comparison of connection performance in the beam analysis.	145
6.1	Model of thin shell saddle-shape cleat connector.	150
6.2	Wire frame model of thin shell saddle-shape cleat connector.	151
6.3	Connection pieces.	153
6.4	Connection No. 1.	154
6.5	Connection No. 2.	155
6.6	Connection No. 3.	156
6.7	Connection No. 4.	157
6.8	Connection No. 5.	157
6.9	Connection No. 6.	158
6.10	3D beam-to-column connection.	159
6.11	Cutaway view of 3D beam-to-column connection.	160
6.12	Erection procedure one for the joint sub-assembly.	161
6.13	Erection procedure two for the joint sub-assembly.	162
6.14	The structural model of new structural system.	163
7.1	Sign convention for member end displacements (a) and forces (b). . .	167
7.2	(a) Member with semi-rigid connection under deformation of joint. (b) Member with rigid connection under deformation of joint. (c) Member with semi-rigid connection under equivalent end-moments. .	170

7.3	Model of the member with semi-rigid connection	171
7.4	Type of the joint with semi-rigid connections of members	172
7.5	Member end rotation of member with semi-rigid connections.	173
7.6	Half beam span under distributed load	181
7.7	Serviceability beam line, and midspan and end support moments equalised line.	184
7.8	Shear displacements at member end i (a) and end j (b).	189
7.9	Members with pinned connection on one-end.	194
7.10	Deformation of a member, (a) rotation of end i, (b)a general state of sway.	200
7.11	The stability functions s and c.	203
7.12	Modified Livesley's function with shear deformation.	205
7.13	Partial distributed load between the joints.	211
7.14	Vertical concentrated load between the joints.	213
7.15	Horizontal concentrated load between the joints.	214
7.16	Flowchart of programme.	216
7.17	The method to obtain moment-rotation ratio k.	218
7.18	Frame A: (a) frame geometries, loading conditions and, (b) the num- bering of members and joints.	220
7.19	Frame B: (a) frame geometries, loading conditions and, (b) the num- bering of members and joints.	221
7.20	Moment-rotation curves of the joint of frames A and B.	222
7.21	Comparison of the results in load-drift for frame A.	222
7.22	Comparison of the results in load-drift for frame B.	223
7.23	Comparison of load-drift behaviour.	223
7.24	Frame dimensions and loading arrange (Mosallam and Bank, 1992).	224
7.25	Moment-rotation curve for portal frame connections.	224

7.26	Load midspan deflection of portal frame.	225
8.1	Frame 1 (a) geometry, loading conditions and, (b) the numbering of members and joints.	229
8.2	Frame 2 (a) geometry, loading conditions and, (b) the numbering of members and joints.	230
8.3	Frame 3 (a) geometry, loading conditions and, (b) the numbering of members and joints.	231
8.4	Load-overall sway curve of frame 1.	233
8.5	Load-overall sway curve of frame 2.	234
8.6	Percentage load-sway increment curve for semi-rigid frame 1 and 2 with, and without including, the effects of second-order and shear deformation.	234
8.7	Mid-span deflection of the top beam of frame 1.	236
8.8	Mid-span deflection of the top beam in the left bay of frame 2.	236
8.9	Mid-span deflection of the top beam in the left bay of frame 3.	237
8.10	Effect of the connection stiffness on the lateral sway of frames.	239
8.11	Effect of connection stiffness on the mid-span deflection.	239
8.12	Effect of connection stiffness on the moment distribution.	240
8.13	Effect of connection stiffness and load on the mid-span deflection.	242
8.14	Effect of connection stiffness and load on the moment distribution.	243
8.15	Effect of the connection stiffness and the member stiffness on the mid-span deflection.	244
8.16	Effect of the connection stiffness and the member stiffness on the mid-span deflection.	245
8.17	Effect of the connection stiffness and the member stiffness on the ratio of mid-span moment and the right side beam-end moment.	245

8.18	Ultimate connection moment and the serviceability beam line.	247
8.19	Connection $m - \phi$ curves and the serviceability beam line.	249
C.1	Member local coordinate system.	284
C.2	Sign convention for member end displacements (a) and forces (b). . .	285
C.3	Example frame 1: (a) frame geometry, loading conditions and, (b) the numbering of elements and joints.	293
C.4	Example frame 2: (a) frame geometry, loading conditions and, (b) the numbering of elements and joints.	295
C.5	Example frame 3.	297
C.6	Example frame 4.	299
C.7	Example frame 5.	300

List of Tables

2.1	Typical mechanical properties for GFRP, CFRP and AFRP (Head, 1996).	12
2.2	Typical minimum ultimate coupon properties of EXTREN 525 series pultruded shapes (MMFG, 1989).	13
3.1	The initial stiffnesses k_{ini} (Bank et al., 1990).	48
3.2	Selected moment-rotation data (Bank et al., 1992).	51
4.1	Summary of connection specimens.	63
4.2	Physical properties of fibreglass-reinforced shape.	67
4.3	Strength of bolt in clearance hole (BS 5950).	67
4.4	The data of the piece-wise moment-rotation curves.	83
4.5	Selected connection properties.	86
4.6	Connection performance.	87
5.1	Summary of connection tests.	93
5.2	Code strengths of Grade 43 steel (BS 5950).	101
5.3	The data of the piece-wise moment-rotation curves.	134
5.4	Connection properties.	141
5.5	Connection performance.	143

8.1	Properties of member.	232
8.2	Results for frame 1.	250
8.3	Results for frame 2.	250
8.4	Results for frame 3.	250

Acknowledgement

I feel specially indebted to Department of Engineering, particularly Dr J.T. Mottram, who has directly supervised the work and given invaluable guidance and very considerable help throughout this research project.

I would also like to thank the workshop technicians, Mr. Colin Banks, Mr. Gary Hackett and Mr. Dennis Smith, who have also offered a lot of help and valuable suggestions on the laboratory tests.

All laboratory investigations involved in this thesis were carried out at the Department of Engineering, University of Warwick.

Grateful thanks is extended to Miss Hazel St.John M.B.E for helping to improve the English.

I appreciate the encouragement and support from my family.

Declaration

The author wishes to declare that, except for commonly understood and accepted ideas, or where specific reference is made to the work of others, the content of the thesis is his own investigation. This thesis has not been submitted previously, in part or in whole, to any university or institution for any degree, diploma or other qualification.

Publications

Mottram, J.T. and Zheng, Y. (1996) *Analysis of Pultruded Frames with Semi-rigid Connection*, 2nd International Conference on Advanced Composite Materials in Bridges and Structures, Montréal (Québec) Canada, 11-14 August 1996, Canadian Society of Civil Engineers, Montreal, (1996), 919-927.

Mottram, J.T. and Zheng, Y. (1996) *State-of-the-Art Review on the Design of Beam-to-column Connections for Pultruded Frames*, Composites Structures 35 (1996), 387-401.

Mottram, J.T. and Zheng, Y. (1998) Analysis of a Pultruded Frame with Various Connection Properties, in Saadatmanesh, H. and Ehsani, M.R. (Eds.), *The Second International Conference on Composites in Infrastructure*, University of Arizona, USA, January 5-7 1998. pp. 261-274.

Notations

a_n	Constant.
A	Cross-sectional area of member.
b	Width of connection.
d	Diameter of bolt hole.
E	Modulus of elasticity.
e	End distance.
$\{\bar{\mathbf{F}}\}^{(e)}$	Vector of local element nodal forces.
$\{\mathbf{F}\}^{(e)}$	Vector of global element nodal forces.
$\{\mathbf{F}\}$	Vector of global structure nodal forces.
F_s	Member fixed-end force due to the rotation of semi-rigid connection.
G	Shear modulus.
I	Second moment of area.
k	Shear coefficient.
k_i, k_j	The ratio of moment and rotation of semi-rigid connection.
\mathbf{k}_{ij}	Sub-element stiffness matrix.
k_{ini}	Initial moment-rotation stiffness.
k_f	Final moment-rotation stiffness.
$[\bar{\mathbf{k}}]^{(e)}$	Element stiffness matrix.

$[\mathbf{k}]^{(e)}$	Global element stiffness matrix.
$[\mathbf{K}]$	Global stiffness matrix.
l	Length.
l_a, l_b	Measured connection slip.
L	Span, length.
M	Moment.
M_e	Beam-end moment.
M_{ms}	Beam midspan moment.
U	Force in X-direction.
P	Axial load.
P_a	External load applied at joint.
P_e	Euler critical load.
P_o	Equivalent joint load due to load between joint.
P_s	Equivalent joint load due to rotation of semi-rigid connection.
r	Slip rotation.
t	Thickness.
V	Force in Y direction.
α_s	Shear coefficient.
β	Member-end rotation.
γ	Shear strain at neutral axis.
$\{\bar{\delta}\}^{(e)}$	Vector of local element displacements.
$\{\delta\}^{(e)}$	Vector of global element displacements.
$\{\delta\}$	Vector of global structure displacements.
δ	Mid-span deflection.

θ	Joint rotation.
ρ	Ratio of the actual axial load P to the Euler critical load P_e
μ	Parameter $\frac{l^2}{12EI}$.
ρ	Curvature of bending.
ϕ	Semi-rigid connection rotation.
ϕ_1 to ϕ_7	Stability functions.
ϕ_e	Beam-end rotation.
ψ	$\frac{\alpha_s}{GA}$.
ω	Distributed load.

Chapter 1

Introduction

The problems associated with the serious corrosion of conventional construction materials, the rise of labour costs in construction, the need to reduce energy consumption and pollution of the environment, and the devastation of earthquakes have led to the use of advanced composites (Head, 1996, 1995). Polymeric composites are the widely used composite materials in structural engineering. They consist of a polymer resin based matrix and fibre reinforcement; the fibres are usually of glass. The materials are also known as fibre reinforced plastics (FRPs). Such materials are light weight, strong, non-corrosive, chemically resistant and have electro-magnetic transparency. These advantages of FRPs make them suitable for use in various forms of structural applications worldwide.

In structural applications the structural members of polymeric composite are generally of E-glass reinforced polyester and have been manufactured by a pultrusion process. Such FRP members are also known as pultruded profiles which can be commercially obtained. Their cross-section shapes are similar to their steel counterparts. Unlike steel, pultruded profiles have anisotropic properties, low elastic moduli and high shear deformation. The anisotropic properties of FRP profiles provide a

higher load bearing ability in the longitudinal direction, but the low strength in the transverse direction. The low Young's modulus and shear stiffness result in the profiles having low member stiffness.

To form a frame the members have to be jointed by a connection. The connections transfer forces between the members and are crucial components in the frame structure. Unfortunately, there is no standard specification or code of practice for connection design. Current connection designs used in pultruded frames are those recommended in the design guidance by the manufacturers. These connections simply mimic steel-type web cleated connections. They are assumed to behave as pins in the frame design. On one hand, such a conservative design assumption makes it difficult for FRP profiles to be competitive with steel or aluminium profiles, especially for primary load-bearing applications (Turvey, 1998). On the other hand, since pultruded profiles have anisotropic properties this type of connection may not be able to perform as required because the cleat pieces have the fibres oriented in the wrong direction (Mottram & Zheng, 1996 b).

Compared with steel the pultruded profiles have lower Young's modulus. For this reason frame design is often governed by the deflection serviceability requirement. This naturally leads to the consideration of increasing the connection stiffness in order to reduce the deflection and such a practical connection is known as a semi-rigid connection. In traditional steel frame design the connection is assumed to be either pinned or rigid. The actual behaviour of a connection is between these two extremes. It is found with steel that using the semi-rigid behaviour in frame design has the merits of reducing beam depth and overall cost (Anderson et al., 1993).

The focus of the current work is to investigate the nature of beam-to-column connections which reflect an understanding of both the properties of FRP materials and the connection's behaviour. In particular, the influence of the semi-rigid beam-to-column connection on the overall response of frames is considered.

The research consists of two principal aspects of a laboratory investigation, ‘pinned’ and ‘semi-rigid’ beam-to-column connections and the formulation of a plane frame analytical tool.

In Chapter 2, a brief introduction to polymer composite materials and their applications is given. Chapter 3 is a literature review covering previous research related to the subject of this thesis. The experimental investigation of pinned beam-to-column connections and the analysis of the results are given in Chapter 4. Chapter 5 reports the experimental investigation of semi-rigid beam-to-column connections, together with the manufacture of a flange cleat component. A number of conceptual designs for connections and a structural system are designed in Chapter 6. In Chapter 7, a plane frame analysis method and computer program is developed. It uses a new approach to model the semi-rigid connections, and it includes the shear deformation of member and the second-order deflection effects. Parametric studies using the author’s frame analysis programme are presented in Chapter 8. The final chapter has a summary, a discussion on the results, and an assessment on the testing is made. These are followed by a list of the further work that needs to be developed.

Chapter 2

Introduction to Polymeric Composite Materials and Their Applications

2.1 Introduction

Polymeric composites are relatively new materials to the building industry. They are often referred to in the literature as fibre reinforced plastic (FRP). If glass fibre is used as the reinforcement, the material is also known as GRP or GFRP. Polymeric composites consist of two distinct constituents — a polymer resin and fibre reinforcement. The fibres with high strength and high stiffness are embedded in, and bonded together, by the low modulus continuous matrix (the polymer). The final material combines the properties of the reinforcement with the processing ability of the plastic. The fibres enhance the low stiffness and strength of the resin and the resin transmits loads into the stiff, brittle fibres and protects them from damage (Mayer, 1993). The fibrous reinforcement may be orientated in such a

way as to provide the greatest strength and stiffness in the direction in which it is needed. Glass and carbon fibres are normally used as the fibre reinforcement in polymer composites. Glass fibre is the predominant type of reinforcement used in FRP structural members. Worldwide 98% of all composites have glass fibres (Mayer, 1993).

Polymeric composite as a new construction material has merged into structural engineering and has attracted the attention of the industry. Its applications are beginning to be seen in a variety of civil engineering structures. Widespread use of this material has been limited due to the reasons such as lack of knowledge, design code, practical experience, confidence and the issue of cost-competitiveness. Available design criteria for composite connectors, components, and systems are very limited (GangaRao & Barbero, 1991).

2.2 History of Polymeric Composites

The history of fibre reinforced plastic (FRP) for load-bearing structures goes back to 1942. Such material was used in the form of lightweight aircraft components, as demanded for the developing agile fighter planes in the Second World War. The use of polymers and composites in the construction industry also commenced during the Second World War. They were used to erect radomes of hand lay-up construction for housing electronic radar equipment (Leggatt, 1984; Hollaway, 1993). After the war, FRP continued to be used, but it remained an expensive material relative to the alternative choices. Since the early 1950s, translucent GRP sheeting has been available (Leggatt, 1984). With developing techniques of GRP manufacture, the construction industry showed growth in using this material during the 1960s. A number of applications, such as Benghazi dome structure (**Figure 2.1**) completed in 1968, and Dubai Airport roof structure (**Figure 2.2**) built in 1972, played an

important role in the development of the composites in construction (Hollaway, 1978, 1993).

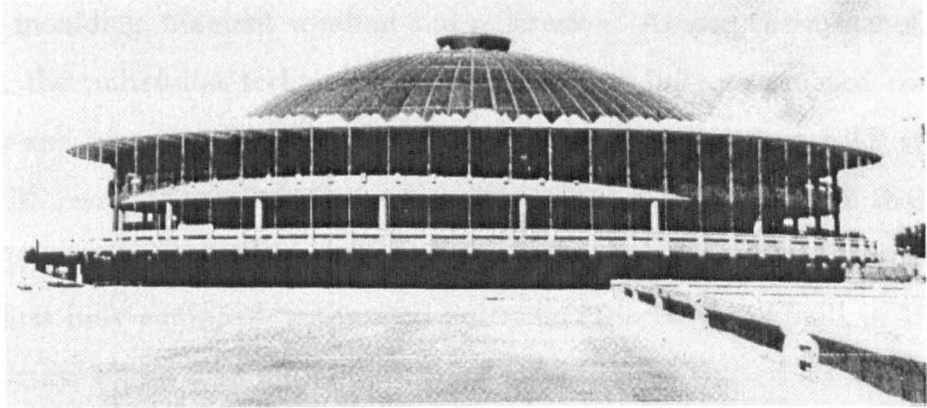


Figure 2.1: GRP dome structure in Benghazi (Hollaway, 1978).

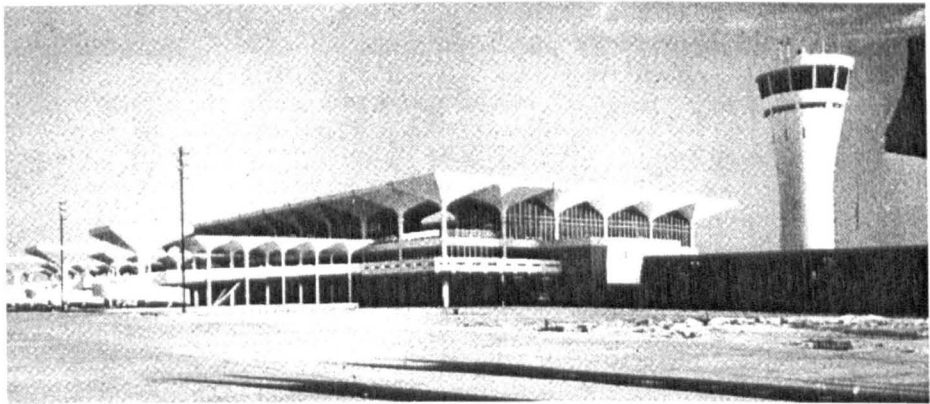


Figure 2.2: GRP roof structure of Dubai Airport (Hollaway, 1978).

Since the later 1980s, due to favourable production costs the FRPs are now being used for a great variety of products in many areas of civil engineering, even though there are limits to their load-bearing capability and stiffness.

With the growing application of the composite material, various manufacturing methods have also been developed and refined. These include contact moulding, pre-preg moulding, resin transfer moulding, press moulding, centrifugal moulding, injection moulding, filament winding and pultrusion. Among these manufacturing methods, the pultrusion technique is one of the few fully automated continuous processes and is one of the most widely used methods to produce FRP structural shapes with constant cross-section and continuous lengths. It is known that pultrusion produces advanced composite materials in the most cost efficient way.

The first fully equipped, automated pultrusion machine was built in 1950-1951 (Goldsworthy, 1991). The initial pultrusion patent in the United States was issued in 1951. The early pultrusion machines were built for production of simple solid rod stock. Most of these machines were designed and built in-house and most were the intermittent pull type (Meyer, 1985).

In 1956, Universal Molded Products Corporation, which became Morrison Molded Fiber Glass Company (MMFG)¹ and is now Strongwell, began producing structural shapes. The company became the early leader in pultruded product development (Smith & Stone, 1990). The inclusion of structural shapes gave a good impetus to the pultrusion business (Meyer, 1985). This technique, comparing with the earlier dominant processing method of hand lay-up contact moulding, makes it possible to produce profiles with higher mechanical properties, at lower manufacturing cost, and with improved quality assurance. Correspondingly, the advent of pultruded structural shapes promoted the application of composite material in structural engineering.

¹MMFG changed its name to Strongwell on July 1, 1997. The company is in Bristol, Virginia USA. Internet: www.strongwell.com

2.3 Advantages of Polymeric Composites

Fiber reinforced polymer composite is called ‘the future material of civil engineering (Ballinger, 1990).’ It has many unique advantages over more conventional materials such as:

- Light-weight, high strength and high stiffness. Composites possess high strength-to-weight ratio. Fibre have a high static and fatigue strength, and composites are up to five times lighter than steel or concrete (Ballinger, 1992). The light weight of composites makes it possible that sub-assemblies can be fabricated in factories and transported to site for quicker and safer erection, which results in shorter construction time and consequently a relatively lower life cycle cost (Mosallam, 1993; Mottram & Zheng, 1996 b). Comparing with coated steel section, calculations for coated composite I beams showed potential weight savings up to 50% (Bishop & Sheard, 1992).
- Mouldability. They can be easily moulded to desired complex shapes. This makes it possible to consolidate the multiple parts in one final shape, thus the fabrication cost can be reduced. The most efficient structural forms may be selected by the mouldability of the material (Hollaway, 1993).
- Non-corrosion and chemical resistant. These material properties make them suitable for use in hostile environments and is the principal reason why they are the preferred materials for the chemical, offshore oil and gas industries. As a result of the resistance, structures require less maintenance, and operational costs are reduced.
- Electro-magnetic transparency. The materials have “low observable” characteristics to current radar, electro-optical, acoustic, and infrared detective techniques. These enable the materials to be substantially used in military aircraft.

Nonmagnetic properties of materials make them suitable to build structures for nonmagnetic environments (e.g., buildings housing magnetic equipment, computer chip manufacturing, etc.).

- Fire resistance.
- Heat and sound damping capabilities.

Above advantages make polymeric composites the most competitive material and this is why they have attracted interest in a large number of different applications.

2.4 FRP Pultruded Composite Profiles

Pultrusion has a high degree of automation allowing the production of cost-effective fibre-reinforced structural components. The process generally consists of pulling the raw fibres, such as continuous rovings and/or continuous glass mats, through a resin bath or impregnator, then into preforming fixture where the section is partially shaped and excess resin and/or air is removed, afterward into a heated die where the section is consolidated and cured. The process of pultrusion allows some latitude for varying the angle of fibres (Ballinger, 1990). **Figure 2.3** shows a typical pultrusion process.

The pultrusion process can produce straight sections having most geometrical cross-sectional shapes at any desired length. The maximum cross-section of pultruded profiles will continue to increase as the process reaches its maturity. The products can be solid or hollow, with variations in shape from bars and rods to complex custom sections. Most of these currently available standard products have steel like cross section shape. **Figure 2.4** shows EXTREN pultruded shapes manufactured by MMFG.

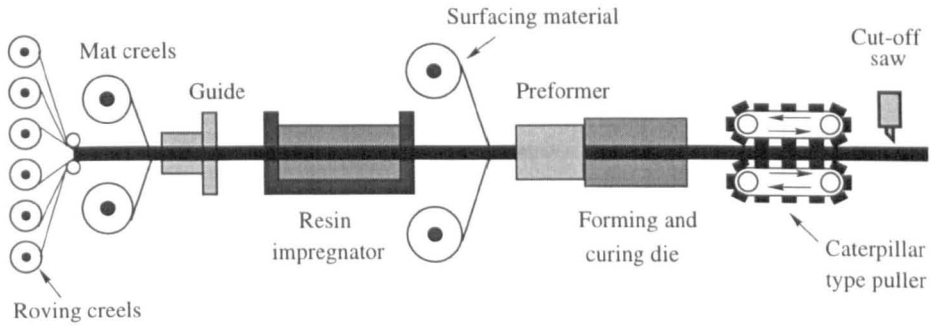


Figure 2.3: Typical pultrusion process used.

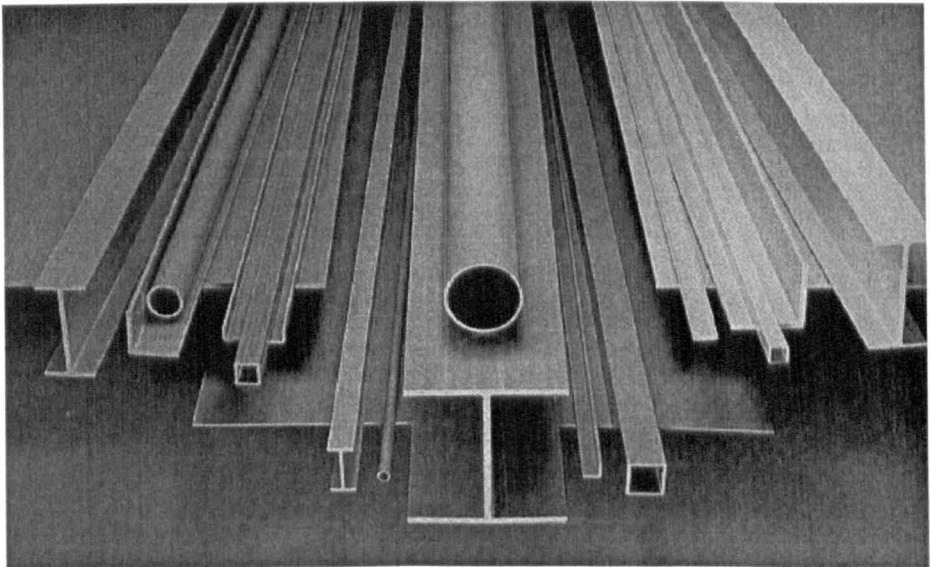


Figure 2.4: Three EXTREN series: Series 500 (left) Series 525 (center) Series 625 (right).

Structural shapes consist of reinforcing materials, resin matrix, together with a surfacing mat to improve the composite surface appearance, chemical resistance and weather resistance, and a variety of ancillary materials such as pigments to impart colour, accelerators to cure the laminating resin, internal release agents, inert fillers, etc. (Meyer, 1985). The reinforcing materials normally used are E type fibreglass continuous strand mats and continuous fibreglass rovings. The laminating resin may be an unsaturated polyester resin, a vinyl ester resin, or an epoxy resin. The majority of all pultruded products currently use polyester resins due to its relatively low cost.

Figure 2.5 shows an exploded view of one type of pultruded construction containing both continuous strand mat and roving reinforcements.

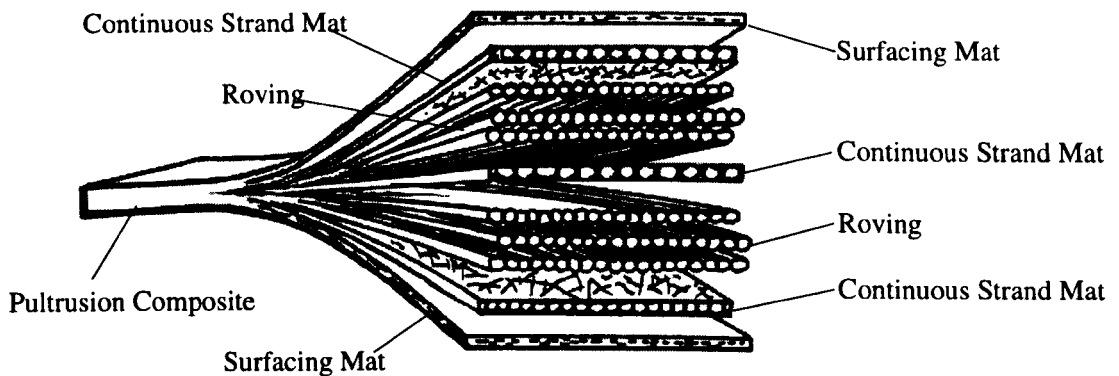


Figure 2.5: Exploded view of pultruded composite.

The strength of the material is determined primarily by the type, orientation, quantity, and location of the glass fibres within the section. Type of resin used determines corrosion resistance, flame retardancy, and maximum operating temperature, as well as contributing significantly to certain strength characteristics (including resistance to impact and fatigue) (MMFG, 1989).

2.5 Properties and Design

As described in previous section, the properties of polymeric composites will depend on the type, the content, the form, and the arrangement of fibres and resin used. Typical polymeric composite properties given by Head (1996), for the three types of fibres continuously laid in the direction of stress, are listed in **Table 2.1**.

Table 2.1: Typical mechanical properties for GFRP, CFRP and AFRP (Head, 1996).

Uni-directional Composite Material	Fibre Content (% by weight)	Density (kg/m ³)	Longitudinal Tensile Modulus (G Pa)	Tensile Strength (M Pa)
Glass/polyester (GFRP)	50 - 80	1600 - 2000	20 - 55	400 - 1800
Carbon/epoxy (CFRP)	65 - 75	1600 - 1900	120 - 250	1200 - 2250
Aramid/epoxy (AFRP)	60 - 70	1050 - 1250	40 - 125	100 - 1800

The composite properties vary widely; this alone makes design work more complex than for conventional material. In addition, the designer needs to consider the effect of loading duration, creep, fatigue resistance, environmental effects, temperature effects, moisture ingress and fire resistance. All of these will vary depending on the choice of fibre and resin configurations (Head, 1996).

This complexity, and associated high design cost, will discourage designers from using the composite material, such that a solution is to provide standard products, like EXTREN structural shapes, with known material properties and well-established design guidance.

Table 2.2 presents the minimum ultimate coupon properties of EXTREN series 525 structural shapes given by MMFG (1989), in which ‘longitudinal’ is for the material properties parallel to the pultrusion direction and ‘transverse’ is in

the perpendicular direction. The coupon properties of structural shapes show that pultruded composites are neither homogeneous nor isotropic; their mechanical properties are directional and locally varying. Due to unidirectional fibre arrangement the material has higher strength acting axially along a profile. It is important to consider both longitudinal and transverse stress in design.

Table 2.2: Typical minimum ultimate coupon properties of EXTREN 525 series pultruded shapes (MMFG, 1989).

Property	Units	Longitudinal	Transverse
Tensile Strength	MPa	207	48.3
Tensile modulus	GPa	17.2	5.52
Compressive strength	MPa	207	103
Compressive modulus	GPa	17.2	6.89
Shear strength	MPa	31.0	
Shear modulus	GPa	2.93	
Flexural strength	MPa	207	68.9
Flexural modulus	GPa	11.0	5.52
Density	kg/m ³	1716 - 1938	

The modulus of elasticity of EXTREN is approximately one-tenth that of steel. As a result, deflection is often a controlling design factor. In comparison with metal the shear modulus is low, and so shear deflection should often be considered in design.

2.6 Applications

FRP's are suitable in all engineering areas, including aerospace, marine, automotive, sport, building and construction. On consulting the literature of the engineering profession, it is found that the number of applications is rapidly growing and that

this growth is expected to continue, at pace, into the next century.

2.6.1 General Applications of Polymer Composites

In the aerospace industry, applications have been developed in the construction of rockets and satellite components, wing skins and small structural beams for aircraft, and even the main rotor blades and rotor head on helicopters (Ballinger, 1990). U.S. Air Force's B-2 stealth bomber aircraft (**Figure 2.6**), developed by Northrop in the 1980s', has a massive carbon fibre reinforced composite structure, including its large wing box, manufactured by LTV (Stonier, 1991). The INTELSAT-V, international telecommunications satellites, each have over 400 individual advanced composite parts, developed in the United States, Europe and Japan (Stonier, 1991). All composite voyager aircraft (Rutan) and business aircraft (Beechcraft) have flown (Charrier, 1990). It is reported that nearly 4 tons of composite material is used in the Airbus A340. This is also the first airliner to have a composite horizontal tailplane which also acts as a fuel tank (Anon, 1992 a).

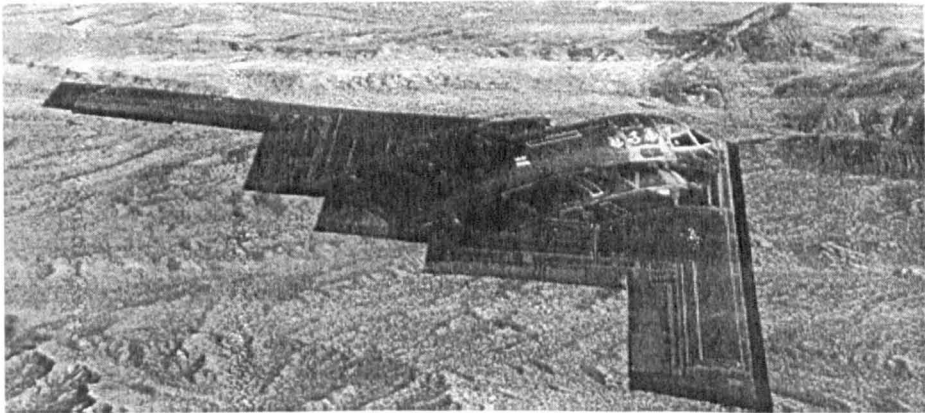


Figure 2.6: First B-2 aircraft during flight testing. (Courtesy U.S.Air Force.)

In the marine industry composites are used in boat hulls. The boat-builders use

a contact moulding process which is simple. Almost all boat hulls up to 20 metres in length are now built from hand lay-up GRP (Leggatt, 1984). The Royal Navy has built the 496 ton H.M.S. Wilton (**Figure 2.7**) (Bailie, 1991). It is also reported that 10 metre high FRP towers are erected as automated solar powered light stations in waters surrounding the islands of the Phillipines (Anon, 1995 a).



Figure 2.7: H.M.S. Wilton, a minehunter whose hull is virtually all glass fabric and polyester resin.

For automotive production the application of composites reduces the number of components, the system cost, the overall weight and the package space. The use of the material has grown considerably in volume and sophistication over the previous 20 years (Charrier, 1990).

Polymeric composites are used appreciably in steering mechanisms, powertrain interior elements and body panels etc. It is claimed that the Espace (**Figure 2.8**), built by Matra Automobile, France, is the only car in the world in which the body consists almost completely of composite materials. The body parts were made of sheet molding compound (SMC) which do not require further finish. (Anon, 1996 a).



Figure 2.8: Composite French Renault Espace.

Composite material has not only been used in the body panels of vehicles, but also been used in load component. The Ford's Contour concept car is featured with a transversely-mounted composite leaf spring (Anon, 1992 b).

In civil engineering, FRP has been extensively used for construction of tanks, pipes and ducts for many years. These products are often manufactured by the filament winding or hand lay-up method. It is the predominant material in the field of small size domestic and industrial tank construction. Its mould-ability into any free shape, light and strong, make it suitable for use as decorative panels of building, walls, partitioning, etc. So far, in the building industry, the composites have been mainly used as large panel units, roof structure and small folded plate systems. **Figure 2.9** shows four domes, up to 50 metres in diameter, covering a airport terminal with GRP external cladding.

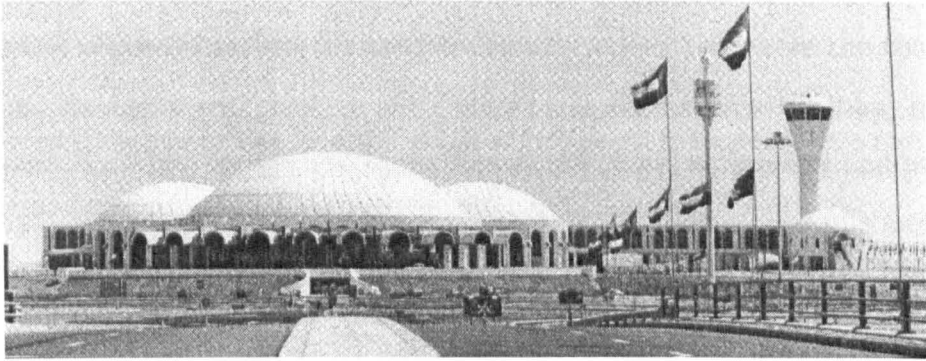


Figure 2.9: GRP domes at Sharjah International Airport 1977 (Leggatt, 1984).

2.6.2 Structural Engineering Applications

Although FRP has been around for more than half century, it still represents a new construction material category for the construction industry, and its applications in this field are still being established. For civil/structural application, both the strength and stiffness of the material are critical. ‘The strength and stiffness properties of the pultrusion composite are not yet fully realized in practice and many structural applications that would be possible are never considered. However, this market must soon be exploited because of the need for more energy efficient structures’ (Hollaway, 1993).

Advances of polymeric composite material give it a tendency to replace conventional materials such as steel, aluminium, and wood in a wide variety of structural applications. However, to date, its application is usually limited to shuttering and cladding, for building folded-plate systems. For various reasons, the introduction into the construction industry of structural, load-supporting elements has been slow (Abd-El-Naby and Hollaway, 1993; Leggatt, 1984). More recently, there have been a number of prominent applications in structural engineering developed on the basis of trial-and-error, overdesign, limited test data, and common sense (GangaRao &

Barbero, 1991).

Polymeric composite materials are particularly attractive where the contents or the ambient condition are corrosive. FRP structures are employed in many segments of the chemical process industries, including chemical, petrochemical and pulp-and-paper plants, pollution-control and sewage-treatment facilities, and offshore oil and gas production rigs (Liskey, 1985).

Pultruded walkways and ladders, fume scrubber structural elements, cable trays and gutters are some of the items now found in corrosive environment (see **Figure 2.10**). FRP standard pultruded sections (wide-flange I-Beam, angle etc.) have been used for hundreds of glass fibre-reinforced outdoor platforms installed at Dow Chemical facilities where the pultruded platforms are expected to last 15-20 years, but wood and steel platforms fail in 3-5 years in such environments (Lass, 1986).

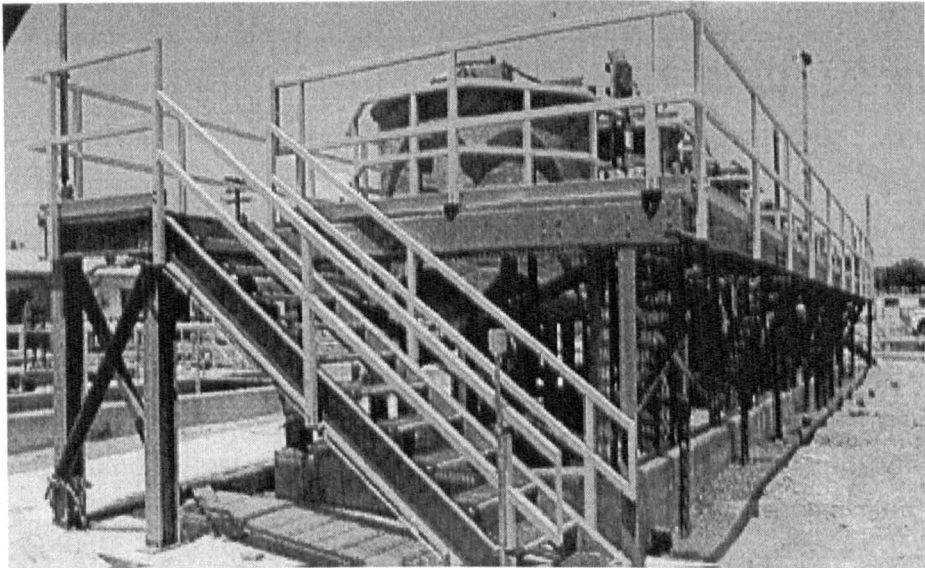


Figure 2.10: Support structure and handrail of this platform surrounding chemical storage tanks are EXTREN.

Figure 2.11 shows one of MMFG's 10' × 250' EXTREN pultruded glass fi-

bre platforms used in a corrosive chlorine operation provided for a petrochemical complex at a Saudi Arabian oil refinery.

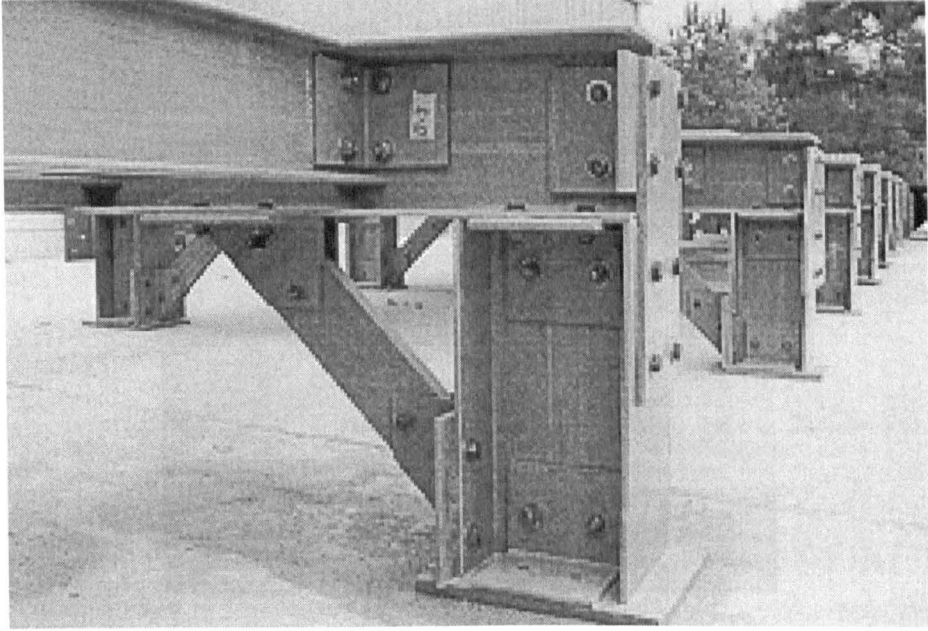


Figure 2.11: Pultruded glass fibre EXTREN platform for a petrochemical complex.

Figure 2.12 shows that EXTREN fibreglass standard pultruded sections used to support 1,000 lineal feet of 54 inch diameter FRP pipes at the Metro Wastewater Treatment in St. Paul, Minnesota, USA (Anon, 1996 b).

Composite materials offer the offshore industry significant savings in platform topside weight and in installation and maintenance cost. One of the largest offshore applications of composites is over 30 tons of fire protection panels, manufactured by Vosper Thornycroft, and supplied to Amerada Hess for the helideck and part of the accommodation area of the Ivanhoe/Rob Roy rig. A composite well bay platform, consisting largely of pultruded decking elements, was installed to replace a heavily corroded steel structure in 1986 on Shell's Southpass 62 production platform in the



Figure 2.12: FRP supports for FRP pipes, image from MMFG Profile, Fall 1996.

Gulf of Mexico.

A handful of GRP bridges and other structures have been successfully built around the world within the last 15 years.

Some of the first applications of fibre-reinforced plastics in complete bridge structures were in China. A number of pedestrian bridges have been built. The first major bridge carrying full highway traffic was the Miyun Bridge (**Figure 2.13**) completed in September 1982 in Miyun Beijing (Head, 1997). **Figure 2.14** shows a glass fibre reinforced plastic cable-stayed pedestrian bridge completed in China in 1986 (Anon, 1994 a). Guanyinqiao pedestrian bridge in Chongqing was completed in May of 1988. It has FRP deck girders suspended from reinforced concrete rigid frames (Bruce, 1990).

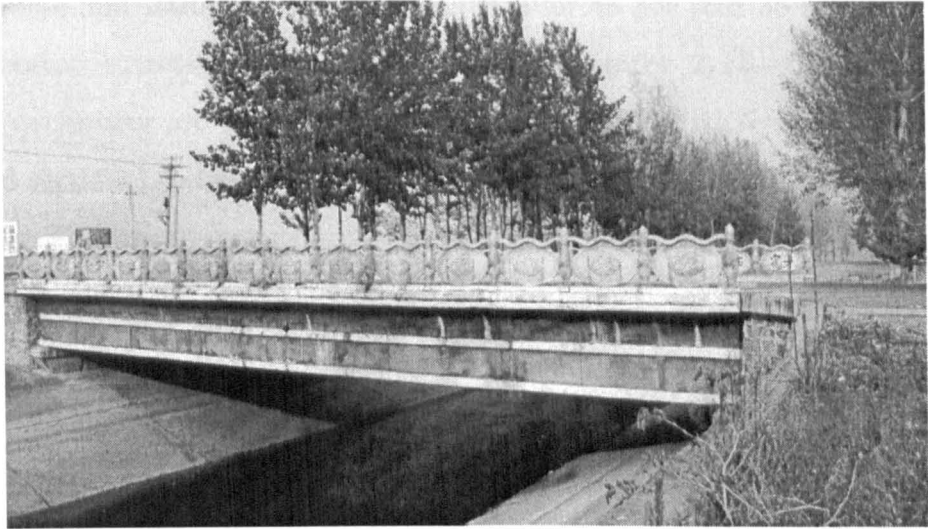


Figure 2.13: Miyun highway bridge in China 1982.

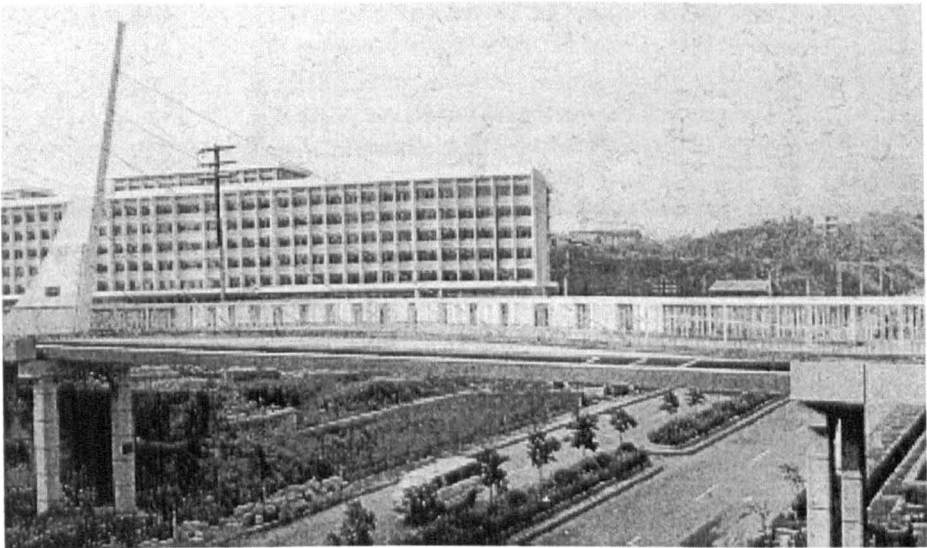


Figure 2.14: GFRP cable-stayed bridge in China 1986.

In America, a number of structures have been fabricated with pultruded profiles. The high-rise Sun Bank building in Orlando, Florida has four 35 ft. high by 35 ft. square rooftop turrets to house radio antennae **Figure 2.15**. These electrically invisible enclosures are made with 10x10x1/2 inch EXTREN wide flange beams (standard sections) and fibreglass nuts and bolts from Morrison Moulded Fiber Glass Company. The turrets are designed to withstand hurricane-force wind (Ballinger, 1990).

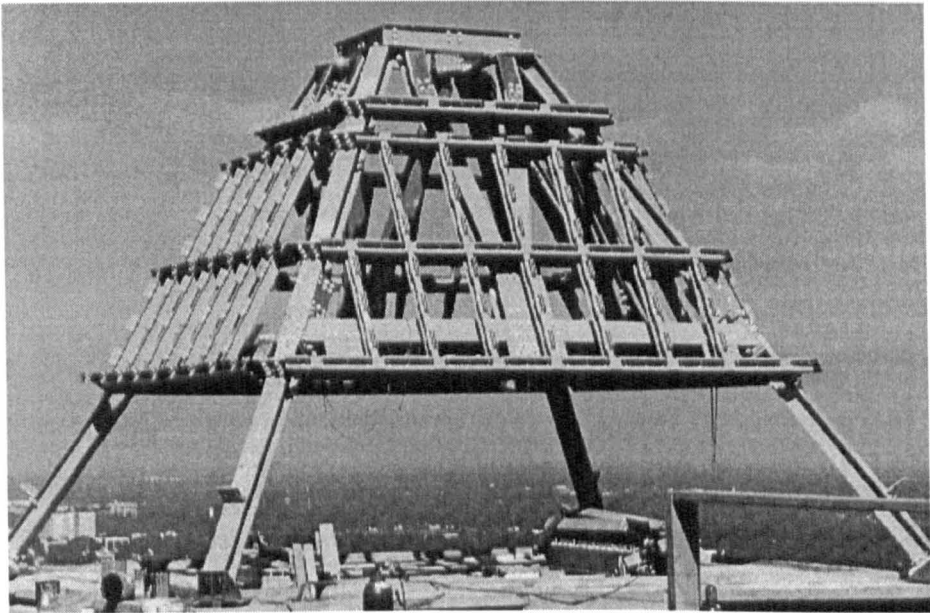


Figure 2.15: Composite turret at top of the Sun Bank building in Orlando, Florida (Photo courtesy of MMFG)

North America's longest fibreglass pedestrian bridge (50 ft. span) made completely of composite materials, is built at Devil's Pool, Fairmount Park, Philadelphia, PA (**Figure 2.16**). The FRP beams were manufactured by Creative Pultrusions Inc. and the bridge was designed by E.T Techtronics. According to the design team 'The project design provided an innovative blend of structural engineering and

environmental design which resulted in significant cost saving (Anon, 1993 a)¹.

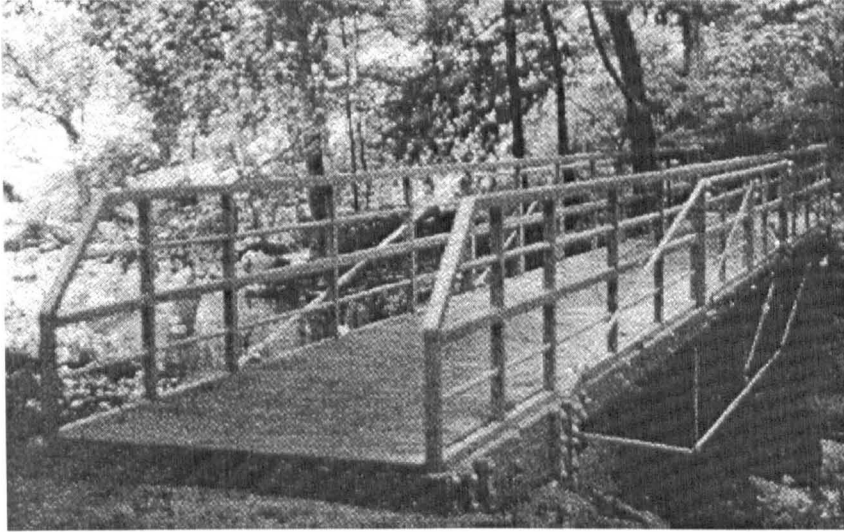


Figure 2.16: Fibreglass pedestrian bridge in Philadelphia 1993.

In the UK, Maunsell Structural Plastic Ltd. ², UK is a key player in developing advanced composite materials for structural engineering. Their advanced composite construction system has been used to install motorway message sign gantries (**Figure 2.17**) (Robbins, 1992).

The nine bridges on the new approach roads to the Second Severn Crossing, opened to traffic on 5 June 1996, are the first in the world to feature full advance composite bridge enclosures (**Figure 2.18**). The Maunsell's bridge enclosures provide a cost-effective solution to long-term maintenance, by reducing the rate of corrosion and minimising future cost. The enclosure system improved safety for maintenance staff and road users and provided a new aesthetic form for bridge structures which has already been widely praised. All the visible superstructure is

²Maunsell House, 160 Croydon Road, Beckenham, Kent BR3 4DE;
Internet: www.maunsell.co.uk

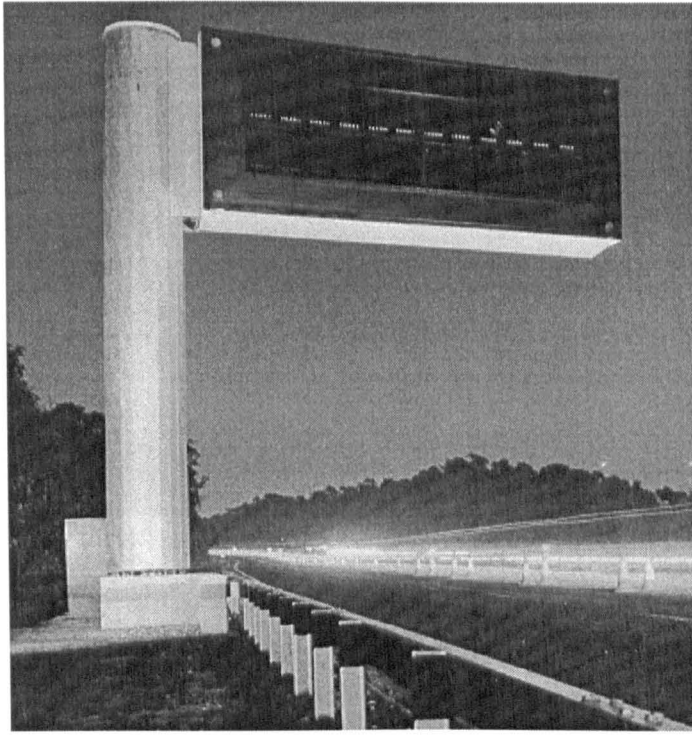


Figure 2.17: Glass fibre reinforced plastic motorway message sign gantries.

of advanced composite material.

Aberfeldy composite cable stayed bridge (**Figure 2.19**) 112 m long with a 63 m span, built by Maunsell and Dundee University, was completed in October 1992. The bridge is stayed from two 18 m high ‘A’ shaped GRP pylons using Parafil cables - Kevlar aramid fibres sheathed in a protective low density polyethylene coat (Anon, 1995 b). The deck, pylons and handrails are made out of pultruded glass fibre reinforced plastic. It is the world’s first major bridge in advanced composite materials and incorporates a number of innovations in structural systems, materials and methods of construction (Anon, 1993 b).

Bonds Mill lift bridge (**Figure 2.20**), completed in July 1994, is the first advanced composite bridge designed by Maunsell Structural Plastics to accommodate



Figure 2.18: Advance composite bridge enclosures (Anon, 1997).

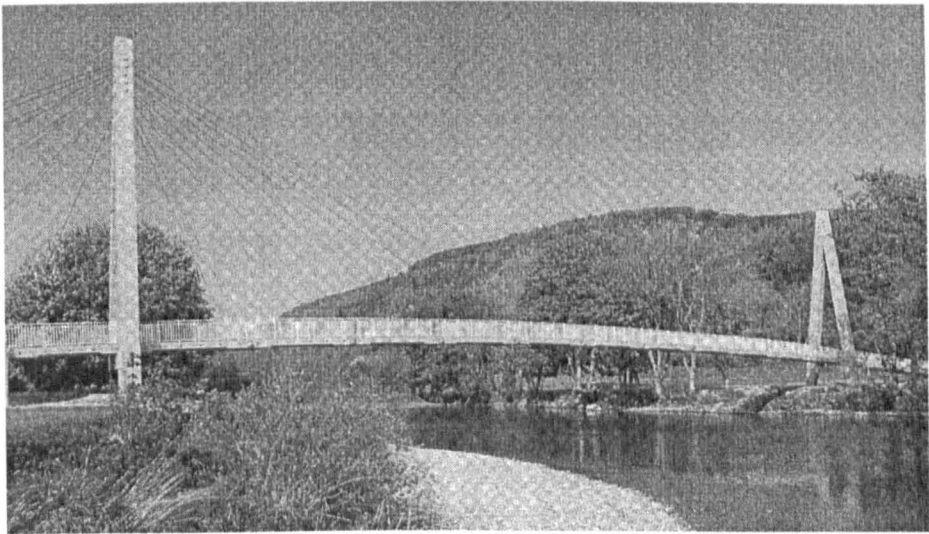


Figure 2.19: Aberfeldy footbridge Scotland, UK 1992.

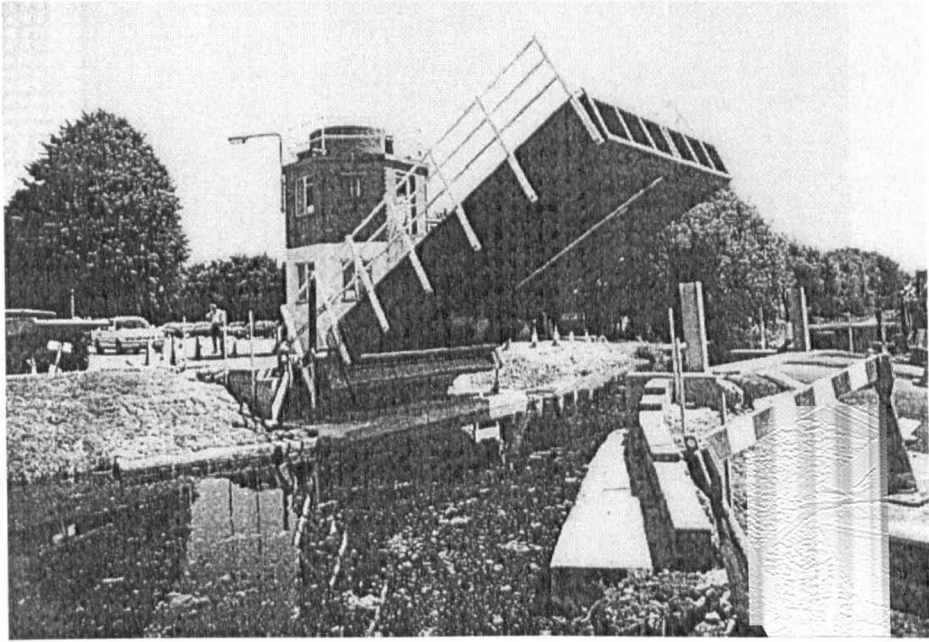


Figure 2.20: Bonds Mill lift bridge Gloucestershire, UK 1994.

full highway traffic loading (Anon, 1994 b).

Europe's first suspension bridge of entire pultruded composite profiles, where the only non-composite materials in the bridge are the steel bearings at the foundation and the bolts holding together the bridge, was constructed by co-operation between RamboØll, a Danish firm of consulting engineers, the authorities of Kolding City, and Fiberline Composite³, A/S in Kolding, Denmark (**Figure 2.21**). The bridge is 40 metre long and 3 metre wide and designed to carry a variety of vehicles, such as bicycles, motorbikes and snow clearing vehicles weighing up to 5 tons. The bridge features 15 different types of pultruded profiles with a ratio of 60% glass fibres and 40% resins used in the structure. It was opened to the public in June 1997.

³Fiberline Composite A/S, Nr.Bjertvej 88, DK-6000 Kolding, Denmark;
Internet: www.fiberline.com

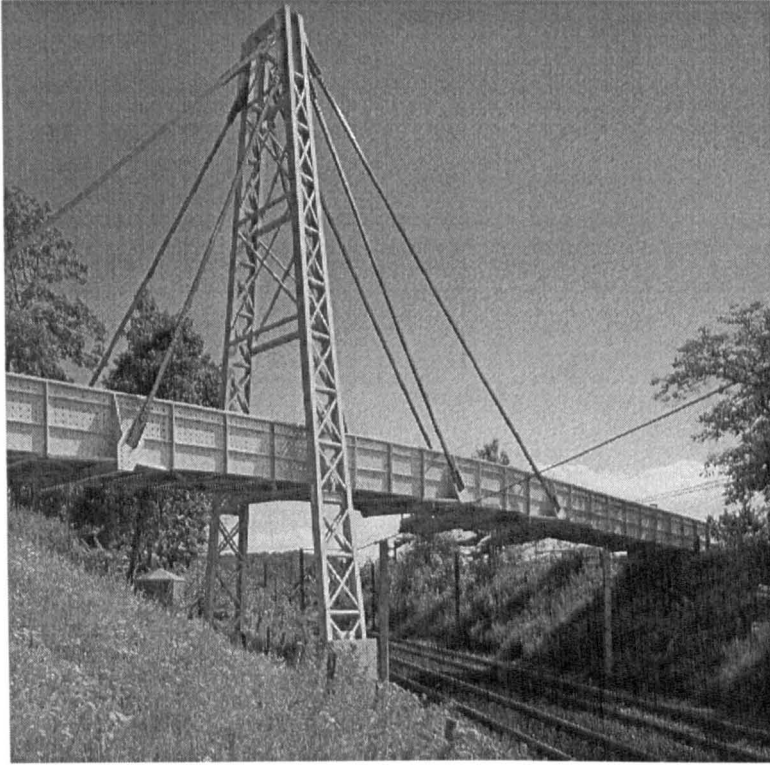


Figure 2.21: Fiberline cable-stayed bridge, Denmark 1997.

The longest stress-ribbon footbridge (**Figure 2.22**) using Aramid fibre composite cable, FiBRA, has been constructed by Tobishima Corporation at a golf course in Nagasaki Prefecture, Japan. The bridge is 73 m long with a clear span of 64 m, using six FiBRA cables in the bridge slab (Anon, 1996 c).

2.7 Conclusions

FRP composites have been shown to be successful structural materials, and have been increasingly used in various forms of structural applications in the construction industry worldwide. The significant advances of composites make them an optimum

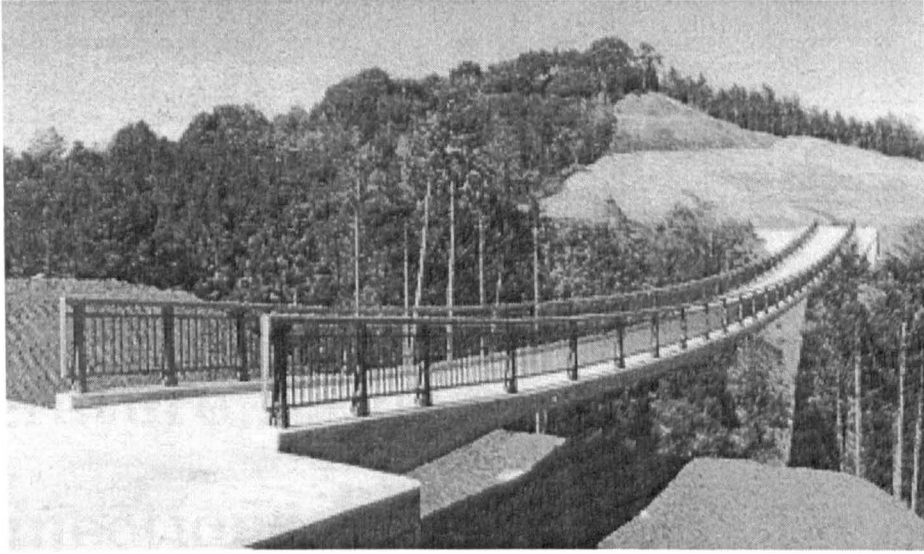


Figure 2.22: Longest stress-ribbon footbridge in Japan 1996.

material choice for corrosive environment, and likely to be most cost effective. There is now no doubt that advanced composites are becoming established as an important structural material for use alongside the conventional materials of steel, concrete and timber. Wide use of FRP structures in innovative construction has been limited by several factors, such as lack of design guidelines, material properties, and design awareness and high material cost (GangaRao & Barbero, 1991).

To address these and other problems, many engineers are working to improve our understanding. Many valuable research projects into the material and its applications have been, and are being carried out. Continuing research and development of a better understanding of the behaviour of structure over their life time will help composites to play a major role in the future construction industry.

Chapter 3

Literature Review on Connections in Polymer Composite Structures

3.1 Introduction

Problems associated with the buildability and durability of structures of conventional construction materials have led to a growing interest in new structural systems of polymeric composite materials (Mottram & Zheng, 1996 b). Due to the nature of these materials and their range of material properties, there are more design factors to be considered than with conventional materials. This makes design more complex and expensive, thereby increasing the overall cost of a project. This complexity and associated higher design cost discourages designers. There is no doubt therefore that the construction industry will need to settle on some standard products and construction systems if designers are to be encouraged to work with these materials in preference to alternative solutions (Head, 1996). Standard pultruded structural

shapes are one of these standard products. They have been successfully used in a number of applications such as the rooftop turrets on the top of Sun Bank building in Orlando (**Figure 2.15**), and the platform shown in **Figure 2.11**.

FRP pultruded structural shapes have been available for more than two decades, yet the development of their application has been relatively slow. One of the reasons for this situation is that structural engineers is still not familiar with this material and its structural elements and connections. The design practice with conventional structural materials relies heavily on approved and legally standing design codes. There is no such recognised design code currently available for building structures fabricated from fibre reinforced polymeric composite materials. The only available design guidance is from pultrusion manufactures, such as Morrison Molded Fiber Glass Co. (MMFG), Creative Pultrusions Inc. ¹, and Fiberline Composites. Recently, EUROCOMP project which finished in 1996, developed a design code EUROCOMP (Clarke, 1996) without legal standing.

As standard pultruded sections resemble their steel counterparts in appearance, steel-type connections are recommended by the manufactures' design guidance such as MMFG (1989). Since the pultruded structural shapes have unidirection fibre reinforcement along their length, the transverse and through-thickness strengths are much lower than the longitudinal. As a consequence, steel-type connections do not perform satisfactorily. It is the aim of this thesis to study the beam-to-column connection for pultruded frame construction. A literature survey has been carried out on FRP composite connections and the related topics such as member and frame.

¹Creative Pultrusions, Inc. 214 Industrial Lane, Po Box 6, Alum Bank, PA 15521-0006 US.
Internet: www.creativepultrusions.com

3.2 Study of Pultruded Members

Commercially produced pultruded FRP structural shapes have been investigated extensively and research has involved: (1) the mechanical properties (Sims, et al., 1987; Bank, 1987, 1989 a, 1989 b, 1989 c; Mottram, 1991), (2) buckling of beams (Bank, et al., 1993, 1994 a), (3) Lateral-torsional buckling (Mottram, 1992; Brooks and Turvey, 1995), and (4) buckling of pultruded FRP column (Hewson, 1978; Barbero and Tomblin, 1992; Brown et al., 1998).

For design purposes both stiffness and strength properties of structural members are required. Due to the nature of pultruded material, the stiffness in longitudinal direction is generally higher than in transverse direction (see **Table 2.2**). Testing to determine the stiffness and the deflection of beams has demonstrated that they have relatively low stiffness, so that frame design will be governed by serviceability requirements. In addition, the transverse shear stiffness of FRP material is primarily derived from the relatively flexible plastic matrix material and the ratio of the longitudinal Young's modulus to shear modulus is higher than the 2.6 value common for isotropic material; therefore, shear deformation effects which are usually neglected in conventional structural analysis, cannot be neglected in the analysis of FRP structures (Bank, 1989 c).

To take account of shear deformation in the deflection of FRP beams Bank (1991), considering anisotropic properties of pultruded FRP material, proposed a new material/structural stiffness property — beam section shear modulus (G_b) which is found from direct experiment on full-size pultruded FRP beam rather than on coupon tests. Proposed (G_b) will replace the term kG (k is shear coefficient and G is shear modulus for isotropic materials) in the isotropic formulation of shear deformation.

3.3 Connection Research

According to joining methods used connections of FRP composite could be classified as mechanical connections, bonded connection or combined connection (Clarke, 1996). The role of connections in a frame is to join members together and to transfer the forces between the members. The behaviour of the connections influences the way in which a complete structure responds to load.

Connections can account for up to 40% of the cost of a steel frame (Fewster, 1995); for a FRP frame, with inefficient connections the cost could be even higher. By recognising the significance of this factor it is very important to improve our knowledge of the behaviour of the connections between members of a structure in order to (COST, 1994):

- be able to control the level of semi-rigidity, by developing practical analytical tools using realistic connection behaviour;
- determine what amount of savings can be achieved by using semi-rigid connections and simplifying accordingly the detailing of the connections;
- gain a better estimation of the level of safety and to provide information for a realistic determination of partial safety factors;
- estimate the energy dissipation in the case of seismic loading and improve seismic design.

The role of connections in structures and their complexity in design due to the inherent properties of composite material gives them a special significance and poses a major challenge to the engineers. During last 10 years, a number of connection investigations have been carried out. The review of this previous work in the context

of frame connections has conveniently been divided into four connection types; adhesively bonded connection, bolted plate-to-plate connection, pinned beam-to-column and semi-rigid beam-to-column connection.

3.3.1 Adhesively Bonded FRP Connections

Adhesive bonding can be used to connect plates, known as adherends, and to transfer load from adherend to adherend. It also can be used to increase the structural efficiency of a laminate structure by bonding a stiffener to a member to increase resistance to local buckling. The strength of the adhesively bonded joint is dependent on the joint type and geometry (Hollaway, 1993).

There is a wide range of adhesives to choose from and the principal options are described by Clarke (1996). Currently, epoxy (thermoset) based and the acrylic (thermoplastic) based toughened adhesives are used for general application. They have proved over the years to be very versatile, easy to use, durable, robust and relatively free from toxic hazards.

There are four basic stresses on bonded joints when they are subjected to load, and they are: tensile, shear, cleavage, and peel. Joints that are subjected to tension or shear stresses are considerably stronger and much more reliable than those subjected to cleavage or peel stresses (Meyer, 1985).

Four typical locations and modes of possible failure of an adhesively bonded joint under in-plane loading are given by Hollaway (1993). They are shown in **Figure 3.1**, and are

1. a failure of the adherend;
2. a shear strength failure of the adhesive;
3. a mode associated with the failure of the adhesive under a peel load;

4. a failure by delamination of the fibrous composite adherends.

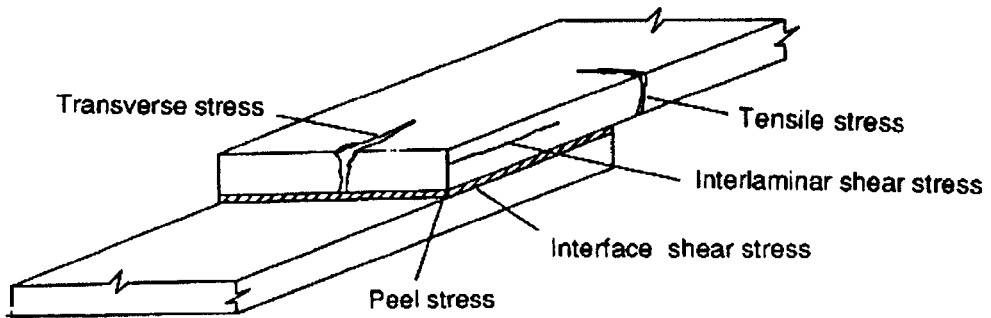


Figure 3.1: Failure modes of an adhesively bonded joint (Hollaway, 1993).

The most important factors to obtain best performance of joint are surface preparation of the areas to be bonded and film thickness in adhesive (Meyer, 1985).

Efficiency of a bonded joint is defined by the ratio of joint strength to adhesive strength. Bonded joints are most efficient when subjected to shear load and least efficient when subjected to peel load, thus joints should be designed so that they are only subjected to shear loads whenever possible (Hollaway, 1993). In addition, the fibre orientation on the bond surface should be parallel to the primary loading direction (Clarke, 1996).

By using solely bonding Gordaninejad et al. (1997) experimentally tested two pultruded beam-to-column connection details. The beam and the column were 6 inch and 12.7 inch Creative Pultrusions' I-sections respectively, and they were joined by pultruded angles bonded by an epoxy structural adhesive. There was no $M - \phi$ curve determined in their test. The failure loads for two specimens were about 3.13 kNm and 5.81 kNm respectively. Their test results show that their connections are not able to develop the full strength of the beam.

3.3.2 Bolted Plate-to-plate Connection

Bolting is the most common method of connection and can be used to form a reliable connection in comparison with bonding. It has the advantage of being cheaper and easier to fabricate than bonded joints. This is because they require very little preparation, and therefore can be more easily constructed on site (Cooper & Turvey, 1995). Bolted joints are relatively easy to inspect and to maintain as they can be disassembled. Experimental behaviour of FRP joints has been extensively investigated for aeronautical applications. It is only in recent years that a number of studies with pultruded FRP material have been carried out with objective of developing our understanding for constructional applications. These investigations identified failure modes for the single bolted joint configuration shown in **Figure 3.2** and found the factors which affect resistance. For the multi-bolted connection the load distribution between bolts and the effect of geometrical parameters on the connection behaviour were also investigated. The literature survey for these topics is summarized in following sections.

Failure Modes

Tests on single bolted joints of lap-joint type (single and double) have shown the effects of width, end distance, hole size, bolt clamping pressure, fibre arrangement and environmental conditions on failure mode and joint strength. The basic failure modes in steel connection are also to be found with FRP material. These six modes are illustrated in **Figure 3.2**.

Generally, as the width to bolt diameter ratio (w/d) increases, assuming that the end distance to bolt diameter ratio (e/d) is large, the failure mode changes from net tension to bearing. Similarly as the e/d ratio increases, assuming that w/d is large, the failure mode changes from shear to bearing. Cleavage failure generally

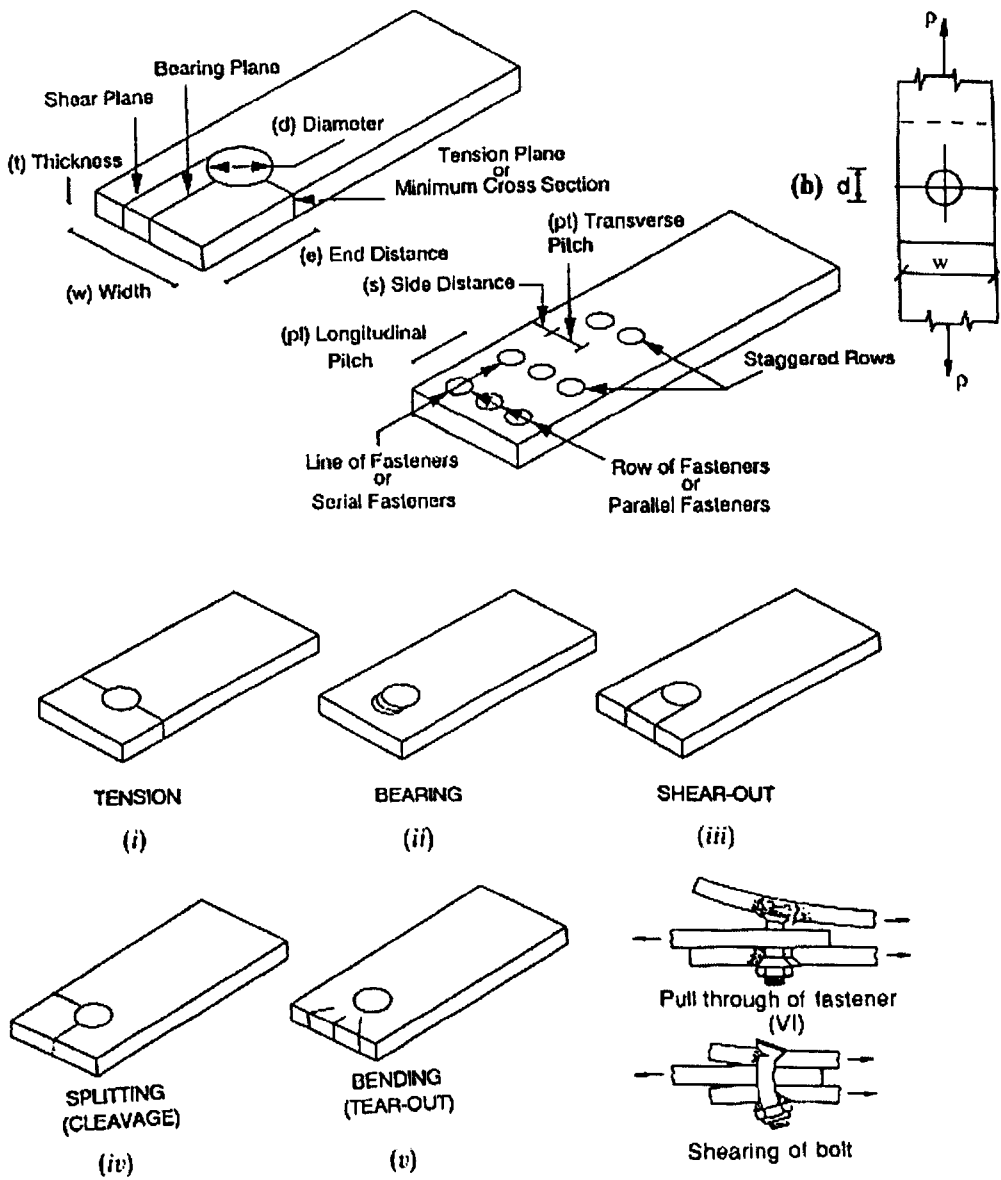


Figure 3.2: Failure modes of bolted connections, (a) joint nomenclature; (b) notation; (c) joint failure modes (Hollaway, 1993).

occurs in FRPs where the percentage of 0° fibres is high (Cooper & Turvey, 1995), and is initiated by transverse tensile failure ahead of the bolt, followed by tensile failure on the minimum area cross-section (Hollaway, 1993). Failure is also possible by pull-out or in a combined tension and bending mode referred to as cleavage (Matthews, 1985). Due to the lower stiffness of the composite plates compared to that of the steel bolt, a shearing failure of the bolt will only occur when bolts are of small diameter and are therefore liable to bend (Hollaway, 1993). Shearing failure of GFRP threaded bolts can also occur because they are weaker than the members joined (Erki, 1995). The bearing failure mode is desirable, because it develops slowly, giving plenty of warning before ultimate failure. As a result it provides confidence and a joint behaviour analogous to that when the plate material is a ductile metal. The shear, tension and cleavage failure modes usually occur suddenly and are normally catastrophic (Cooper & Turvey, 1995); such joint failure should be avoided if the structure's performance is to remain safe.

Effect of Parameters on the Behaviour of Bolted Connections

1. Geometry of Connection

Geometry is one of the major factors which affect the connection failure mode, and includes width (w), end distance (e), bolt hole size (d) and thickness of connection section (t) (see **Figure 3.2** (b)). For convenience, the ratio of (w/d) and (e/d) are usually used to define the required width and end distance respectively.

The end distance and the width are interrelated factors for failure modes and strength of connection, and they are also highly dependent on the fibre orientation of the composite. Abd-El-Naby and Hollaway (1993 a) demonstrated that increasing the end distance increased the strength of the joint until a

critical end distance was reached – any further increase of the end distance over that value did not result in a corresponding increase in the strength of the joint. It was found that critical end distance did increase with the width of the plate.

The critical end distance and the critical width are also affected by clamping torque to bolt. With increasing clamping torque, the critical end distance and the width are increased (Cooper & Turvey 1995).

To obtain optimum performance, as a general rule the width and end distance should be approximately $4d$ (Matthews, 1985). The ratio of e/d and w/d suggested by Cooper and Turvey (1995) are 3 and 4, respectively. They also recommended the e/d and the w/d ratio as 4 for EXTREN 500 series $8 \times 8 \times 3/8$ inch WF section, in comparison with the range of 2 to 4.5 and 1.5 to 3.5, respectively, for the ratios recommended by MMFG (1989), and with 3 and 2, respectively, for the ratios commonly used values from MMFG's data. The tests, conducted by Rosner and Rizkalla (1995), on 9.5mm, 12.7mm and 19.05mm thick pultruded flat sheet with 20.6mm diameter of hole size showed generally that the member thickness had little effect on the bearing stresses and the mode of failure. Matthews (1985) found the bearing strength did reduce when the hole diameter was larger or thickness for a given diameter was small because there was gross bending of the laminate on loaded side of the hole. Matthews (1985) suggested that the ratio of bolt hole diameter to composite thickness (d/t) should be less than 3.

2. Fibre Arrangement

Matthews (1985) noted that fibre lay-up is a key factor in determining strength. To obtain optimum bearing strength the material should not be strongly anisotropic and a combination of 0° and 45° fibre orientation, with between

35-65% of 0° fibre lay-up, is generally preferred. The stacking sequence should be as homogeneous as possible.

The fibre direction of the unidirectional fibre layers in pultruded material controls the failure mode and as the angle of loading with respect to the unidirection fibres increase, both strength and stiffness decrease (Erki, 1995). This was also found in the test programme of Rosner and Rizkalla (1995) who reported that the ultimate strength of connections with fibre orientation of 45° and 90° with respect to the direction of the applied load was 18% and 24% lower than the corresponding connection with a 0° fibre orientation, respectively.

For some pultruded lay-ups, Abd-El-Naby and Hollaway (1993 a) found that bearing failure cannot be achieved because of the low shear strength of the material.

3. Bolt Hole Clearance

For obtaining maximum connection strength, bolt hole and washer should be reamed to size (Hollaway, 1993). But for the buildability reason it is necessary to have a bolt hole clearance in practical construction.

To investigate the effect of bolt hole clearance on the ultimate load capacity of the bolted joints, Yuan and Liu (1996) conducted tests with single bolted joints fabricated from 9.525 mm thick EXTREN Series 500 Flat Sheet. They found that with an increase of bolt hole clearance the ultimate load of the connection decreased and there was little effect on the ultimate load of the connection with a bolt hole clearance less than 0.794 mm ($d = \text{bolt diameter} + 1.588\text{mm}$). The percentage decrease of ultimate load with the increase of the clearance given by Yuan and Liu (1996) is plotted in **Figure 3.3**.

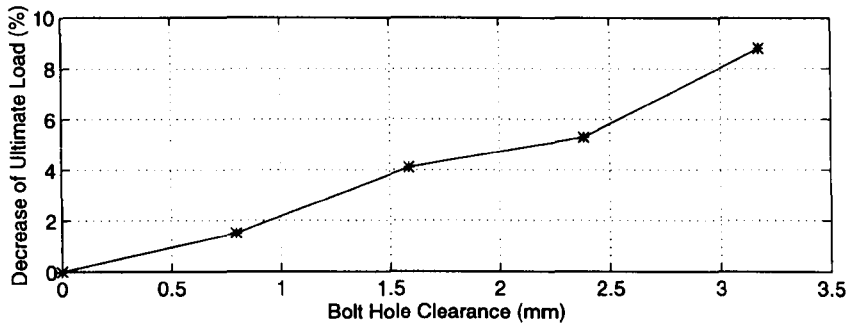


Figure 3.3: Effect of bolt hole clearance on ultimate load.

The presence of a clearance will also allow the connection to slip under joint loading. Rosner and Rizkalla (1995) conducted tests with the single bolted joints where the joints were fastened by 19 mm high strength bolt tightened to a torque of 32.5 N m. The bolt hole clearance was 1.6 mm. The test showed that the slipping occurred in the initial loading stage.

4. Bolt Clamping Pressure and Confinement

Matthews (1985) noted that clamping strongly influenced joint behaviour and bolts must be fully tightened in order to obtain maximum connection strength. He explained that the compressive stresses around the loaded portion of the circumference generated by the fastener cause tensile stresses in the through-thickness direction which because of the low strength in that direction, can lead to early bearing failure if adequate restraint is not provided. Confirmation of this effect is given by Abd-El-Naby and Hollaway (1993 a) and Cooper and Turvey (1995). In addition, Abd-El-Naby and Hollaway (1993 a) replaced the washer by steel plates and composite plates covering all the potential damage area in a single bolted joint and found that there is a trend of increasing strength with increasing confinement area and the material used for clamping

influences the behaviour of the joint as well.

Furthermore, using high-strength structural bolts, tightened to a torque of 32.5 N.m, Rosner and Rizkalla (1995) showed this joint set-up was adequate to remove most of the influence of the material thickness.

The stiffness of the fastener affects the stiffness and maximum load carrying capacity of the joint. Erki (1995) tested the joint with three different types of fasteners; steel threaded rod, GFRP threaded rod and GFRP threaded rod with GFRP pipe sleeve. She found that joints with a GFRP threaded rod gave half the strength of the joints with a steel threaded rod. The joints with a GFRP threaded rod and GFRP pipe sleeve were at least a third stronger than the joints with a GFRP threaded rod alone. All joints joined by a GFRP threaded rod failed initially by crushing of the vinyl ester moulded threads, followed by breaking of the rod, with little damage to the GFRP plates. This joint behaviour is contrary to that found with steel bolts and explains why in practice FRP bolts are only used in the structures which cannot contain any steel. Most pultruded structures such as those introduced in chapter 2 have mechanical fastening by stainless steel bolts.

Multi-bolted Joint

The load distribution between two bolts in series, in a pultruded composite plate, was investigated by Abd-El-Naby and Hollaway (1993 b). They found that the load distribution between the bolts tended to approach uniformity near failure; this, however, was obstructed by premature tensile and shear failure. For the case where bearing failure develops, the load distribution is uniform and, accordingly, the load per bolt is equal to the strength of a single-bolt joint. Redistribution will occur if bearing is the mode of failure.

The influence of the geometric parameters, including the width of the member, the edge distance, the bolt pattern, number of bolts and orientation of the uni-directional fibres, on the strength and the failure mode of multi-bolted joints was investigated by Hassan et al. (1997 a, 1997 b). They tested 105 multi-bolted double shear lap joints and found that the load is equally shared among the bolts for the connections with one row of bolts; whereas, for the connections with more than one row of bolts, the load distribution is not even. They also found that the increase in the ultimate capacity of the connection is not directly proportional to the increase of the number of bolts and e/d ratio has a significant effect on the mode of failure. Their tests show that the effect of fibre orientation on ultimate strengths of connection are similar to single bolted joints.

3.3.3 Review on Pinned Beam-to-column Connection

The beam-to-column connection of pultruded fibre-reinforced plastic (FRP) structural sections plays an important role in frame structures. Mosallam and Bank (1992) performed a study on a portal frame subjected to short-term static loads, and indicated that the flexibility of the beam-to-column frame connection has been shown to control the overall behaviour of the frame. It has been shown that, unlike in steel structures where accounting for connection flexibility is recommended, the inclusion of connection flexibility in the analysis of pultruded FRP frame structures is vital.

To study the behaviour of different connection designs and see whether they had adequate performance for semi-rigid action, Bank et al. (1990, 1992) conducted the first test programme in the late 80's in America. One of these connections was a double web angle connection (**W**) (Bank et al., 1990). The beam and column were

made from **Pultex**² 1625 wide flange 8x8x3/8 inch pultruded glass reinforced vinyl ester and the web cleats were cut from 6x6x1/2 inch equal leg angles. The detail of the **W** connection is shown in **Figure 3.4** (a). No adhesive bonding was applied. The beam, column and web cleats were bolted together with pultruded threaded rods and Superstud 3/4 inch nuts and all FRP nuts were tightened to a torque of 40.67 N m. The connection was tested in the loading set-up shown in **Figure 3.5**. Only initial connection stiffness tests were conducted and results gave a very low initial stiffness 0.028 kNm/mrad. The test was terminated at a connection rotation ϕ of only 5 mrad. Since the purpose of their experimental investigation was to examine the semi-rigid behaviour of the different connections, little attention was paid to this 'pinned' web cleated connection.

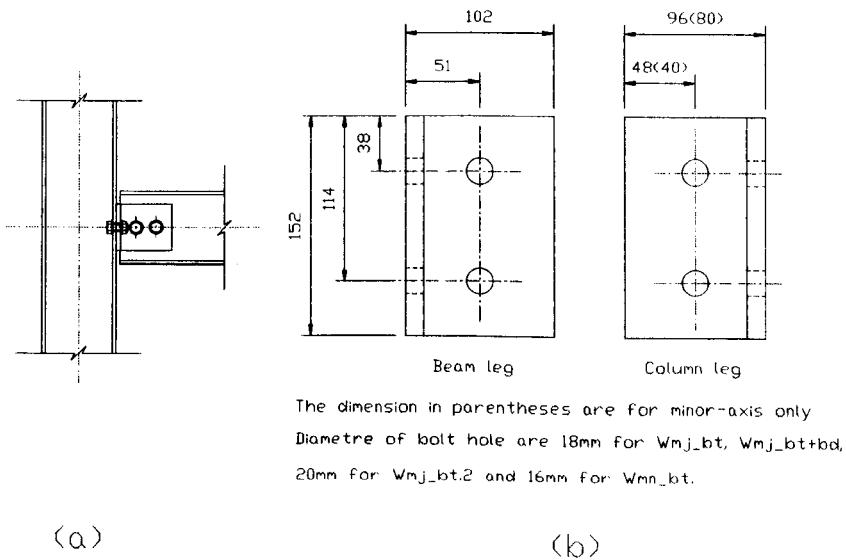


Figure 3.4: Web cleated connections, (a) Bank et al. (1990), (b) Mottram (1994).

²Manufactured by Creative Pultrusions, Inc.

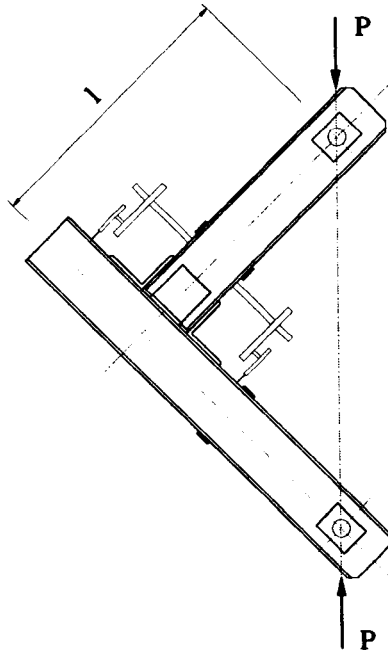


Figure 3.5: Experimental set-up (Bank et al. 1990).

On questioning whether the connections recommended by Design Manual (MMFG, 1989) have adequate performance for the requirement of frame design, Mottram (1994) conducted five tests to study the behaviour of web cleated connections as part of the EU468:EUROCOMP project. The web cleated connections were cut from pultruded 6x6x1/2 inch equal leg angle. The beam and column members were made from 8x8x3/8 inch wide flange (WF) section. The beam and column members were jointed by the web cleats. In his test programme, three connection tests, labelled, **Wmj_bt**, **Wmj_bt.2** and **Wmn_bt** had bolting fastening, one connection test labelled **Wmj_bt+bd** had bolting and bonding fastening, and one labelled **Wmj_bd** had bonding fastening alone. The details of the web cleats are shown Figure 3.4 (b).

Unlike the tests conducted by Bank et al. (1990) which had a test configuration

for external connections, external columns and the column oriented to be major axis, Mottram's tests were internal columns with the column oriented to be major (m_j) and minor (m_n) axis, respectively. By criticizing Bank's loading set-up that subjected the beam to moment, shear and a parasitic compression loading, Mottram (1994) took the form of two back-to-back cantilever beams with a central column, which is the standard method in Europe to determine connection properties. His test configuration was similar to that shown in **Figure 4.3**, and used by the author for his test programme.

The results of Mottram's connection tests showed that the initial moment-rotation behaviour of each connection was linear. Both connection moment and rotation when the behaviour became non-linear was low. Non-linear behaviour was gradual for the bolted only connection and pronounced for those with bonding. Splitting between the reinforcement layer, at the top of the web cleats, was the first visual mode of failure, except if bonding was present. Major-axis connection had considerable flexibility due to deformation of column flange.

In analysis of the connections, Mottram (1996) stated that the rotation of the connection at first failure is the most relevant connection property for the purpose of design and this rotation may be used to determine a simply supported beam's maximum deflection.

By defining connection failure as visual material failure, such as cracking and debonding, he found that only **Wmn_bt**, **Wmj_bt.2** met the requirement of the rotation 12.8 mrad (without including shear deformation) for a maximum deflection 1/250 required by serviceability limit state. None of the connections tested provided an adequate rotation for the MMFG maximum deflection limit of 1/100 of the beam span.

These connection rotations for **Wmn_bt**, **Wmj_bt.2** at first failure are questioned by the author because they fall in the non-linear part of the $M - \phi$ curve, and

this means material may already have some failure before the visible ‘first failure’. As Bank et al (1992) stated ‘the non-linearity in the $M - \phi$ curves can be related to the damage that develops in the connection during the loading.’ This was verified by the experimental investigation in this thesis.

3.3.4 Semi-rigid Beam-to-column Connection

Steel frames are usually designed on the basis that beam-to-column connection are either pinned or rigid. The actual stiffness though is between these two extremes, resulting in what is termed ‘semi-rigid’ behaviour. Stiffness and resistance of the connections will influence the response of the frame as a whole. For steel frames this has been recognized and studied extensively (Anderson et al., 1992).

As standard pultruded members resemble their steel counterparts in appearance, it has been the practice to use knowledge available from the behaviour of steelwork. In the design of pultruded frames, the forms of the connection, which are given in MMFG (1989), are simply copies of steel practice and are assumed to be nominally pinned connections. On the one hand, these connections will perform differently to those of steel due to the anisotropic nature of material (Mosallam et al., 1994 b). On the other hand, the result of treating such connections as nominally pinned in design is to have a conservative over-estimation of the member stresses and deformation. If the actual characteristics of the connection are used in the frame design, in term of economics, the depth of the beam and the overall cost could be reduced, or in term of serviceability, the beam span could be increased, thus making frames more economical and attractive.

Frames of pultruded structural profiles have members connected using bolting on its own or combined with adhesive bonding. Bolting is the main connection method used in pultruded frames because it has been shown that the bonding strength for

pultruded frames is much weaker than welding strength for steel work; this is due to the physical structure of pultruded material and the fact that adhesive connections are weak in tension (often known as peel or cleavage failure).

To study the semi-rigid behaviour of the connection in pultruded frames, Bank et al. (1990) conducted the first test programme to determine the moment-rotation behaviour of different connection designs to see whether they had adequate performance for semi-rigid action (Mosallam, 1990; Bank et al., 1994 b). Four different beam-to-column connection tests were conducted using **Pultex** 1625 wide flange 8x8x3/8 inch pultruded glass reinforced vinylester beams and 6x6x1/2 inch equal leg angles cleats, and bolted together with pultruded threaded rods and superstud 3/4 inch nuts. The connection details for each of these tests are different and they are shown in **Figure 3.6**.

Figure 3.6 consists of: (a) connection with double web angles (**W**) (see **Section 3.3.3**), (b) connection with seat and double web angles (**SW**), (c) connection with top and seat angles (**TS**), and (d) connection with top, seat and double web angles (**TSW**). All connections had mechanical fastening by pultruded threaded rods and compression moulded nuts and all the nuts were tightened to a torque 30 ft-lbs (40.67 N m).

The configuration of experimental loading set-up used by Bank et al. (1990) is the same as shown in **Figure 3.5**. The measurement of the connection rotation was achieved by using two 0.0001 inch displacement indicators attached to a bar parallel to the column and fixed to the beam. The connection moment was obtained by $P \times l \times \cos 45^\circ$, where P is load and l is the distance from the loading pin to the intersection of the beam and column centrelines which is 914.4 mm (36 inches).

The initial stiffnesses k_{ini} for four connections were obtained from the moment-rotation curves. The values of the initial stiffnesses k_{ini} are given in **Table 3.1**

Connection **TSW** was loaded to ultimate failure. The moment-rotation char-

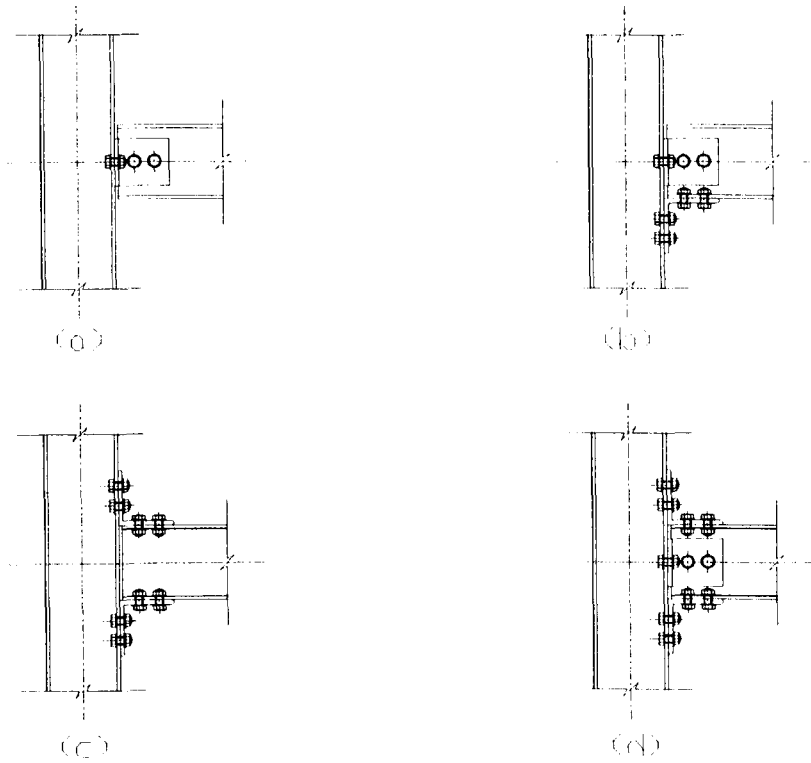


Figure 3.6: Pultruded FRP beam-to-column connection (Bank et al., 1990).

Table 3.1: The initial stiffnesses k_{ini} (Bank et al., 1990).

Connections	k_{ini} (kNm/rad)
TSW	791
TS	678
SW	169
W	28

acteristic of the connection was given to a maximum rotation of 25 mrad because the displacement gauges reached their full range (0.4 in.) in measurement. Without measurement of the rotation, the connection was loaded to ultimate failure at a load 2,050 lbs ($M=52.3$ k-in.=5.9 kNm). They described the progressive failure of connection **TSW** as due to cracks developing in the top leg-angle, followed by the flange of the column separating away from the web behind the top tension angle, thus creating a hollow internal cavity in the pultruded section. Ultimate failure of the connection was due to this failure of the column member.

Further connection tests were carried out by Bank et al. (1992), aimed at improving the structural performance of the beam-to-column connection designed and at developing a prototype semi-rigid connection suitable for pultruded framed structures. The reason for this trial and error approach was that all four connection details in **Figure 3.6** had $M - \phi$ behaviour that made them unsuitable for designing frames as semi-rigid.

Figure 3.7 shows the subsequent four connections, in which (a) is connection **TSW** described previously, (b) is the same as connection **TSW** in all details except two back-to-back 6x6x1/2 inch pultruded angles have been bolted to the column section to reinforce the column web/flange junction, (c) is the connection with a change of top cleat construction from that in connection (b) (which copies steel practice). The new cleat was a built-up part and it consisted of two Creative Pultrusions' 6 inch Tee Flanges and a triangular pultruded 1/2 inch (gusset) plate (with its longitudinal direction at 45 degree to the beam section), and (d) is a connection, referred to as the 'prototype' connection by Bank et al. (1992), in which built-up parts were used to replace both top and bottom cleats. These cleat pieces consisted of a gusset plate bonded into a Tee Flange section. This combination of three part components created a monolithic 3-dimensional continuous part. To further increase stiffness and strength of the connection, the column and beam members were stiff-

ened by using 2x2x1/4 inch pultruded square tubes through which threaded FRP rods connected the flanges of beam and the flange of the column.

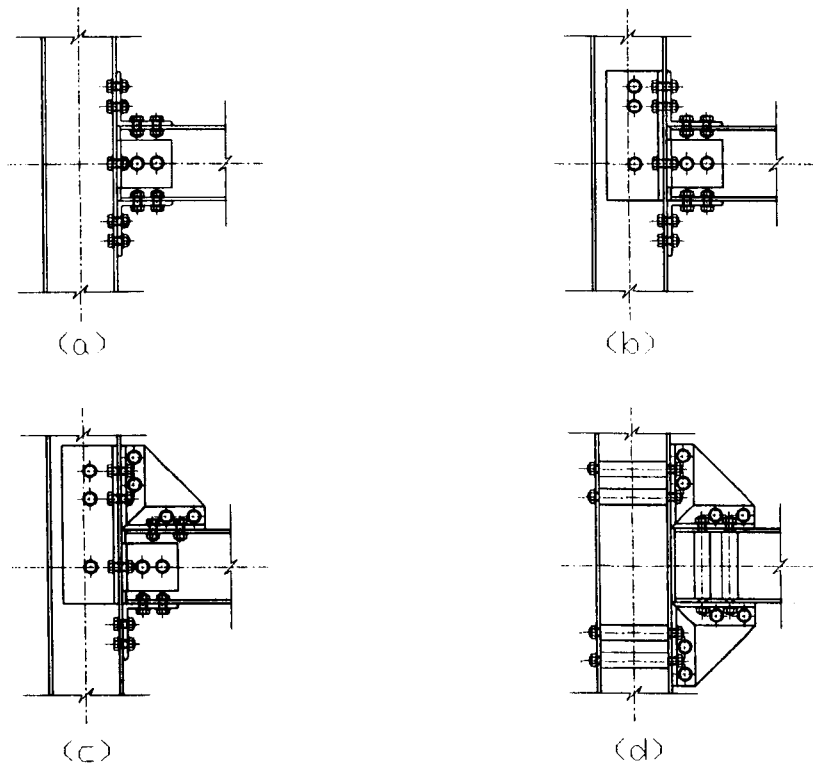


Figure 3.7: Pultruded FRP beam-to-column connection (Bank et al., 1992).

As described above connection **TSW** failed in the column at the junction between the web and the flange. In order to prevent this type of failure occurring in connection (b) (**Figure 3.7**) two FRP angles were bolted into the column interior. Following the test it was observed that there had indeed been an increase in ultimate connection strength, but that the initial stiffness was unchanged. Ultimate failure of connection (b) occurred in the top cleat angle due to a combination of radial tensile cracking and the nuts ‘punching’ through the pultruded angle. Connection (c) uli-

mately failed due to a transverse tensile failure of the Tee Flange web. Flange/web separation in the unstiffened beam section below the top clip also occurred. Connection (d) is reported to have given a substantial improvement in both strength and rotational stiffness. In comparison with connection **TSW**, connection (d) gave a 196% increase in strength, and a 272% increase in initial stiffness. Connection (d) failed in shear at the adhesive bond between gusset plate and the Tee Flange. Fracture was sudden and provided an unsafe ultimate mode of failure.

The initial rotation stiffness, k_{ini} , final rotation stiffness, k_f , the ultimate moment capacity, M_{ult} , and the ultimate connection rotation, θ_{ult} , are given in **Table 3.2**

Table 3.2: Selected moment-rotation data (Bank et al., 1992).

Connections	k_{ini} kip-in/rad (kNm/mrad)	k_f kip-in/rad (kNm/mrad)	M_{ult} kip-in (kNm)	θ_{ult} rad (mrad)
(a)	6,993 (0.79)	333 (0.037)	55.0 (6.21)	0.0380 (38)
(b)	6,993 (0.79)	455 (0.051)	76.5 (8.64)	0.0590 (59)
(c)	9,091 (1.027)	617 (0.070)	114.6 (12.95)	0.0883 (88.8)
(d)	26,041 (2.942)	7,194 (0.812)	162.9 (18.41)	0.0200 (20)

The loading set-up used by Bank et al. (1990) subjected a beam to moment, shear and a parasitic compression loading. This provides not only the connection moment but also an equally increasing compressive force on the connection through the beam. This parasitic compression force may affect the behaviour of the connection. For this and other reasons, Bass and Mottram (1994) conducted five internal beam-to-column tests having flange cleated connections of a standard pultruded leg-angle section. They used the different test set-up as shown in **Figure 4.3**, and the purpose of this test programme was to observe the behaviour of connection and web cleated connection made of pultruded section and to find out if it was possible to have an acceptable semi-rigid connection.

The connection details and their specimen labels are shown in **Figure 3.8**. Note that the two minor-axis connection were novel; all previous tests had been with the column in the major-axis position.

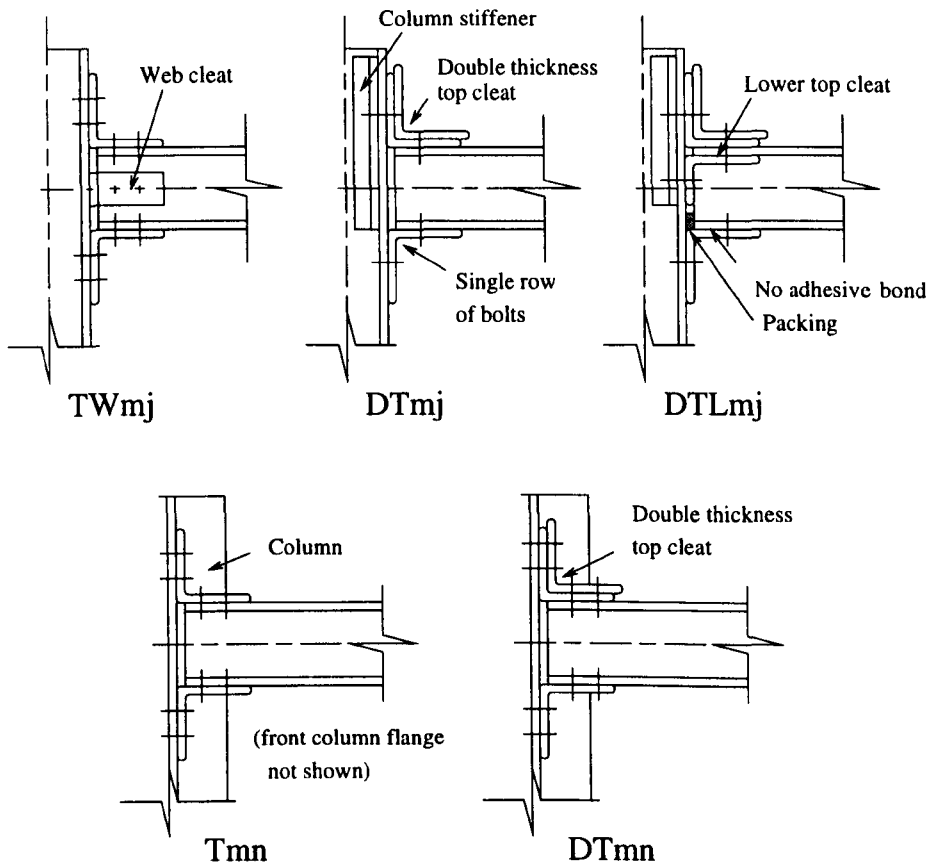


Figure 3.8: Connection details (Bass & Mottram, 1994).

Results from their **DTmj** and **DTmn** tests showed that minor-axis connection was stiffer than its equivalent major-axis connection, but that their ultimate strength was about the same. This difference in the $M - \phi$ behaviour clearly showed that with the major-axis connections considerable attention will be needed to design a connection that minimises the inherent flexibility of the column flanges. Such a problem is not present when the column is in the minor-axis orientation because the

web, when the connection is internal, and the two connections are equally loaded, acts as a 'rigid' boundary. From this series of tests, it was found that connection **DTLmj** was stiffer and stronger than the other two major connections and gave a similar $M - \phi$ behaviour to connection (d) in **Figure 3.7**. As with all tests for connections that were supposed to be semi-rigid the top cleat piece was the weak point. This weakness meant that the moment, when failure first became visible in the connection, was too low for the joint stiffness to be useful in semi-rigid design.

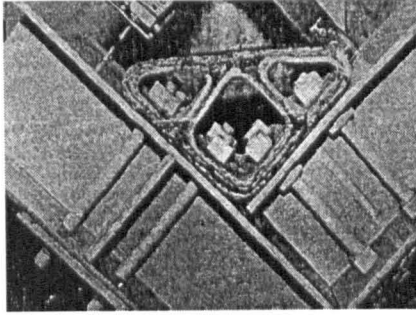
Bass and Mottram (1994) made the following recommendations using their data and those data of Bank.

Future research should concentrate on developing a cleat piece (ideally for all connection types) having suitable shape, reinforcement placement and cost to meet its needs.

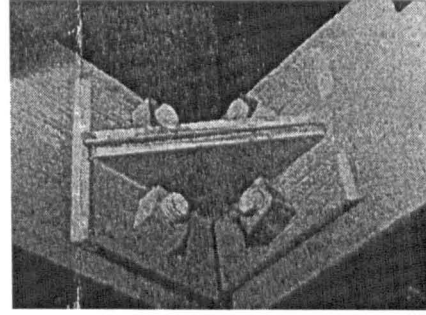
To optimize connections for semi-rigid action, studies are needed to be made on details such as; number of bolts, their position and type, effect of column stiffeners, jointing by bolting, bonding or a combination of both.

Independent to Bass and Mottram (1994), Bank et al. (1996) had implemented their recommendation and the four modified connections, shown in **Figure 3.9**, were tested. For connection (a) a moulded multi-cell 8 inch connection (**Figure 3.9 (a)**) was processed using three separate rigid polyurethane foam mandrels and combined to fabricate connection detail. In connection (b) a back-to-back wide flange 6 inch connection detail (**Figure 3.9 (b)**) was constructed by taking two pieces of 6 inch wide flange section cut at 45° (to the beam axis) and bonding to form a right-angled "brace". For connection (c) the back-to-back wide flange 8 inch connection detail (**Figure 3.9 (c)**) was of the same type as in the connection (b) but was instead fabricated from two sections cut from 8 inch wide flange beams. Finally connection

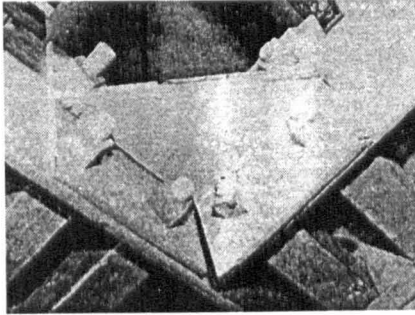
(d) had a 6x1/2 inch wrapped angle connection (**Figure 3.9** (d)). This innovation connection piece was developed by wrapping a standard 6x1/2 inch pultruded vinylester angle with two layers of Fabmat 2415.



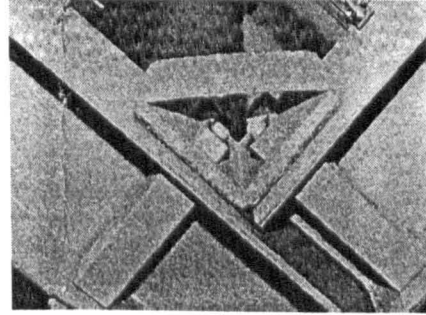
(a) Molded multicell 8 inch connection.



(b) Back-to-back wide-flange 6 inch connection.



(c) Back-to-back wide-flange 8 inch connection.



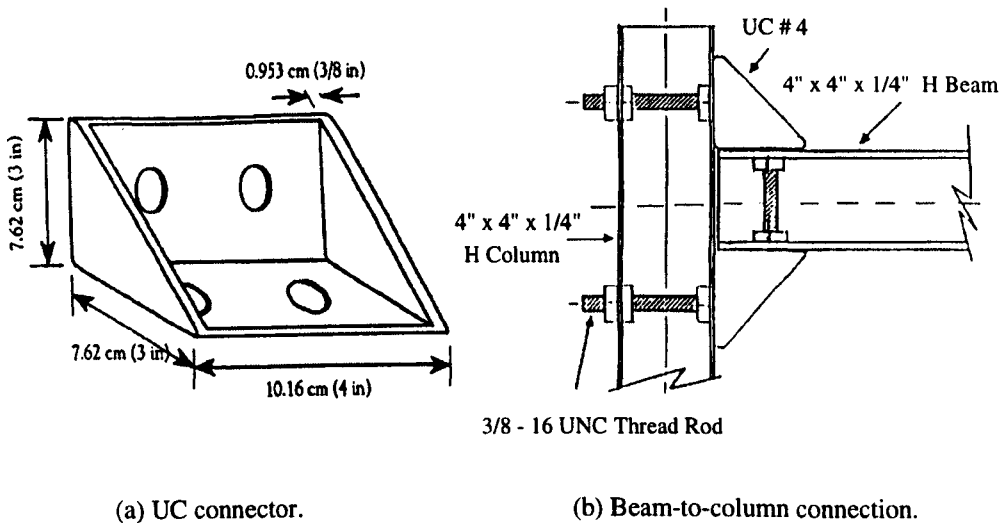
(d) 6 x 1/2 wrapped angle connection.

Figure 3.9: The beam-to-column connections (Bank et al., 1996).

Results from the four new connection tests showed that the failure moment for connection (a) was much higher than the other three connections. It was 270 kip-in (30 kNm). Connection failed by thread stripping of pultruded rods in the top brace of the connection.

From evaluation of available information of experimental connection test programmes, Mosallam (1994) developed his universal connector (UC) (**Figure 3.10** (a)). This novel cleat piece presented a positive step in the development of practical

FRP structural connections (Mosallam, et al., 1994 a, 1994 b). The UC connection has the conventional leg-angle shape of pultruded and steel standard cleats, but with side ribs to substantially increase its stiffness and strength. Mosallam (1994) shows that the UC connector can be used to develop connection design details for all possible types of frame connection.



(a) UC connector.

(b) Beam-to-column connection.

Figure 3.10: Mosallam's universal connector and beam-to-column connection (Mosallam et al., 1994 a).

To demonstrate the structural performance of the UC connector, an external joint fabricated from two UC connectors and two 4x4x1/4 inch PFRP E glass/vinyl ester H-sections was tested. The connection detail is given in (**Figure 3.10** (b)).

The results of the single test showed that significant improvement in both the strength and the stiffness of the connection was achieved. The failure of the connection was gradual and was in a form of punching shear by the nuts at the column-side. Hair line cracks had developed in the left diagonal stiffener of the UC connector (**Figure 3.11**), and their presence suggests to the author that the Mossallam's UC connector is not ideal for its intended application.

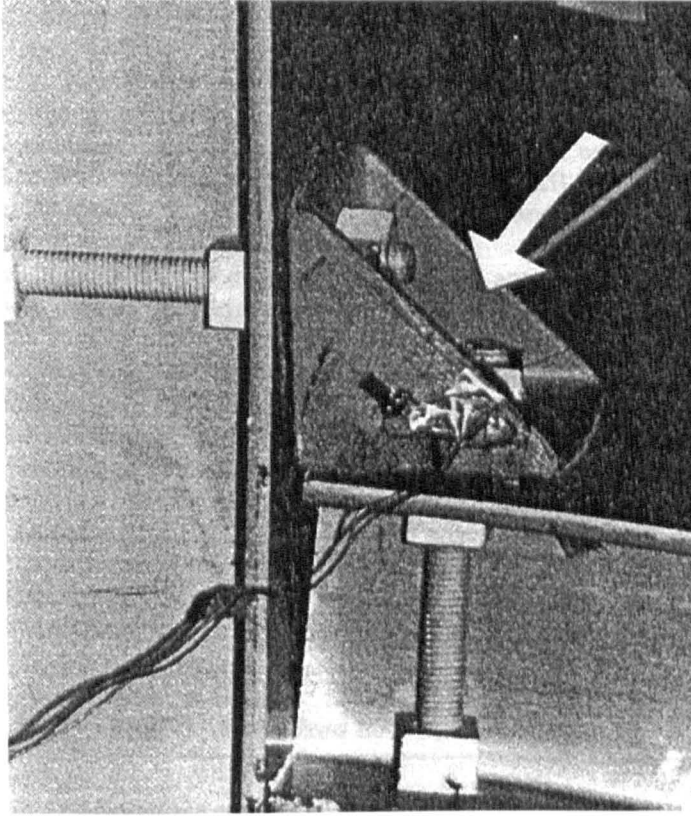


Figure 3.11: The diagonal cracks in the UC connector.

Unfortunately, it is impossible to compare properties of Mosallam's 4-inch UC connection with others in this review, because all other connections were fabricated from different sizes of beam and column members (Mottram and Zheng, 1996 b).

A final series beam-to-column tests was conducted by Turvey and Cooper (1996 a, 1996 b). Their tests involved conventional and unconventional connection tests. The conventional connections were bolted web or web and flange cleated connections, and their novel unconventional connection was four bolted cruciform web plates connection shown in **Figure 3.12**. In order to establish the initial connection stiffness, their tests were conducted at low load.

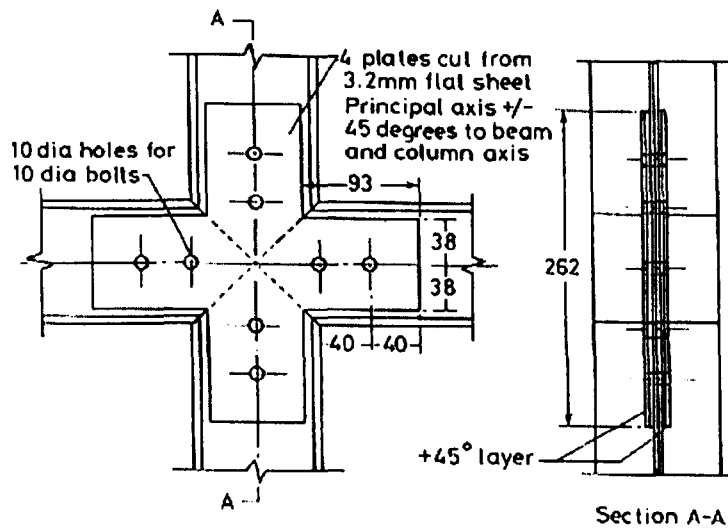


Figure 3.12: The cruciform plate connection (Turvey and Cooper, 1996 a, 1996 b).

3.4 Study of Pultruded Frames

There are few FRP frame tests found in this literature survey and those that have been reported are all for portal frames. The first pultruded FRP portal frame tests were carried out by Mosallam (1990). He conducted two frame tests; the first was on a portal frame subjected to short-term static loads (Mosallam and Bank, 1992) and the second was the frame subjected to a sustained load, approximately one quarter of the frame initial failure load, for 10,000 hours (Mosallam and Bank, 1991). Both frames were loaded symmetrically at third points along the beam.

The results of "short-term" tests showed that serviceability and ultimate failure of a frame was dominated by performance of the beam-to-column connections, local buckling and eventual failure of the compression flange of the beam. It was observed that 'the stiffness and strength of the web-flange intersection of the pultruded FRP WF section have been identified as having a major influence on the beam-to-column stiffness of the frame, and the critical buckling load and postbuckling stiffness of the

section' (Mosallam and Bank, 1992).

The results of long-term loading showed that a significant portion of creep occurred during the first 2000 hours. After this duration the rate of creep became almost constant. The short-term mid-span deflection had increased by 12.8%, after 3500 hours, from 7.13 mm to 8.04 mm (Bank and Mosallam, 1990).

A computer code of frame analysis, which included of the effects of both shear deformation and of connection flexibility, was used to predict the deformation of frames and the results agreed well with the experimental data (Mosallam and Bank, 1992).

Turvey (1996) conducted a portal frame test and his frame is shown in **Figure 3.13**. It was fabricated from 8x8x3/8 inch WF pultruded sections of EXTREN 500 Series. The beam and two columns were 2540 mm and 2286 mm respectively. The beam was connected at its end to the column in major axis. The beam-to-column connections were web cleated connections recommended by MMFG (1989) and the cleats (76x76x9.5 mm) were cut from 6x6x3/8 inch pultruded equal leg angle. The connections were bolted only and they were tightened to a torque of 100 Nm. The columns were supported by pinned connections. The geometry of portal frame was identical to that of Mosallam's 'short-term' frame, but the beam-to-column and column base connections were different. Instead of loading at third point of the beam, the frame was loaded with a concentrated load at the mid-span.

The frame was tested under a low load flexural mode, a low load sway mode, and an ultimate load flexural mode. In the latter loading situation the frame failed when the load reached about 40 kN and the mid-span deflection was about 20 mm (this was about 1.5 times of the deflection serviceability requirement (span/200)). Instead of the expected mode of failure being in a beam-to-column connection itself, flexural tension cracking failure of the beam flange occurred in the vicinity of the point load. Frame analysis was also performed, but all of the models grossly underestimated

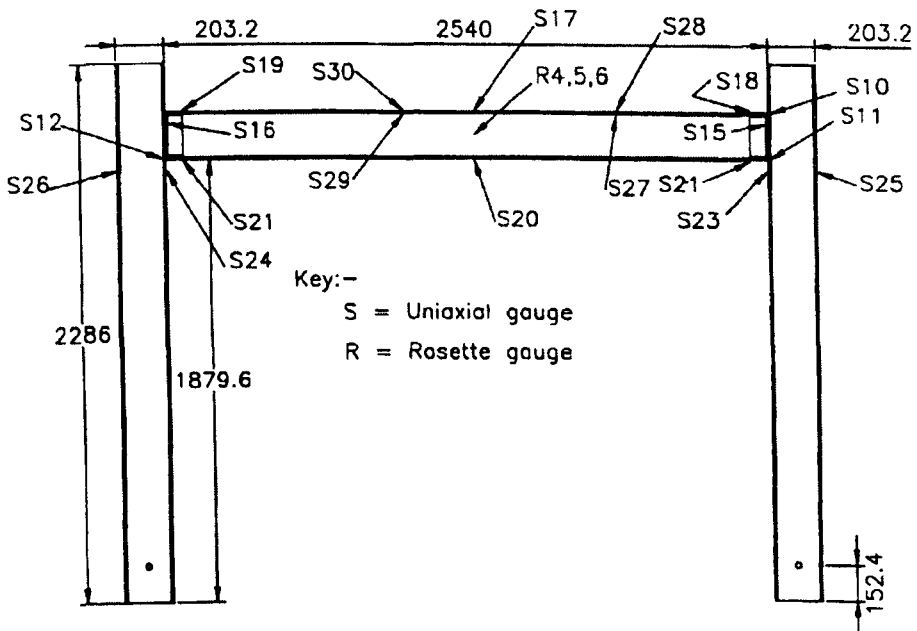


Figure 3.13: Pultruded GRP frame layout (Turvey, 1996).

the sway mode deflection at the top of the columns, and all but one underestimated the flexural mode beam mid-span deflection.

3.5 Summary

The survey of literature has shown that:

- Our understanding of the behaviour and design of plate-to-plate joint has benefited from previous research for application of such joints in other engineering industries.
- Testing of plate-to-plate joint of pultruded material has been made by a number of researchers and their results are of limited value because there is a lack of standardization.

-
- The pinned beam-to-column connections recommended by manufacturers have received little attention and the only significant research on such connections was carried out by Mottram (1994): Test results for the small number of pinned connections has shown that they may perform satisfactorily.
 - The development of semi-rigid beam-to-column connections has been studied by a small number of researchers: Although a few models of such connections have been developed from their research, and the moment-rotation behaviour of these connections has been significantly improved, there is still no one design that can satisfy all the aspects of semi-rigid frame design.
 - The shear deformation of FRP pultruded sections needs to be counted in pultruded frame analysis.

Chapter 4

Experimental Investigation on Pinned Beam-to-column Connections

4.1 Introduction

As standard pultruded members resemble their steel counterparts in appearance, it has been the practice to use knowledge available from the behaviour of steelwork. Due to the difference of the material properties, structural engineers need to know the behaviour of both frame members and the connections between frame members. The research and analysis of standard pultruded structural members has been discussed by Bank (1989 a, 1989 b, 1989 c), Mottram (1991) and Turvey (1996). The analysis and design of connections for pultruded frame structures has received little attention, although connection design is often the most critical aspect of the design process. This experimental investigation is a continuation of the research on the nominally pinned connections undertaken by Mottram (1994), which is detailed

in chapter 3.

For current design of pultruded frames, the connections as given in MMFG (1989), mimic those in steel practice with web cleats, and are assumed to behave as a nominally pinned connection. Due to the differences in material properties between FRP and steel, one can expect that a similar form of the connection will perform differently, and until experimental evidence is available copying steel practice cannot reliably be stated to result in a safe connection behaviour, and thereby safe frame behaviour.

Frames of pultruded section have members connected by web cleats using bolting on its own or combined with adhesive bonding. Bolting is the main connection method used because it has been shown that the bonding strength for pultruded frames is much weaker than welding strength for steel work; this is mainly due to the material properties of pultruded members.

The experimental investigation involved three web cleat connections and they are assumed as pinned connections in the frame design. The aim of this experimental investigation is to examine the behaviour of the MMFG's web cleated connection on 10x10x1/2 inch wide flange members and to study aspects of the behaviour not yet answered by previous research (Mottram, 1994).

For this purpose, a cruciform plane frame subassembly was tested. It consisted of a column and two back-to-back cantilever beams connected by web cleat connections cut from 6x6x1/2 inch (152.4x152.4x12.7 mm) equal-leg angle (see **Figure 4.7**). The column and beams are made from wide flange (WF) pultruded FRP shape. The WF sections used for the column and beam in the tests were 10x10x1/2 inch (254x254x12.7 mm) EXTREN 525 series standard pultruded fibreglass structural shapes.

4.2 Description of Connection Specimens

A description of the tests and the labelling system used herein follows that used by Mottram (1994) and is presented in **Table 4.1**. For example, label **Wmj10_bt+bd** defines connection to be **W**eb cleated with **m**ajor-axis column, **10**x10x1/2 inch WF beam and column members, and jointing by combined **b**olting and **b**onding.

Table 4.1: Summary of connection specimens.

Label	Connection details	Column axis	Jointing
Wmj10_bt	Web cleats	major	bolting
Wmj10_bt+bd	Web cleats	major	bolting + bonding
Wmn10_bt	Web cleats	minor	bolting

4.2.1 Connection Wmj10_bt

Connection **Wmj10_bt** shown in **Figure 4.1** consisted of web cleats which were positioned on the central line of the beam web and were connected to the column flange. Further details of the connection and the subassembly of the frame are given in figures in **Appendix A**.

This major-axis connection was basically the same as the connection recommended in the MMFG's Design Manual (MMFG, 1989), but two modifications were made to ease the buildability. First, a 10 mm end clearance between the beam-end and column flange was adopted in which 5 mm is for clearance and 5 mm is for tolerance. This conformed with the latest edition of MMFG design manual (new engineering drawings, 1995) that followed the EUROCOMP testing by Mottram (1996). Second, the bolt hole was slightly moved off from the centre line of cleat

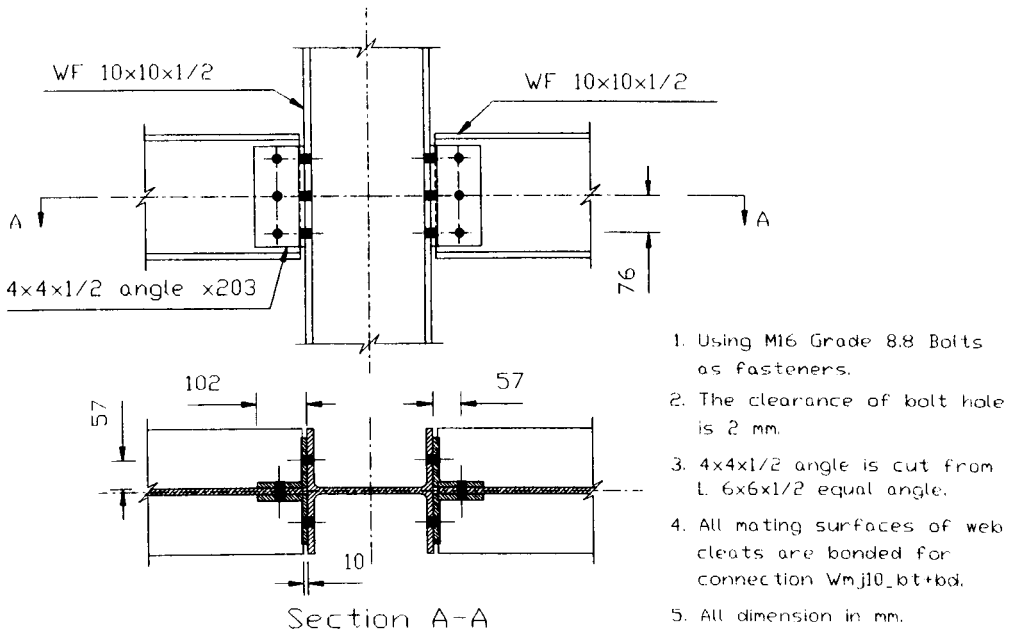


Figure 4.1: Configuration of connections **Wmj10_bt** and **Wmj10_bt+bd**.

leg. In MMFG's Design Manual (MMFG, 1989), combination of mechanical fasteners with adhesive applied to the mating surfaces is recommended. For practical reasons, bolting only was also investigated here. All mechanical fasteners used were M16 grade 8.8 steel bolts with 30 mm diameter standard size washers. The bolts were tightened to a torque of 100 N m, instead of 23.8 N m used in the 8 inch section connection tests (Mottram, 1994). This higher torque was used by Turvey (1996) in a pinned connected rectangular portal frame test and there was no slip and no material damage reported. The bolt hole clearance is 2 mm, with which the effect on the ultimate load of the connection is about 2% according to Yuan and Liu (1996) (see **Figure 3.3**).

4.2.2 Connection Wmj10_bt+bd

Connection **Wmj10_bt+bd** was identical to connection **Wmj10_bt** (see **Figure 4.1**), except that the method of connecting was combined mechanical fastening and adhesive bonding. All the mating surfaces of the cleats and beam and column members were adhesively bonded. Lengths of copper wire at 0.25 mm diameter were laid on the prepared mating surface after adhesive was applied to obtain a minimum bond thickness of 0.25 mm. The adhesive system used was Araldite 2015. The method of bonding follows that described by Bass (1994).

Details of the connection and the subassembly of the frame are given in figures in **Appendix A**.

4.2.3 Connection Wmn10_bt

For this connection, the web cleats connected the beam web to the column web for a minor-axis connection. Due to a limitation on working space between flange outstands, the length of legs of the web cleats connected to the column web were shorter than the legs connected to the beam web. The end clearance employed was 10 mm and only mechanical fasteners were used in this connection.

Figure 4.2 shows fabrication of connection **Wmn10_bt**. Further details of the connection and the subassembly of the frame are given in figures in **Appendix A**.

4.3 Material Specification and Connection Details

Pieces for the web cleats were cut from 6x6x1/2 inch (152.4x152.4x12.7 mm) equal-leg angle of the MMFG EXTREN 525 series (MMFG, 1989). Column and beam

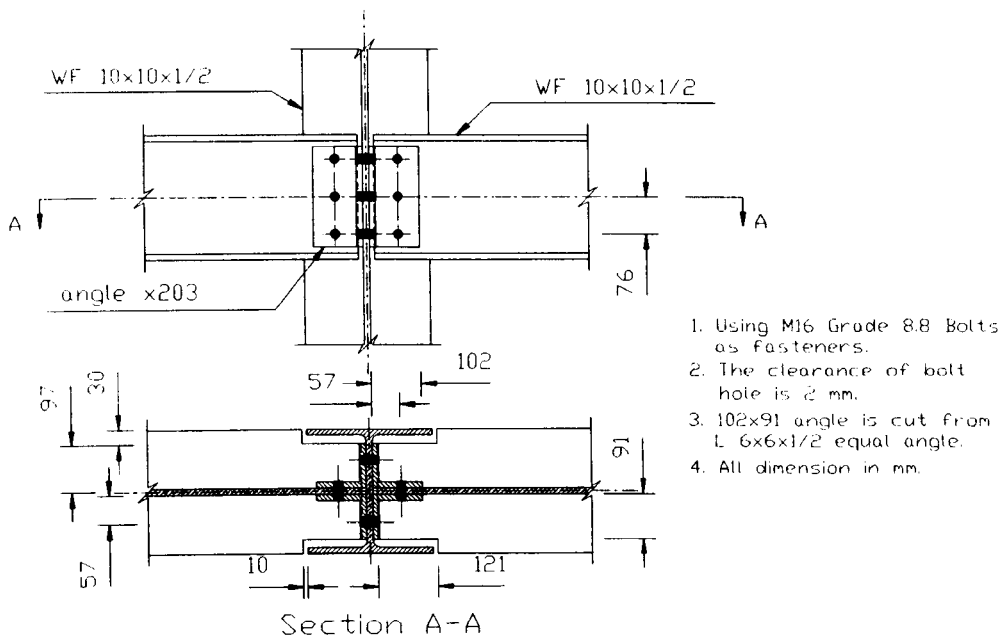


Figure 4.2: Configuration of connection **Wmn10.bt**.

members were 10x10x1/2 inch (254x254x12.7 mm) WF members, and were fabricated from standard **Pultex** fibreglass structural shapes manufactured by Creative Pultrusions. The physical properties of fibreglass-reinforced structural shapes given by MMFG (1989) and Creative Pultrusions (1988) are listed in **Table 4.2**.

All connections had mechanical fastening by M16 grade 8.8 steel bolts. The material physical properties of the bolts used in the connections tested here, given by BS 5950, are listed in **Table 4.3**.

The adhesive system used was Araldite 2015.

Table 4.2: Physical properties of fibreglass-reinforced shape.

Property	MMFG	Creative Pultrusions
Bearing Strength, LW	206.8 N/mm ²	
Tensile Strength, LW	206.8 N/mm ²	206.8 N/mm ²
Compressive Strength, CW	103.4 N/mm ²	103.4 N/mm ²
Tensile Modulus, LW	17.2 kN/mm ²	17.2 kN/mm ²
Compressive Modulus, LW	17.2 kN/mm ²	17.2 kN/mm ²

Note: LW — LengthWise, CW — CrossWise.

Table 4.3: Strength of bolt in clearance hole (BS 5950).

Property	grade 4.6	grade 8.8
Shear Strength, P_s	160 N/mm ²	375 N/mm ²
Bearing Strength, P_{bb}	460 N/mm ²	1035 N/mm ²
Tensile Strength, P_t	195 N/mm ²	450 N/mm ²

4.4 Test Method

4.4.1 Test Equipment and Loading Set-up

The loading equipment used for the connection tests are tensile manual hydraulic jacks. The measurement of rotation, displacement and load was achieved by using electronic transducers: Lucas Accustar Electronic Clinometer, displacement transducer and tension load cell, respectively. The data were recorded using an ORION delta (3531D) data acquisition system and personal computer.

The rotation transducer, clinometer, were linear over a range of 10 ± 1 degrees with a resolution of 0.12 mrad. Two ranges of the displacement transducers were 50 mm and 100 mm and the capacity of the tension load cells were 20 kN.

The test configuration of the frame adopted in the tests were central column supporting two nominally identical cantilevers in major and minor axis orientations respectively. This is shown in **Figure 4.3**. This testing was used by Bass and Mottram (1994).

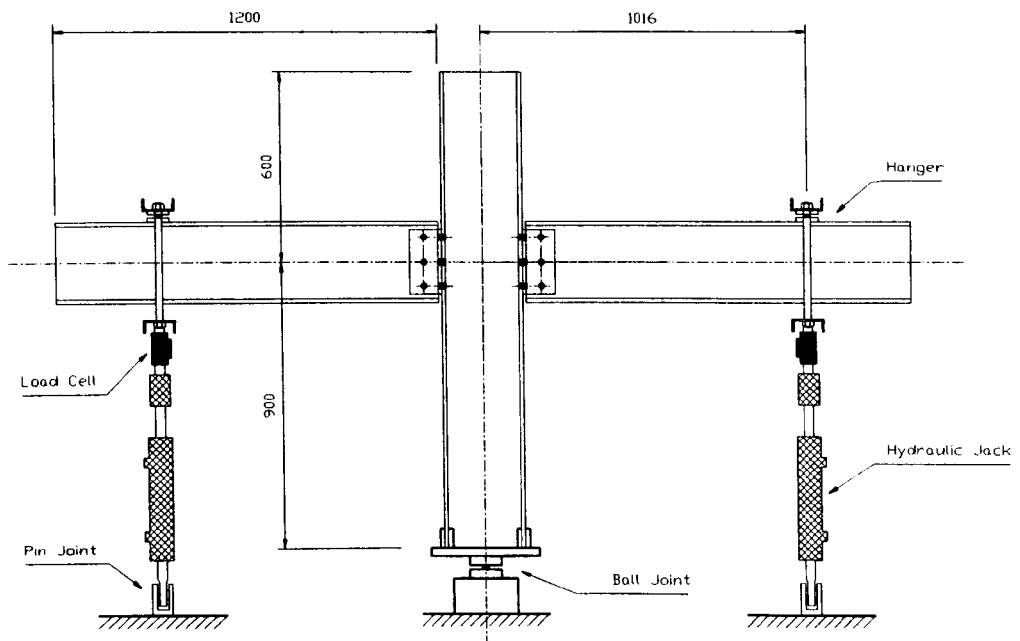


Figure 4.3: Test arrangement and loading set-up.

The cantilevers and column were 1.2 m and 1.5 m in length, respectively. The beams were fixed to the column at a height of 0.9 m. Both beams were loaded at a position 1.016 m from the centre of the column, which gave the ratio of loading arm to beam depth of 4.

With this loading arrangement, the connections will be subjected to an in-plane moment and shear. The column member was seated on a base plate support with central ball joint regard as a pinned connection, the column will not be subjected to in-plane bending action and both side connections will be subjected to the same

bending moment (assuming that the column remains in vertical position).

4.4.2 Test Measurement and Data Processing

The arrangement of the transducers which were used to measure displacement and rotation in the tests is shown in **Appendix A**, drawing No. 003. The various arrangements of the transducers on the three subassembly test frames are also shown in photographs in **Figures 4.7, 4.10 and 4.14**. The measurement of the rotations was achieved by using five clinometers which are labelled as C1 to C5 from left to right. The rotation of cantilevers at a loading point was measured by clinometers C1 and C5. The beam end rotation of the cantilevers was measured by clinometers C2 and C4, a distance of 130 mm from the end of beam nearest the column. The rotation of the column was measured at the centre of the column web for major-axis tests and from the column flange for minor-axis test.

The vertical deflection of the cantilevers was measured directly above each load point by 100 mm displacement transducers (HS 100), these are labelled transducers L1 and L2. The relative horizontal slip of the cantilevers and web cleats was measured by 50 mm displacement transducers (HS 50) at the levels of the top and bottom bolt centres, which are labelled transducers LTL, LBL, LTR and LBR, respectively. The vertical slip of the end of the cantilevers was measured by 25 mm transducers (HS 25) underneath the cantilevers, a distance of 20 mm from the column face.

All transducers were connected to the data logger (data acquisition system), from which the data were recorded during the tests and sent to the computer for data processing.

Short-term data was obtained immediately after the application of each loading increment, or of stroke, and after a time lapse of 5 to 10 minutes.

To calculate the connection rotation, the relative rotation of the column and a

beam was obtained from the difference of column rotation and beam-end rotation as measured by clinometers C2, C3 and C4. This rotation difference was taken to represent the connection rotation, if there was no slip between beam and web cleat. In the event that slip occurred the relative rotation of the column and beam was deducted from the rotation due to slip, to obtain the true connection rotation.

Rotation due to slip was calculated from the geometry and the slip displacements measured by the displacement transducers. **Figure 4.4** shows the web cleat connection with a slip rotation r . LTR and LBR are **Top Right** and **Bottom Right** displacement transducers. They are fixed to the beam web in such a way that in the test they remain parallel. The distance between a pair of the two LSC displacement transducers is represented by l . If the slip at the top transducer is represented by la and at bottom transducer is represented by lb , the rotation r from connection slippage is given by

$$r = \arctan\left(\frac{la + lb}{l}\right). \quad (4.1)$$

The moment that a connection transmitted was determined by multiplying the load by the distance between the loading point and the centre of the column. The distance used was 1.016 m and it was assumed that as a beam deforms the loading remains vertical and at a constant distance from the centre of the column.

4.4.3 Methods of Testing

Frames were loaded in increments of connection moment until the connection behaviour became nonlinear; the control was then transferred to connection rotation ϕ . At a rotation above 12.5 mrad, a first unloading and reloading cycle was applied to the specimen, and there afterwards, additional cycles of the unloading and reloading procedure were performed in each test. The purpose of this procedure was to determine the extent of permanent deformation and change in connection stiffness.

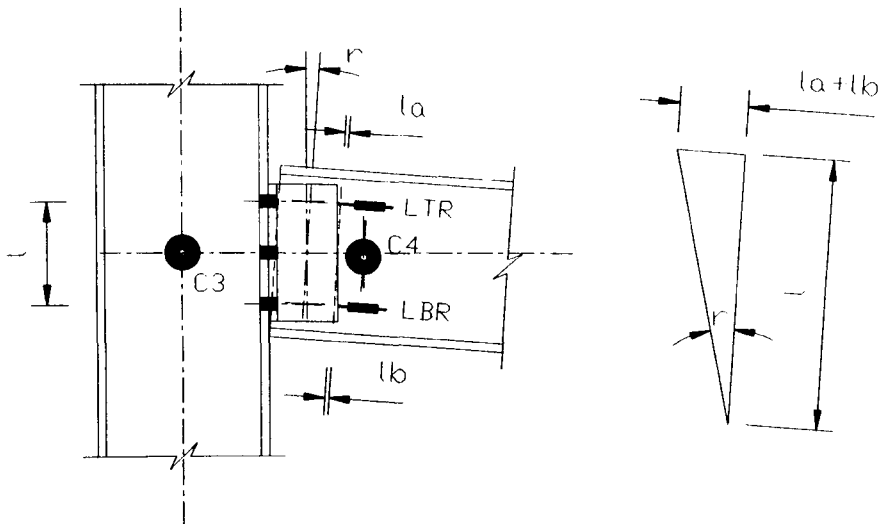


Figure 4.4: The rotation due to slipping.

A time interval of 5 to 10 minutes elapsed between each load increment to carry out visual inspection for any failure and to take measurements from the transducers detailed above. All data were recorded immediately after an increment was applied and again just before the next one was applied. After the ultimate moment had been reached, each connection was taken to either ultimate failure or until rotation was excessive. Test duration was between 1 and 3 hours.

4.5 Descriptions of Tests

4.5.1 Test of Connection Wmj10_bt

The moment-rotation behaviour of connection Wmj10_bt for both left and right side web cleated connections is plotted in Figure 4.5, in which both data taken immediately after the application of the each loading increment and after a time lapse of 5 to 10 minutes are represented. The reduction in moment can be observed

after the time lapse. The higher the value of moment, the larger the decrease gets.

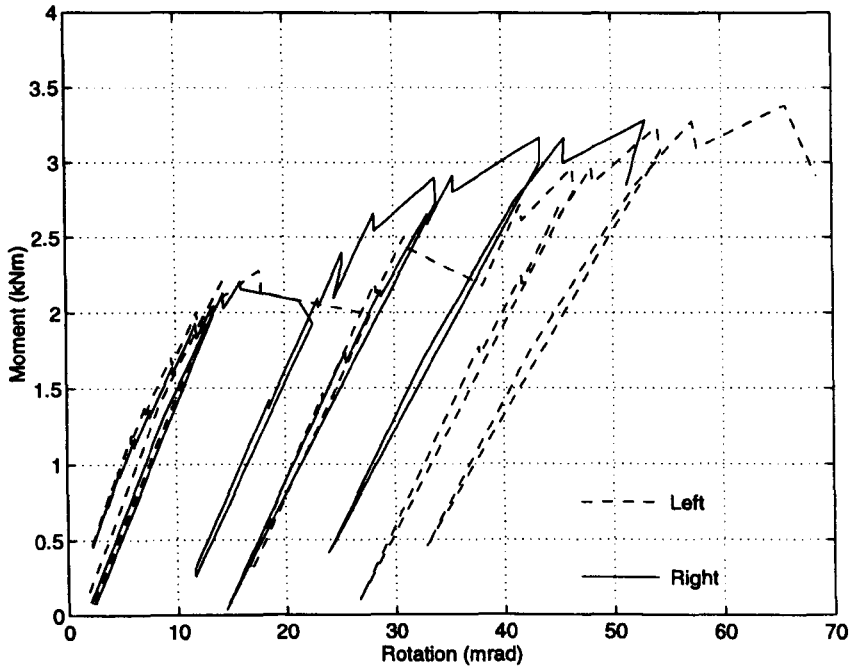


Figure 4.5: Moment-rotation curves of **Wmj10_bt**.

During the test prying action at the web cleats was observed. The opening-up between the top of the web cleats and column flanges gradually developed as the deformation gradually increased.

First connection slippage occurred in both connections when the loading was about 2.2 kNm and rotation was about 14 mrad. The resulting increase in rotation can be seen in **Figure 4.5**. Further slipping occurred as the load increased.

Figure 4.6 shows the connection moment rotation behaviour of left and right connections of connection **Wmj10_bt** by removing the rotation due to slippage using the method described in **Section 4.4.2**

The moment-rotation behaviour for connection **Wmj10_bt** was nonlinear when moment was greater than 0.5 kNm. The part of the nonlinear rotation of the

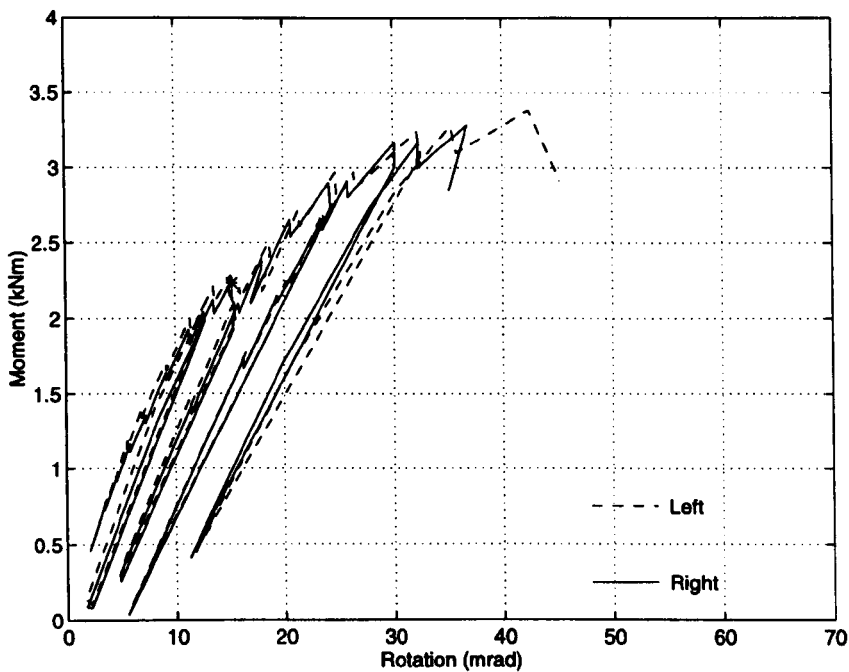


Figure 4.6: Moment-rotation curves of **Wmj10_bt** (without slip).

connections was unrecoverable in this short-term test and this can be seen from the unloading and reloading curves. This aspect of connection behaviour will be discussed further in **Section 4.6**

From the unloading curves in **Figure 4.6**, it can be seen that the permanent connection rotation increased with the increase of the maximum rotation that the connection experienced. Unloading at about 30 mrad gave a permanent rotation of about 10 mrad in both left and right connections.

The reloading curves were linear and were virtually parallel to the unloading curves. The reloading connection stiffness was the same as its initial value showing that the nonlinear rotation part of the rotation was permanent.

Splitting cracks, at the top of web cleats in connections **Wmj10_bt** were detected visually between the layers in the pultruded material when the moment exceeded

2.2 kNm and the connection rotation was about 14 mrad.

As the connection rotation was further increased up to 36 mrad (right) and 42 mrad (left), the left connection failed by gross splitting and ‘tearing’ at the top of the web cleats, and by gross material fracturing across the top leg section of the web cleat, level with the bolt position on the top of the left web cleats. The left connection failed completely and no further moment could be carried. **Figure 4.7** shows the deformation of connection **Wmj10_bt** at failure, and **Figure 4.8** shows the visible details of the ultimate failure of the left side web cleat connection. The right connection did not fail completely; there were extensive splitting cracks at the top of the web cleats.

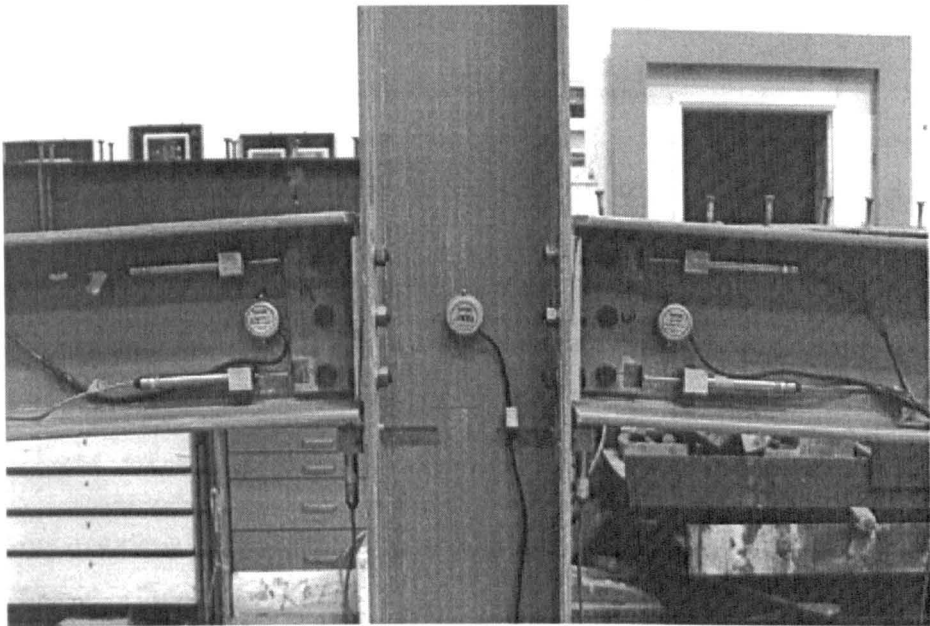


Figure 4.7: The deformation of connection **Wmj10_bt** at failure.

There was no significant deformation of the column flanges (see **Figure 4.7**), such that the bowing deformation seen with an 8 inch WF column (Bass and Mottram, 1994; Mottram, 1994) was significantly reduced when the larger section col-

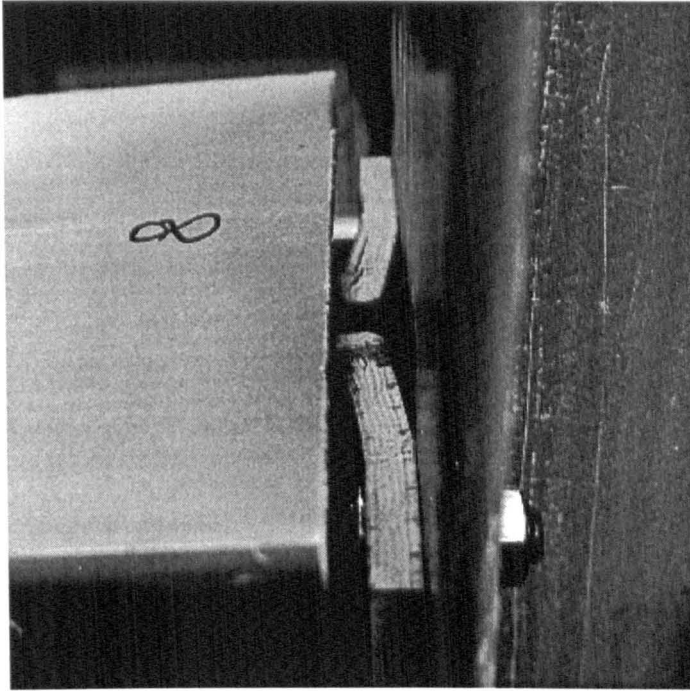


Figure 4.8: Ultimate failure mode of left side connection of test **Wmj10_bt**.

umn was used. This change in joint deformation is attributed to the flange thickness increasing from 9.53 to 12.7 mm; thereby increasing the bending stiffness.

4.5.2 Test of Connection **Wmj10_bt+bd**

The moment-rotation behaviour of connections **Wmj10_bt+bd** is presented in **Figure 4.9**. Due to the adhesive bond applied to the mating surfaces, no slip occurred, hence the measured moment and rotation shown in **Figure 4.9** give the true $M - \phi$ response.

The moment-rotation behaviour of connections **Wmj10_bt+bd** went nonlinear when the moment was greater than 1.5 kNm.

Debonding at the interface of web cleats and column flange started when the

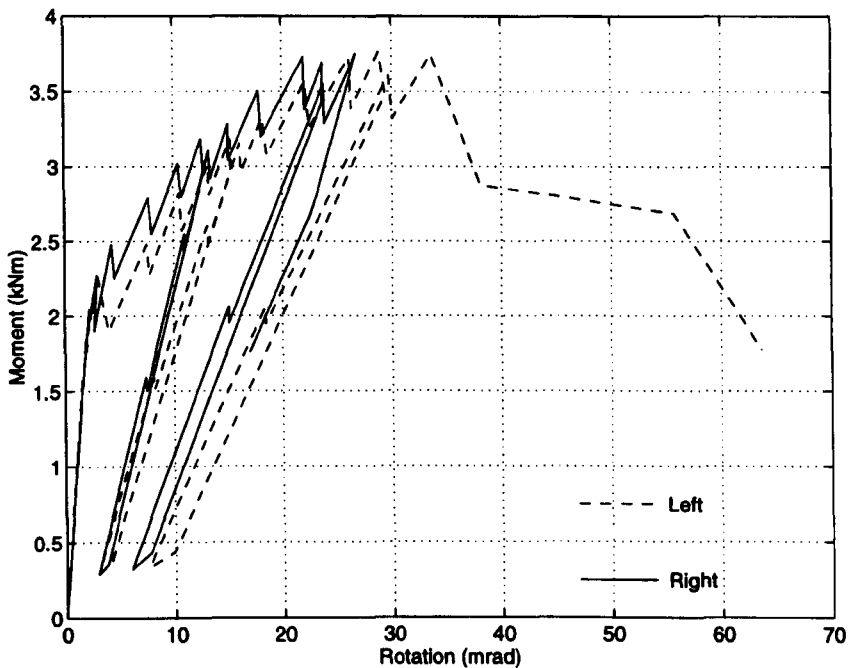


Figure 4.9: Moment-rotation curves of **Wmj10_bt+bd**.

moment exceeded 2.48 kNm (immediately after the loading increment) and was signalled by acoustic emission. After this loading, the connections were inspected and it was found that the debonding on the interface of the cleats and the column on both sides occurred. The moment and the rotation recorded for both sides were 2.81 kNm and 10.44 mrad for the left side connection and 2.82 kNm and 7.58 mrad for the right side connection, respectively. More important to the connection behaviour is the significant increase in rotation ϕ , and gradual decrease in the stiffness, after debonding was seen to have started.

A reloading curve was linear and it virtually followed the unloading one. The reloading connection stiffness was lower than its initial value and gradually decreased with the development of debonding failure. Finally, the reloading connection stiffness stabilized and the final reloading connection stiffness was virtually the same as

found in the test of connection **Wmj10_bt**.

Connection **Wmj10_bt+bd** gave the same value of permanent connection rotation as for connection **Wmj10_bt** when the same maximum rotation was experienced (see **Figures 4.6** and **4.9**). This observation suggests that the debonding under prying action had been fully developed and the remaining adhesive bonding was having no effect on the connection stiffness. Once the debond failure had fully developed the connection was equivalent to that when connection is by mechanical fastening and slip is ignored.

A barely visible surface crack at the fillet on the top of the right web cleat was detected before the test started and this crack developed during the test. The splitting cracks at the top of the web cleats on both connections developed from the start of the loading.

The connection's ultimate mode of failure was similar to that of connection **Wmj10_bt**. The left connection failed by gross splitting and 'tearing' at the top of the web cleats, and severe cracking across the section at the bolt position on the top of the left web cleats. The left connection failed when the moment exceeded 3.74 kNm and the rotation was greater than 33.5 mrad. No further moment load could be carried. The right connection did not fail completely, but there were severe splitting cracks at the top of the web cleats.

Figure 4.10 shows the deformation of connection **Wmj10_bt+bd** after failure and **Figure 4.11** shows the visible details of ultimate failure on left side.

4.5.3 Test of Connection **Wmn10_bt**

The moment rotation behaviour of connection **Wmn10_bt** is presented in **Figure 4.12**.

First slippage occurred on the right side when the moment exceeded 1.75 kNm,

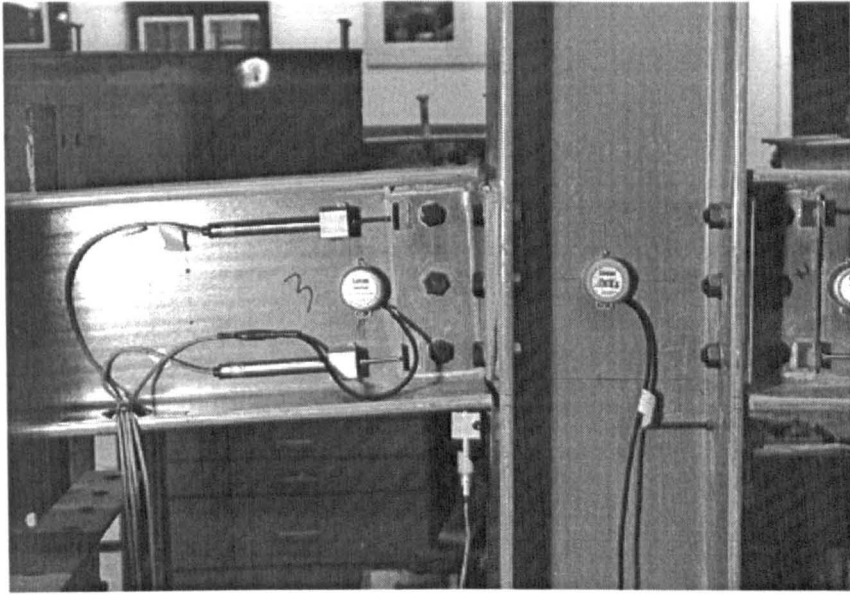


Figure 4.10: The deformation of connection **Wmj10_bt+bd** at failure.

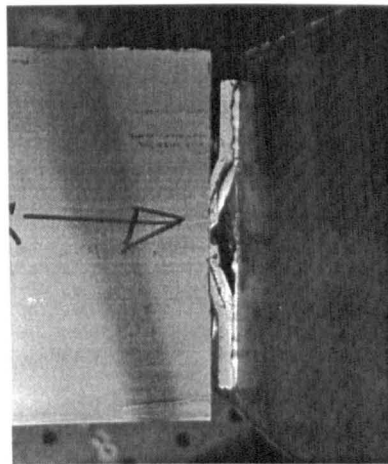


Figure 4.11: Ultimate failure mode of left side connection of test **Wmj10_bt+bd**.

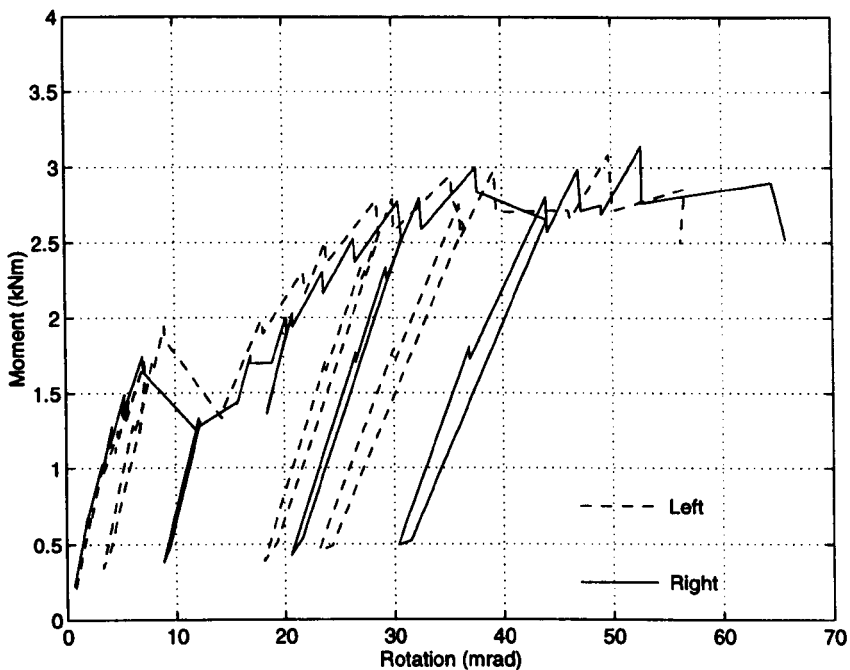


Figure 4.12: Moment-rotation curves of **Wmn10_bt**.

and was accompanied by a loud bang. Throughout the rest of the test there was slippage after each load increment. The same response was observed for the left side connection when the moment exceeded 1.95 kNm.

Figure 4.13 shows the moment-rotation behaviour after compensation for the rotation due to slip. Unloading at about 20 mrad gave a permanent rotation of about 8 mrad in both left and right connections.

At failure, the delamination damage (due to the poor through-thickness strength) between laminae on both side web cleats was well developed. Material fracturing in the right side cleats, at the bolt position, was observed when the rotation was greater than 40 mrad (20 mrad of connection rotation without slip). The ultimate moment was 3 kNm.

Figure 4.14 shows the deformation of specimen **Wmn10_bt** at failure and

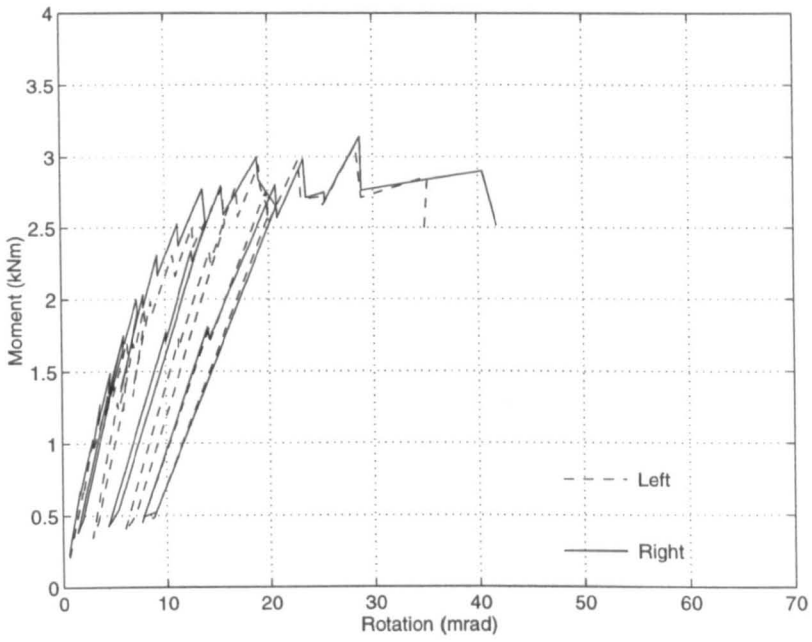


Figure 4.13: Moment-rotation curves of **Wmn10_bt** (without slip).

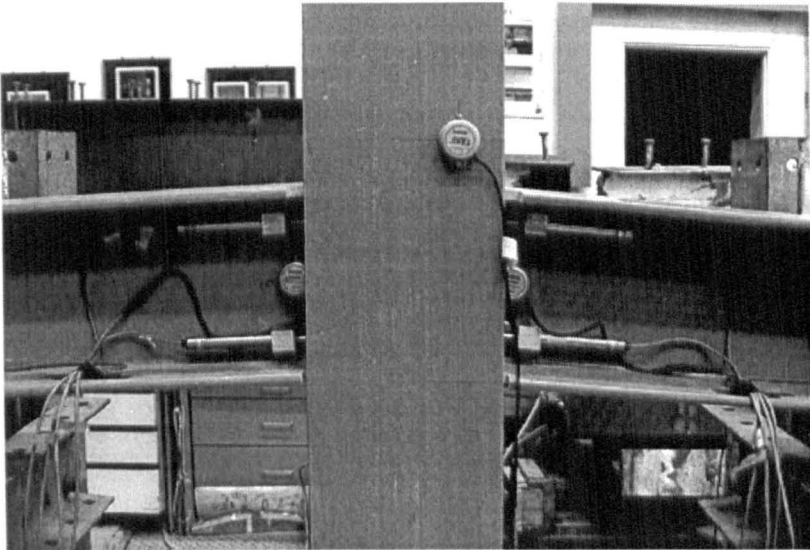


Figure 4.14: The deformation of connection **Wmn10_bt** at failure.

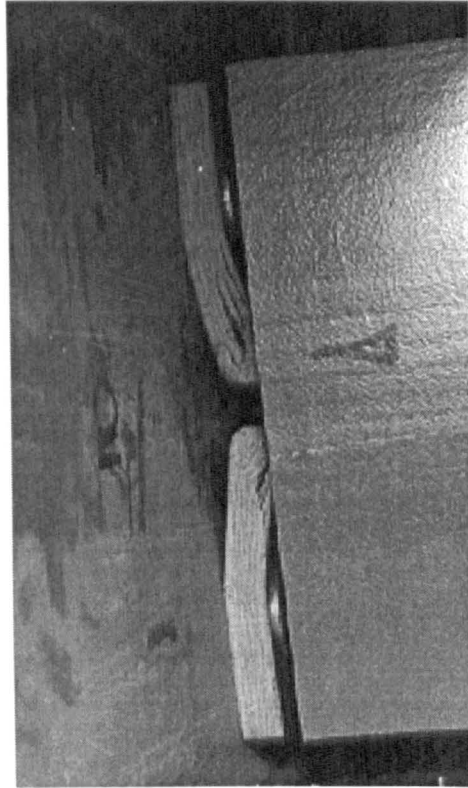


Figure 4.15: Ultimate failure mode of right side connection of test **Wmn10_bt**.

Figure 4.15 shows details of the ultimate failure of right side.

4.6 Discussion and Analysis of the Test Results

The three web cleated connections tested here had the same failure mode of delamination cracks at the top of web cleat. This was due to the prying action, inherent with web cleated connection. Their moment-rotation behaviour was nonlinear. **Figure 4.16** shows the linear piece-wise moment-rotation curves for these three web cleated connections. Each curve is the mean values of the left and right connections taken after a time lapse of 5 to 10 minutes and the slip effects on the rotation

have been removed. The data of these piece-wise moment-rotation curves are given in **Table 4.4**. These data are available for input to numerical analysis of frame behaviour.

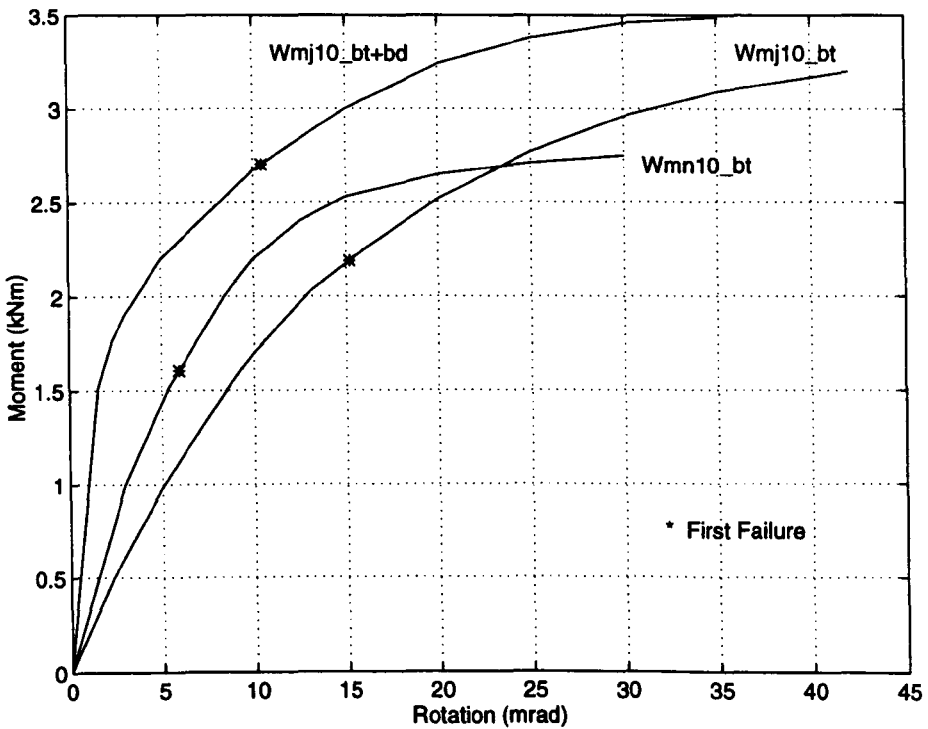


Figure 4.16: Piece-wise moment-rotation curves.

The $M - \phi$ curves of the three connection tests consist of two phases. The first phase is the initial elastic deformation phase, and the second phase is the nonlinear elastic material damage phase. Since pultruded FRP has elastic material properties, there is no viscoelastic deformation in the short-term test. For a bolted connection, as the reloading stiffness of the connection is the same as initial connection stiffness this nonlinear phase of the curve can actually be treated as linear elastic deformation plus permanent deformation (the connection rotation after unloading), i.e. amount of connection rotation in nonlinear phase is equal to the sum of the linear

Table 4.4: The data of the piece-wise moment-rotation curves.

Wmj10_bt		Wmj10_bt+bd		Wmn10_bt	
<i>M</i> (kNm)	ϕ (mrad)	<i>M</i> (kNm)	ϕ (mrad)	<i>M</i> (kNm)	ϕ (mrad)
0	0	0	0	0	0
0.5	2.3	1.5	1.52	1.0	2.98
1.0	5.1	1.76	2.3	1.5	5.3
1.5	8.5	1.9	3.0	2.0	8.4
1.7	10.0	2.2	5.0	2.2	10.0
2.02	13.0	2.67	10.0	2.4	12.5
2.25	16.0	3.00	15.0	2.53	15.0
2.52	20.0	3.24	20.0	2.65	20.0
2.77	25.0	3.38	25.0	2.71	25.0
2.96	30.0	3.46	30.0	2.75	30.0
3.09	35.0	3.49	35.0		
3.20	42.0				

rotation and permanent rotation (see **Figures 4.6** and **4.13**). For the bolted and bonded connection this relation becomes more complicated due to the bonding initially increasing the stiffness of the connection and later to the debonding gradually decreasing the connection stiffness (see **Figures 4.9**).

The linear relationship of moment-rotation reloading curve (see **Figures 4.6**, **4.9** and **4.13**) showed the elastic property of each connection, even after damage had developed in it.

It can be seen that the initial stiffness of connection **Wmj10_bt+bd** is higher than for connection **Wmj10_bt** and **Wmn10_bt** and the moment at which the curve starts to be nonlinear is also higher. This difference in performance is due to the adhesive bonding. The application of bonding is to resist the initial prying action and prevents the opening-up between the top of the cleats and column flange. This resulted in the initial stiffness increase.

Test data from connections **Wmj10_bt** and **Wmj10_bt+bd** confirmed the ob-

observation made by Mottram (1994) that adequate support rotation was not attainable without adhesive bonding failure, (the MMFG (1989) recommended connection has combined bolting and bonding). These test data also showed that after adhesive bonding failure, **Wmj10.bt** and **Wmj10.bt+bd** gave identical reloading stiffness; meaning under this loading condition the two connections have the same structural behaviour.

For the final reloading curve the flexibility of the column flange in the major-axis connections results in less stiff moment-rotation behaviour than in the minor-axis connection (see **Figures 4.6, 4.9 and 4.13**). This can be seen by comparing the moment-rotation behaviour of the three connections. In comparison with the results of 8 inch WF section connections (Mottram 1994), the effect of column flange is significantly less than the connection tests on 8 inch column and beam members of pultruded shape. In other words, 10 inch pinned connections are stiffer and stronger than the 8 inch connections. For major-axis connections this difference is more than 1.5 times and for the minor-axis connection the difference in both strength and stiffness is smaller. There were two reasons for these differences. One is that, for major-axis connection, 1/2 inch flange of 10 inch pultruded column member is much stiffer than 3/8 inch flange of 8 inch column member. It offered more stiffness and resistance to prying action and flange 'bowing' deformation. The second reason is that, for minor-axis connection with two cantilever beams connected to column web, the stiffness and strength of the column no longer affects the performance of the connection. Thus the $M - \phi$ behaviour observed is due solely to the deformation of the web cleats. As the web cleats used in both full-sized 8 and 10 inch WF section connection tests were cut from the same size of equal-leg angle (6x6x1/2 inch), it is not surprising to find that they both gave similar $M - \phi$ curves.

The data recorded at a time lapse of 5 to 10 minutes after each loading showed a relaxation in load and rotation on the linear part of $M - \phi$ curve and a relaxation

in load and a slight increase in rotation when the $M - \phi$ curve was nonlinear. The magnitude of the relaxation grew with the increase of M applied. This phenomenon suggests that damage in the connections started when the nonlinear behaviour occurred and that its rate of development corresponded to the rotation imposed.

From these short-term tests, it is clear that the permanent rotation, suggested by Mottram (1994) to be due to slip, is not due to slip alone, but also has a contribution from permanent deformation of the connection itself. It was found that the permanent rotation was induced when the curve started to show nonlinear behaviour and grew with rotation. Since nonlinear connection behaviour is due to the damage that develops in the connection during the loading, this may suggest that permanent rotation is related to the damage of connection material and its value is directly proportional to the extent of damage in the connection.

There were two types of damage observed, delamination cracks and debonding. The cracking in the web cleats was the reason for the permanent rotation as it was observed that the cracks did not close up after unloading, whereas debonding did not cause the permanent rotation, but a reduction in connection stiffness, which can be seen by comparing the plot of connection **Wmj10.bt+bd** test (Figure 4.9) with the plot of connection **Wmj10.bt** test (Figure 4.6).

Table 4.5 presents the connection properties of initial secant stiffness, k_{ini} , moment, M_{ini} and rotation, ϕ_{ini} ; and $M_{12.8}$ and stiffness $k_{12.8}$ when the connection rotation is 12.8 mrad (ie. beam deflection is at $L/250$). Generally, a 10 inch connection is stiffer and stronger in moment resistant than the equivalent 8 inch connections. The comparison made on the connections in major-axis and the connections in the minor-axis shows that stiffness and strength of the major-axis connections have increased more than for the minor-axis. This is due to much higher flange stiffness from the wall thickness being 12.7 mm, instead of 9.5 mm, while the effect of web cleat itself is relatively small. This evidence shows that there is no real benefit in

having three bolts instead of two. Two steel bolts are adequate to transmit the shear force (see Mottram, 1994).

Table 4.5: Selected connection properties.

Connection	M_{ini} kNm	ϕ_{ini} mrad	$k_{ini} = M_{ini}/\phi_{ini}$ kNm/mrad	$M_{12.8}$ kNm	$k_{12.8} = M_{12.8}/12.8$ kNm/mrad
Wmj_bt †	0.14	1.22	0.1148	0.83	0.0645
Wmj_bt.2 †	0.29	3.21	0.0903	1.05	0.0822
Wmj_bt + bd †	0.81	2.07	0.3889	1.32	0.1035
Wmn_bt †	0.46	2.08	0.2212	2.24	0.1753
Wmj10_bt	0.5	2.3	0.2174	2.00	0.1563
Wmj10_bt + bd	1.5	1.52	0.9868	2.86	0.2234
Wmn10_bt	1.0	2.98	0.3356	2.42	0.1891
W †	1.25	5.00	0.0280		

† Mottram (1994). ‡ Bank (1990).

The three web cleated connections tested are assumed as pinned connections in Design Manual (MMFG, 1989); however, even these ‘pinned’ connections possess an ability to resist moment. This will result in some reserve in safety, if these connections are used as pinned connections in the frame design. To illustrate the role played by these connections, a simple example of a 5 meter span 10 inch WF pultruded beam with different beam end connections is given. The elastic modulus, cross-section area and moment of inertia of the beam are given as $E = 1720 \text{ kN/cm}^2$, $A = 93.9 \text{ cm}^2$ and $I = 10600 \text{ cm}^4$ respectively (MMFG, 1989). The calculation was made by using the method and computer programme discussed in Chapter 7. Results are shown in Table 4.6, in which, ω represents a uniformly distributed load, δ represents mid-span deflection, M_m represents mid-span moment, M_e , and ϕ_e , represent beam-end moment, and beam-end rotation, respectively. A limiting value for deflection $L/250$ is used, which is recommended as in EUROCOMP clause 4.5.2 to general public access flooring (Clarke, 1996), and this gives a 20 mm allowance

of deflection. The value of load ω is determined for a simply supported beam with perfectly pinned connections at both ends. With this load, the three connections give a reduction of 15 to 22 % in deflection respectively. If mid-span deflection is 20 mm, the three connections show a load increase from 17 to 24 %. In other word, these connection details when treated as a pinned connection have a 17 to 24 % load reserve.

Table 4.6: Connection performance.

Beam End Connection	ω kN/m	Load Factor	δ mm	Deflection Factor	M_{ms} kNm	M_e kNm	ϕ_e mrad
<i>Pin</i>	4.517	1	20	1	14.12	0	12.8
<i>Fixed end</i>	4.517	1	4	0.2	4.71	9.41	0
	22.592	5.00	20	1	23.53	47.07	0
Wmj10_bt	4.517	1	17.03	0.85	12.37	1.75	10.425
	5.264	1.17	20	1	14.51	1.94	12.274
Wmj10_bt+bd	4.517	1	15.58	0.78	11.52	2.60	9.262
	5.595	1.24	20	1	14.68	2.81	12.039
Wmn10_bt	4.517	1	16.29	0.81	11.94	2.18	9.835
	5.429	1.20	20	1	14.59	2.37	12.156

Note: the second line for each connection gives the results for the beam has 20mm mid span deflection.

The results of this comparison are also illustrated in **Figure 4.17**. Since the result in **Table 4.6** for the 'Fixed end' connection shows a big difference to the others, and the aim of this comparison is to illustrate the difference between a pinned and the web cleated connections, only the comparison of the pinned and the web cleated connections are given in **Figure 4.17**.

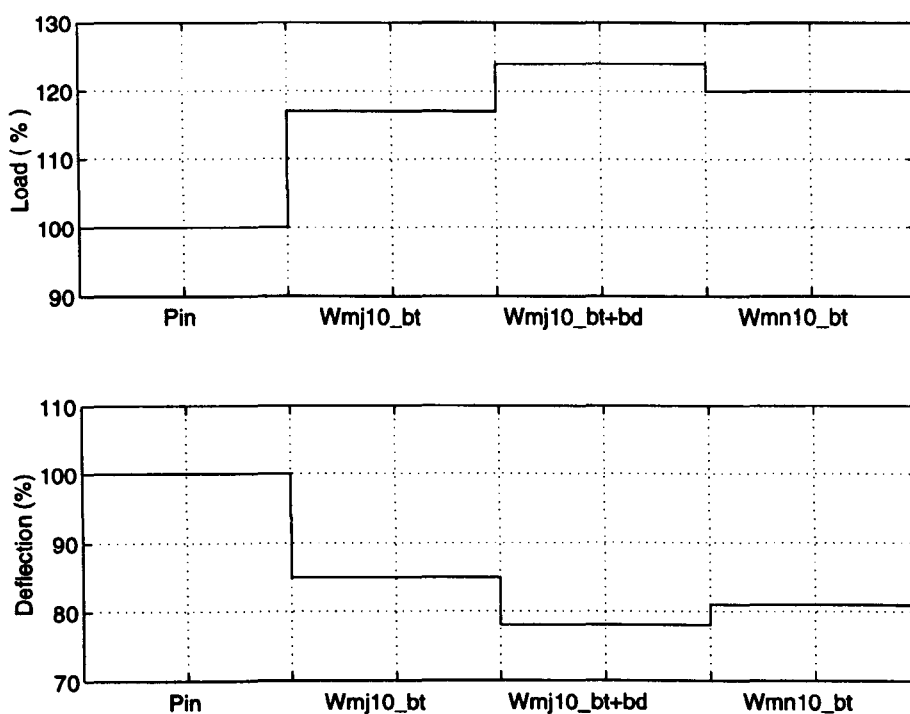


Figure 4.17: Load and mid-span deflection comparison of the beam with different beam-end connections.

4.7 Conclusions from the Pinned Beam-to-column Connection Tests

- The short-term moment-rotation behaviour of three 10 inch WF beam-to-column web cleated connections has been determined.
- Initial moment-rotation behaviour of each connection was linear. The moment at which the curve goes nonlinear was low, at 1.5, 1.0 and 0.5 kNm for connections **Wmj10_bt+bd**, **Wmn10_bt** and **Wmj10_bt**, respectively. The start of the nonlinear behaviour was gradual for the bolted connections and pronounced for the connection with bonding and bolting.

- Compared to an 8 inch flange of 3/8 inch thickness, the 10 inch flange of 1/2 inch thickness pultruded column is stiffer and there is no significant column flange 'bowing' deformation produced.
- As the rotation of the connection increases the magnitude of the permanent rotation increases. This permanent rotation is due to deterioration of the connection. Eventually, the damage to the web cleats as the connection rotates leads to its ultimate failure. Further research is required to determine the long-term permanent rotation.
- Combined bonding and bolting can prevent slipping between beam and web cleats at all load levels.
- Application of bonding improves the initial stiffness of the connection. However as debonding could not be prevented, and developed during the test, the stiffness of a reloading curve gradually tended to the curve obtained when the connection was bolted only. It does not seem necessary to include the expensive practice of adhesive bonding, unless it is to prevent the inherent slip.
- Web cleat failure is gradual with the mode that of delamination crack growth at the top of the web cleat. This type of failure is difficult to prevent by using pultruded composite profiles because all such material has poor through thickness strength; there is no fibre reinforcement in this direction.
- None of these three 'pinned' connections can meet the 21.3 mrad rotation requirement, without material damage, as needed to satisfies MMFG design for beam with a maximum deflection of $L/150$. The maximum rotation of the three connections were all greater than 30 mrad. If a limited amount of the material damage is acceptable, these three connections can meet the rotation

requirement for pinned connections. **Table 4.6** shows that the actual beam end-rotations for the design load (ie. the beam deflection achieves $1/250$) are less than 10.5 mrad (without counting the rotation due to slip), or approximately $1/3$ the connection rotation at ultimate failure.

Chapter 5

Experimental Investigation on Semi-rigid Beam-to-column Connections

5.1 Introduction

Traditional steel frame design is usually based on the assumption that the connections are either pinned or rigid. However, actual behaviour of a connection is between these two extremes, and this leads naturally to the semi-rigid behaviour of connections in frame design. By including such behaviour, frame design is 'semi-continuous', and with steel this has been found to have the merits of reducing beam depth and overall cost. To date, the research on semi-rigid connections has led semi-rigid frame design to be a possible practice in steel frame design through clauses in Eurocode 3 (1992). For frame of pultruded members and polymeric composite connections, the possibility and the feasibility on semi-rigid frame design, and the benefit from such design, need to be proved, which is one of the main purposes of

this investigation.

FRP pultruded structural members are more flexible by a factor of 10 than the traditional structural material of steel and the connections recommended by design guide (MMFG, 1989) have low stiffness (see $M - \phi$ results in **chapter 4** for example) such that they must be treated as pinned; consequently, the deflection and the instabilities of members in frames will often govern their design. To quote Bass & Mottram (1994), 'the design of pultruded frames should be based on preventing instabilities and limiting deflection, and not strength as is often the case with steel'. This can be achieved by increasing the stiffness and the resistance of the connection, which will reduce the deflection of the members for any design loading and influence the response of the frame as a whole. It will also increase the resistance to buckling instabilities such as lateral torsional buckling. Such a connection is known as a semi-rigid connection.

In current pultruded frame construction, the form of the connections given in design manuals (MMFG, 1989; Anon, 1995) are web cleated connections which are simply a copy of steel practice; they are assumed to be pinned connections. For semi-rigid connections of FRP pultruded frames, there is no design guidance available. Although, in steel work some types of connections are used as semi-rigid connections, they are not suitable for pultruded frame practice due to the different material properties and the different fastening methods (Bass & Mottram, 1994). Thus the types of connection for pultruded frames will not necessarily copy exactly steel practice.

To study the behaviour of semi-rigid connections and to develop practical semi-rigid connections for pultruded frames, two steel angle cleated connections and two pre-preg cleated connections on 8x8x3/8 inch (203.2x203.2x9.5 mm) wide flange pultruded section have been designed and tested in a laboratory investigation. Moment-rotation behaviour for each connection is reported as well as detailed description of

the test and failure modes of each of the connections. Results of a load analysis for a 6 metre span beam with the connections tested is presented to demonstrate the benefit of the semi-rigid connection. The serviceability beam line (see Section 7.4.8) has been used in the analysis as an aid to quickly show the merits expected. A linear moment-rotation curve of moment equalised connection (MEC) is presented, which is suggested as the ideal connection stiffness for semi-rigid connection design.

5.2 Connection Description

A description of the tests and the labelling system used herein follows that used by Mottram (1994), and it is presented in Table 5.1. For example, label **Tmj** defines connection to be **Top** cleated with **major**-axis column.

Table 5.1: Summary of connection tests.

Label	Connection details	Column axis	Note
STmj	Steel top and bottom cleats	major	bolting, column stiffeners
STmn	Steel top and bottom cleats	minor	bolting
Tmj	Top and seat cleats	major	column stiffeners †
TLmj	Top, low and seat cleats	major	column and beam stiffeners †

† bolting and bonding.

The description of the four connections is given in following sections. The engineering drawings for these connections and the frame subassembly are presented in **Appendix B**.

5.2.1 Connection STmj

This connection used two 100x100x8 steel leg-angle cleat and eight steel nuts and bolts. The configuration of connection **STmj** consisted of steel top and seat angle cleats, as shown in **Figure 5.1**.

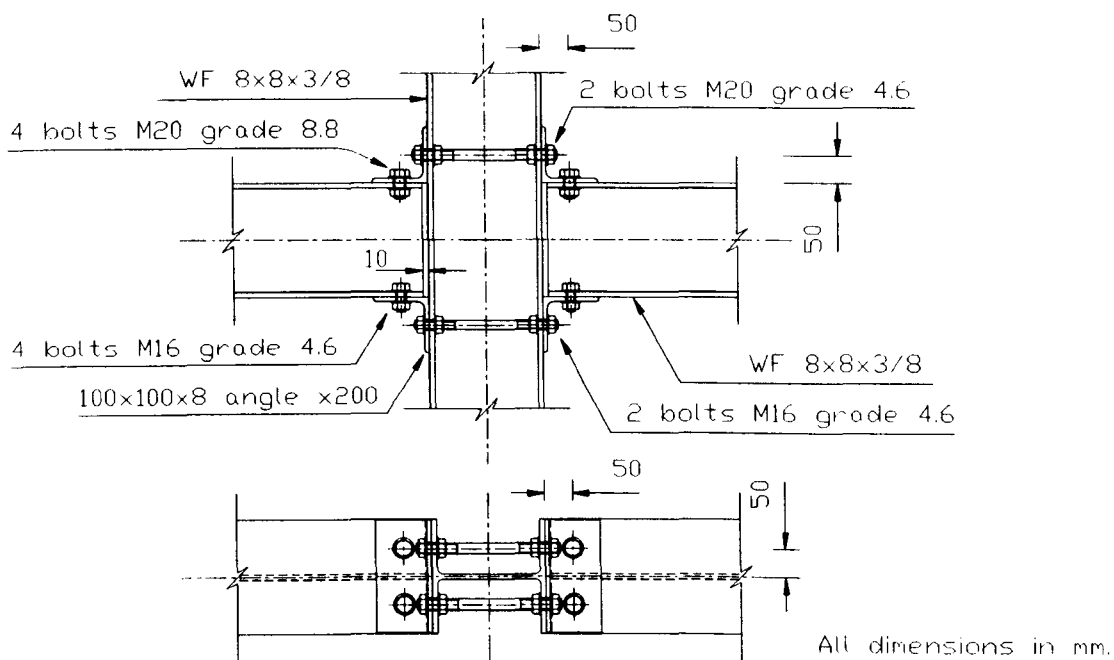


Figure 5.1: Configuration of connection **STmj**.

The top and bottom angle cleats were joined to the beam and column member by one row of bolts in each steel angle leg, in which the horizontal bolts extended to cross both sides of column flanges and steel angle cleats. These continuous bolts were included to stiffen the column flanges and thereby restrict the column flange induced prying action seen with pinned connections in **chapter 4**. A second reason why the stiffening was necessary was because in previous tests (Bass & Mottram, 1994) flange deformation made the connection's $M - \phi$ behaviour too flexible. These

long stiffening bolt were manufactured from mild steel studding of diameter 20 mm. The rest of the mechanical fastenings were M16 grade 4.6 and M20 grade 8.8 steel bolts. 30 mm diameter standard size washer were used and bolts were tightened to a torque of 100 N m. This higher torque was used by Turvey (1996) in pinned connected rectangular portal frame tests and his test gave no slip. The width of each steel angle cleat was 200 mm. For buildability, the bolt hole clearance was 2 mm; the same as in steel practice.

Full engineering details of connection **STmj** are given in **Appendix B**.

5.2.2 Connection **STmn**

Connection **STmn** was similar to connection **STmj**, except that the beams were connected to the minor-axis of the column, using steel angle cleats of width 165 mm. The details of the connection is shown in **Figure 5.2** .

The aim of this connection test was to examine the performance of the steel angle cleated connection without the effect of column flange deformation. In previous semi-rigid connection tests, with pultruded top and bottom cleats, cleat failure was the most common type of failure. This is not unexpected because of the poor through thickness properties of pultruded angle cleat material. It was therefore decided to find out if steel could be used for the cleat piece. This was a rational approach, because it would remove the through thickness strength problem when the material is composite. Moreover it was of interest to know whether there would be any other structural problem that would appear if the cleat was not the first component in the joint to fail. Full engineering details of the connections are given in **Appendix B**.

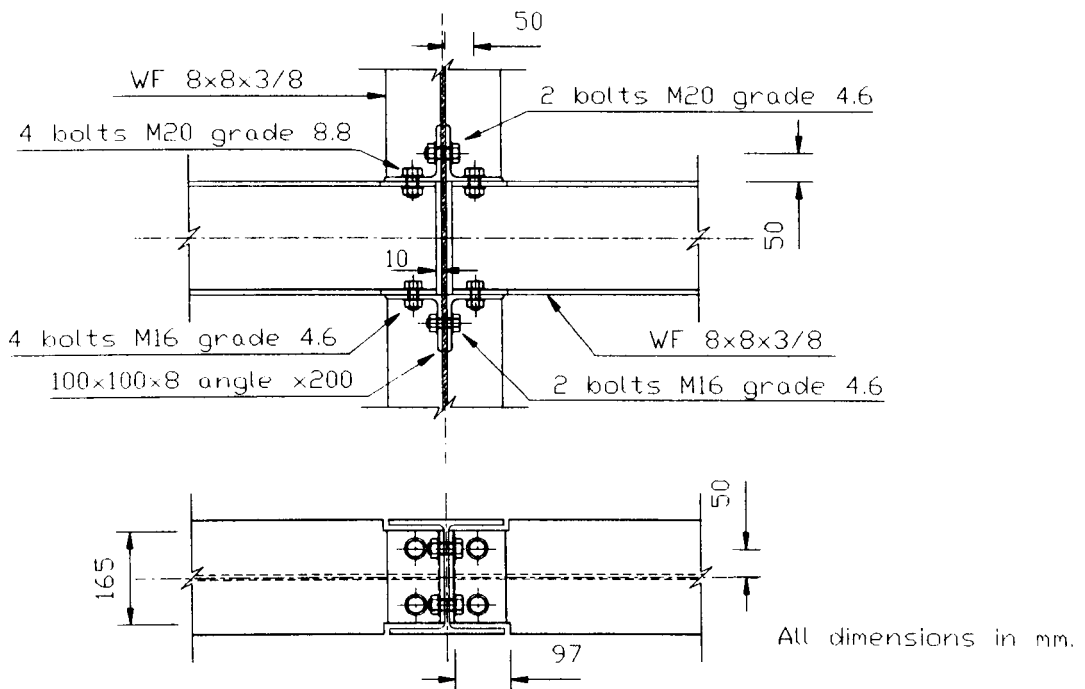


Figure 5.2: Configuration of connection **STmn**.

5.2.3 Connection **Tmj**

Connection **Tmj**, as shown in Figure 5.3, followed an unsuccessful attempt to develop a similar ‘all-composite’ connection by Mottram (1994) and consisted of top cleat, seat cleat and column stiffener. The top cleats were pre-preg angle made of E-glass woven fibre saturated with epoxy resin. Details of how the pre-preg cleat was made are given in Section 5.4. The pre-preg material was manufactured by Advanced Composite Group Ltd, Derby. The seat cleat were cut from 6x6x1/2 inch equal leg pultruded angle and the column stiffener was 1 inch composite bolt¹ which effectively reinforced the column flanges by connecting them together. The

¹MMFG fibrebolt, MMFG, 1989.

intention of this connection was to develop an all-polymeric composite connection for application where steel was claimed not to be suitable.

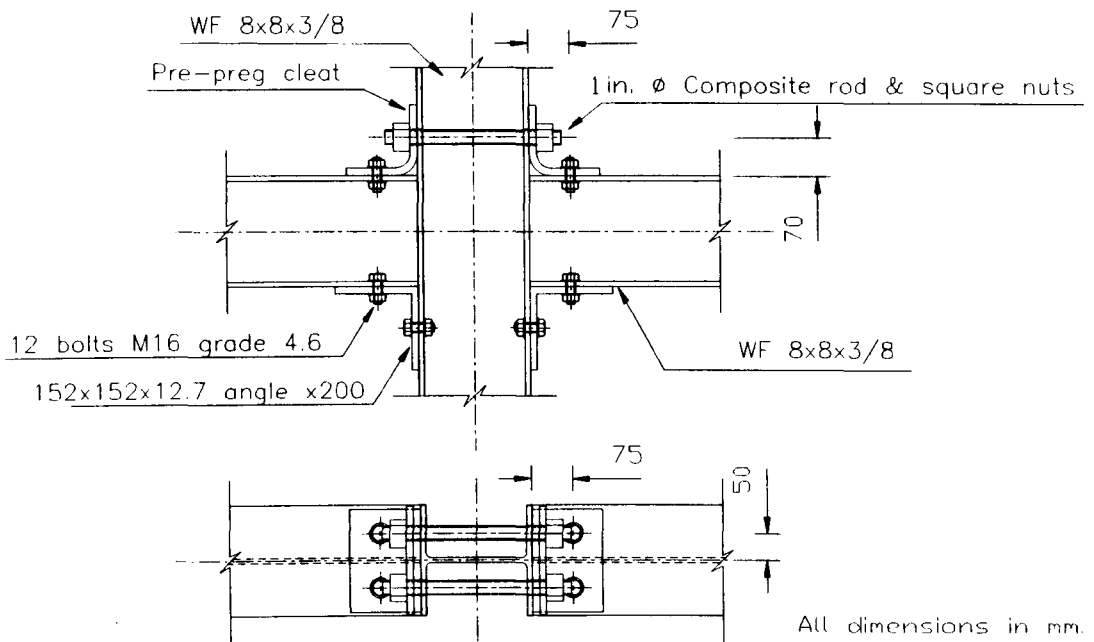


Figure 5.3: Configuration of connection **Tmj**.

The top and seat cleats connected two cantilever beams to the column flanges in the major-axis position. The connection was jointed by a combination of bolting and bonding. All other bolts were M16 grade 4.6 steel bolts. All steel bolts were tightened to a torque of 28.3 kNm and the composite bolts were initially tightened by hand only. The mating surface of top and seat cleats and the flanges of the beam and column were partially bonded from the centre line of the bolt hole to the end of cleat legs (as shown in **Figure 5.4**) with the Araldite 2015 adhesive system. To obtain a minimum bond thickness of 0.25 mm, lengths of copper wire were laid on the prepared mating surface after the adhesive had been applied. The procedure for bonding is given in the thesis by Bass (1994).

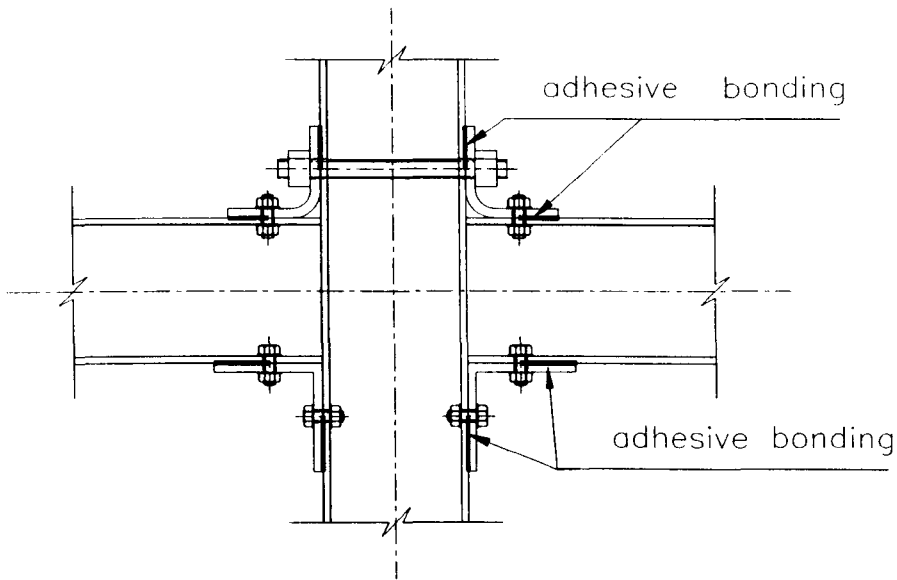


Figure 5.4: Bonding in of connection **Tmj**.

No clearance between the beam end and the surface of the column flange was allowed in this connection design. This detail was included to increase the stiffness in the connection and together with the limited regions of bonding to prevent any connection slip. Full engineering details of connection **Tmj** are given in **Appendix B**.

5.2.4 Connection **TLmj**

Connection **TLmj** was designed using knowledge obtained from the previous connection tests, especially that from connection **Tmj**. Like connection **Tmj**, it had a top pre-preg cleat, seat pultruded angle cleat and composite bolts for column stiffeners. Beside these details, there were two lower top pultruded angle cleats to increase further the stiffness of connection, and two M16 continuous steel bolts through both top and bottom beam flanges to reinforce the beam flange. This latter detail was introduced to reduce the rotation flexibility caused by the deformation

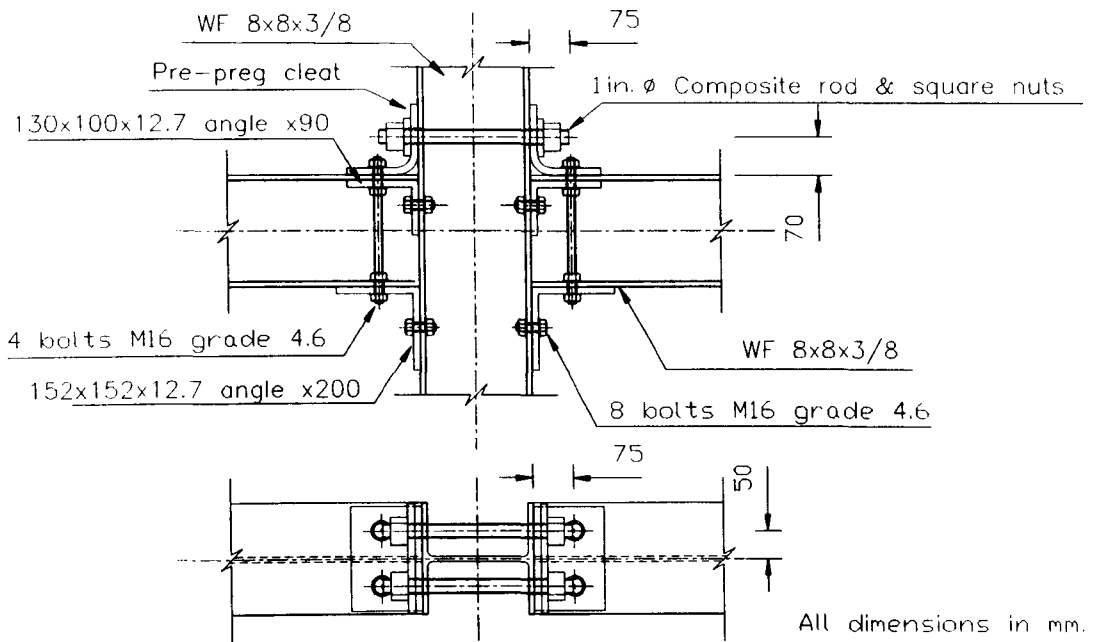


Figure 5.5: Configuration of connection **TLMj**.

of the beam flange seen in the test on connection **Tmj**. The test with connection **Tmj** (see Section 5.6.3) also showed that the connection stiffness was affected by the actual orientation of the square composite nuts (see Figure 5.38). A rectangular plate stiffener cut from a 6x6x1/2 inch pultruded equal leg angle was therefore placed between the pre-preg cleat and the square composite nut (see Figure 5.5). This detail not only eliminated the effect of the composite nut orientation, but also increased the stiffness of the pre-preg cleat. Unlike connection **Tmj**, all mating surfaces of cleats and beam and column flanges were bonded. The adhesive system and the procedure used were the same as that used when fabricating connection **Tmj**. Figure 5.5 shows the fabrication of the connection and Figure 5.6 shows application of the adhesive bonding material on to the angle cleats. For the engineering details of the connection, refer to the figures in Appendix B.

No clearance distance between the beam end and the surface of the column flange was used in this connection.

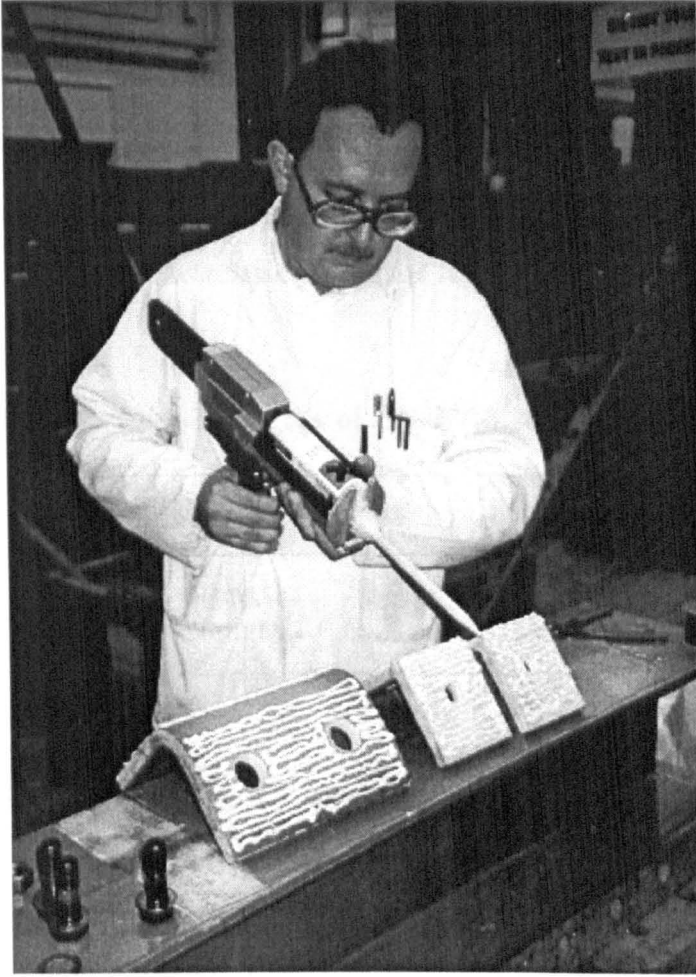


Figure 5.6: Application of the adhesive to cleats for connection **TLmj**.

5.3 Material Specification

The pieces for the low cleats and seat cleat used in connection **TLmj** and **Tmj** were cut from 6x6x1/2 inch (152.4x152.4x12.7 mm) equal-leg angle and column

and beam members were 8x8x3/8 inch (203.2x203.2x9.5 mm) standard wide flange (WF) section. These pultruded sections were from the EXTREN 525 range of fibreglass structural shapes, manufactured by MMFG. The material physical properties of fibreglass-reinforced structural shapes given by MMFG (1989) are listed in **Table 4.2**. These properties were determined by using ASTM coupon tests and represented the minimum properties measured.

The cleats used in connection **STmj** and **STmn** were of 100x100x8 steel equal leg angle in Grade 43. Characteristic strengths for the steel angle are presented in **Table 5.2**.

Table 5.2: Code strengths of Grade 43 steel (BS 5950).

Property	Strength
Bearing strength, P_{bb}	460N/mm ²
Design strength, P_y	275N/mm ²

The bolts used in the connection were M16 in grade 4.6 and 8.8 and M20 in grade 4.6 and 8.8. The 16 mm diameter bolts used as beam flange stiffener and fasteners were made of mild steel. 30 mm diameter standard size of steel washers were used with all bolt fasteners. Characteristic strengths for the bolts are listed in **Table 4.3**.

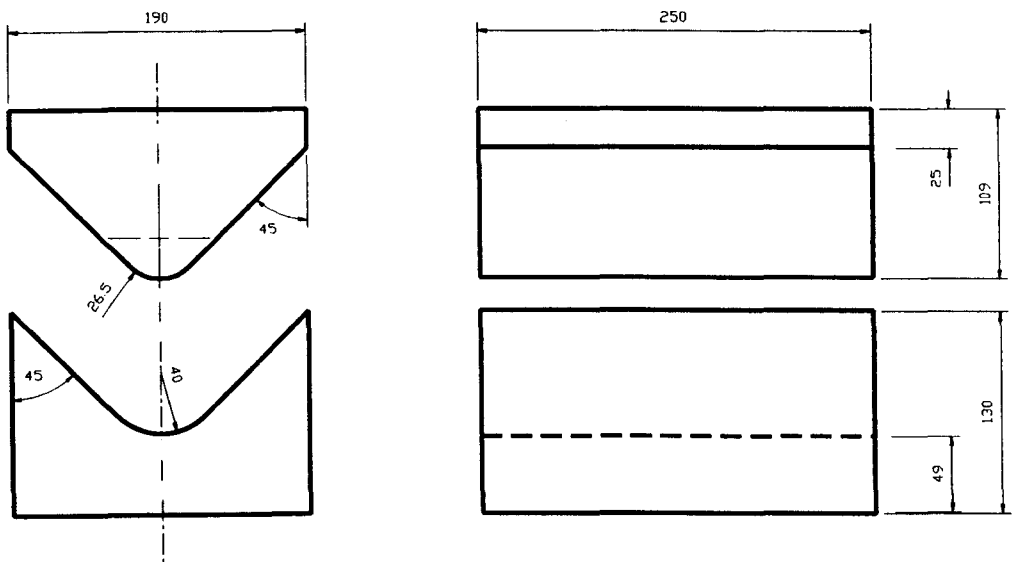
The adhesive system used was the same as that used in the pinned connections (**Section 4.3**).

5.4 Manufacture of Pre-preg Cleats

The material chosen for the polymeric composite pre-preg cleat piece was the pre-preg GF007/LTM25/300A2S (manufactured by Advanced Composites Group Ltd., UK). It had bi-directional reinforcement of E-glass Woven Rovings at 850 g/m^2 , and an epoxy resin at a weight fraction of 32%. Advantages of this material for fabrication of the cleat piece were that it had a high nominal lamina thickness of 0.58 mm (evaluated by using the rule of mixtures and manufacturer's data), and a minimum curing temperature of 50° C (24 hours).

Pre-preg cleat was manufactured using a pressure moulding process. The structural shape of the cleat was improved by having a generous fillet, of maximum radius 40 mm, at the knee of the two legs, and was introduced to alleviate the through-thickness stress that had caused delamination failure in the pultruded leg-angle; this had been found to be the weakness of connection **DTLmj** (Bass & Mottram, 1994), when trying to develop a semi-rigid connection using pultruded materials for the connection pieces. The mould is made of steel and the mould, designed by Dr J.T. Mottram at University of Warwick, is shown in **Figure 5.7**. The male and the female steel mould parts were machined such that when mould was closed up the gap between them gave a constant thickness of 14 mm along the length of the cleat's profile. The cleat comprised of 24 layers of pre-preg, which were laid out manually on the female mould layer by layer.

To release the pre-preg cleat from the mould, the mould surface was prepared with mould releasing agent Frekote Mold Release 700-NC and a layer of fine woven glass cloth was placed over the surface of each male and female mould. 24 layers of the pre-preg material was laid up in the female mould by hand, and an unconsolidated and uncured cleat was between 18 and 20 mm thick. A fine woven glass cloth was placed over a uncured cleat before the male mould was placed on the top. The



Material: mild steel.
All dimensions in mm.

Figure 5.7: The detail of steel mould for pre-preg cleat.

ready-to-cure pre-preg cleat in the female mould is shown in **Figure 5.8**.

The pre-preg material is stored in a freezer at -20°C . It cures under room temperature conditions and, therefore, once it has become in thermal equilibrium with room temperature, moulders must work quickly. For this reason the individual layers were cut while the material was still cold and stored in the freezer for use on the next day. The rectangular layers of 200 by 200 mm were cut out using a Stanley knife and it is likely that the fibre orientation was not exactly normal to the side edges of the layer. There was a second problem found when the laminate was built up; it prevented the lay-up from having the actual bi-directional arrangement expected. At room temperature the resin became very tacky. This made it extremely difficult under manual operation to position each layer in exactly the correct location. The

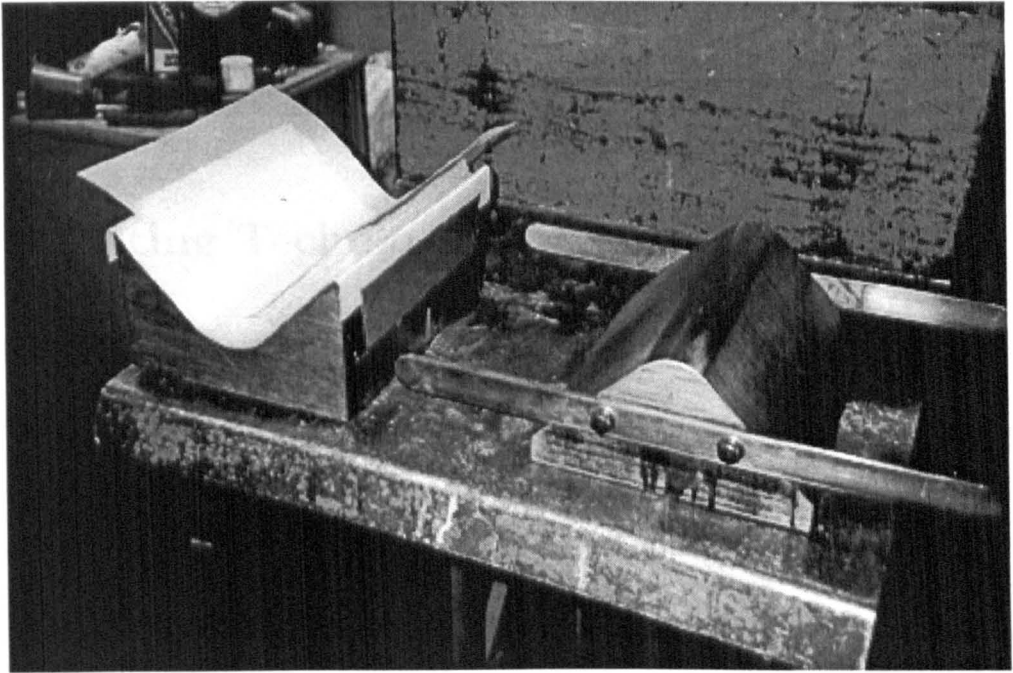


Figure 5.8: The uncured pre-preg cleat in the steel mould.

two problems encountered when manufacturing the cleat were not too serious and it is the author's opinion that they did not affect the structural performance of the pre-preg cleats. However, for completeness of the work it has been necessary here to provide the information for those who want to repeat the method of manufacture.

To cure the laminate, the mould was put into a Moore heated press, and the unconsolidated laminate was subjected to a pressure of 70 psi for 1 hour. Using a K-type thermocouple, the plates of the press were kept at a constant temperature of 100°C. The maximum temperature on the surface of the curing laminate was found to be 60°C. The mould parts were prevented from moving together by stops, such that the cured thickness was exactly 14 mm. The colour of the composite was slightly brown. Both these physical conditions were indications that the manufacturing process had been successful. Finally, the mould and cleat were removed from the

Moore heated press and the cleat was released from the mould after the mould had cooled down. The consolidated cleat was cut and drilled to the finished size (**Appendix B** gives engineering drawing).

5.5 Testing Techniques

5.5.1 Test Equipment and Loading Arrangement

The loading equipment, the measurement tools and the test configuration of the frame are the same as those used by the author to test web cleated connections in **Chapter 4** except that the capacity of the tension load cells were 45 kN. The 6 mm electrical resistance strain gauge (FLA-6-11) used to measure the strain of mild steel were 6mm long and the gauge resistance was $120 \pm 0.3 \Omega$.

5.5.2 Methods and Procedure of Test

Connections were loaded in increments of the connection moment of about 1 kNm. Once the $M - \phi$ curve started to show non-linear behaviour, the specimen was first unloaded and reloaded. Afterwards, additional cycles of unloading and reloading were performed. The purpose of this cyclic procedure was to determine the extent of permanent deformation and thus any change in the connection's stiffness. A time interval of 5 to 10 minutes elapsed between each load increment to carry out visual inspection for failure and to take measurements. All data were recorded immediately after an increment was applied and again just before the next one was applied. After the maximum moment had been reached, each connection was taken to either ultimate failure or until rotation was excessive. Test duration was between 1 and 3 hours.

5.5.3 Test Measurement

Test Measurement for Connection ST_{mj} and ST_{mn}

The arrangement of the transducers which were used to measure displacement and rotation in the tests is shown in drawing No. 004 in **Appendix B**. The measurement of the rotations was achieved by using five clinometers, which is the same as that in pinned connection described in **Section 4.4.2**. But the clinometers C2 and C4 were 100 mm distance from the end of the beams. The rotation of the column member was measured at the centre of the column web for the major-axis tests and by fitting the clinometer to the column flange in the minor-axis test.

The vertical deflection of the cantilevers was measured directly above each load point using 100 mm displacement transducers (HS 100), which is the same as pinned connection tests (see **Section 4.4.2**). The relative horizontal slip of the cantilevers and the top and seat cleats was measured by 25 mm displacement transducers (HS 25). These are transducers labelled LTL, LBL, LTR and LBR, on the centre of the top and bottom flanges of the cantilevers.

The FLA-6-11 strain gauges located on the centre of the horizontal leg of each steel cleat was 5 mm from end of the fillet radius. These gauges were used to measure the surface direct strain to find out if yielding occurred. The strain of the column stiffeners bolts was measured on the top surface of each bolt by FLA-6-11 strain gauges.

The arrangement of transducers in the tests of connection ST_{mj} and ST_{mn} are shown in **Figures 5.9 and 5.10** respectively.

All transducers were connected to the data logger (data acquisition system), from which the data were recorded during a test and sent to the computer for data processing.

Short-term data were obtained immediately after the application of the each

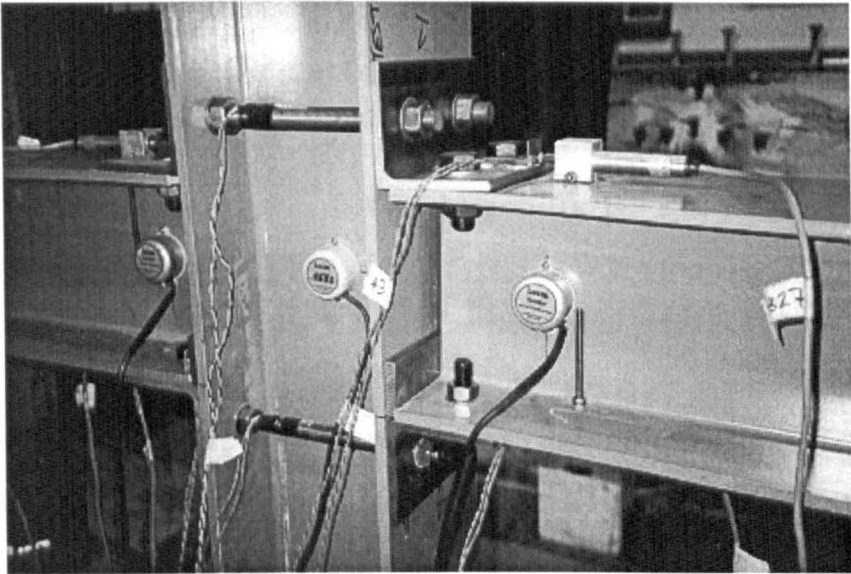


Figure 5.9: The transducers arrangement for the tests on connection **STmj**.

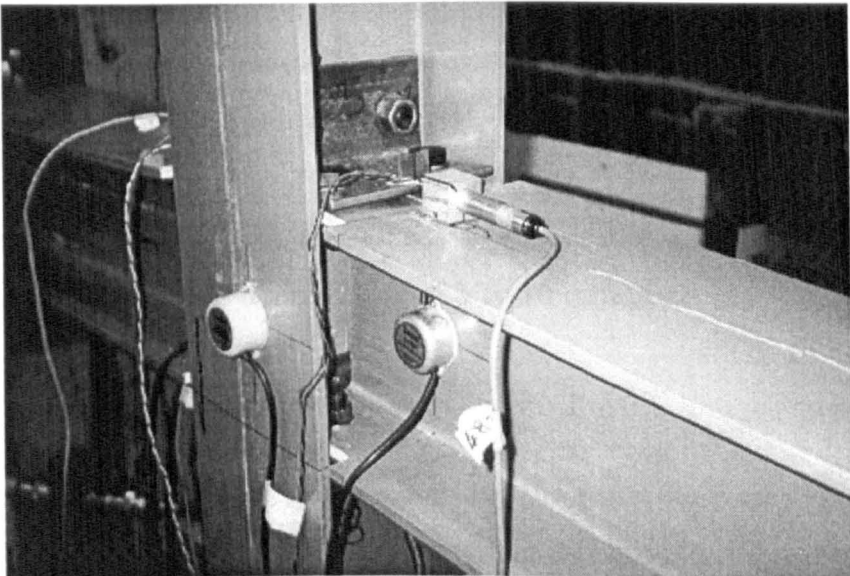


Figure 5.10: The transducers arrangement for the test on connection **STmn**.

loading increment and after a time lapse of 5 to 10 minutes.

Test Measurements for Connection Tmj and TLMj

The arrangement of the transducers used to measure displacement and rotation in the tests is shown in drawing No. 004 in **Appendix B**. The measurement of the rotations was achieved by using five clinometers, which is the same as that in pinned connection described in **Section 4.4.2**. The beam end rotation of the cantilevers was measured by clinometers C2 and C4, 75 mm away from the end of beam. The rotation of the column was measured at the centre of the column web for major axis tests and at the column flange for minor axis tests.

The vertical deflection of the cantilevers was measured directly above each load point by 100 mm displacement transducers (HS 100), these are transducers L1 and L2. The relative horizontal slip of the cantilevers and top and seat cleats was measured by 50 mm displacement transducers (HS 50); these are transducers LTL, LBL, LTR and LBR, at the level of the top and seat legs.

All transducers were connected to the data logger (data acquisition system), from which the data were recorded during the tests and sent to the computer for data processing.

Short-term data was obtained immediately after the application of the each loading increment and after a time lapse of 5 to 10 minutes.

5.5.4 Data Processing

The connection rotation was calculated using the same method as described in **Section 4.4.2**. Rotation from slip was calculated by **Equation 4.1**, but distance l was measured between two transducers which were fixed onto the the surface of top and bottom beam flanges (see **Figure 5.11**).

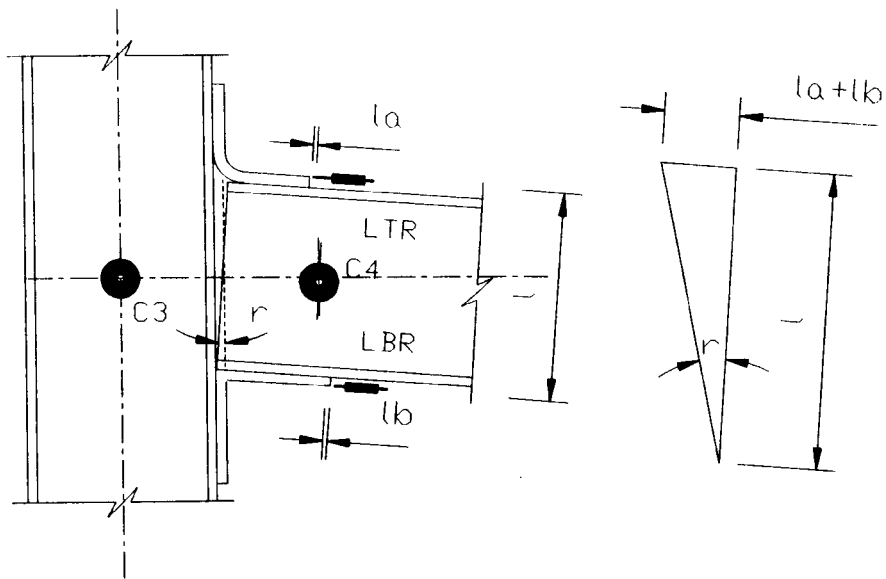


Figure 5.11: The rotation due to slipping.

The moment that a connection transmitted was determined by multiplying the vertical load by the distance between the loading point and the centre of the column. The distance used was 1.016 meter.

5.6 Descriptions of Tests

5.6.1 Test of Connection STmj

In the early stage of the loading slippage occurred between the beam member and the top steel cleats. This slip first occurred on the top right side of the cruciform specimen. The moment was over 4 kNm and the slip caused the rotation of the right side connection to increase to about 7 mrad (see **Figure 5.12**, point A). Following this first noticeable slip there was subsequent movement in both connections due

to slippage between connection pieces and members. Due to this slip movement, the right-side connection rotation was larger than the left side, at 17.8 mrad, for a moment of only 8 kNm (point C in **Figure 5.12**). Obviously, this part of the moment-rotation behaviour does not reflect the true behaviour of the connection, and hence to avoid spurious results, the specimen was unloaded. After unloading, a 10 mm thick steel plate packing was put into the clearance gap on each side between the bottom flange of the beam-end and the column flange (see **Figures 5.9** and **5.13**). The presence of the packing was to resist further slip movement in the connection. The unloading and reloading curve showed similar stiffness to the initial stiffness of the connection (see **Figure 5.12**).

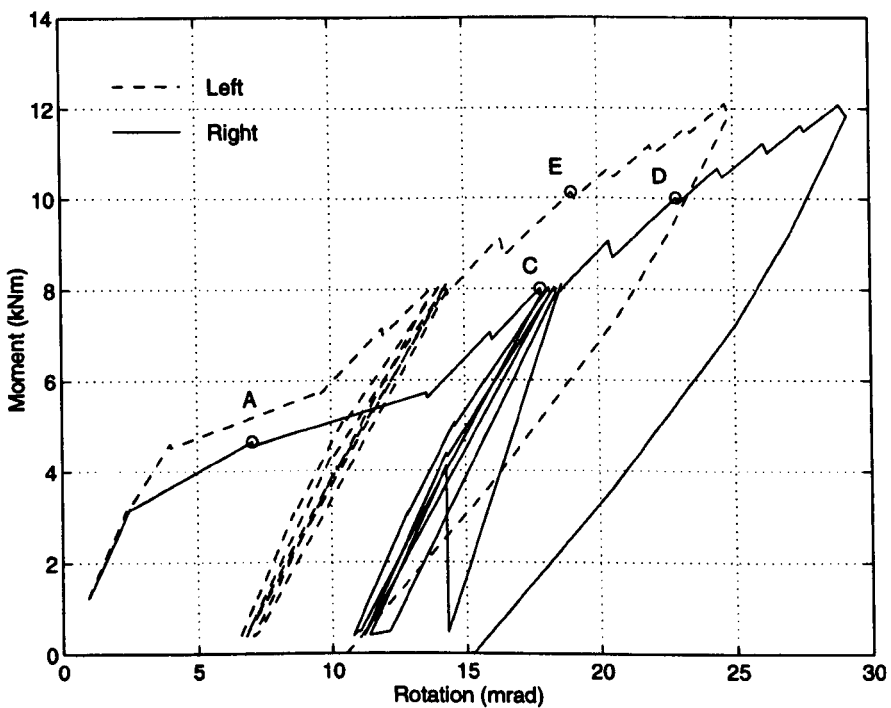


Figure 5.12: Moment-rotation curves for connection STmj.

When the moment was increased to 10 kNm (point D and E in **Figure 5.12**),

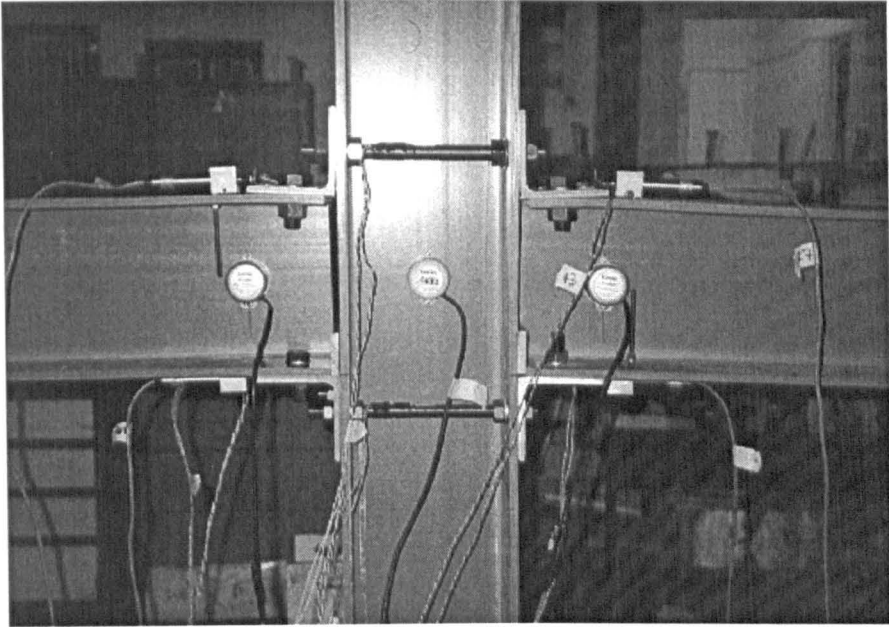


Figure 5.13: The deformation of connection **STmj** and the deflection of the beams.

the first acoustic emission was heard. Cracking was then visually observed in both beams along the interface of the web and the top flange, and adjacent to the top cleat. Finally, the connection moment was further increased to 12 kNm. There was no significant additional failure. Only slight surface cracking along the internal radius of the web and the top flange of each beam could be observed. There was no buckling of the beams or column members. The final deformation of the connection and the deflection of the beams are shown in **Figure 5.13**.

The moment-rotation behaviour of connection **STmj** is given in **Figure 5.12**, in which both data taken immediately after a loading increment and after a time elapse of 5 to 10 minutes are presented. The curves show that relaxation was small throughout the test. In this figure, it is shown that the left-side and right-side curves are not coincident, which is due to the problem of connection slip. This can be clearly seen in the moment-slip curve shown in **Figure 5.16**.

The moment-strain curves for the upper surface of the cleats are presented in **Figure 5.14**. The difference between the left-side and the right-side connection slip reflected in these curves shows a slightly larger strain in the right-side bottom cleat. This was due to the larger right-side top connection slip allowing the right-side beam to have a larger rotation than on the left-side. This in turn meant the bending deformation of the right-side bottom cleat was larger than the left-side, thus the strain at the right-side cleat was slightly larger than on the left-side.

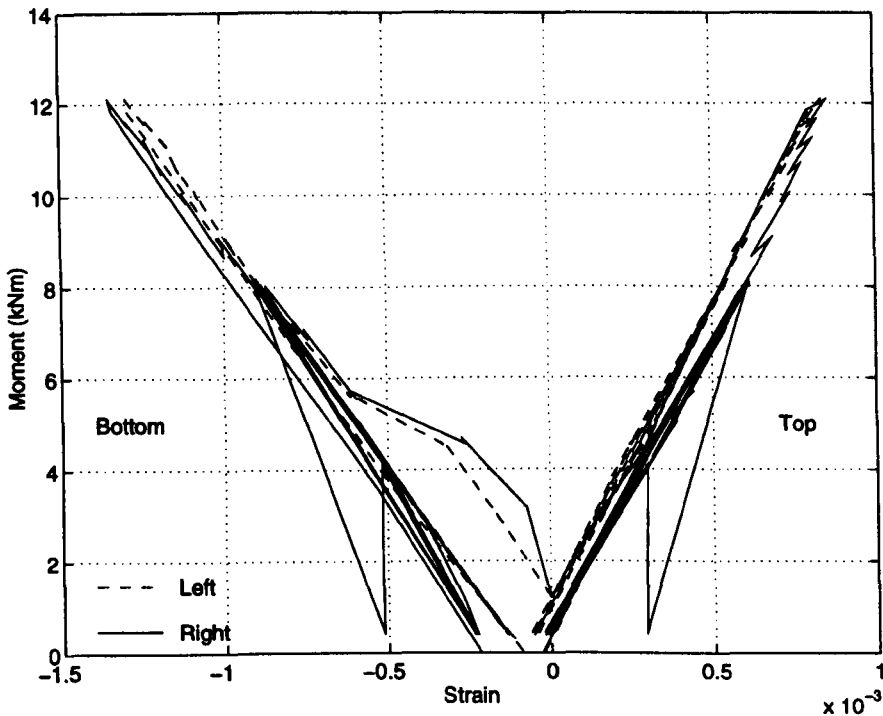


Figure 5.14: Moment-strain curves for the steel cleats in connection **STmj**.

Figure 5.14 shows that the direct strain on the surface of the bottom cleats is larger than the equivalent strain in the top cleats. It also shows, through the load cycle curves, that a permanent deformation developed. This can be seen more clearly in **Figure 5.15** where the strain-rotation curves for top and bottom cleats

are presented. The final permanent strain for the bottom cleats may indicate that yielding of the steel has occurred.

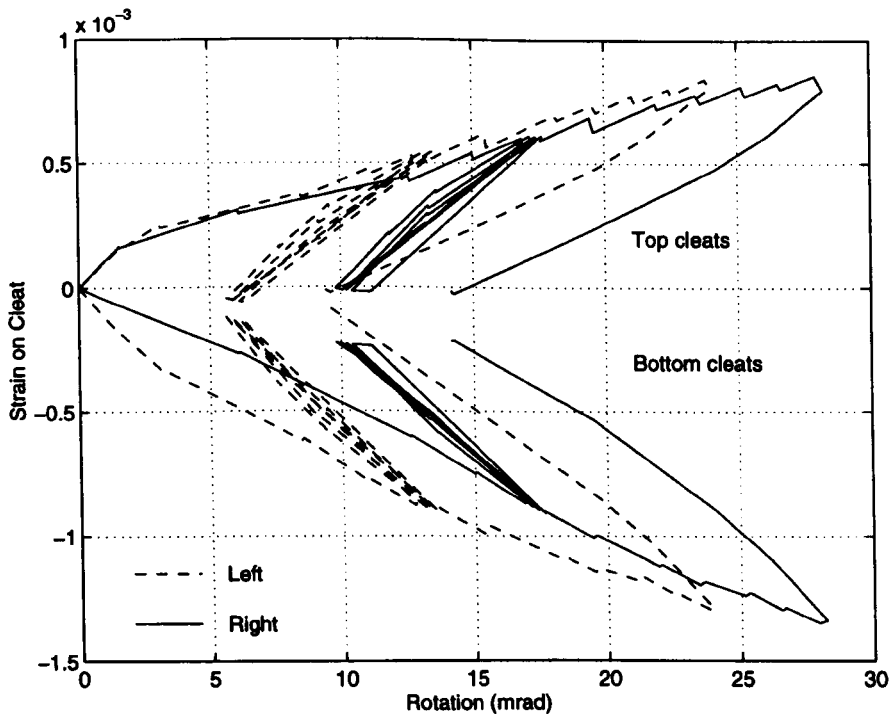


Figure 5.15: Strain-rotation curves for the cleats in connections **STmj**.

The moment-slip curves for the two connections are plotted in **Figure 5.16**. They show that the slip associated with top cleats is larger than for the bottom ones and that no significant slip movement occurred between the beam and its bottom cleat before, and after, the steel packing was introduced.

Due to the flexibility of the beam member, and its flanges in particular, the bending deformation of the beam caused the gap to increase significantly between the horizontal cleat leg and the top flange of the beam (see **Figures 5.9** and **5.13**), and this, throughout the test, resulted in an increase in the slip measured by the displacement transducer mounted between the steel cleat leg and the beam top

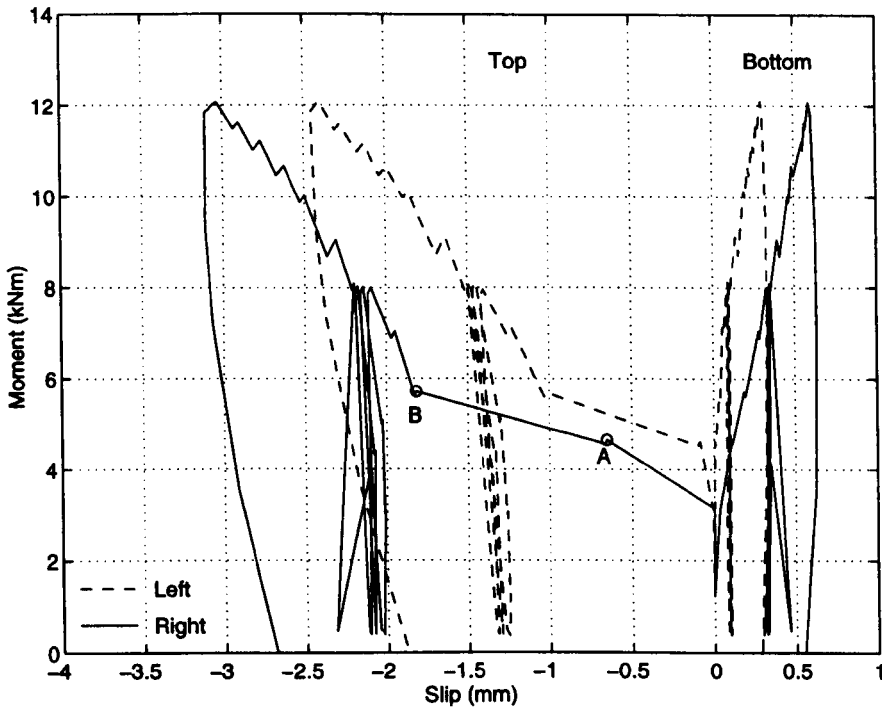


Figure 5.16: Moment-slip curves for connection STmj.

flange. This continuous increase in slip, with increase in the moment, is shown in **Figure 5.16**, and may be explained as the result of such deformation. In contrast the sudden increase in slip, such as from point A to point B in **Figure 5.16**, represents the real slip movement between the beam and the steel cleat.

In **Figure 5.16**, the slip measured at the top of the connection is negative and is much higher than the positive slip at the bottom. It is the addition of the two values of slip that with **Equation 4.1** determines the rotation r due to these inherent effects.

Figure 5.17 presents the moment-strain curves for the column bolts used as column flange stiffeners. It shows that the upper-most surface of the four bolts has compressive strain. This tells us that the top bolts were under bending action and

that the deformation was downward.

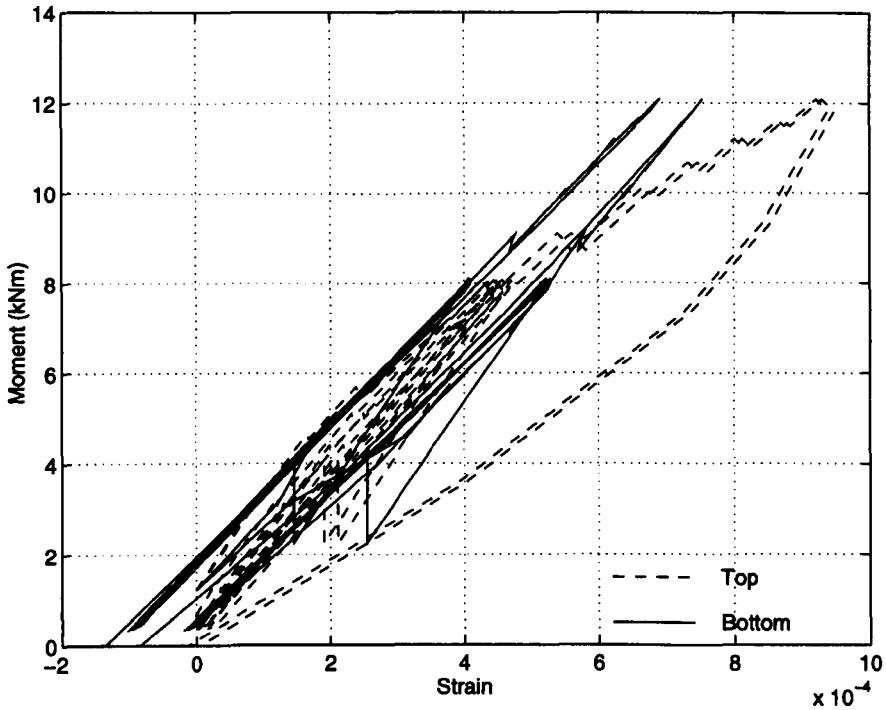


Figure 5.17: Moment-strain curves for the column bolts in connection **STmj**.

5.6.2 Test of Connection **STmn**

The moment-rotation curves for connection **STmn** are presented in **Figure 5.18**, in which both data taken immediately after a loading increment and after a time elapse of 5 to 10 minutes are given. The small difference between the two sets of data show that relaxation was small throughout the test. Note that there was a similar response for both left and right connection.

First slippage occurred in the right-side connection between the beam and the top steel cleat when the moment was 5 kNm. Continuous slippage in both left and right connection was then found on increasing moment. Due to an extremely large

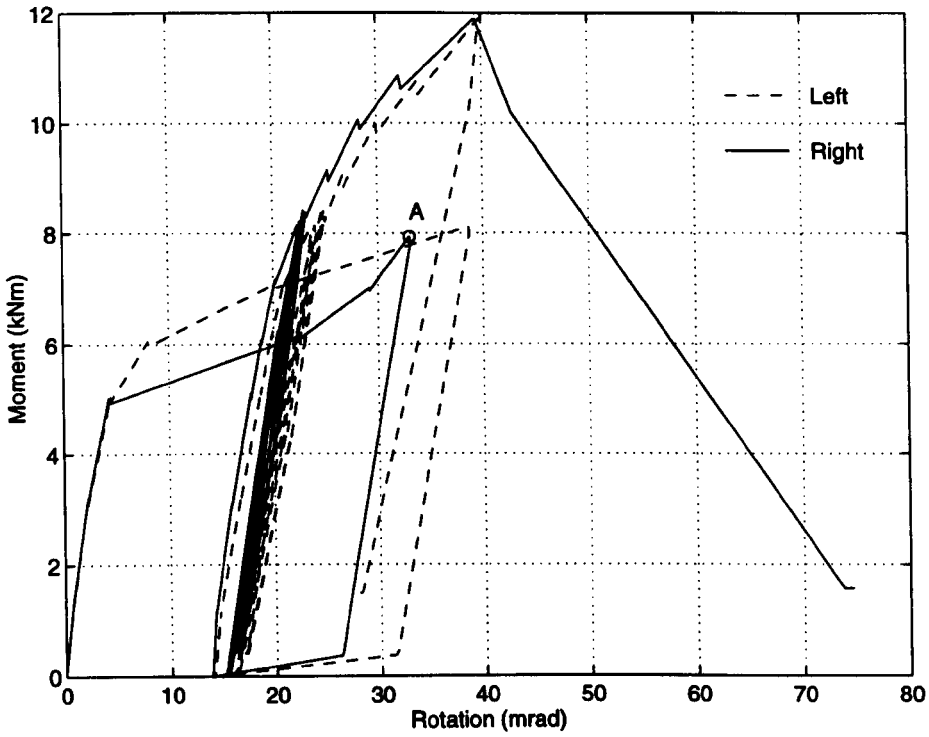


Figure 5.18: Moment-rotation curves for connection **STmn**.

slip movement (see **Figure 5.18**, point A), the frame was unloaded when moment was 8 kNm. After unloading, a 10 mm wide steel package was placed into the gap between the beam-end and the column web (see **Figures 5.10** and **5.19**), then the frame was reloaded following the test procedure given in **Section 5.5.2**. After repeating loading and unloading cycles, the frame was finally loaded to ultimate failure, and the failure moment load was about 12 kNm.

In the final part of the test when the moment was greater than 8 kNm, a crack along the internal radius of the web and the top flange of the beam, and near to the joint itself (see **Figure 5.19**) was observed. The moment was 11 kNm. When the moment was finally increased to 12 kNm, the top flange of the right-side beam fractured at the narrow net section where the two bolt holes were, and two corner



Figure 5.19: Failure of the right-side beam in connection **STmn**.

pieces of the top flange sheared off. **Figures 5.19** and **5.20** show that there was separation of the reinforcement layers in the top flange near the surface and slight surface cracking along the internal radius of the web and the top flange. When ultimate failure of the right connection occurred the strength of the connection disappeared. No buckling deformation in the beam or column members were observed. The final deformation of the specimen is shown in **Figure 5.21**

The direct strain for the horizontal legs of the steel cleat against the applied moment and the connection rotation are plotted in **Figures 5.22** and **5.23**, respectively. **Figure 5.22** shows that the surface of horizontal legs of the bottom cleat angles with the strain gauge on it had compressive strain whereas the surface of

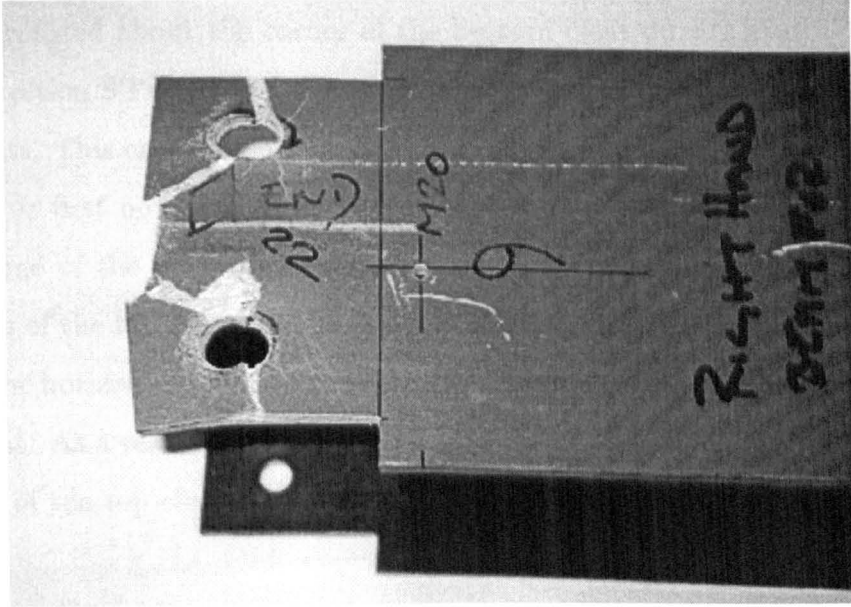


Figure 5.20: Failure mode of the right-side beam in connection **STmn**.

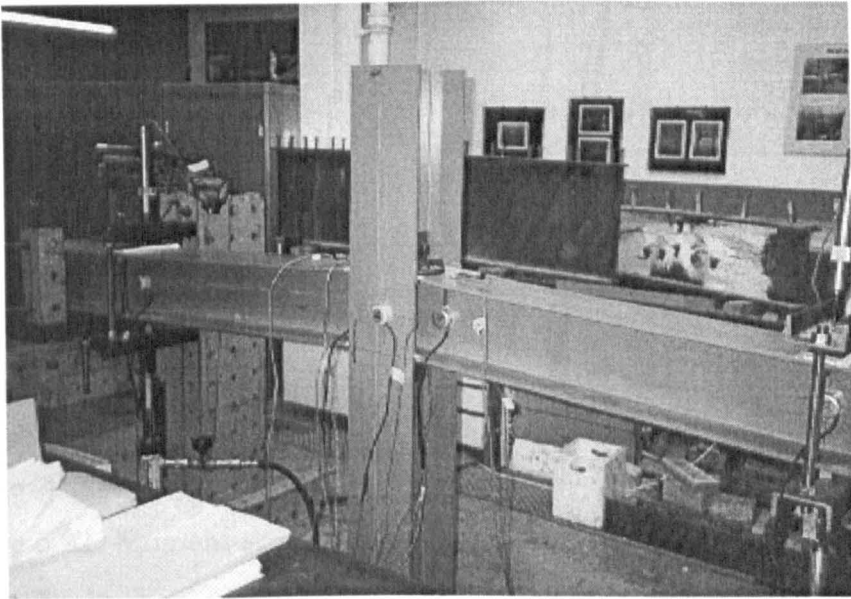


Figure 5.21: Final deflection of the beams in connection **STmn**.

horizontal legs of the top cleat angles had tension strain. This result indicates the connection rotated about the corner of the bottom cleat during loading. As in the test of connection **STmj**, the strain of the bottom cleats is larger than the strain of the top cleats. This can also be seen from the data in **Figure 5.23**. To explain what happens, it is first noted that the leg of the steel angle cleat is much stiffer than the top flange of the pultruded beam. When the specimen was loaded, a bowing deformation of the top flange of the beam occurred, which made the bending deformation of the horizontal leg of the top cleat less than that of the horizontal leg of the bottom cleat. As a result of this response in the connection, the measured strain on the surface of the top cleat was smaller than on its equivalent in the the bottom cleat.

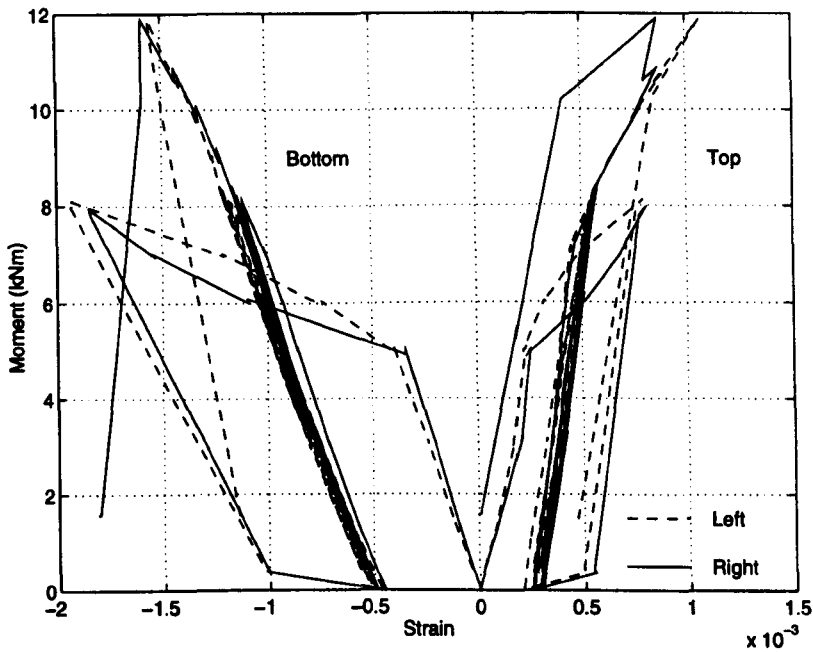


Figure 5.22: Moment-strain curves for the cleats of connection **STmn**.

The slip (between the cleat and the beam) against moment is presented in **Figure 5.24**. It shows that at the bottom-right of the joint there was reverse slip. This

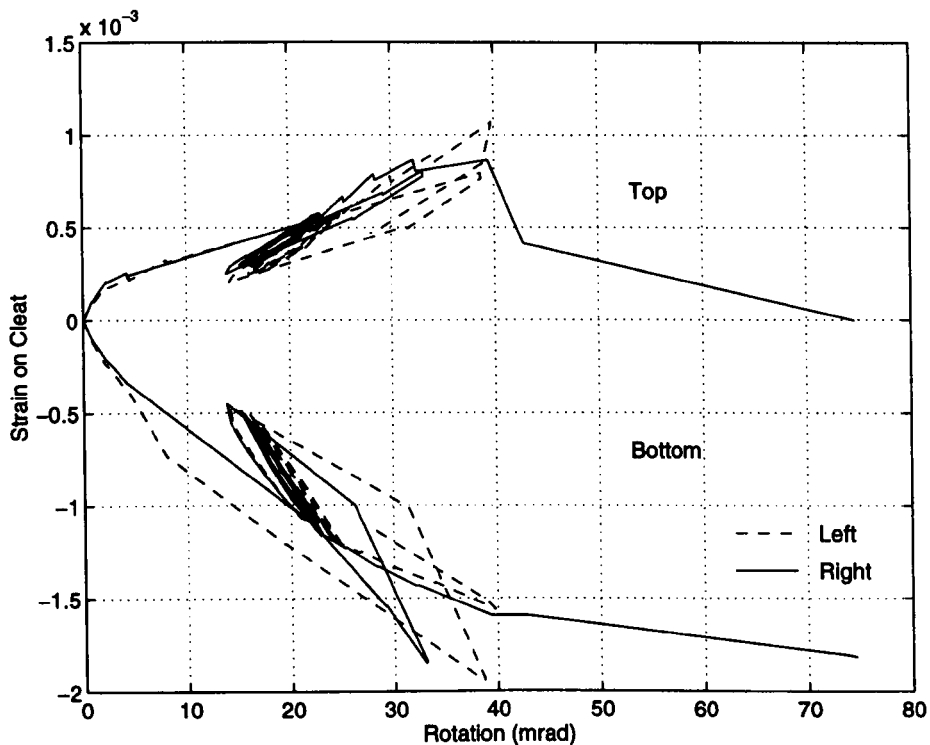


Figure 5.23: Strain-rotation curves for the cleats of connection **STmn**.

was due to the effect of inserting the steel package between the beam-end and the column, which forced the beam to move away from the column.

Just prior to ultimate failure, **Figure 5.25** shows the large gap that existed between the top steel angle cleat and the top flange of beam in the right-side connection. This local deformation made measurement of slip by the displacement transducer mounted on the beam flange inaccurate and as such the data in **Figure 5.24** should be interpreted accordingly.

Note that the bending deformation enabled the stiffer steel cleat leg to separate from the surface of the top flange and thereby reduce the frictional force needed to resist slip movement. As a result of this slip in connection **STmn** was much higher

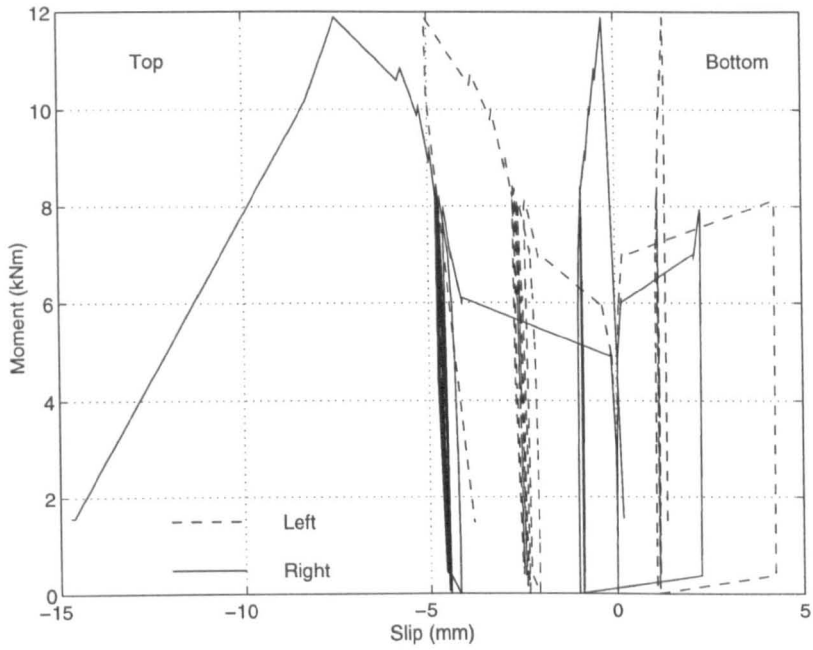


Figure 5.24: Moment-slip curves for connection **STmn**.

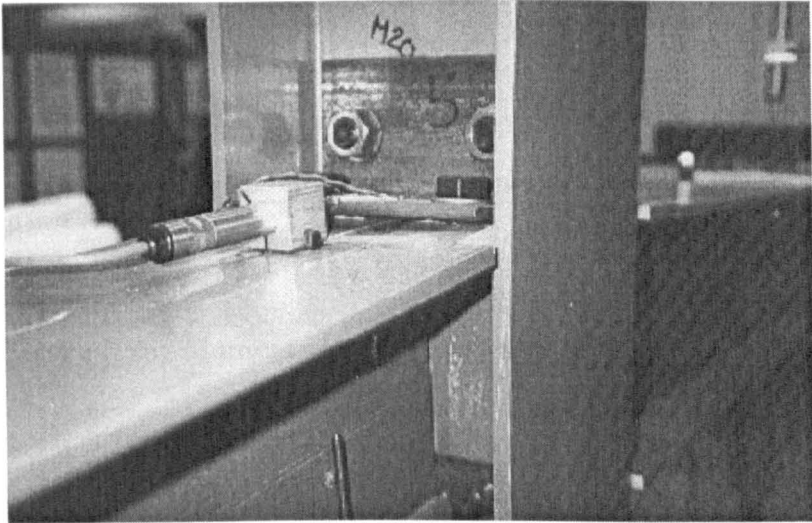


Figure 5.25: Gap between the top cleat and right-side beam in the test of connection **STmn**.

than in connection **STmj**.

5.6.3 Test of Connection **Tmj**

The moment-rotation behaviour of connection **Tmj** is presented in **Figure 5.26**, with data for the two connections (left and right connections) taken immediately after each loading increment and after a time lapse of 5 minutes.

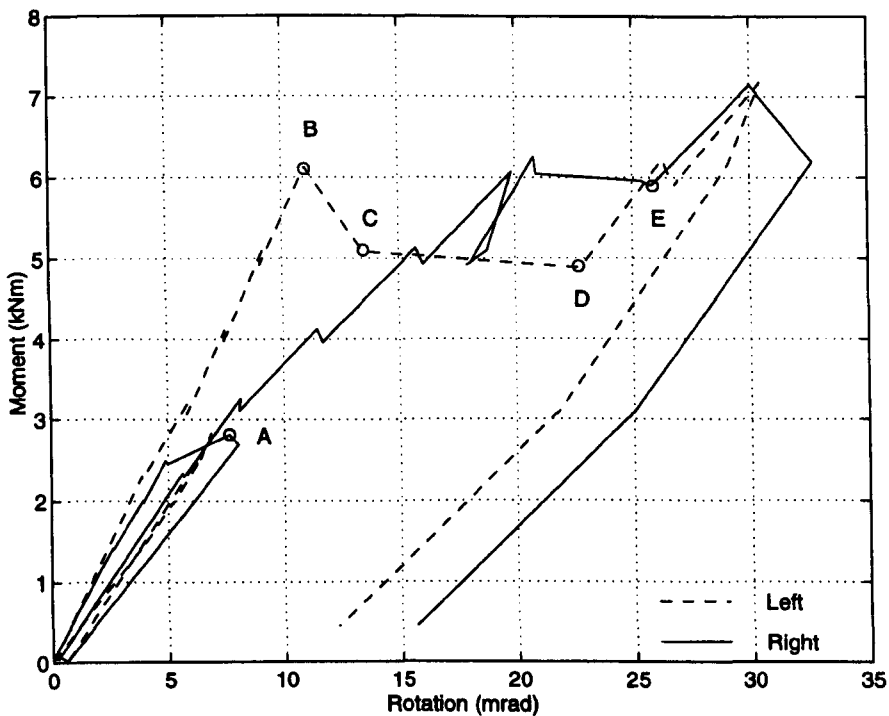


Figure 5.26: Moment-rotation curves for connection **Tmj**.

It can be seen in **Figure 5.26** that slip occurred during the test. The moment-slip curves for the two connections are plotted in **Figure 5.27**. There was little slip at the bottom of the connection. Slippage at the top of the connection was significant when the moment exceeded 5 kNm. These slippages resulted in large

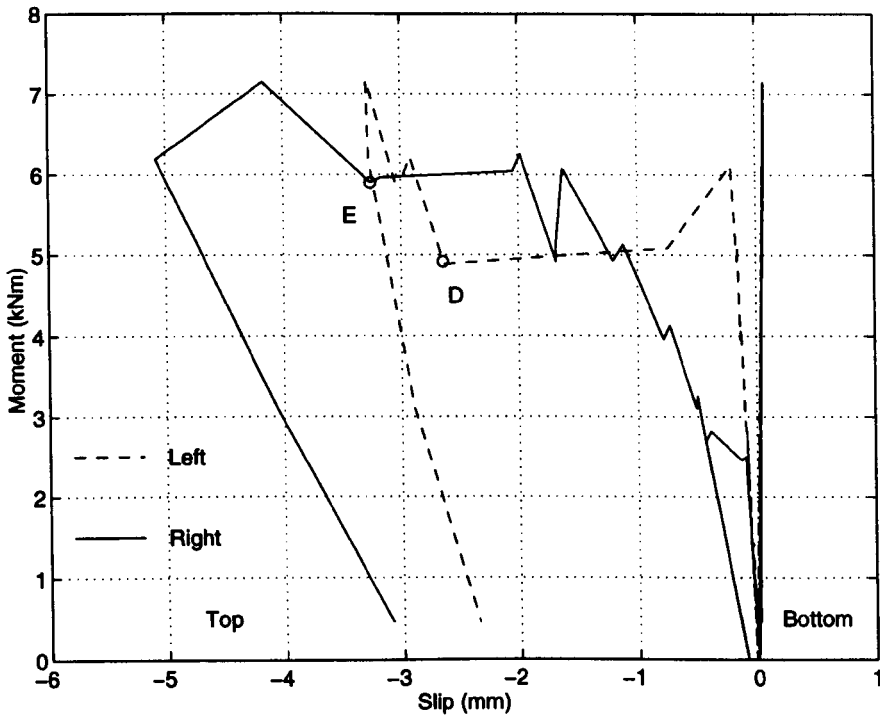


Figure 5.27: Moment-slip curves for connection **Tmj**.

connection rotation and was the reason why this connection design proved not to meet the requirements needed for a practical semi-rigid 8 inch connection.

By eliminating the rotation due to slip from the moment-rotation curve in **Figure 5.26**, the connection moment-rotation behaviour without connection slip is obtained and this is given in **Figure 5.28**.

Due to the fact that the two composite bolts were only hand tightened, each connection was too flexible during the early stage of loading and the top pre-preg cleat and column flange separated at the low moment of 2.4 kNm. When the moment had increased to 2.7 kNm, adhesive debonding at the mating surface of top right cleat (see **Figure 5.4**) and the beam flange occurred. This deterioration in the specimen was signalled by a loud 'bang'. The connection showed rather lower stiffness than

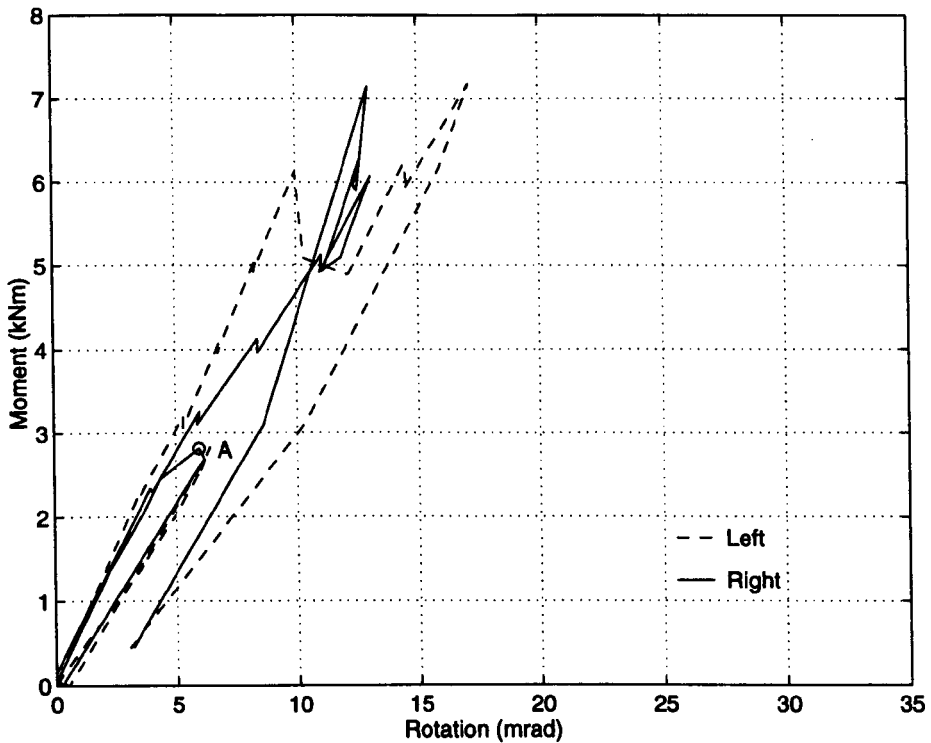


Figure 5.28: Moment-rotation curve of connection T_{mj} (without slip).

was expected based on the results of the set of tests using pultruded connection pieces by Bass and Mottram (1994). Therefore, the specimen was unloaded (point A in **Figure 5.26**) and the composite bolts were re-tightened so that column and cleat would not separate. During the second loading of the specimen, debonding of top left-cleat, over the mating surface of the cleat and the beam flange, occurred when the moment exceeded 3 kNm and this continued as the moment increased. After 5 minutes at the moment of 6 kNm (point B in **Figure 5.26**), horizontal slip in the left connection occurred between the top cleat and beam occurred with a 'bang', and this was followed by the moment reducing slightly to 5.1 kNm (point C in **Figure 5.26**). The moment was again increased to 6 kNm and slip increased significantly to 2.6

mm on the left side connection, and was accompanied by the moment dropping to 4.8 kNm (point D in **Figure 5.26** and **5.27**). With moment increased to 6.5 kNm, the debonding of the mating surface between the top right pre-preg cleat and the beam top flange developed completely. There was an audible ‘bang’ and there was a slip increase on the right-side connection (point E in **Figure 5.26** and **5.27**). When the moment increased to 7 kNm slip continued to grow. A crack at the fillet of the top flange and the web of the beam was observed. The test on connection **Tmj** was terminated because it was obvious that the connection did not have the structural performance required.

Figure 5.29 shows the specimen and its deformation at the end of the test and just prior to unloading. Even at such a low connection moment of 7 kNm the local connection deformation can be clearly observed. It also can be seen that on the right-side, the opening-up of the bonded mating surface between the top flange of the beam and the end-part of the cleat’s horizontal leg was larger than that for the left-side connection.

Due to this opening-up deformation, the measured connection slip was larger than it actually was. As a consequence of this deterioration in the connection there was an over-estimation when the rotation was compensated for the effect of slip.

This effect can clearly be seen when it is noted that the $M - \phi$ curve for the right connection in **Figure 5.28** gives a higher connection stiffness than the equivalent curve for the left connection.

Because this ‘phantom’ of increase in stiffness occurs once debonding has occurred, the effect becomes apparent when the moment exceeded 5 kNm. Subsequently, there was an over-estimation of the effect of the slip on the connection rotation in **Figure 5.28** because such deformation had occurred. Since the open-up deformation on the right-side of the connection was relatively larger than on the left-side, the over-estimate of the slip made the stiffness of the right-side connection

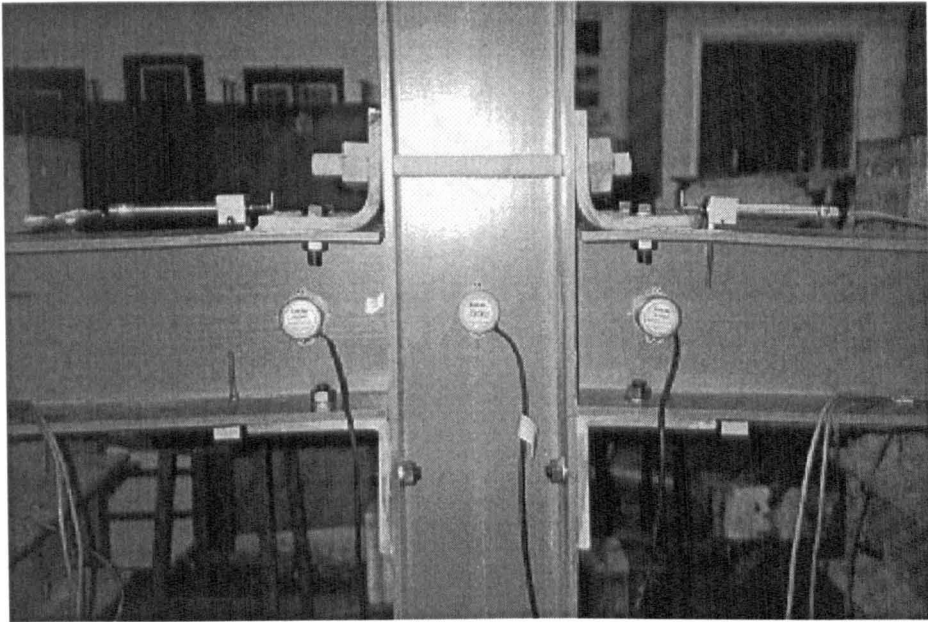


Figure 5.29: Deformation of specimen with connection **Tmj**.

show an increase when the moment was over 5 kNm, whereas this effect on left-side was small.

5.6.4 Test of Connection **TLmj**

The moment-rotation behaviour of connection **TLmj** is plotted in **Figure 5.30**, with data taken immediately after each loading increment and after a time lapse of 5 minutes. The modifications to connection **Tmj**, providing the details for connection **TLmj**, eliminated connection slip such that there was no need to compensate for it. **Figure 5.30** presents the actual $M - \phi$ behaviour. Note that the behaviour of the two connections is similar throughout the whole of the test and this feature is certainly one advantage of the choice of connection details.

The initial moment-rotation behaviour of the connection is linear and no debond-

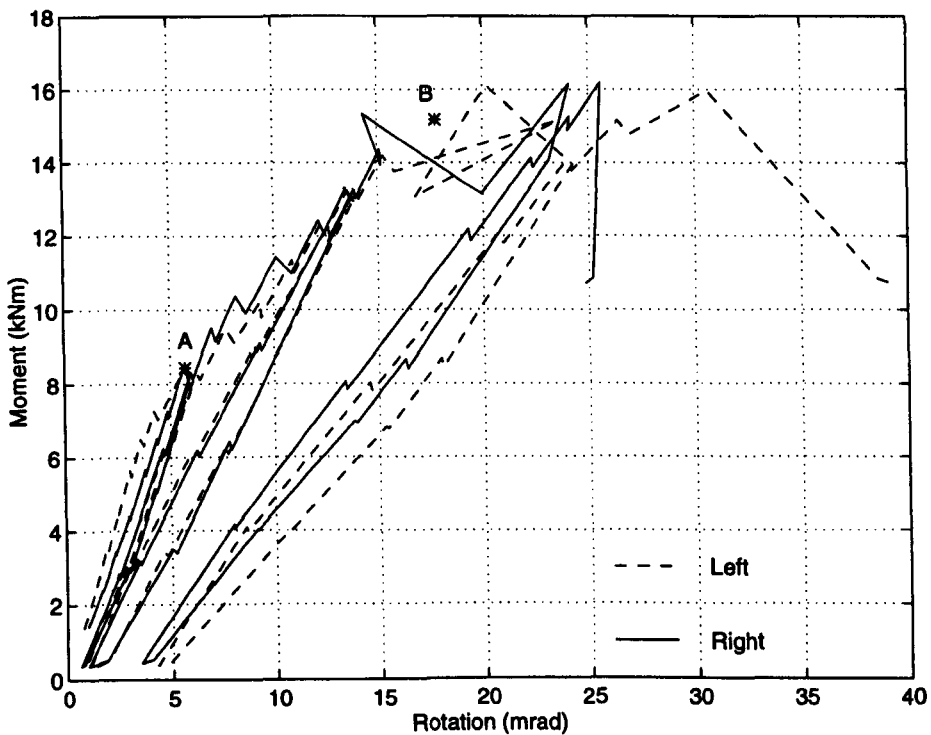


Figure 5.30: Moment-rotation curves of TLMj.

ing or material failure occurred when M was below 4 kNm. A faint crack noise associated with material damage was heard when the moment was just above 4 kNm, but no visual sign of cracking or debonding was observed. Later in the test, this acoustic emission would provide evidence that there was debonding damage growth. When the moment increased to 8.19 kNm (point A in **Figure 5.30**), debonding was first observed at the mating surface of the top left cleat and beam flange from the centre line of the bolts to the corner of the cleats (see **Figure 5.32**).

The moment-rotation curve started to show non-linear behaviour when the moment was 6 kNm and the rotation was 3.39 mrad, for left-side connection, and at a moment of 8 kNm and the rotation of 5.82 mrad, for right-side connection.

The initial stiffness of the left-side connection was slightly higher than the right-

side connection, and the moment-rotation of both connections became similar when M was > 8 kNm; after debonding on the left-side had occurred. The first reloading cycle, from the rotation ϕ of 5.6 mrad, was carried out at this stage in the test and the unloading and the reloading part of the curve gave a similar stiffness to initial loading curve. This indicated that the stiffness was not significantly reduced by the developing debond failure at this stage.

After the moment had increased to 9.27 kNm, debonding was observed on the mating surface of top right cleat and beam flange. Debonding over the mating surface of the top-left cleat and column flange occurred when the moment and the rotation were 11.15 kNm and 10.4 mrad, respectively. Then after a further moment increment had been applied, debonding between the top right cleat and the column flange occurred. The moment was 12.1 kNm and the rotation was 13.5 mrad. After adhesive debonding had fully developed on both sides, the specimen was unloaded from 14.0 kNm and reloaded to observe the change of the connection stiffness. This second cycle of loading showed that both connections had reduced stiffness, the loss of stiffness being due to the development of four regions of debond failure. During the reloading of the connections, delamination cracks in the right-side cleat, around the fillet (**Figure 5.31**), occurred (with loud acoustic emission) at the moment of 15.2 kNm and the rotation of 17.8 mrad (point B in **Figure 5.30**). Further moment increase to 16.05 kNm caused delamination failure to be visible on both sides. Even though there were significant delamination cracks in both pre-preg cleats, they were still able to sustain the applied moment of 14 kNm. The distance between the two column flanges, at the bolt level of the two lower top pultruded cleats, opened up to about 5 mm. This caused the column flange bowing deformation, as observed by Bass and Mottram (1994), and they found it to reduce significantly the stiffness of their semi-rigid connections of pultruded section. It was at this late stage in the test that tension failure along the interface between the web and flange of the

column could be clearly observed (see **Figure 5.34**). The final reloading cycle showed a further reduction in the stiffness of both connections, this being due to the development of the material failures just described. Even though the connection was considered failed, further moment was applied to the connections to obtain the behaviour of the connection up to ultimate failure. This occurred when the moment was 16 kNm, the rotation was 31 mrad on the left, and 26 mrad on the right, with the thread stripping on the 1 inch composite bolt. **Figure 5.33** shows this failure which occurred on the left-side. As no additional moment could be sustained the test was terminated.

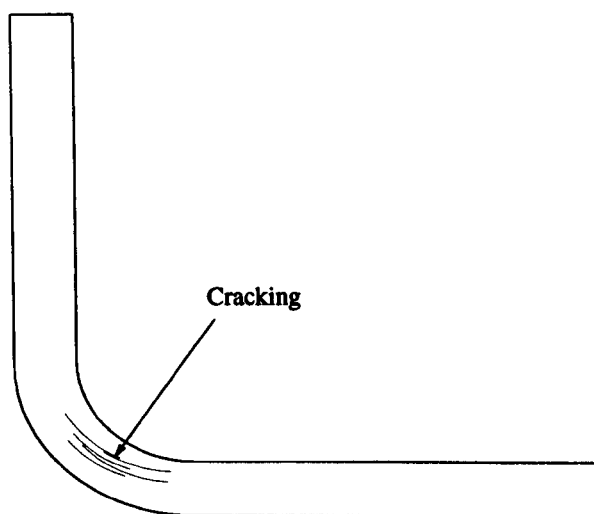


Figure 5.31: Crack on pre-peg cleat.

Figure 5.32 shows the deformation of connection **TLmj** at the end of the test. **Figures 5.33** and **5.34** show the thread stripping failure and the tension failure at the interface of the web and the flange of the column, respectively.

Throughout the duration of the test no slip was monitored by the two horizontal

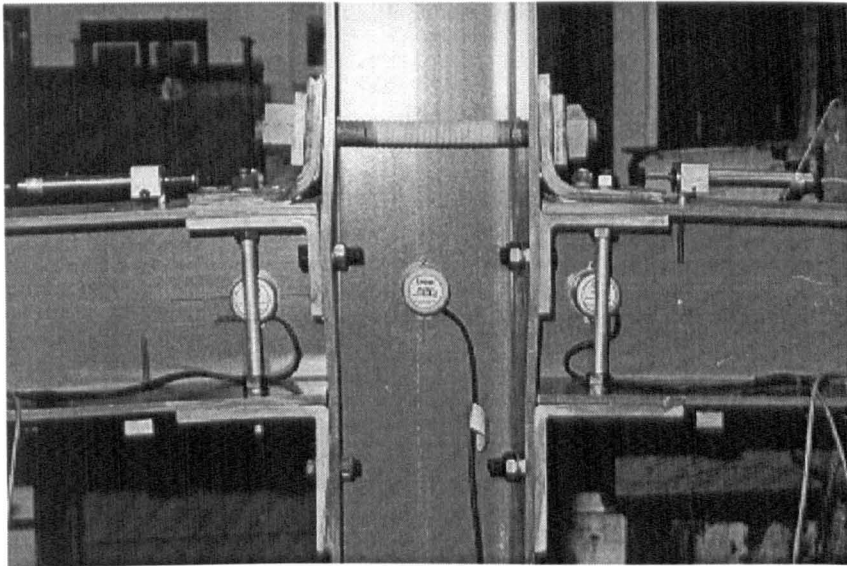


Figure 5.32: Deformation of connection **TLmj** at the end of the test.

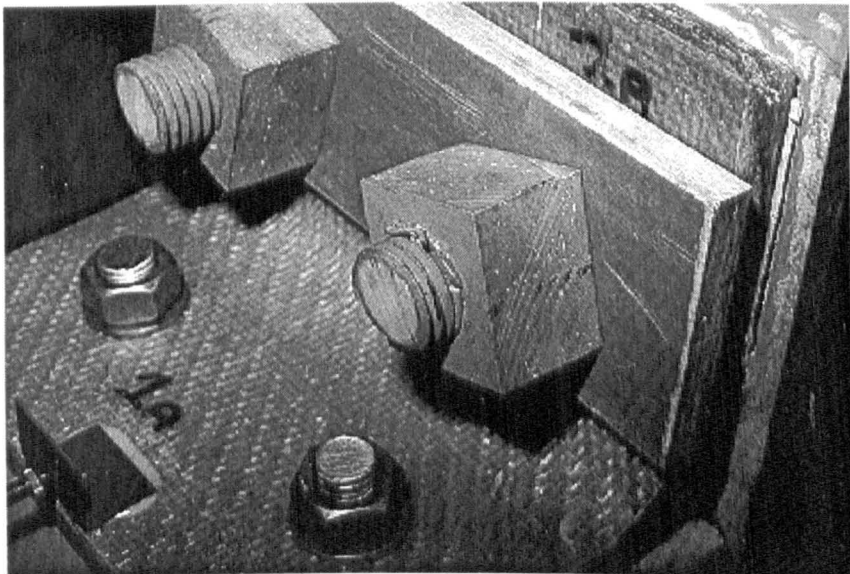


Figure 5.33: Ultimate connection failure due to thread stripping of the composite bolt.

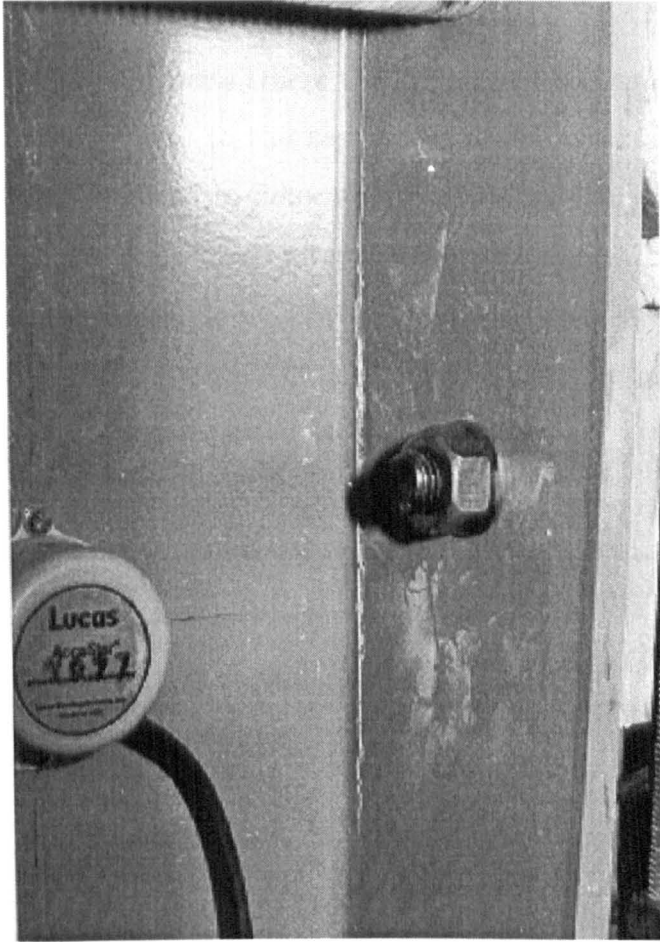


Figure 5.34: Cracking along the interface of the web and the flange of the column.

displacement transducers (**Figure 5.32**). After releasing all load from the connection, the column flange bowing deformation could still be clearly visible. As this deformation did not disappear it was observed that permanent strain of the flanges had been induced.

5.7 Discussion and Analysis of the Test Results

We will first consider the two tests where the connection pieces were of steel. The slip measured was affected due to the separation of the cleat and the beam top flange, and it could not be used to determine the rotation due to the slip. It was noticed that no further slip occurred after the steel packing had been introduced in connection specimens **STmj** and **STmn**. It follows therefore that the moment-rotation behaviour for connections **STmj** and **STmn** can be represented by this part of their curves and these are given in **Figure 5.35**.

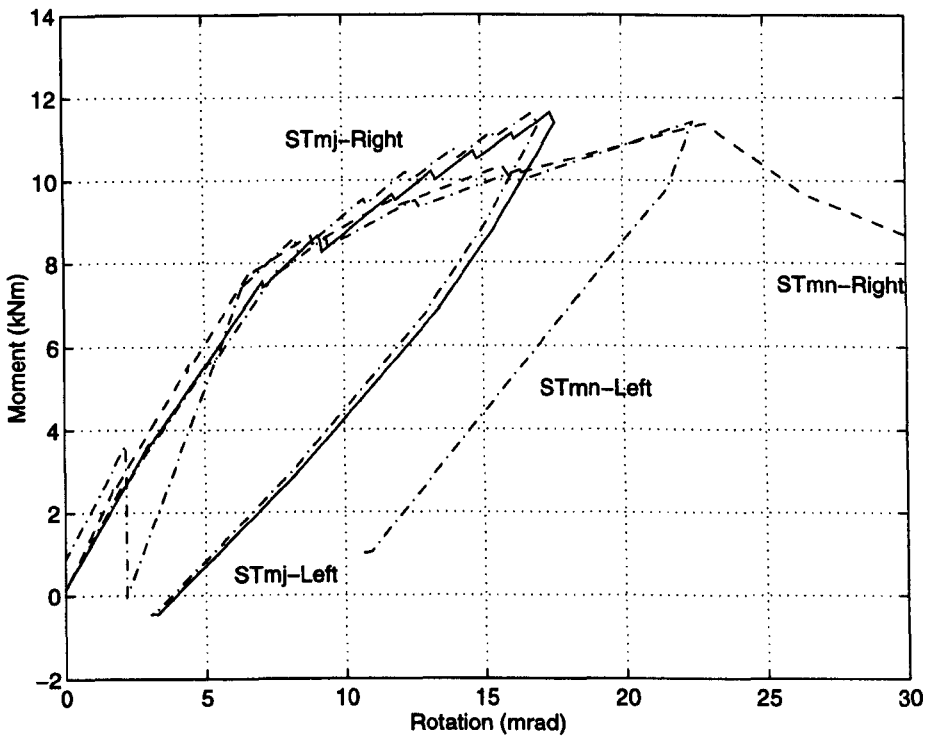


Figure 5.35: Moment-rotation curves for connections **STmj** and **STmn**.

The simplified linear piece-wise moment-rotation curves, obtained from the data of the mean values of the left and right connections taken after lapse of 5 to 10

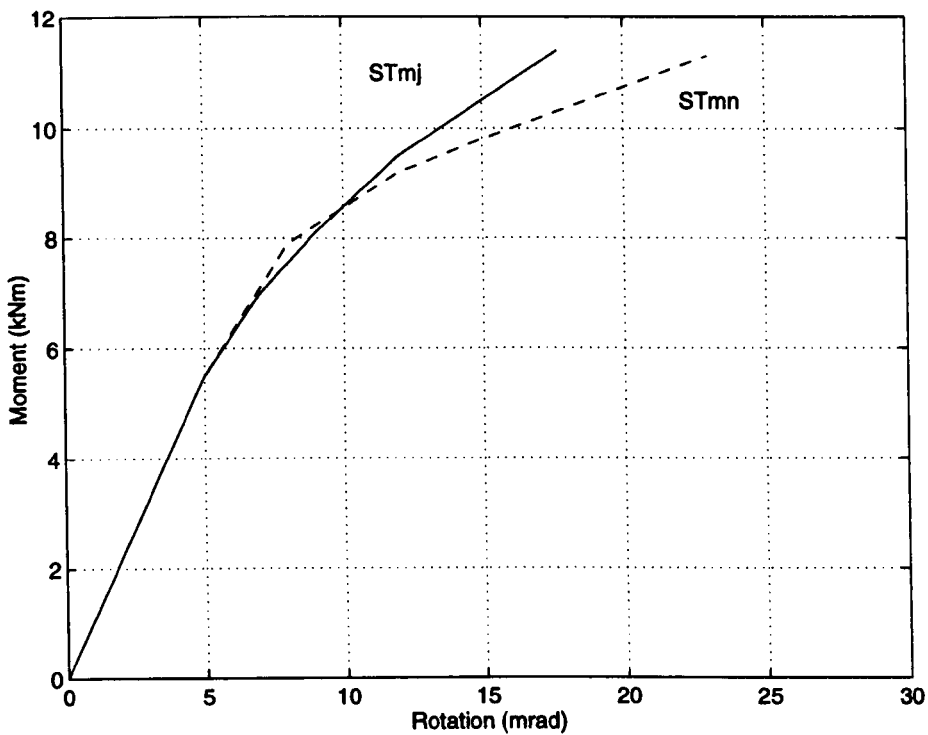


Figure 5.36: Simplified linear piece-wise moment-rotation curves for connections **STmj** and **STmn**.

minutes (see **Figure 5.35**), are presented in **Figure 5.36**, and the corresponding data is given in **Table 5.3**. This data represented the mean connection properties and was from the $M - \phi$ data recorded at least 5 minutes after the load increment had been applied.

It can be seen that:

- the moment rotation curves for both major and minor axis connection are almost identical.
- the column stiffeners in the major-axis connection worked satisfactory.
- the connection stiffness k (moment/rotation) is almost linear up to moment 8

Table 5.3: The data of the piece-wise moment-rotation curves.

STmj		STmn		Tmj		TLmj	
M	ϕ	M	ϕ	M	ϕ	M	ϕ
(kNm)	(mrad)	(kNm)	(mrad)	(kNm)	(mrad)	(kNm)	(mrad)
0	0	0	0	0	0	0	0
5.5	5	5.5	5	3	5.2	6	4
7	7	7.9	8	4.3	8	7.1	5
8.1	9	9.2	12	5.9	12	8	5.9
9.5	12	9.8	15	7	15	9	7
10.5	15	11.3	23			10	8.2
11.4	17.7					11.2	10
						12.7	12.5
						13.8	15
						14.6	17.5
						15.1	20
						15.5	22.5
						15.8	25
						16	30

kNm and then gradually declines.

- the rotation capacity of both connections is in excess of 15 mrad.

In both tests, no buckling occurred in beam and column members. This observation suggests that this type of connection is acceptable for the properties of 8 inch pultruded section. The bottom cleats gave a higher surface strain than the top cleats. As the results of there being a different deformation in the cleats the distance between the two cleats increased. This induced the top flange of the beam to bend upward. Yielding of the steel was measured before the test was terminated, and this showed the necessity to strengthen the bottom cleat. That is to use a leg-angle of thickness $> 8\text{mm}$.

Now we will consider the two 'all-composite' connection tests.

The moment-rotation behaviour of the two pre-preg cleated connections **Tmj** and **TLmj** are presented as simplified linear piece-wise moment-rotation curves in **Figure 5.37**. Each of these curves represents the mean values of the data from left and right connections 5 to 10 minutes after the moment/rotation increment was applied. For connection **Tmj**, the slip effect on the rotation had been removed using the method described in **Section 5.5.4**. The data for these piece-wise moment-rotation curves are given in **Table 5.3**. For comparison, the $M - \phi$ curves of Bank's novel prototype connection (**Figure 3.7 (d)**) and Bass & Mottram's **DTLmj** connection (**Figure 3.8**) are also given in **Figure 5.37**.

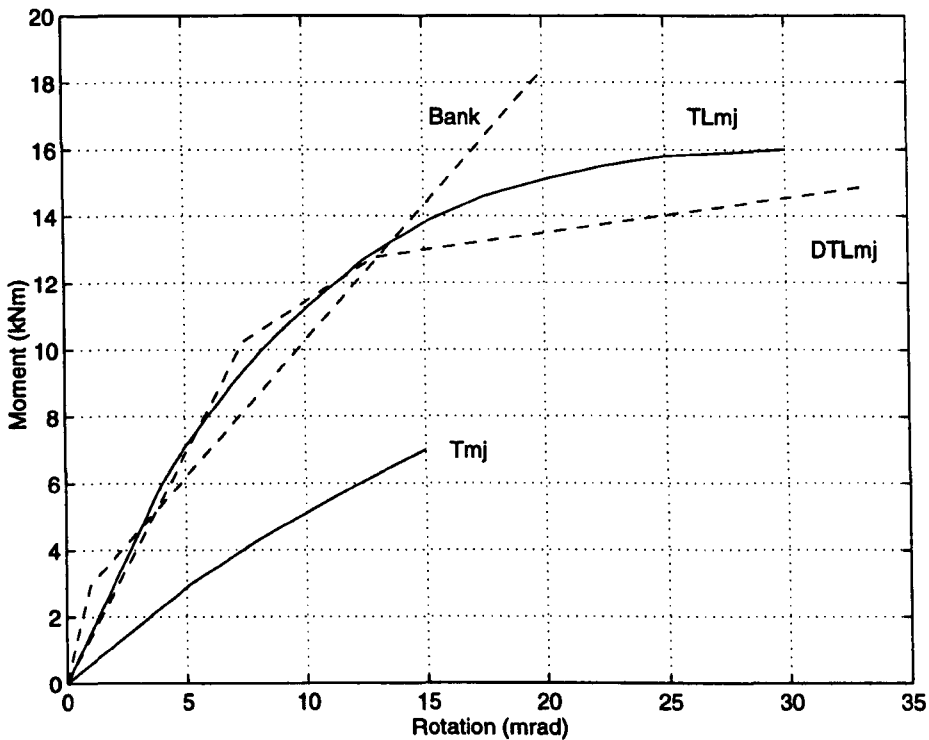


Figure 5.37: Simplified linear piece-wise moment-rotation curves.

It can be seen that both connections **Tmj** and **TLmj** possess a gradually changing non-linear moment-rotation behaviour. Their $M - \phi$ curves consist of two

phases, one is a linear elastic phase which is related to initial linear elastic deformation, the second is a non-linear elastic phase, which is related to the debonding, the cracking in the pre-preg cleat, and the bowing deformation of column flange.

Figure 5.37 shows that the $M - \phi$ curves of connections **TLmj**, **DTLmj** and **Bank** closely resemble each other when M is below 13 kNm. Connections **TLmj** and **DTLmj** gave a higher stiffness than Bank's connection for $M \leq 12$ kNm, and more rotation capacity for $M > 12$ kNm. This higher rotation capacity is due to the flexibility of the member flange, and if the flanges of members are reinforced, the stiffness of connection will increase. As a consequence of stiffening a connection, its rotation capacity may be sacrificed. This is an important consideration when further consideration is being given to the development of semi-rigid connection details.

Due to its lower than expected stiffness the test with connection **Tmj** was terminated before ultimate connection failure. On examination of the connection it was found that several factors led to these unsatisfactory results. The first factor was the stiffness of pre-preg cleat itself. Compared with the top cleat in connection **DTLmj**, the section of 24 layers pre-preg cleat was only 14 mm thick and 190 mm wide, whereas the double top angle cleats of connection **DTLmj** was 25.4 mm of thickness and 200 mm of width. This meant the pre-preg cleat had only 30 % stiffness of the double thickness pultruded cleat, in which $E_{pre-preg}$ was taken as 24kN/m^2 and $E_{pultruded}$ as 5.5kN/m^2 (see Table 2.2). The second factor was the flexibility of the beam flanges of the 8 inch WF section. As the beam rotated under loading the top flange of the beam beneath pre-preg cleat bent upward. This resulted in an increase in connection rotation and thereby manifested itself as a reduction in stiffness. The third factor was the slackness of the composite bolts. One reason for the composite bolts only having the nuts 'finger tight' was a concern that too high pretension would limit their resistance. In the event, and after the bolts were tightened using a spanner the connection design itself was found to limit

the connection structural performance; the 1 inch composite bolts were acceptable. The fourth, and final, factor was the debonding on the mating surface of the beams and pre-preg cleats. This factor caused slippage between the beams and the cleats at lower loading levels.

There were two reasons why complete debonding developed at such an early loading stage in connection **Tmj**. The first reason was the choice of bonding surfaces shown in **Figure 5.4**. Due to bolt action, the mating surface between the beam's top flange and the front part of the top cleat leg (from the centre line of bolts to the end of cleat leg) was subjected to prying action. In contrast, the mating surface between the beam and the rear part of the top cleat leg was subjected to bearing and shearing action. To prevent slip between the cleat and the beam it is obvious that the choice of bonded surfaces should be the rear part of the cleat leg rather than the front part of the cleat leg. The second reason was the result of exposed glass fibres on the mating surface of the beam members, and this was because these members had been used in a previous connection test with cleats bonded to them. Removing the bonded cleat from the beam had caused the surface layer of the pultruded beams to be damaged and to expose beneath a CFM fibre layer. It was this surface that was used to bond to and its through thickness strength was lower than might have been expected. Ignorance of how the exposed fibre layer would reduce the bonded strength led to the connection poor performance. However, by choosing to bond to a damaged pultruded material we have observed that this should not be done in practice.

The initial moment-rotation curve of the right-side connection in test **Tmj** was stiffer than the left-side connection. This situation was reversed on reloading after unloading the specimen and re-tightening of the square composite nuts. This phenomenon was recognized to be due to the change of the position of the square composite nuts after tightening up (**Figure 5.38**), which affected the stiffness of the

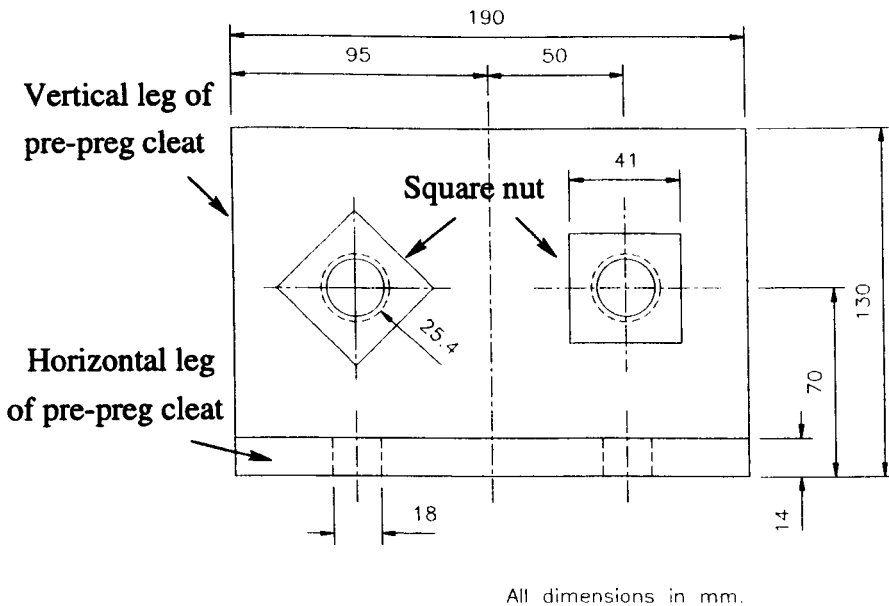


Figure 5.38: The position of the square composite nuts and the pre-preg cleat of connection T_{mj} .

vertical leg of the pre-preg cleats. In **Figure 5.38**, the position of the square nut on the left will increase the connection stiffness, whereas the position of the square nut on the right will minimise the connection stiffness.

In view of the above deficiencies in the details of connection T_{mj} , several modifications were introduced in connection TL_{mj} (see **Figures 5.5** and **5.32**). Two rectangular plates were cut from 6x6x1/2 inch pultruded equal leg angle and each one was placed against a vertical leg of a pre-preg cleat. This modification helped to eliminate the effect of the position of the composite nuts and the plate also had the function of increasing the stiffness of the vertical cleat leg. In order to increase the overall connection stiffness, lower top pultruded cleats were cut from 6x6x1/2 inch equal leg angle and fitted underneath the top flange of the beams and steel bolts of 16 mm diameter were extended to both top and bottom flanges to reinforce the

beam section. This improvement resulted in a much stiffer and stronger connection. It can be seen from the $M - \phi$ curves in **Figure 5.37** that the initial stiffness of connection **TLmj** and the moment at which the connection starts to behave nonlinearly are significantly higher than those properties for connection **Tmj**.

Application of the adhesive bonding increased the initial stiffness of the connection and later as the debonding gradually developed, the connection stiffness decreased correspondingly (**Figure 5.30**). After debonding was complete the final reloading stiffness of the connection was constant and independent of the number of load cycles. The linear relationship of the final moment-rotation reloading curve (**Figure 5.30**) showed the elastic response of the connection design, even after damage had developed in it.

At the ultimate failure of connection **TLmj** the column flange had, level with the bolts connecting the lower top cleat, opened up by about 10 mm, which contributed to the connection rotation of more than 30 mrad. In other words, if such bowing deformation of the column was further reduced by additional stiffeners, the connection could be even stiffer.

The two pre-preg cleat connection tests showed the capability of such cleats to resist failure due to prying action at low moments and therefore overcame one deficiency of the semi-rigid cleated connections using pultruded sections (Bass & Mottram, 1994). The cleats did start to fail by delamination, when the moment was 15 kNm and the rotation was 17.7 mrad. Despite the presence of delamination cracks, connection **TLmj** did not lose its ability to sustain a high moment and still had potential to sustain further moment increments. The two connections (left and right) ultimately failed by thread stripping of a composite bolt. Unfortunately, this mode of failure is sudden and catastrophic. It is interesting to note that even though the connection experienced a rotation of 30 mrad and a moment of 16 kNm, no damage had developed in the lower top pultruded cleat. In the previous connection

tests by Bass and Mottram (1994) it was usual to observe delaminations in pultruded sections used as top cleats. This suggests that cleats of pultruded leg-angle are more suitable to be used as lower top cleat rather than top flange cleat.

Figure 5.30 shows that connection **TLMj** had permanent deformation when unloaded. This permanent rotation was induced when the curve started to show non-linear behaviour and increased with rotation. Since non-linear connection behaviour is related to the damage that develops in the connection during the loading, this may suggest that permanent rotation is related to the damage of connection material and its value is directly proportional to the extent of damage in the connection.

There were three types of damage observed, delamination cracks, permanent column flange bowing (caused by column flanges open up) and adhesive debonding. Material fracture and column flange bowing were most likely the types of damage that gave the permanent rotation observed. It was noted that delamination cracks did not close up and the bowing deformation of the column flange remained, even after the specimen was unloaded. Debonding was believed not to cause any permanent rotation, just a reduction in the connection's stiffness.

Figure 5.26 and **5.30** show that the initial $M - \phi$ unloading curve was linear, but when non-linear behaviour of the connection appeared, the curvature of the unloading curve was increased with the increase of rotation which the connection was subjected to. This is to be contrasted to the reloading which was linear on all occasions.

Table 5.4 presents the connection properties of initial stiffness, k_{ini} , moment, M_{ini} and rotation, ϕ_{ini} , and at ultimate failure the moment M_{ult} and ϕ_{ult} .

For a practical semi-rigid connection slip is not acceptable for two reasons. First, if such slip occurs in a connection, its actual stiffness will be greatly reduced. Second, there is uncertainty to 'where' and 'when' such slip will occur. Therefore, the author considers connection slip as a major problem when developing a practical semi-rigid

Table 5.4: Connection properties.

Connection	M_{ini} kNm	ϕ_{ini} mrad	$k_{ini} = M_{ini}/\phi_{ini}$ kNm/mrad	M_{ult} kNm	ϕ_{ult} mrad
Tmj	3	5.2	0.6		
TLmj	6	4	1.5	16	30
DTLmj †	2.5	1.9	1.3	14.9	33.4
Bank ‡	2.9	1	2.9	18.4	20.3

† Mottram (1994). ‡ Bank et al. (1994 b).

connection, and this problem needs to be solved. In the test for connection **TLmj** such connection slip was successfully prevented by using full adhesive bonding, but this practice is believed not to be practical. It not only increases the connection cost, but also involves a complicated fabrication work. Moreover, by having bonding in the method of connection, the frame can no longer be disassembled and so one potential advantage of a light weight frame is lost. For these three reasons, it would be sensible to develop a connection that did not need bonding and still met the requirements needed for semi-rigid action to benefit design of frame.

It was noteworthy that no slip occurred throughout the whole test procedure of connection **TLmj**, even though debonding developed. This raised the question ‘what was it that resisted the slip?’ After the test was terminated the specimen was dismounted. It was found that the composite bolts were quite easy to remove, whereas the steel bolts of the beam flange stiffener were not easy to take apart. This is believed to be the result of some grease being applied to the composite bolts, but not to the steel bolts. All bolt hole were filled with the epoxy adhesive used to bond surfaces of the connection. This bonding material had squeezed into the holes during the fabrication of the connection. The clearance holes were therefore grouted and because the bolts were now fixed-in, they were able to resist connection slip. This observation may lead to a solution to the problem of the connection slip for

semi-rigid connection design by only applying an adhesive bonding material to the bolt hole. This will simplify the connection fabrication procedure. No preparation work will be needed and the bonding material can be applied at the time of frame fabrication. If this is successful, it will greatly save on labour and material costs and make such connection application practical. Such practice has a secondary advantage of protecting exposed fibres on the surface of the drilled bolt holes.

5.8 Benefits of Semi-rigid Connections

Semi-rigid connections possess both a stiffness and a moment resistance which will be of benefit in frame design. To illustrate the role played by these connections and the benefit which can be achieved, a simple example of a 6 meter span, 8 inch WF pultruded beam with different beam end connections is now given. The elastic modulus, cross-section area and moment of inertia of the beam are given as $E = 1720 \text{ kN/cm}^2$, $A = 56.3 \text{ cm}^2$ and $I = 4128 \text{ cm}^4$, respectively (MMFG, 1989). Analysis was carried out by using computing programme developed in **Chapter 7** and the linear piece-wise moment-rotation curves shown in **Figure 5.37** were used to represent the behaviour of the connections. The results of this analysis are given in **Table 5.5**, in which ω represents distributed load, δ represents mid-span deflection, M_{ms} represents mid-span moment, M_e and ϕ_e represent beam-end moment and beam-end rotation, respectively. A limiting values for deflection $L/250$ is used, which is the serviceability limit state recommended to general public access flooring (Clarke, 1996), and this gives a 24 mm allowance of deflection. For a perfectly pinned connection, the distributed load ω is determined and used to determine the benefit of connection stiffness. With this load value, the three connections (**Tmj**, **TLmj** and **DTLmj**) give a reduction of 57 to 74 % in deflection respectively. If the mid-span deflection is kept constant at 24 mm, the four 'semi-rigid' connections

show a load increase from 123 to 215 %. In other words, to design for the beam with pinned connection is to lose 2.2 to 3.2 times the loading that can actually be applied.

Table 5.5: Connection performance.

Beam End Connection	ω kN/m	Load Factor	δ mm	Deflection Factor	M_{ms} kNm	M_e kNm	ϕ_e mrad
Pin	1.012	1	24	1	4.55	0	12.8
Fixed end	1.012	1	4.8	0.2	1.52	3.04	0
	5.061	5.00	24	1	7.59	15.18	0
Tmj	1.012	1	10.40	0.43	2.40	2.15	3.730
	2.253	2.23	24	1	5.48	4.65	8.880
TLmj	1.012	1	7.42	0.31	1.93	2.62	1.748
	3.167	3.13	24	1	6.17	8.08	5.989
DTLmj	1.012	1	7.62	0.32	1.96	2.59	1.877
	3.190	3.15	24	1	6.19	8.17	5.916
Bank	1.012	1	6.24	0.26	1.75	2.81	0.956
	2.995	2.96	24	1	6.04	7.44	6.533

Note: the second line for each connection gives the results for the beam has 24mm mid span deflection.

The results of this comparison are also illustrated in **Figures 5.39** and **5.40**.

The performance of the connections in the above beam analysis is illustrated in **Figure 5.41**, in which the serviceability beam-line (see **Section 7.4.8**) and beam-line are also presented. It can be seen that when the deflection reaches 24 mm (the serviceability limit), the connection has a moment and rotation indicated as the intersection point of $M - \phi$ curve and the serviceability beam-line, whereas the intersection point of $M - \phi$ curve and the beam-line given the moment and the rotation when the load is kept as the same as simply supported beam (see the first row for each connection in **Table 5.5**).

If the ultimate moment of a member is higher than the moment of the intersection of $M - \phi$ curve and the serviceability beam-line, then the serviceability beam-line can

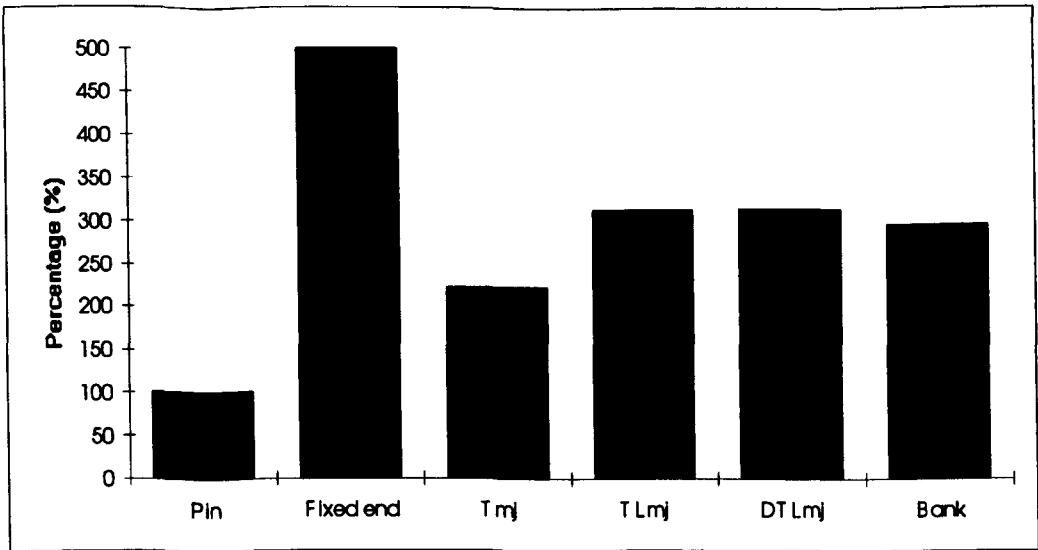


Figure 5.39: Comparison of load increase for the beam with different beam-end connections.

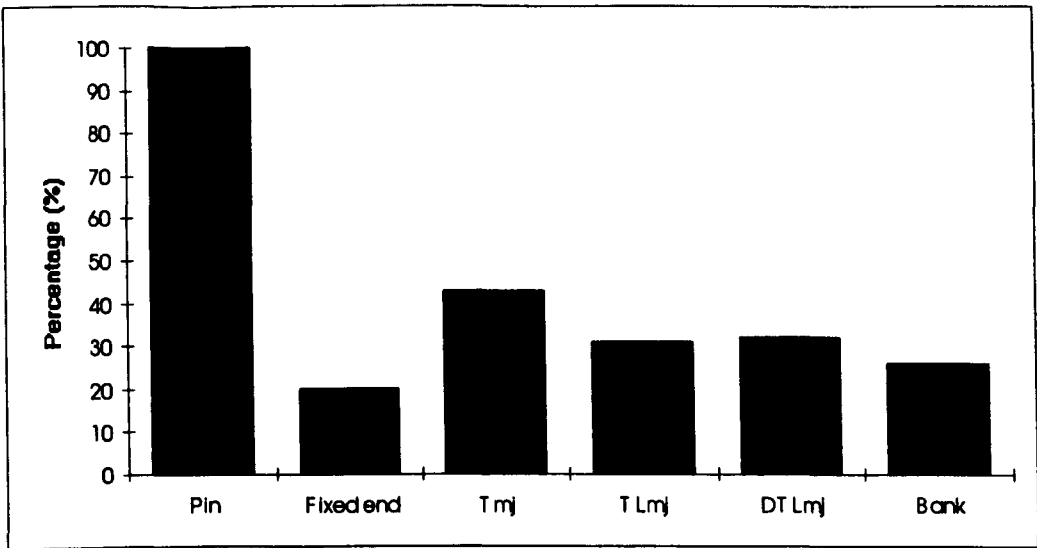


Figure 5.40: Comparison of the middle span deflection for the beam with different beam-end connections.

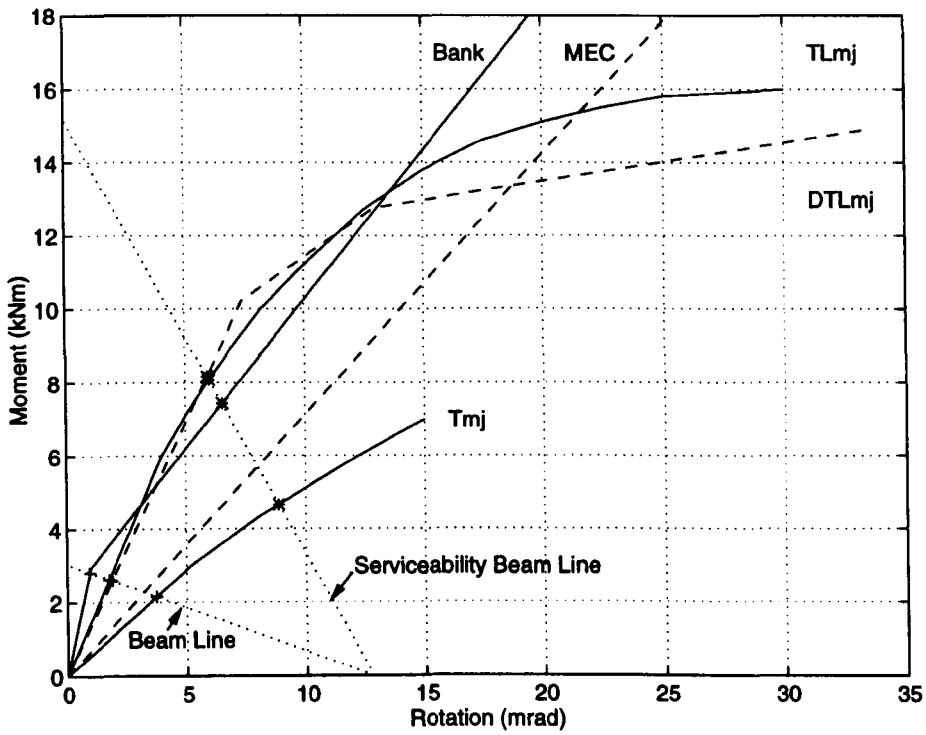


Figure 5.41: Comparison of connection performance in the beam analysis.

be used in design. This is always going to be the situation for frames of pultruded section. Such an approach to design will therefore result in a more economical design than by simply using the conventional beam-line (Nethercot, 1985).

The linear line **MEC** represents a **Moment Equalised Connection** which means the connection with this $M - \phi$ behaviour can make the beam-end moment and the middle span moment equal (see **Section 7.4.8**). The intersection point of the $M - \phi$ curve of the connection and the serviceability beam line is below the **MEC** line, which indicates that the beam-end moment is less than the mid-span moment, whereas is above the the **MEC** line, which means that the beam-end moment is higher than the mid-span moment. The greatest benefit of semi-rigid connection can be achieved by using a connection with moment-rotation behaviour like the

MEC line. It is author's view that the ideal connection stiffness for the design of semi-rigid connection will be close to the MEC line.

5.9 Conclusions

From above analysis and discussion of the connection tests the following conclusions are drawn:

- The short-term moment-rotation behaviour of four 8 inch WF beam-to-column cleated connection has been determined.
- Initial moment-rotation behaviour of each connection was linear. The moment at which the curve showed non-linear was 5.5 kNm for both connections **STmj** and **STmn** and was 3 and 6 kNm for connections **Tmj** and **TLmj**, respectively. The start of nonlinearity behaviour was gradual for both connections.
- The moment-rotation curve of connection **TLmj** is smooth and the stiffness of the connection decrease gradually.
- As the rotation of the connection increases the value of the permanent rotation due to connection deterioration increases.
- Bonding and bolting can prevent slippage between the beam and the cleats at all load levels, and therefore make the connection stiffer.
- Application of bonding improves the initial stiffness of the connection. However, as debonding could not be prevented from developing, the stiffness of a reloading curve gradually tended to the curve for bolted only connection. It seems it is not necessary to include bonding in connection design, unless it is there to prevent the inherent slip.

-
- Delamination cracks at the fillet of the pre-preg cleat angle developed during testing. After these cracks occurred the cleat had not reached ultimate failure and was able still to sustain a high connection moment.
 - It is acceptable to use standard steel section for cleat pieces.
 - Stiffeners on the column flange resist the deformation caused by beam action and reduce inherent prying action.
 - Leading to material failure, large deformations of the top flange of the beam, adjacent to the connection, suggests that long bolts connecting the top and the seat cleats are needed to minimise this deformation.
 - The stiffness of connection $TLmj$ can be increased further by reinforcing the column flange where bowing deformation has been found. However, this will be accompanied by loss in the rotation capacity of the connection, and how much this capacity can be reduced without the connection becoming too 'brittle' is a subject for further investigation.
 - The test evidence showed that the beam rotated about the corner of the seat cleat. This can be used to determine the load for the cleat design.
 - Slip is the main problem for this type of connection detail, and there is a need to solve this problem.
 - A solution to prevent connection slip is suggested for cleated connections.

Chapter 6

Conceptual Design of Beam-to-Column Connections for Pultruded Frames

6.1 Introduction

The application of semi-rigid connection can provide the best structural performance for pultruded frame construction (Mottram and Zheng, 1996). Benefits of semi-rigid action in frame design have attracted the attention of a number of researchers. However, the difficulties in developing practical connections, because of the anisotropic properties of the material, have made such connections a major engineering challenge. A few attempts to develop appropriate connections have been made by Bank et al. (1996), Bass and Mottram (1994) and Mosallam et al. (1994 a, 1994 b). All of their connection details had bolted cleats and different modifications to make structural performance more acceptable. Laboratory testing of these connection prototypes has exposed deficiencies which still need to be addressed.

Recognising that the design and detailing of its connections has a major influence on overall economics and buildability of a frame, a conceptual design exercise is carried out using knowledge obtained from the connection research, including that given in **Chapters 4 and 5**. These new design details are principally for beam-to-column internal joints, but can readily be adapted to external beam-to-column, and column-to-base joints. The first alternative is a 'thin shell' cleat piece. The method of connection is bolting and this approach continues what is the current practice of mimicking steelwork. There follows six concepts based on mechanical interlocking pieces whose mating surfaces would be adhesively bonded. The final concept does not consider joining of I-shaped sections and is a more radical solution. It uses box and flat sheet profiles in a novel structural way to construct frames that do not mimic what we see routinely in steelwork.

When creating the various alternative concepts the author considered how each would be manufactured and, to minimise their cost, required parts consolidation where possible. The optimisation of the different connection pieces, in terms of their exact shape, fibre placement and manufacture was, however, outside the scope of his work. Here the concepts themselves will be presented with the object of encouraging future research to concentrate on such approaches that best meet the requirements of the industry.

6.2 Thin Shell Cleat

The connection tests in **Chapters 5** having conventional leg-angle cleats of pre-preg material showed that, although the material's modulus was sufficient, the 14 mm leg thickness gave a connection with too much flexibility, and thus there was not adequate connections stiffness (see **Sections 5.6.3 and 5.6.4**). By modifying the leg-angle cleat with side ribs, Mosallam et al. (1994 a) found significant improvement

in the stiffness of leg-angle cleated connection. The stiffness of flat sheet material can easily be improved by changing the shape. Widely used industrial methods to increase rigidity of thin materials are troughing, ribbing and sandwich construction. The simplest and most economical means of providing rigidity to thin FRP materials is to use curvature (Leggatt, 1984); this is often straightforward to achieve because many composite material processes require a closed mould which can accommodate such change of shape.

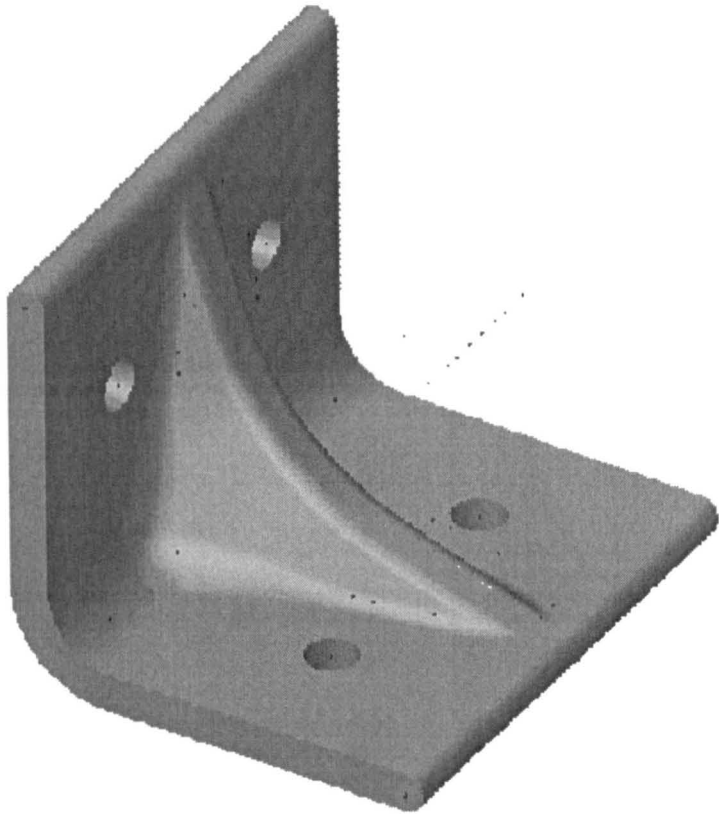


Figure 6.1: Model of thin shell saddle-shape cleat connector.

The proposed cleat connector shown in **Figure 6.1** has shell structure with constant thickness and has a 3D curved surface to provide inherent higher rigidity

than the conventional 2D curved flat leg-angle cleat.

The cleat has a saddle shaped ribbing at its centre and to further increase stiffness there is a generous radius in the fillet region. The transition between the ribbing and the flat legs is smooth. This design feature is to minimise stress concentrations and will allow the cleat to act as a shell structure. The flat portions of a leg provide a mating surface for connection of the cleat to a member. **Figure 6.2** shows three views of wire frame model of the saddle-shape shell cleat.

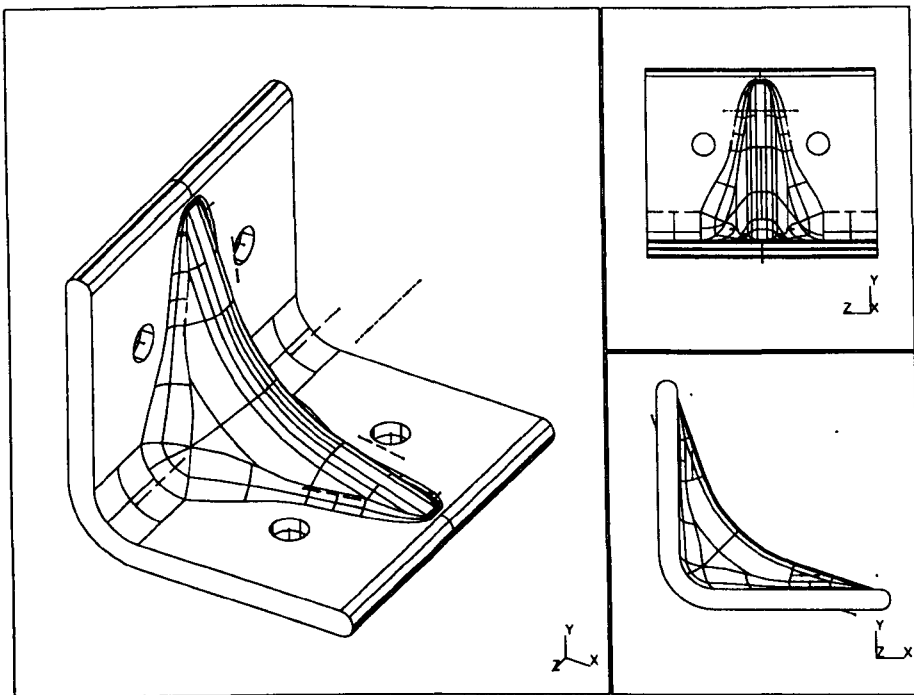


Figure 6.2: Wire frame model of thin shell saddle-shape cleat connector.

By choosing a cleat design with central saddle a higher second moment of area is obtained. Its smooth curved shell structure avoids the high stress concentration

found at the edge of side rib of Mossallam's UC connector (see **Figures 3.10** and **3.11**) (Mosallam et al., 1994 a).

Such a cleat piece can be used to connect many of standard structural profiles or can be used to stiffen members (Mosallam et al., 1994 a). The exact shape for a practical cleat will be a function of the processing method, probably RTM or pressure moulding, and the properties of the composite material.

6.3 Beam-to-column Connections

From the test results given in **Chapters 4** and **5** it has been found that, not only do connection pieces need to be stiffer, there is also a need for the beam and column members themselves to be stiffened and strengthened. These two factors were considered when creating six conceptual designs for beam-to-column connections with wide flange pultruded profiles. In addition, ease of fabrication and erection, both in a workshop or on site, were considered. This has led the author to choose adhesive bonding and mechanical interlocking as the preferred methods of connection. By minimising the number of bolts there is a reduced need to drill and to protect the exposed fibres with a coating of resin.

To construct the six beam-to-column connections, six connection pieces are proposed, and their geometries are shown in **Figure 6.3**. These pieces fit together and are able to transfer forces by using a toggle and adhesive bonding to provide the necessary continuity. A large range of alternative connection details are feasible using the six pieces in different combinations. Connection details No. 1 to 4 comprise entirely a number of these connection pieces, whereas connections No. 5 and 6 also include bolting. Each of the six connection alternatives will be introduced and the order in which they are presented does not indicate any preference. Future research will be needed before the most appropriate detailing can be recommended.

One aspect that will need specific attention is that of tolerances because, without high quality pieces, joint assemble could be difficult and likely to lead to potentially damaging residual stresses.

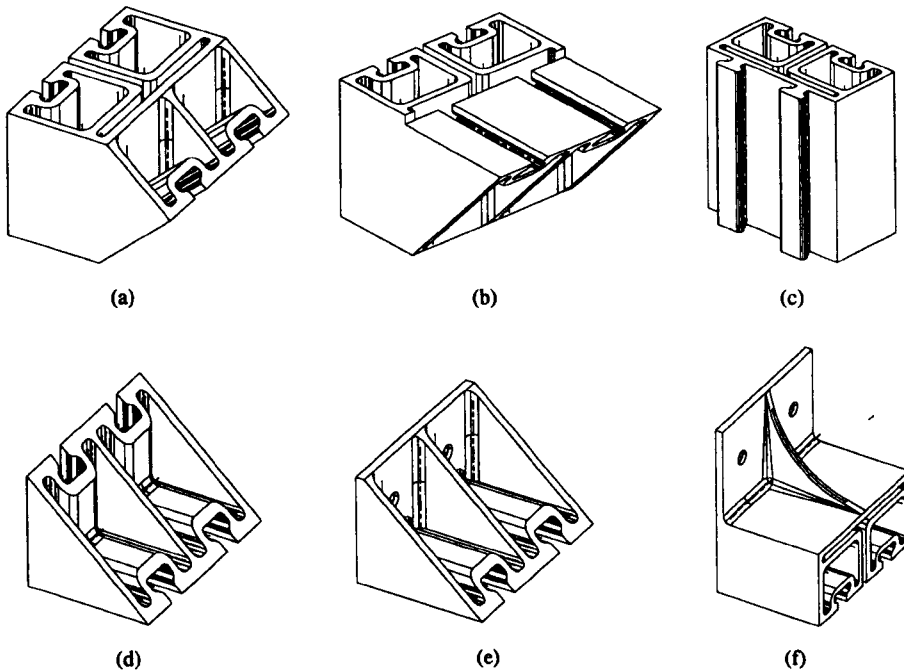


Figure 6.3: Connection pieces.

6.3.1 Connection No. 1

Connection No. 1 is shown in **Figure 6.4**, and it uses piece type (a) (see **Figure 6.3**). All six pieces are identical and they have two slots on each mating surface for toggle connectors.

These connection components can be slid onto beam or column members and bonded at the correct location under factory conditions. When erecting a frame on site the column and beam members with their connection pieces in place will

be positioned such that placement of the toggles will make the final connection. A suitable adhesive would be applied, just prior to the mating surfaces being brought into contact. The presence of the toggles will ensure that the joint can immediately transfer the forces of erection before the adhesive cures. Once the adhesive has cured it will become the principal loading carrier and the toggle will serve as a mechanical 'fail safe' back-up should the bond later fail in service.

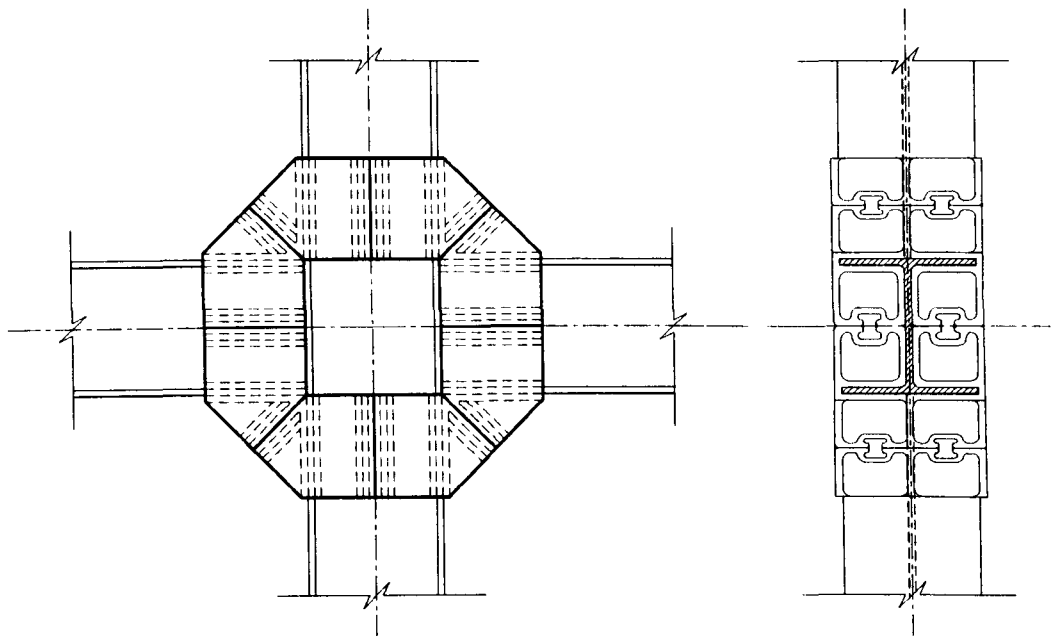


Figure 6.4: Connection No. 1.

6.3.2 Connection No. 2

Connection No. 2 is shown in **Figure 6.5**, and it consists of the three different pieces (a), (b) and (c) (see **Figure 6.3**).

Piece (b) is used at the base of the joint. The reason for this specific piece is to have, during assembly, increased support capability and minimal slippage between

the various components in the joint. The arrangement of pieces is symmetrical about the column's centre line.

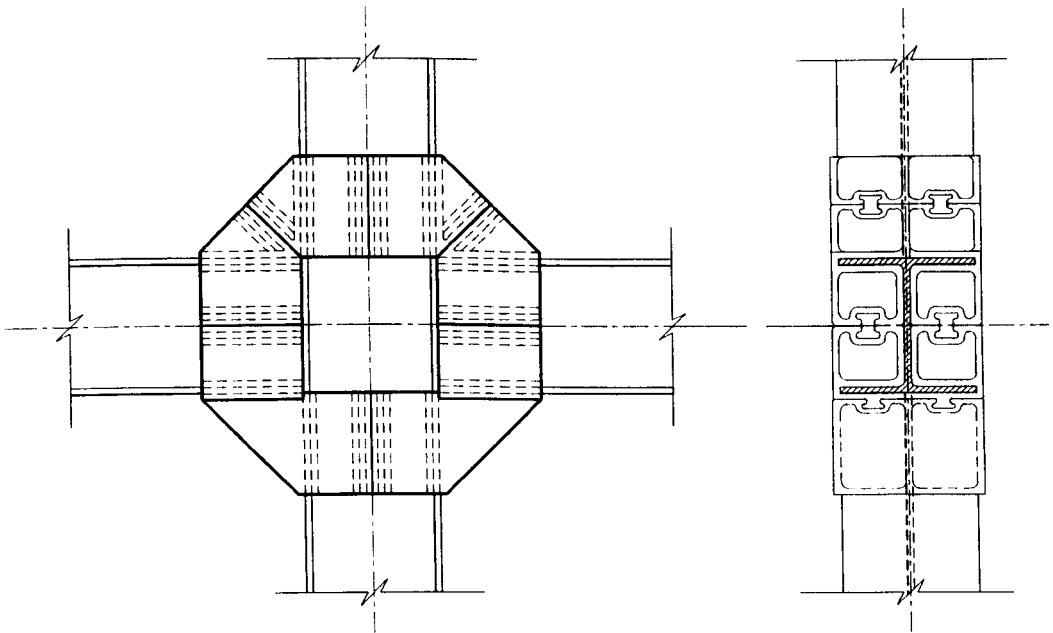


Figure 6.5: Connection No. 2.

6.3.3 Connection No. 3

Connection No. 3 is shown in **Figure 6.6**. It is assembled from eight connection pieces. Four each of pieces (b) and (c) are used (see **Figure 6.3**). The arrangement of these pieces is symmetrical about column and the beam centre lines.

6.3.4 Connection No. 4

Connection No. 4 is shown in **Figure 6.7**, and it consists of eight pieces of type (c) and four pieces of type (d) (see **Figure 6.3**). The diagonal part of the connection

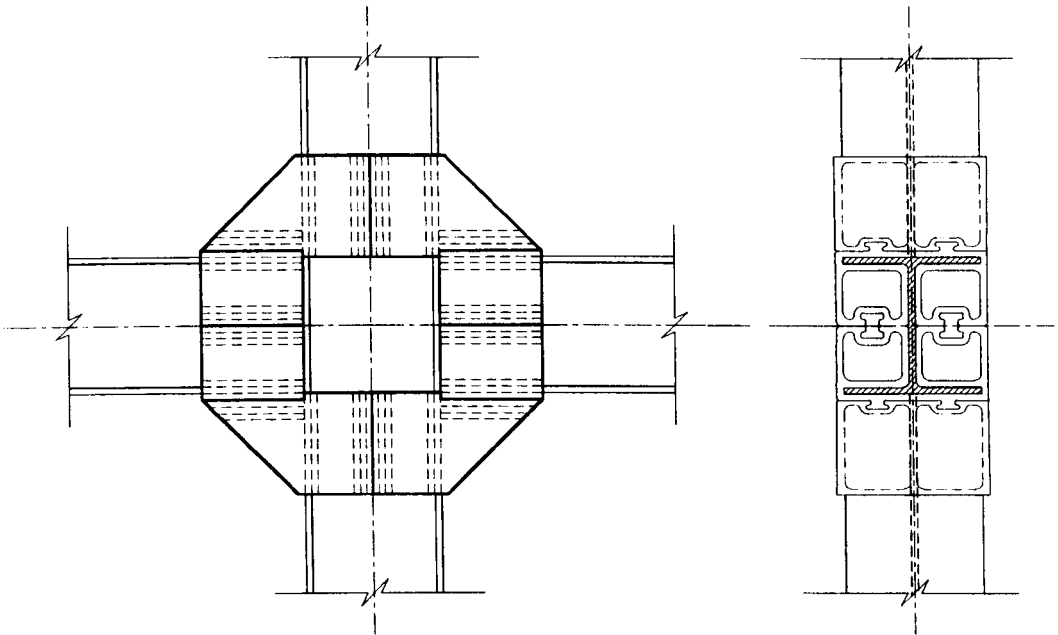


Figure 6.6: Connection No. 3.

is cut off as one component. Connection pieces for column and beam members are identical. Their arrangement is symmetrical about column and the beam centre lines.

6.3.5 Connection No. 5

Connection No. 5 is shown in **Figure 6.8**, and it consists of eight pieces (four (c) and four (e), (see **Figure 6.3**)) and four bolts to provide column flange stiffening. The arrangement of pieces is symmetrical about column and beam centre lines.

This connection will behave similarly to conventional cleated connections. Connection piece type (c) is used to stiffen the beams while the bolts stiffen the column member.

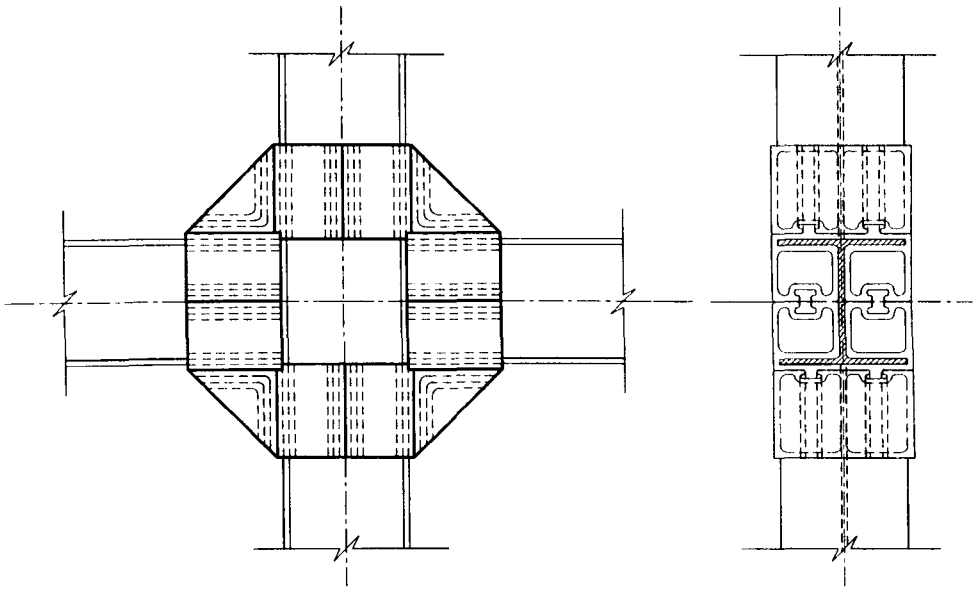


Figure 6.7: Connection No. 4.

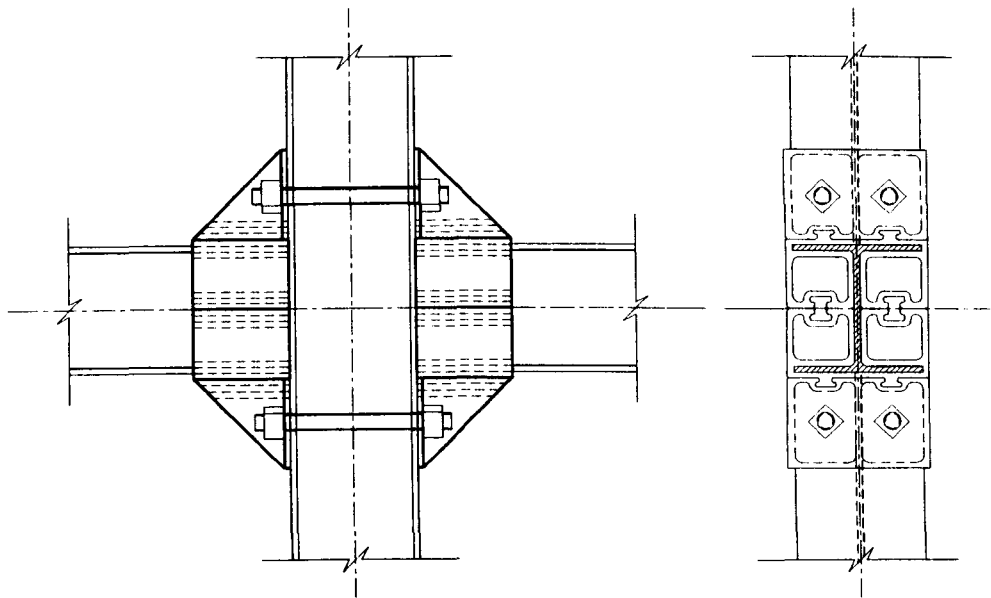


Figure 6.8: Connection No. 5.

6.3.6 Connection No. 6

Connection No. 6 is similar to No. 5 except that instead of eight pieces the connection has four pieces of type (f). This beam-to-column connection concept is shown in **Figure 6.9**). The curved central rib of piece (f) is used to stiffen the leg which connects to the column member.

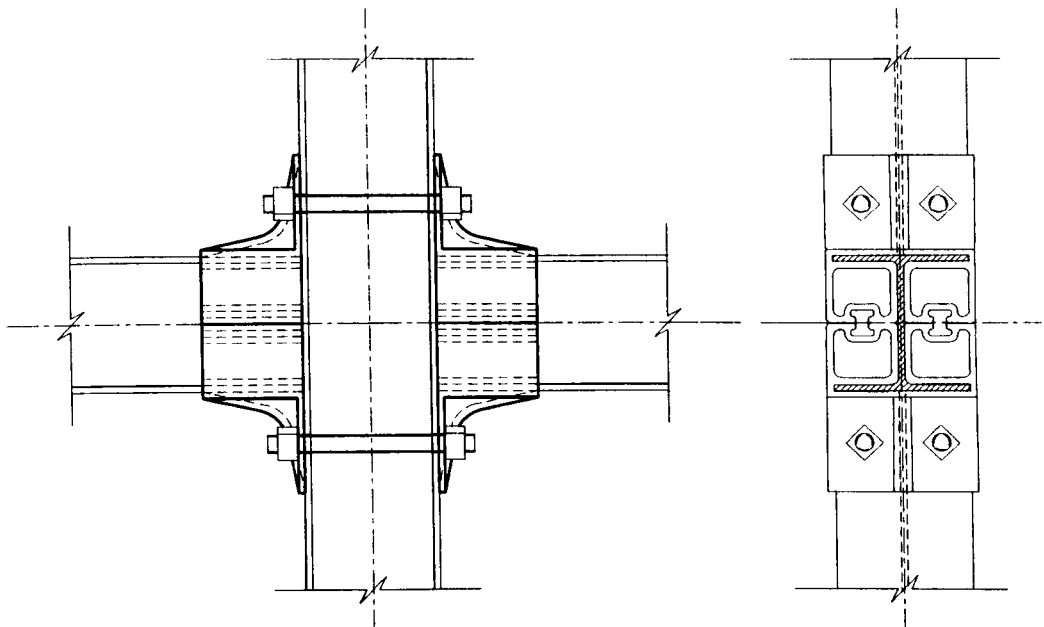


Figure 6.9: Connection No. 6.

6.4 Structural System Concept

A new structural system is shown in **Figure 6.10**. It consists of beam and column members which are assembled from pultruded standard box and flat sheet profiles. Such members can be prepared in the factory or on site. It can also be manufactured as a single profile by the pultrusion process. It is envisaged that this system can be

used in multistorey building construction. The proposal is an approach that does not mimic practice in steel work and it is the opinion of the author that such an approach should make better utilization of available standard profiles.

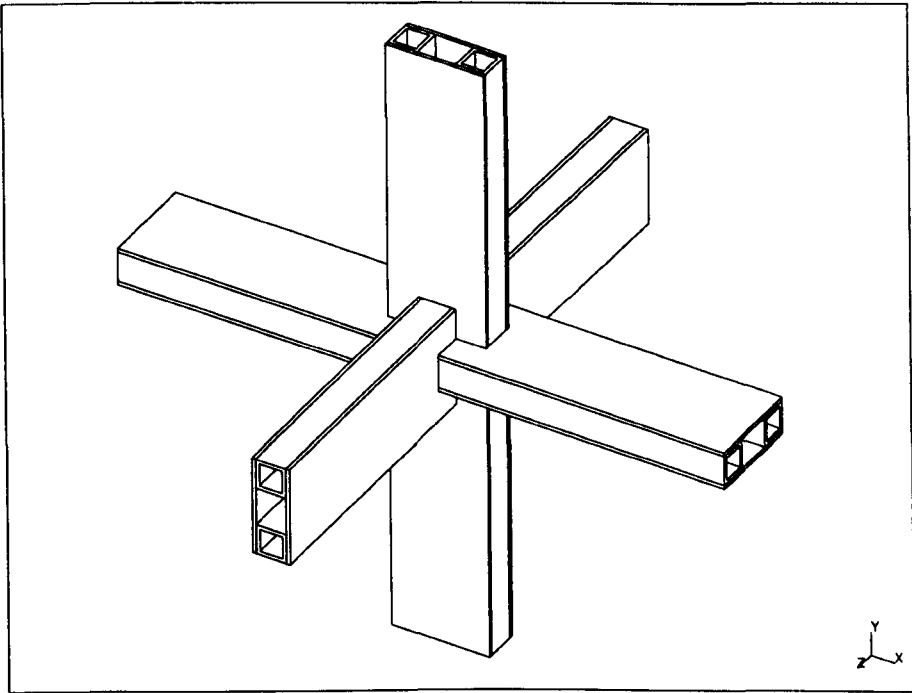


Figure 6.10: 3D beam-to-column connection.

An exposed drawing of the connection details of the system is shown in **Figure 6.11**, in which it can be seen that short box sections are placed adjacent to the joint and between the two box sections in a member. These short box sections are bonded and therefore provide additional strength and stiffness to members and the joint itself. In this structural system beams and column members go through the joint itself and are inter-locked together by each other to form a strong continuous

connection.

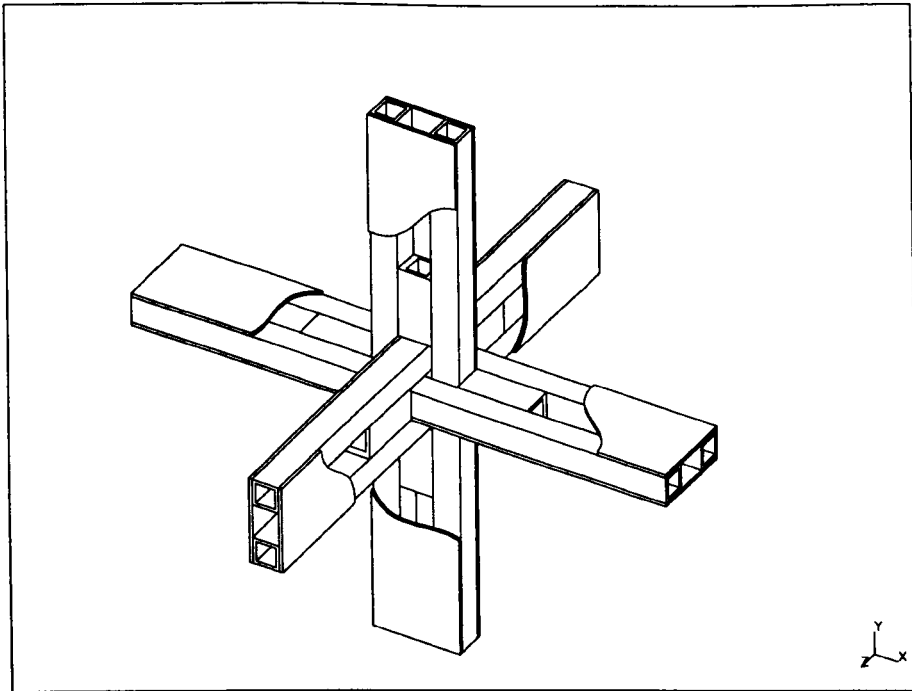


Figure 6.11: Cutaway view of 3D beam-to-column connection.

Two erection procedures for the joint sub-assembly (see **Figure 6.10**) will now be given. The first one is as shown in **Figure 6.12**. The column member is erected first (**Figure 6.12 (a)**) and then a beam sub-assembly is put through the slot in the column assembly (**Figure 6.12 (b)**). Next, a second beam sub-assembly, half-assembled of which two main box sections are bonded with a short box section and two half sheet plates on one side of member, is put through the slot of the first beam sub-assembly (**Figure 6.12 (c)**). Finally, the other two half sheet plate and another short box section are bonded to the other side of second beam to complete

the joint assembly (see **Figure 6.12** (d)).

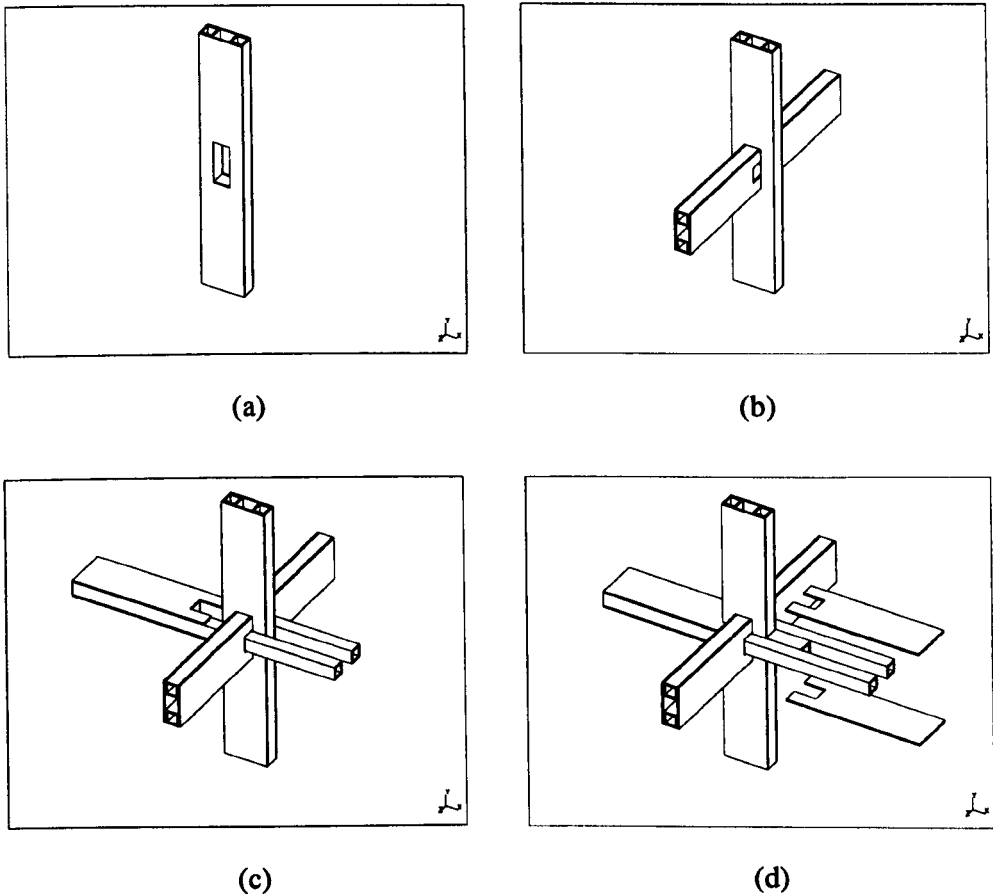


Figure 6.12: Erection procedure one for the joint sub-assembly.

The second procedure of assembly is shown in **Figure 6.13**. After the column is erected a box section is put through the slot in the column (see **Figure 6.13** (a)). Next a complete beam sub-assembly is put over the end of the column section and slid into place (**Figure 6.13** (b)). Two short box sections and top box section of vertical standing beam are then spliced into position (**Figure 6.13** (c)) to make the complete joint. Finally, the plates of the vertical beam sub-assembly are bonded on

to the box sections (**Figure 6.13** (d)).

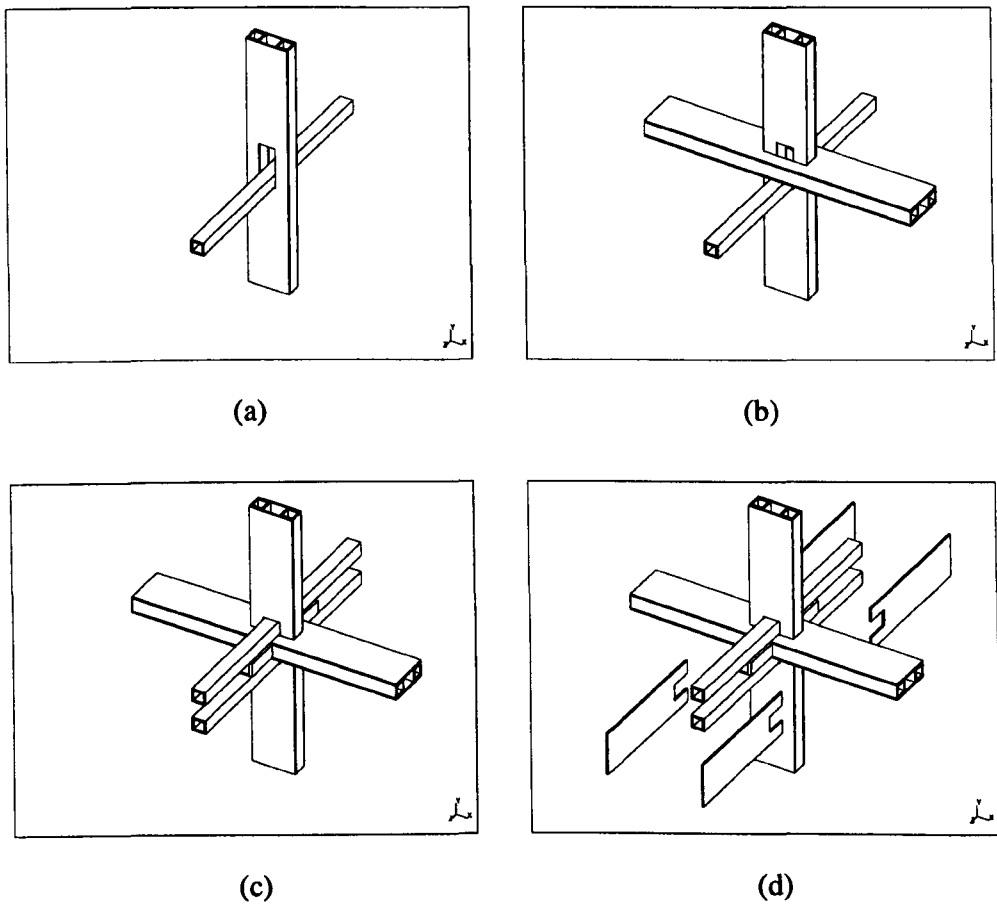


Figure 6.13: Erection procedure two for the joint sub-assembly.

Figure 6.14 shows a two bays three stories, five metre span frame structure model by using this new structure system.

6.5 Summary

To make best use of the properties and the processing technology for FRP materials a number of futuristic connection details have been proposed. It is the intention

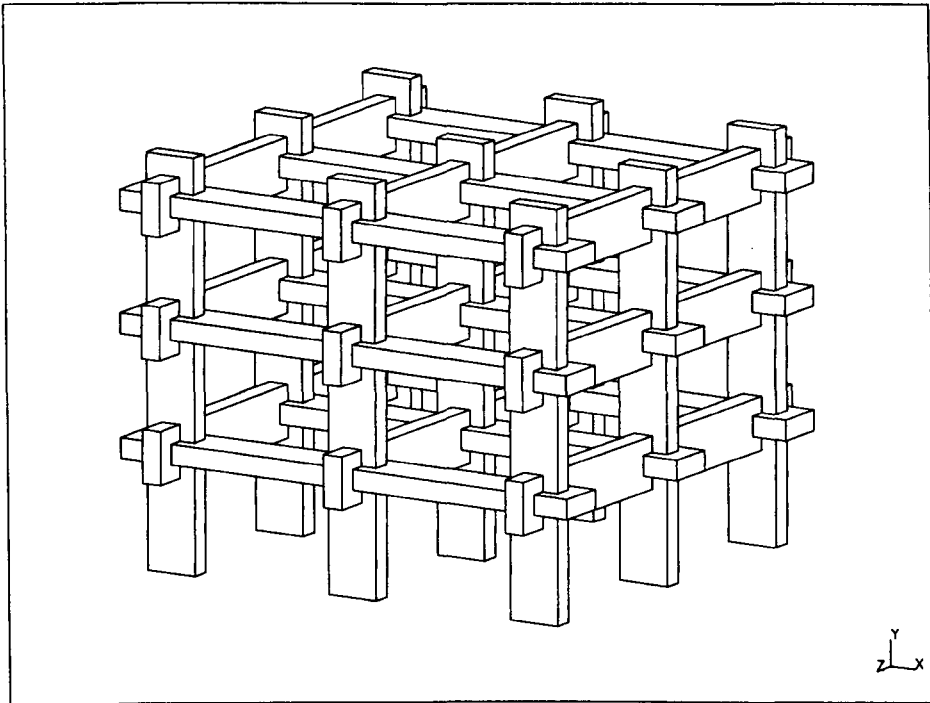


Figure 6.14: The structural model of new structural system.

that one of concepts given will be the catalyst for the development of a semi-rigid connection that meets all specifications for use in practice. The first proposal continues the theme of mimicking steel practice of cleated connection pieces and is a thin shell cleat with central saddle shaped ribbing. This connection piece has the potential to be used to construct many joint types with a majority of the available structural profiles. Six concepts are presented for beam-to-column connections that have column and beam members of WF section. These connections are formed using a number of new connection pieces, whose function is to provide the method of connection by a combination of mechanical interlocking and adhesive bonding. Two connections do, however, have a minimum number of bolts. Finally, in an attempt to be more radical and move outside of the scope dictated by steelwork practice a

new structural system is given.

None of the concepts have been studied in depth and so for any of them to become reality much further research and development work will be needed. It is the author's hope that the concepts presented will encourage those studying frames to focus much more on how joints (through their connection details) and the members affect the overall structural behaviour.

Chapter 7

The Computer Analysis of Plane Frame Structures

7.1 Introduction

For practical beam members of steel, the deflection due to shear is about 1% of that due to bending; it is therefore not surprising that frame analysis for steel does not include shear deformation. The situation is very different when the material of the members is a polymeric composite because the much lower ratio of G/E means that shear deflection can readily be equivalent to 10% of that due to bending. For this reason it is necessary to develop analysis with the option of shear deformation.

An elastic analysis for plane frame structures with, or without, semi-rigid connections is developed based on the matrix displacement method of analysis. There are also the options of having fully rigid or fully pinned connections. The program is written in C program language. Other options of the analysis are second-order deflection effects of the frame and shear deformation of the members. For the second-order effects, the stability function approach as introduced by Livesley (1956) is used

in the analysis. The shearing effect is considered in deriving the beam member end forces and displacement equations, which is based on the shear deformation analysis of Timoshenko and Gere (1972). For combining the second-order effects and shearing effects, a stability function is derived; corresponding ϕ functions used in matrix method of analysis are also given. A Gauss-elimination method is used to solve the set of linear simultaneous equation.

A new method is developed from the matrix displacement method to cope with the connection possessing semi-rigid $M - \phi$ behaviour. When compared to the method of Majid and Anderson (1968), this new method not only saves computing store space, but also is capable of dealing with multiple types of nonlinear semi-rigid connection at one joint.

7.2 Sign Conventions and Axes

The following development of the stiffness matrix method for frame analysis will be based on a plane frame, and, therefore, for the development of the beam element a local Cartesian $x - y$ coordinate system will be used. The x axis is assumed to be positive toward the right and the y axis positive upward, as shown in **Figure 7.1**. The $x - y$ plane is a plane of symmetry of the member and all loads act in this plane. The deflection of the member is also in this plane.

As two-dimensional structures are being considered, only three degrees of freedom occur at each end of the member, and to each there is a corresponding force component. The vectors of member-end displacements represented by \bar{u} , \bar{v} and $\bar{\theta}$ and forces represented by \bar{U} , \bar{V} and \bar{M} are given in **Figure 7.1 (a)** and **(b)**, respectively.

The positive sign convention to be used in the following discussion is as given in **Figure 7.1**.

In the local coordinate system, the member's centroidal axis coincides with the

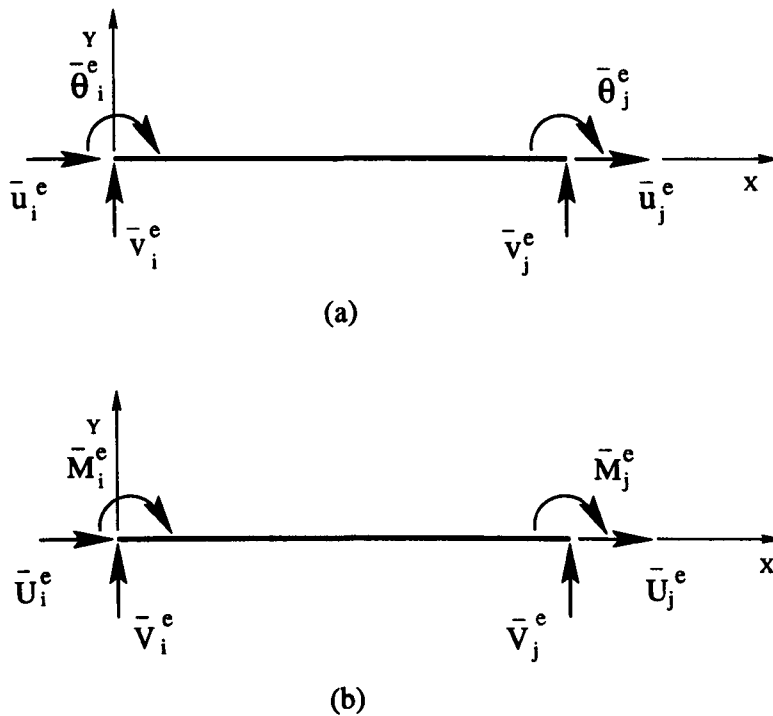


Figure 7.1: Sign convention for member end displacements (a) and forces (b).

x axis. The two nodes of a member are assigned with i and j , and the positive direction of the member is from i to j .

7.3 Matrix Stiffness Method

For a beam member, shown in **Figure 7.1**, with both ends being rigidly connected and without considering the effects of axial load on bending deflection and of shear deformation, the relation of member end forces $\{\bar{\mathbf{F}}\}^{(e)}$ and member end displacements $\{\bar{\delta}\}^{(e)}$ can be written as

$$\{\bar{\mathbf{F}}\}^{(e)} = [\bar{\mathbf{k}}]^{(e)} \{\bar{\delta}\}^{(e)} \quad (7.1)$$

where $[\bar{k}]^{(e)}$ is local member stiffness matrix. The full form of **Equation 7.1** is well-known and is

$$\begin{Bmatrix} \bar{U}_i^e \\ \bar{V}_i^e \\ \bar{M}_i^e \\ \bar{U}_j^e \\ \bar{V}_j^e \\ \bar{M}_j^e \end{Bmatrix} = \begin{bmatrix} \frac{EA}{l} & 0 & 0 & -\frac{EA}{l} & 0 & 0 \\ 0 & \frac{12EI}{l^3} & -\frac{6EI}{l^2} & 0 & -\frac{12EI}{l^3} & -\frac{6EI}{l^2} \\ 0 & -\frac{6EI}{l^2} & \frac{4EI}{l} & 0 & \frac{6EI}{l^2} & \frac{2EI}{l} \\ -\frac{EA}{l} & 0 & 0 & \frac{EA}{l} & 0 & 0 \\ 0 & -\frac{12EI}{l^3} & \frac{6EI}{l^2} & 0 & \frac{12EI}{l^3} & \frac{6EI}{l^2} \\ 0 & -\frac{6EI}{l^2} & \frac{2EI}{l} & 0 & \frac{6EI}{l^2} & \frac{4EI}{l} \end{bmatrix} \begin{Bmatrix} \bar{u}_i^e \\ \bar{v}_i^e \\ \bar{\theta}_i^e \\ \bar{u}_j^e \\ \bar{v}_j^e \\ \bar{\theta}_j^e \end{Bmatrix} \quad (7.2)$$

It is convenient to separate the terms associated with the end i and j of the member. **Equation 7.2** can be written in the compact form of

$$\begin{Bmatrix} \bar{F}_i^e \\ \bar{F}_j^e \end{Bmatrix} = \begin{bmatrix} k_{11} & k_{12} \\ k_{21} & k_{22} \end{bmatrix} \begin{Bmatrix} \bar{\delta}_i^e \\ \bar{\delta}_j^e \end{Bmatrix} \quad (7.3)$$

where $[k_{12}] = [k_{21}]^T$, and we will return to this form later.

7.4 Semi-rigid Connection

‘Steel frames for buildings are usually designed on the basis that beam-to-column connections are either pinned or rigid. The actual stiffness though will fall somewhere between these extremes, giving what is generally termed ‘semi-rigid’ behaviour (Anderson et al., 1993).’ On the basis of semi-rigid behaviour of connections, to design steel frame structures as ‘semi-continuous’ has the advantage of reducing beam depth and overall cost.’

A method for nonlinear elastic analysis of very large rigidly connected plane frame based on matrix method has been described by Majid and Anderson (1968)

and Majid (1972), in which the overall stiffness matrix of the structure is changed due to contributing an extra element hinge rotation in the displacement vectors. Benterkia (1991), using the same method, converted original programs written by Anderson and Lok (1985) in Algol to Fortran 77 and used successive estimates of the secant stiffness of the connection instead of fixing the rotation of the connection before each iteration to improve the convergence of the program. In his program the secondary effects of axial load on column stiffness are included by calculating stability functions from displacements of the previous iteration.

The proposed method of analysis for semi-rigidly connected plane frame structure is based on the matrix method, but different from the above method in a number of respects. Compared with the above method, the new method leads to saving computer storage and time. It is described in what follows.

For convenience, the joint will be termed as an arbitrary point at which two or more members meet; it is really a mathematical point which represents the joint in analysis, while the connection is termed as a part which connects the member to joint, and this is illustrated in **Figure 7.5**.

7.4.1 Analysis of the Performance of Semi-rigid Connection

The end rotation of a member with a semi-rigid connection is partly due to the rotation of the joint and partly due to the rotation of the connection.

Deformations and stresses of a member with semi-rigid connection can be treated as the results of a member under the sum of two systems of loads. These are the actual loads applied and the extra loads due to connection rotation.

To calculate the displacement of a member with semi-rigid connection, as shown in **Figure 7.2 (a)**, it can be divided into two parts. The first part is to render

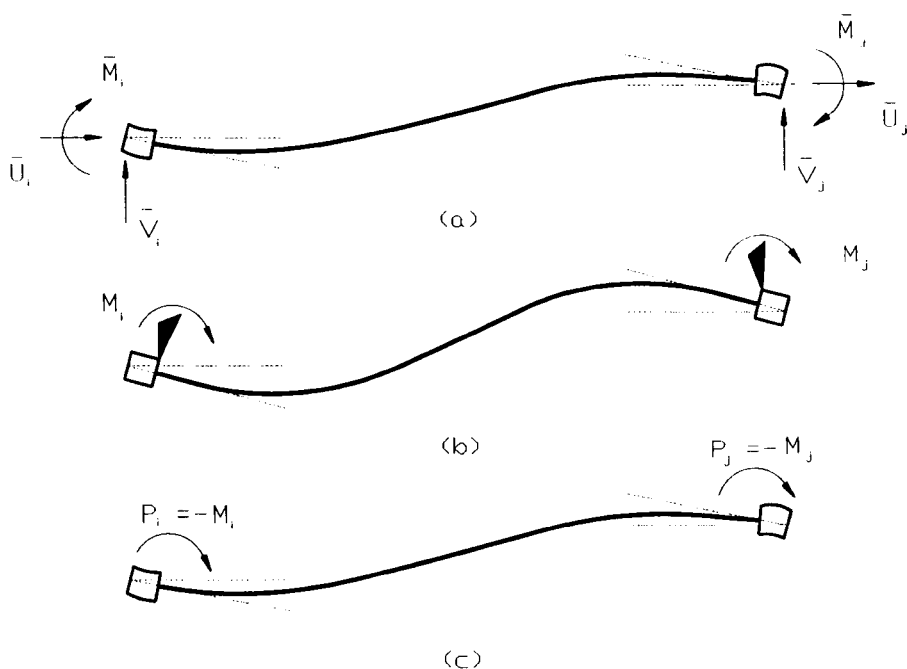


Figure 7.2: (a) Member with semi-rigid connection under deformation of joint. (b) Member with rigid connection under deformation of joint. (c) Member with semi-rigid connection under equivalent end-moments.

the structure kinematically determinate by imagining all the joints of the structure clamped against displacement and to resist the rotation of the connection by adding restraints (black triangle) at the member ends (**Figure 7.2 (b)**). This is what is known as the fully 'rigid state'. The second part is to remove restraints and allow the connection to rotate (**Figure 7.2 (c)**). This is equivalent to applying a moment at the joints with a value equal to the restraint moment action in the opposite direction.

7.4.2 Model of Element in Semi-rigid Frame

In the proposed method, the semi-rigid connection is assumed to be part of the member located at each end of the member. The semi-rigid connections at each end of the member do not necessarily have the same moment-rotation ($M - \phi$) behaviour. They can possess different semi-rigid behaviour. The model of the member with semi-rigid connections is illustrated in **Figure 7.3**, it being equivalent to the member alone (see **Figure 7.1**).

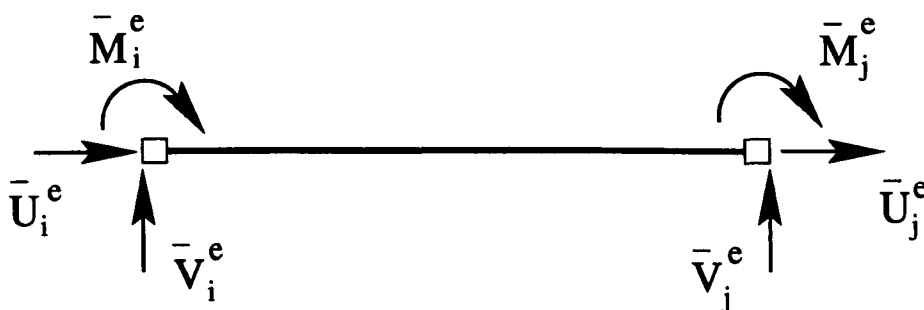


Figure 7.3: Model of the member with semi-rigid connection

In **Figure 7.3**, a square box at each end of the member is used to represent the semi-rigid connection.

In the mathematical model, the size of the connection can be ignored. We will assume the length of the members are based on the centrelines of the adjoining members. Such an assumption is common in the development of frame analyses. As a consequence of this assumption, only the rotational displacement of the connection is of concern.

Due to the assumption that a semi-rigid connection is no longer part of the joint, but is part of the member, its rotation (ϕ) does not appear as a joint displacement term in the new element's stiffness matrix. Instead, it can be imagined to be part of the member's stiffness influencing joint equilibrium.

With this assumption in the model, it can deal with a joint having one semi-rigid connection, and also can deal with a joint having multiple semi-rigid connections with different semi-rigid connection characteristics at one joint. This is illustrated in **Figure 7.4**.

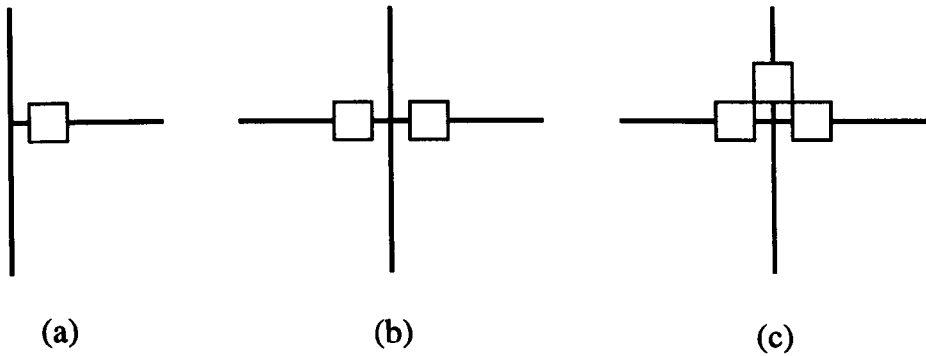


Figure 7.4: Type of the joint with semi-rigid connections of members

In **Figure 7.4**, (a) is the joint of three members with one semi-rigid connection, (b) is the joint of four members with two semi-rigid connection, and (c) is the joint of four members, three of them having semi-rigid connection.

7.4.3 Member-end Rotation

By having a semi-rigid connection present, the rotation of the member-end is not equal to the rotation of the joint in a loaded frame structure. This is because the member has been given an extra degree of freedom by the semi-rigid connection at the end. At a given stage of loading, if the joint has rotation θ and the semi-rigid connection gives a rotation represented by ϕ , as illustrated in **Figure 7.5**, then the member-end rotation β is the sum of joint rotation and semi-rigid connection rotation, and can be written as:

$$\beta = \theta + \phi \quad (7.4)$$

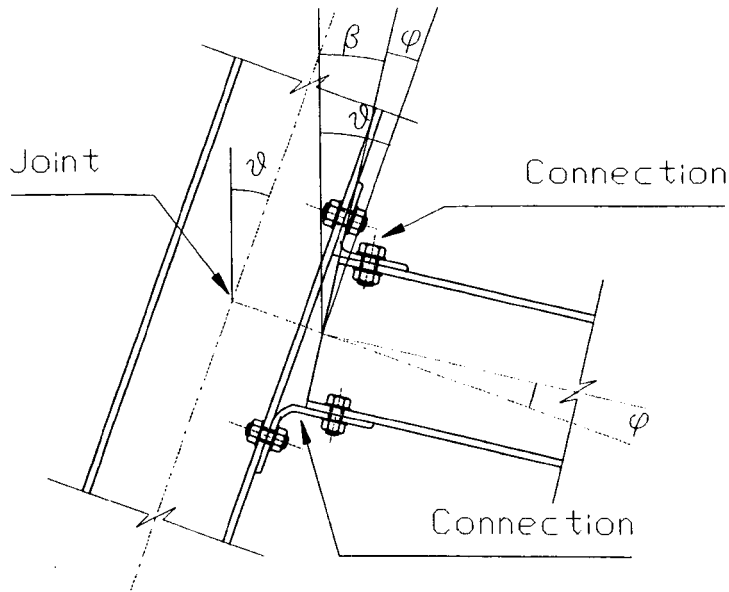


Figure 7.5: Member end rotation of member with semi-rigid connections.

7.4.4 Member-end Forces

Since member-end rotation is the sum of joint rotation and semi-rigid connection rotation, the relationships between element forces and displacements can be written as:

$$\bar{V}_i^e = \frac{12EI}{l^3} \bar{v}_i^e - \frac{6EI}{l^2} (\bar{\theta}_i^e + \bar{\phi}_i^e) - \frac{12EI}{l^3} \bar{v}_j^e - \frac{6EI}{l^2} (\bar{\theta}_j^e + \bar{\phi}_j^e) \quad (7.5)$$

$$\bar{V}_j^e = -\frac{12EI}{l^3} \bar{v}_i^e + \frac{6EI}{l^2} (\bar{\theta}_i^e + \bar{\phi}_i^e) + \frac{12EI}{l^3} \bar{v}_j^e + \frac{6EI}{l^2} (\bar{\theta}_j^e + \bar{\phi}_j^e) \quad (7.6)$$

$$\bar{M}_i^e = -\frac{6EI}{l^2} \bar{v}_i^e + \frac{4EI}{l} (\bar{\theta}_i^e + \bar{\phi}_i^e) + \frac{6EI}{l^2} \bar{v}_j^e + \frac{2EI}{l} (\bar{\theta}_j^e + \bar{\phi}_j^e) \quad (7.7)$$

$$\bar{M}_j^e = -\frac{6EI}{l^2} \bar{v}_i^e + \frac{2EI}{l} (\bar{\theta}_i^e + \bar{\phi}_i^e) + \frac{6EI}{l^2} \bar{v}_j^e + \frac{4EI}{l} (\bar{\theta}_j^e + \bar{\phi}_j^e) \quad (7.8)$$

These four equations can be rearranged to give:

$$\bar{V}_i^e = \frac{12EI}{l^3} \bar{v}_i^e - \frac{6EI}{l^2} \bar{\theta}_i^e - \frac{12EI}{l^3} \bar{v}_j^e - \frac{6EI}{l^2} \bar{\theta}_j^e - \frac{6EI}{l^2} (\bar{\phi}_i^e + \bar{\phi}_j^e) \quad (7.9)$$

$$\bar{V}_j^e = -\frac{12EI}{l^3} \bar{v}_i^e + \frac{6EI}{l^2} \bar{\theta}_i^e + \frac{12EI}{l^3} \bar{v}_j^e + \frac{6EI}{l^2} \bar{\theta}_j^e + \frac{6EI}{l^2} (\bar{\phi}_i^e + \bar{\phi}_j^e) \quad (7.10)$$

$$\bar{M}_i^e = -\frac{6EI}{l^2} \bar{v}_i^e + \frac{4EI}{l} \bar{\theta}_i^e + \frac{6EI}{l^2} \bar{v}_j^e + \frac{2EI}{l} \bar{\theta}_j^e + \frac{EI}{l} (4\bar{\phi}_i^e + 2\bar{\phi}_j^e) \quad (7.11)$$

$$\bar{M}_j^e = -\frac{6EI}{l^2} \bar{v}_i^e + \frac{2EI}{l} \bar{\theta}_i^e + \frac{6EI}{l^2} \bar{v}_j^e + \frac{4EI}{l} \bar{\theta}_j^e + \frac{EI}{l} (2\bar{\phi}_i^e + 4\bar{\phi}_j^e) \quad (7.12)$$

Using $\{\bar{\mathbf{F}}\}^{(e)}$ to represent the forces vector for the member and $\{\bar{\delta}\}^{(e)}$ to represent the joint displacement vector, the relationship between member end-forces and displacement is written as:

$$\{\bar{\mathbf{F}}\}^{(e)} = [\bar{\mathbf{k}}]^{(e)} \{\bar{\delta}\}^{(e)} + \{\bar{\mathbf{F}}_s\}^{(e)} \quad (7.13)$$

where

$$\{\bar{\mathbf{F}}\}^{(e)} = \begin{Bmatrix} \bar{U}_i^e \\ \bar{V}_i^e \\ \bar{M}_i^e \\ \bar{U}_j^e \\ \bar{V}_j^e \\ \bar{M}_j^e \end{Bmatrix}; \quad \{\bar{\delta}\}^{(e)} = \begin{Bmatrix} \bar{u}_i^e \\ \bar{v}_i^e \\ \bar{\theta}_i^e \\ \bar{u}_j^e \\ \bar{v}_j^e \\ \bar{\theta}_j^e \end{Bmatrix}; \quad \{\bar{\mathbf{F}}_s\}^{(e)} = \begin{Bmatrix} 0 \\ -\frac{6EI}{l^2} (\bar{\phi}_i^e + \bar{\phi}_j^e) \\ \frac{EI}{l} (4\bar{\phi}_i^e + 2\bar{\phi}_j^e) \\ 0 \\ \frac{6EI}{l^2} (\bar{\phi}_i^e + \bar{\phi}_j^e) \\ \frac{EI}{l} (2\bar{\phi}_i^e + 4\bar{\phi}_j^e) \end{Bmatrix}$$

where $[\bar{\mathbf{k}}]^{(e)}$ is the 6x6 local member stiffness matrix as follows:

$$[\bar{\mathbf{k}}]^{(e)} = \begin{bmatrix} \frac{EA}{l} & 0 & 0 & -\frac{EA}{l} & 0 & 0 \\ 0 & \frac{12EI}{l^3} & -\frac{6EI}{l^2} & 0 & -\frac{12EI}{l^3} & -\frac{6EI}{l^2} \\ 0 & -\frac{6EI}{l^2} & \frac{4EI}{l} & 0 & \frac{6EI}{l^2} & \frac{2EI}{l} \\ -\frac{EA}{l} & 0 & 0 & \frac{EA}{l} & 0 & 0 \\ 0 & -\frac{12EI}{l^3} & \frac{6EI}{l^2} & 0 & \frac{12EI}{l^3} & \frac{6EI}{l^2} \\ 0 & -\frac{6EI}{l^2} & \frac{2EI}{l} & 0 & \frac{6EI}{l^2} & \frac{4EI}{l} \end{bmatrix} \quad (7.14)$$

Equation 7.13 shows that the member-end force consists of two parts, ‘rigid’ and ‘semi-rigid’. The first part is due to joint displacement, representing the relationship of the member end forces and the displacement of a member in a plane frame that is rigidly connected to the joints at both ends. The second part is due to semi-rigid connection response, representing member end forces produced by semi-rigid connection deformation.

The member stiffness relations in **Equation 7.13** may now be rewritten in terms of the structure coordinate system:

$$\{\mathbf{F}\}^{(e)} = [\mathbf{k}]^{(e)} \{\delta\}^{(e)} + \{\mathbf{F}_s\}^{(e)} \quad (7.15)$$

where:

$$[\mathbf{k}]^{(e)} = [\mathbf{T}]^T [\bar{\mathbf{k}}]^{(e)} [\mathbf{T}] \quad (7.16)$$

$$\{\mathbf{F}_s\}^{(e)} = [\mathbf{T}]^T \{\bar{\mathbf{F}}_s\}^{(e)} \quad (7.17)$$

where $[\mathbf{T}]$ is coordinate transformation matrix. The full form of the transformation

matrix $[\mathbf{T}]$ is given as follows:

$$[\mathbf{T}] = \begin{bmatrix} \text{Cos}\alpha & \text{Sin}\alpha & 0 & 0 & 0 & 0 \\ -\text{Sin}\alpha & \text{Cos}\alpha & 0 & 0 & 0 & 0 \\ 0 & 0 & 1 & 0 & 0 & 0 \\ 0 & 0 & 0 & \text{Cos}\alpha & \text{Sin}\alpha & 0 \\ 0 & 0 & 0 & -\text{Sin}\alpha & \text{Cos}\alpha & 0 \\ 0 & 0 & 0 & 0 & 0 & 1 \end{bmatrix} \quad (7.18)$$

where α is the anti-clockwise angle between the x-axis of the global coordinate system of the frame and the x-axis of the local coordinate system of the element.

It should be pointed out that not only the local stiffness matrix $[\bar{\mathbf{k}}]^{(e)}$ and the displacement transformation matrix $[\mathbf{T}]$ of the element do not change, but nor does the overall stiffness matrix $[\mathbf{k}]^{(e)}$. It can be seen that except for $\{\mathbf{F}_s\}^{(e)}$, **Equation 7.15** for the member with semi-rigid connections is exactly the same as for a rigid connected member. The member stiffness matrix does not alter by taking $\{\mathbf{F}_s\}^{(e)}$ out of it. In what follows, it will be seen that $\{\mathbf{F}_s\}^{(e)}$ may be treated as a set of equivalent joint loads, therefore keeping the size of stiffness matrix to 6x6, thereby reducing the calculation needed if the semi-rigid connection is treated by using the method of Majid and Anderson (1968).

7.4.5 Static Equilibrium

Where several members in a structure meet at a joint there must be static equilibrium between the forces on the members and external loads. Equilibrium equations of joints for the structure can be written in matrix format:

$$[\mathbf{k}]\{\delta\} + \{\mathbf{F}_s\} = \{\mathbf{P}_0\} + \{\mathbf{P}_a\} \quad (7.19)$$

where $\{\mathbf{P}_0\}$ is equivalent joint loads from any loading along the length of member, and $\{\mathbf{P}_a\}$ is external loads applied at joint.

By moving $\{\mathbf{F}_s\}$ to the right-hand side, it is found that the left-hand side of **Equation 7.20** is exactly the same as for rigid frame analysis. Therefore, stiffness matrix for plane frame with rigid joints can still be used in semi-rigidly connected frame analysis, the only difference is to add the equivalent loads due to semi-rigid connection deformation to the total load on right-hand side of the equation. That is

$$[\mathbf{k}]\{\delta\} = \{\mathbf{P}_0\} + \{\mathbf{P}_a\} - \{\mathbf{F}_s\} \quad (7.20)$$

7.4.6 Solution Method

As pointed out earlier, to take into account the effect of semi-rigid connection, the local stiffness matrix $[\bar{\mathbf{k}}]^{(e)}$ and the displacement transformation matrix $[\mathbf{T}]$ of the element do not change, nor does the overall stiffness matrix $[\mathbf{k}]^{(e)}$, only member's equivalent joint loads need to be modified to include the member's fixed-end forces due to the rotation of the semi-rigid connection. These modifications are summarized as follows.

Member's Fixed-end Forces

The member's fixed-end forces due to the rotation of the semi-rigid connection can be obtained from **Equation 7.13**, and they are used to determine member deformation

in the second part.

$$\{\bar{\mathbf{F}}_s\}^{(e)} = \begin{Bmatrix} 0 \\ -\frac{6EI}{l^2}(\bar{\phi}_i^e + \bar{\phi}_j^e) \\ \frac{EI}{l}(4\bar{\phi}_i^e + 2\bar{\phi}_j^e) \\ 0 \\ +\frac{6EI}{l^2}(\bar{\phi}_i^e + \bar{\phi}_j^e) \\ \frac{EI}{l}(2\bar{\phi}_i^e + 4\bar{\phi}_j^e) \end{Bmatrix} \quad (7.21)$$

Member's Equivalent Joint Loads $\{\mathbf{P}_s\}^{(e)}$

The superimposed equivalent loads applied to the joint are in the opposite direction to member's fixed-end forces (ie. $\{\bar{\mathbf{F}}_s\}^{(e)}$). By using the coordinate transformation matrix $[\mathbf{T}]$, these forces can be transformed to the member's superimposed equivalent joint loads $\{\mathbf{P}_s\}^{(e)}$ in terms of the global coordinate system.

$$\{\mathbf{P}_s\}^{(e)} = -\{\mathbf{F}_s\}^{(e)} = -[\mathbf{T}]^T \{\bar{\mathbf{F}}_s\}^{(e)} \quad (7.22)$$

The member's equivalent joint loads $\{\mathbf{P}_s\}^{(e)}$ are assembled to obtain the total frame equivalent joint loads $\{\mathbf{P}_s\}$.

Total Equivalent Joint Loads $\{\mathbf{P}\}$

The total equivalent joint loads $\{\mathbf{P}\}$ are given by:

$$\{\mathbf{P}\} = \{\mathbf{P}_s\} + \{\mathbf{P}_0\} + \{\mathbf{P}_a\} \quad (7.23)$$

where $\{\mathbf{P}_s\}$ is equivalent joint loads caused by semi-rigid effect, $\{\mathbf{P}_0\}$ is equivalent joint loads caused by any loading between joints, and $\{\mathbf{P}_a\}$ is external loads applied at joint.

7.4.7 Member End Rotation ϕ

For a member with both ends having a semi-rigid connection, it is found that the program does not converge by simply using equation $\bar{M}_i^e = -k_i\phi_i$ and $\bar{M}_j^e = -k_j\phi_j$ to calculate the semi-rigid rotations ϕ_i and ϕ_j , respectively; note that \bar{M}_i^e and \bar{M}_j^e are taken to be the member end-moments obtained from the last iterative process. This is due to the carry-over effect of the rotation of semi-rigid connection at the other end. Therefore, if the member is semi-rigidly connected at both ends, the rotations of the two semi-rigid connections should be considered together, while the rotation of each semi-rigid connection is determined.

By assuming the nonlinear moment-rotation curve of the semi-rigid connection to have the form $M(\phi) = -k\phi$, where semi-rigid connection ratio k is a function of ϕ (ie. $k(\phi)$), and using \bar{M}^e to represent the member-end moment if connection is rigid, the member end-moments for semi-rigid connection can be written as;

$$\bar{M}_i^e + \frac{4EI}{l}\bar{\phi}_i^e + \frac{2EI}{l}\bar{\phi}_j^e = -k_i\bar{\phi}_i^e \quad (7.24)$$

$$\bar{M}_j^e + \frac{2EI}{l}\bar{\phi}_i^e + \frac{4EI}{l}\bar{\phi}_j^e = -k_j\bar{\phi}_j^e \quad (7.25)$$

Allowing $B = \frac{EI}{l}$, **Equations 7.24 and 7.25** can be written as;

$$\bar{M}_i^e + 4B\bar{\phi}_i^e + 2B\bar{\phi}_j^e = -k_i\bar{\phi}_i^e \quad (7.26)$$

$$\bar{M}_j^e + 2B\bar{\phi}_i^e + 4B\bar{\phi}_j^e = -k_j\bar{\phi}_j^e \quad (7.27)$$

Rearranging **Equation 7.26** gives;

$$\bar{\phi}_j^e = -\frac{k_i}{2B}\bar{\phi}_i^e - \frac{\bar{M}_i^e}{2B} - 2\bar{\phi}_i^e$$

$$= -\frac{\bar{M}_i^e}{2B} - \left(\frac{k_i}{2B} + 2\right)\bar{\phi}_i^e \quad (7.28)$$

Now substitute for $\bar{\phi}_j^e$ in **Equation 7.27** to obtain;

$$\bar{M}_j^e + 2B\bar{\phi}_i^e + 4B\left[-\frac{\bar{M}_i^e}{2B} - \left(\frac{k_i}{2B} + 2\right)\bar{\phi}_i^e\right] = -k_j\left[-\frac{\bar{M}_i^e}{2B} - \left(\frac{k_i}{2B} + 2\right)\bar{\phi}_i^e\right] \quad (7.29)$$

This can be rearranged to give $\bar{\phi}_i^e$ as:

$$\bar{\phi}_i^e = \frac{\left(\frac{k_i}{2B} + 2\right)\bar{M}_i^e - \bar{M}_j^e}{-2k_i - 6B - 2k_j - \frac{k_i k_j}{2B}} \quad (7.30)$$

A similar expression for $\bar{\phi}_j^e$ can also be obtained by substitution for $\bar{\phi}_i^e$ in **Equation 7.28**.

7.4.8 Beam Analysis

Beam End Rotation ϕ_e

According to the support conditions and symmetry of the beam in **Figure 7.6** , the displacements of the beam element are $\bar{v}_i^e = \bar{\theta}_i^e = \bar{\theta}_j^e = \bar{\phi}_j^e = 0$. For a semi-rigid connection $M = -k\phi$ (where k is the function of ϕ), and using **Equations 7.6** and **7.7** , the middle span shear force \bar{V}_j^e and the beam end moment \bar{M}_i^e can be written as:

$$\bar{M}_i^e = \frac{4EI}{l}\bar{\phi}_i^e + \frac{6EI}{l^2}\bar{v}_j^e - \frac{\omega l^2}{12} = -k\bar{\phi}_i^e \quad (7.31)$$

$$\bar{V}_j^e = \frac{6EI}{l^2}\bar{\phi}_i^e + \frac{12EI}{l^3}\bar{v}_j^e + \frac{\omega l}{2} = 0 \quad (7.32)$$

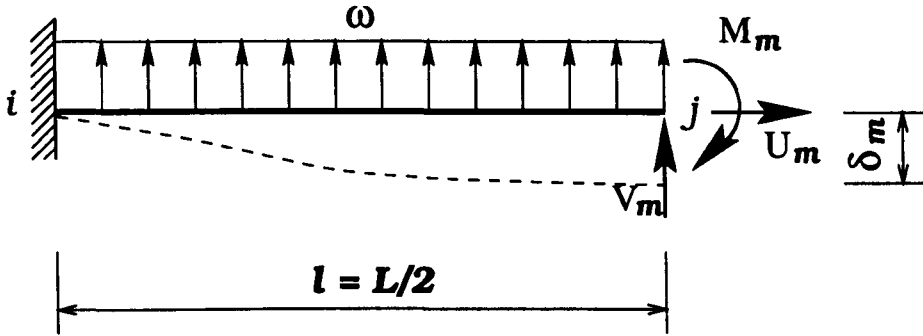


Figure 7.6: Half beam span under distributed load

where $\frac{\omega l^2}{12}$ and $\frac{\omega l}{2}$ are fixed-end internal forces due to uniformly distributed load ω . From **Equation 7.32**, the middle span displacement \bar{v}_j^e is obtained as;

$$\bar{v}_j^e = -\frac{l}{2}\bar{\phi}_i^e - \frac{\omega l^4}{24EI} \quad (7.33)$$

On substitution of \bar{v}_j^e , **Equation 7.31** can be written as:

$$\begin{aligned} \frac{4EI}{l}\bar{\phi}_i^e + \frac{6EI}{l^2}\left(-\frac{l}{2}\bar{\phi}_i^e - \frac{\omega l^4}{24EI}\right) - \frac{\omega l^2}{12} + k\bar{\phi}_i^e &= 0 \\ \frac{EI}{l}\bar{\phi}_i^e - \frac{\omega l^2}{3} + k\bar{\phi}_i^e &= 0 \end{aligned}$$

and this gives

$$\phi_e = \bar{\phi}_i^e = \frac{\omega L^3}{24(EI + k\frac{L}{2})} \quad (7.34)$$

where $l = L/2$ is half span length for the beam problem defined in **Figure 7.6**. If the deformations of the connections are neglected, the effect is the same as if we assume that the connection is infinitely rigid in bending ($k = \infty$); ϕ_e becomes zero in the foregoing equation. If the restraint of the connections are neglected, the effect is the same as if we assume that the beam is pinned connected ($k = 0$); $\phi_e = \frac{\omega L^3}{24EI}$

and it is the case of a simply supported beam.

Mid-span Deflection δ_m

Since the vertical displacement at end j of the member is the middle span displacement of the beam, its expression δ_m can be obtained from **Equation 7.33** following substitution for $\bar{\phi}_i^e$,

$$\begin{aligned}\delta_m = \bar{v}_j^e &= -\frac{l}{2}\bar{\phi}_i^e - \frac{\omega l^4}{24EI} \\ &= -\frac{l}{2}\left[\frac{\omega L^3}{24(EI + kl)}\right] - \frac{\omega l^4}{24EI} \\ &= -\frac{\omega L^4}{384}\left(\frac{4}{EI + kl} + \frac{1}{EI}\right) \\ \delta_m &= -\frac{\omega L^4}{384}\left(\frac{4}{EI + k\frac{L}{2}} + \frac{1}{EI}\right)\end{aligned}\quad (7.35)$$

If the rotation of the connection at end i is neglected in the foregoing result, the effect is the same as if we assume that the connection is infinitely rigid ($k = \infty$); then $\delta_m = -\frac{\omega L^4}{384EI}$ and this is the well-known form of the mid-span deflection for a rigidly connected beam under distributed load. If k becomes zero, then the preceding result is for a simply supported beam, $\delta_m = -\frac{5\omega L^4}{384EI}$.

Beam End Moment M_e

An expression for the beam end-moment M , is derived from **Equations 7.31, 7.34** and **7.35**

$$\begin{aligned}M_e = \bar{M}_i^e &= \frac{4EI}{l} \frac{\omega L^3}{24(EI + kl)} + \frac{6EI}{l^2} \left[-\frac{\omega L^4}{384} \left(\frac{4}{EI + kl} + \frac{1}{EI} \right) \right] - \frac{\omega l^2}{12} \\ &= \frac{EI\omega L^2}{3(EI + kl)} - \frac{EI\omega L^2}{16} \left(\frac{4}{EI + kl} + \frac{1}{EI} \right) - \frac{\omega L^2}{48}\end{aligned}$$

$$= \frac{\omega L^2}{12} \left(\frac{EI}{EI + kl} - 1 \right)$$

$$M_e = \frac{\omega L^2}{12} \left(\frac{EI}{EI + k\frac{L}{2}} - 1 \right) \quad (7.36)$$

If k is zero, $M = 0$ and it is end-moment of a simply supported beam. If k is infinite, $M_e = -\frac{\omega L^2}{12}$, and it is fixed end moment of a rigidly connected beam.

Middle Span Moment M_m

The middle span moment of the beam can be obtained by substitution for $\bar{\phi}_i^e$ and \bar{v}_j^e in **Equation 7.8** and adding the equivalent joint load of $\frac{\omega l^2}{12}$ caused by distributed load between joints. This is given

$$\begin{aligned} M_m = \bar{M}_j^e &= \frac{2EI}{l} \frac{\omega L^3}{24(EI + kl)} + \frac{6EI}{l^2} \left[-\frac{\omega L^4}{384} \left(\frac{4}{EI + kl} + \frac{1}{EI} \right) \right] + \frac{\omega l^2}{12} \\ &= \frac{EI\omega L^2}{6(EI + kl)} - \frac{EI\omega L^2}{16} \left(\frac{4}{EI + kl} + \frac{1}{EI} \right) + \frac{\omega L^2}{48} \\ &= -\frac{\omega L^2}{12} \left(\frac{EI}{EI + kl} + \frac{1}{2} \right) \end{aligned}$$

$$M_m = -\frac{\omega L^2}{12} \left(\frac{EI}{EI + k\frac{L}{2}} + \frac{1}{2} \right) \quad (7.37)$$

If k is zero, $M_m = -\frac{\omega L^2}{8}$ and it is mid-span moment of simply supported beam. If k is infinite, $M_m = -\frac{\omega L^2}{24}$, and it is the mid-span moment of a beam with fixed ends.

Serviceability Beam Line

In the case that the beam design is controlled by the deflection limit of the serviceability requirement, the beam line shown in **Figure 7.7** cannot meet the requirement of such design. Therefore, a serviceability beam line is proposed for such design.

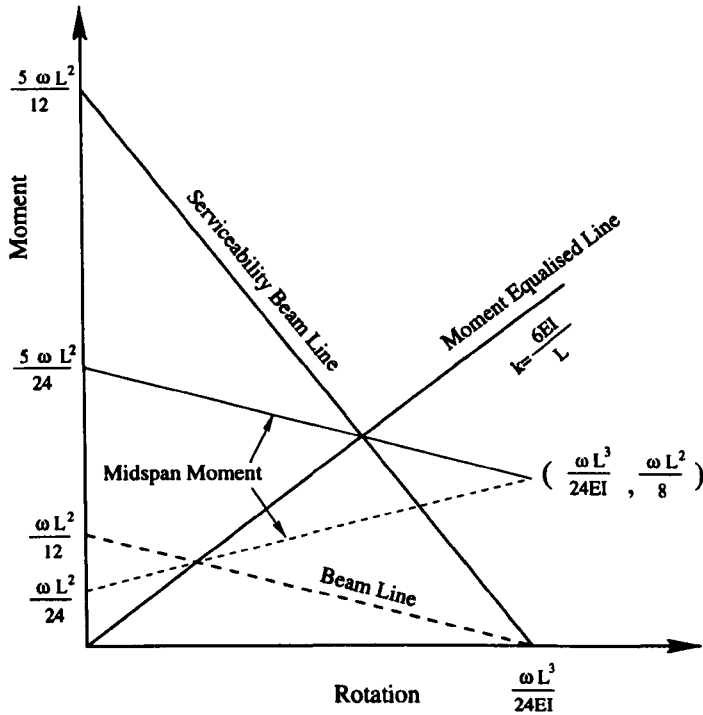


Figure 7.7: Serviceability beam line, and midspan and end support moments equalised line.

Referring to the beam of **Figure 7.6**, and assuming it is simply supported at the ends, the maximum midspan deflection δ_s , allowed by serviceability limit will occur at a distributed load

$$\omega = \frac{384EI}{5L^4} \delta_s. \tag{7.38}$$

For the other extreme condition that the beam is fully fixed at the both ends, the maximum midspan deflection δ_s , will occur at the distributed load

$$\omega_r = \frac{384EI}{L^4} \delta_s. \tag{7.39}$$

Clearly, $\omega_r \neq \omega$; the beam with fully fixed ends requires 5 times the load for

the maximum deflection δ_s allowed by serviceability. Thus the beam line drawn for a constant load ω will not correspond to a constant level of maximum midspan deflection required by serviceability for a beam.

By constructing of a beam line representing this condition a serviceability beam-line is obtained. The serviceability beam-line is shown in **Figure 7.7**, which represents the beams for various end support conditions (from pinned to rigid) under distributed load with maximum deflection allowed by serviceability requirement. The serviceability beam line can be written as:

$$M_e = -\frac{10EI}{L}\phi_e + \frac{5\omega L^2}{12} \quad (7.40)$$

In **Figure 7.7** the beam line for a constant load is also given in dashed line. The both midspan moment lines, one for the constant load and one for the constant midspan deflection, are given in dashed line and solid line, respectively. At the intersections of midspan moment lines and beam lines (give the beam-end moment) the midspan moment is equal to beam-end moment. If we draw a line through these two intersection point, a moment equalised line is obtained. This line passes through the original point and represents the moment-rotation behaviour of a connection. For a beam with such connection under distributed load, the midspan moment and end support moments will be equalized. This line is named moment equalised line (MEL) and the corresponding connection called moment equalised connection (MEC). The stiffness of MEC can be obtained as $k = \frac{6EI}{L}$.

7.5 Effect of Shear deformations

Deflection of a beam subjected to normal loading is the combination of the bending deformations and the shear deformation. In this section, the relationship between

member end-forces and displacements will be deduced from the deflection of member by considering both bending deformations and shear deformations.

Timoshenko and Gere (1972) analysed shear stress in the beam and noted that the shear stress τ varies parabolically from top to bottom of the beam; it follows that the shear strain $\gamma = \tau/G$ must vary in the same manner. Thus, cross sections of the beam which were originally plane surfaces become warped. At the neutral surface the angles are equal to the shear strain $\gamma = \tau_{max}/G$. As long as the shear force V remains constant along the beam, the warping of all cross sections is the same. Thus, the stretching or the shortening of longitudinal fibres produced by the bending moment is unaffected by the shear strains, and the distribution of the normal stresses σ is the same as it is in pure bending. The slope of the deflection curve of the beam due to shear alone is approximately equal to the shear strain at the neutral axis.

It is assumed that the shear stress is uniform on the cross section. Thus shear does not produce rotation of the member section, and each section remains parallel to other sections under deformation due to shear alone.

Therefore, the deflection of the member is due to bending moment and shear, whereas the rotation of the member section is due to bending moment alone.

7.5.1 Shearing deformations

The slope of the deflection curve of the beam due to shear alone, as Timoshenko and Gere (1972) explained, is approximately equal to the shear strain at the neutral axis. This gives the following expression for slope:

$$\frac{dy_s}{dx} = -\gamma = -\frac{\alpha_s \bar{V}_i^e}{GA} = \frac{\alpha_s \bar{V}_j^e}{GA} \quad (7.41)$$

in which \bar{V}^e is the shear force and A is the cross-section area of the beam, \bar{V}^e/A is the average shear stress, α_s is a numerical factor (or shear coefficient) by which the average shear stress must be multiplied to obtain the shear stress at the centroid of the cross section, and G is the modulus of elasticity in shear. For an I beam α_s is approximately equal to $\frac{A}{A_w}$, where A_w is the area of the web of the beam. The quantity GA/α_s is known as the shearing rigidity of the beam.

Sign convention to be used for shear deformation is assigned as that clockwise rotation is positive.

7.5.2 Bending deformations

By assuming that deflection of the beam is very small, the differential equation of the deflection curve of the beam by bending has a familiar form

$$\frac{d^2 y_b}{dx^2} = \frac{1}{\rho} = \frac{M(x)}{EI} \quad (7.42)$$

where ρ is curvature of the deflection curve. For a beam element which does not have any intermediate loading, as shown in **Figure 7.1**, we have $M(x) = \bar{V}_i^e x + \bar{M}_i^e$. Multiplying both sides of **Equation 7.42** by dx and integrating, we obtained

$$\begin{aligned} \frac{dy_b}{dx} &= \frac{1}{EI} \int M(x) dx + C_1 \\ &= \frac{1}{EI} \left(\frac{\bar{V}_i^e}{2} x^2 + \bar{M}_i^e x \right) + C_1 \end{aligned} \quad (7.43)$$

where C_1 is a constant of integration. This constant can be evaluated by considering the displacement boundary condition of the member. Where $x = 0$, the slope of the deflection curve at the left-end of the member is equal to the rotation of the left-end

of the member, represented by θ_i , which may be expressed more succinctly as

$$y'_b(0) = -\bar{\theta}_i^e$$

applying this condition to **Equation 7.43** gives

$$C_1 = -\bar{\theta}_i^e$$

and

$$\frac{dy_b}{dx} = \frac{\bar{V}_i^e}{2EI}x^2 + \frac{\bar{M}_i^e}{EI}x - \bar{\theta}_i^e \quad (7.44)$$

By using the same method, the bending deformation can also be represented by \bar{V}_j^e and \bar{M}_j^e . Since $M(x) = -\bar{M}_j^e + \bar{V}_j^e(l-x)$, the slope of the beam deflection curve by bending gives:

$$\begin{aligned} \frac{dy_b}{dx} &= \frac{1}{EI} \int M(x)dx + C_1 \\ &= \frac{\bar{V}_j^e l}{EI}x - \frac{\bar{V}_j^e}{2EI}x^2 - \frac{\bar{M}_j^e}{EI}x + C_1 \end{aligned} \quad (7.45)$$

where $x = 0$, the slope of deflection curve at the left-end of the member is equal to the rotation of the left-end of the member $\bar{\theta}_i^e$, thus $C_1 = -\bar{\theta}_i^e$, hence **Equation 7.45** can be rewritten as

$$\frac{dy_b}{dx} = \frac{\bar{V}_j^e l}{EI}x - \frac{\bar{V}_j^e}{2EI}x^2 - \frac{\bar{M}_j^e}{EI}x - \bar{\theta}_i^e \quad (7.46)$$

7.5.3 Total Slope of the Beam

At any section of the beam, the total deflection of the beam is the sum of the bending deflection and shear deflection and the total slope of the beam, therefore, is the sum

of the bending slope and shear slope as illustrated in **Figure 7.8**. **Figure 7.8 (a)** shows the end i displacement of the member with bending and shear action. This relation can be written as

$$\frac{dy_b}{dx} + \frac{dy_s}{dx} = \frac{x^2}{2EI} \bar{V}_i^e + \frac{x}{EI} \bar{M}_i^e - \bar{\theta}_i^e - \gamma \quad (7.47)$$

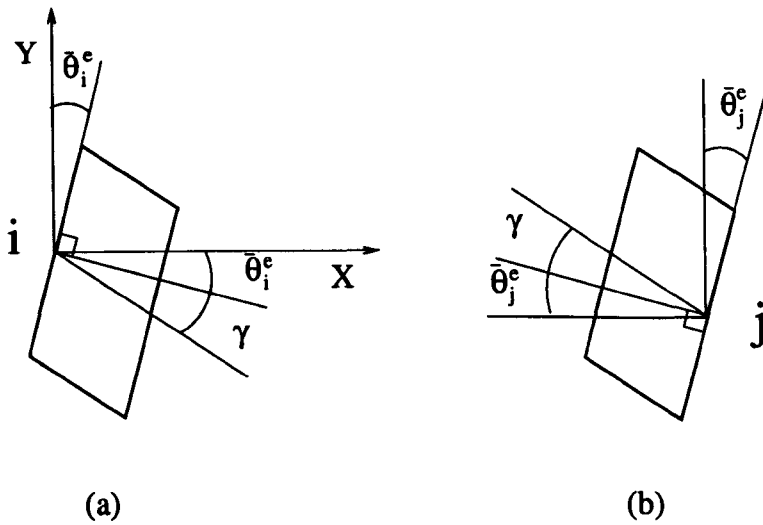


Figure 7.8: Shear displacements at member end i (a) and end j (b).

When $x = l$, the slope of the deflection curve at the right-end of the member is equal to the sum of the right-end rotation of the member and shear slope, represented by $\bar{\theta}_j^e$ and γ as shown in **Figure 7.8 (b)**. Thus **Equation 7.47** gives:

$$-\bar{\theta}_j^e - \gamma = \frac{1}{EI} \left(\frac{l^2}{2} \bar{V}_i^e + \bar{M}_i^e l \right) - \bar{\theta}_i^e - \gamma \quad (7.48)$$

Rearranging gives

$$\bar{\theta}_i^e - \bar{\theta}_j^e = \frac{l^2}{2EI} \bar{V}_i^e + \frac{l}{EI} \bar{M}_i^e \quad (7.49)$$

Similarly, the relation of member end rotations $\bar{\theta}_i^e$, $\bar{\theta}_j^e$ and member end forces \bar{V}_j^e \bar{M}_j^e can be obtained as

$$\bar{\theta}_i^e - \bar{\theta}_j^e = \frac{l^2}{2EI} \bar{V}_j^e - \frac{l}{EI} \bar{M}_j^e \quad (7.50)$$

Equations 7.49 and **7.50** are the relationship of member end rotation $\bar{\theta}_i^e$ and $\bar{\theta}_j^e$ and member end force \bar{M}_i^e , \bar{V}_i^e , \bar{V}_j^e and \bar{M}_j^e . Since there are four unknown variables \bar{M}_i^e , \bar{V}_i^e , \bar{V}_j^e and \bar{M}_j^e but only two equations, **Equations 7.49** and **7.50** still could not be solved with given member end-rotations $\bar{\theta}_i^e$ and $\bar{\theta}_j^e$. To obtain the four member end-forces \bar{M}_i^e , \bar{V}_i^e , \bar{V}_j^e and \bar{M}_j^e , we need two more equations. **Equations 7.49** and **7.50** will be used later to obtain the relationship of the individual member end-forces and member end-displacements.

7.5.4 Total Deflection of the Beam

The total deflection of the beam is the sum of the bending deflection and shear deflection. Thus, the deflection of the beam due to shear and bending moment can be obtained by integrating the slope equations of **Equation 7.47** as follows.

From **Equations 7.41** and **7.47**, The total slope of the deflection curve of the beam can be written as:

$$\frac{dy}{dx} = \frac{dy_b}{dx} + \frac{dy_s}{dx} = \frac{x^2}{2EI} \bar{V}_i^e + \frac{x}{EI} \bar{M}_i^e - \bar{\theta}_i^e - \frac{\alpha_s \bar{V}_i^e}{GA}. \quad (7.51)$$

Integrating this equation gives the total deflection of the beam as:

$$y = \frac{x^3}{6EI} \bar{V}_i^e + \frac{x^2}{2EI} \bar{M}_i^e - \bar{\theta}_i^e x - \frac{\alpha_s \bar{V}_i^e}{GA} x + C_2, \quad (7.52)$$

where C_2 is a constant of integration. This constant can be evaluated by considering the boundary conditions of the member. Where $x = 0$, deflection y is equal to the

displacement of the member at the left-end \bar{v}_i , thus, from **Equation 7.52** we obtain $C_2 = \bar{v}_i^e$. When $x = l$, the deflection at the right-end of the member is equal to the deflection of the right-end of the member, represented by \bar{v}_j^e . **Equation 7.52** now gives:

$$\bar{v}_i^e - \bar{v}_j^e - l\bar{\theta}_i^e = -\left(\frac{l^3}{6EI} - \frac{\alpha_s l}{GA}\right)\bar{V}_i^e - \frac{l^2}{2EI}\bar{M}_i^e. \quad (7.53)$$

Similarly, total deflection of the member due to shear and bending moment can also be obtained by integrating the relationship obtained by summing **Equations 7.41** and **7.46**. This gives:

$$y = \frac{\bar{V}_j^e l}{2EI}x^2 - \frac{\bar{V}_j^e}{6EI}x^3 - \frac{\bar{M}_j^e}{2EI}x^2 - \bar{\theta}_i^e x + \frac{\alpha_s \bar{V}_j^e}{GA}x + C_2 \quad (7.54)$$

Considering the boundary condition, when $x = 0$, $y = \bar{v}_i^e$, and $C_2 = \bar{v}_i^e$. When $x = l$, $y = \bar{v}_j^e$, and **Equation 7.54** gives:

$$\bar{v}_i^e - \bar{v}_j^e - l\bar{\theta}_i^e = -\left(\frac{l^3}{3EI} + \frac{\alpha_s l}{GA}\right)\bar{V}_j^e + \frac{l^2}{2EI}\bar{M}_j^e. \quad (7.55)$$

7.5.5 Derivation of Member End Forces

Member with Both Ends Rigid Connection

From **Equations 7.49** and **7.53**, the shear force at the left-end of the member \bar{V}_i^e and the moment at the left-end of the member \bar{M}_i^e can be obtained as follows:

$$\bar{V}_i^e = \frac{1}{l(\mu + \psi)}\left(\bar{v}_i^e - \frac{l}{2}\bar{\theta}_i^e - \bar{v}_j^e - \frac{l}{2}\bar{\theta}_j^e\right) \quad (7.56)$$

$$\bar{M}_i^e = \frac{1}{l(\mu + \psi)}\left[-\frac{l}{2}\bar{v}_i^e + \left(\frac{l^2}{3} + \psi EI\right)\bar{\theta}_i^e + \frac{l}{2}\bar{v}_j^e + \left(\frac{l^2}{6} - \psi EI\right)\bar{\theta}_j^e\right] \quad (7.57)$$

where $\mu = \frac{l^2}{12EI}$ and $\psi = \frac{\alpha_s}{GA}$.

By solving **Equations 7.50** and **7.55** the shear force at the right-end \bar{V}_j^e and moment at right-end \bar{M}_j^e can be obtained as follows.

$$\bar{V}_j^e = \frac{1}{l(\mu + \psi)}(-\bar{v}_i^e + \frac{l}{2}\bar{\theta}_i^e + \bar{v}_j^e + \frac{l}{2}\bar{\theta}_j^e) \quad (7.58)$$

$$\bar{M}_j^e = \frac{1}{l(\mu + \psi)}[-\frac{l}{2}\bar{v}_i^e + (\frac{l^2}{6} - \psi EI)\bar{\theta}_i^e + \frac{l}{2}\bar{v}_j^e + (\frac{l^2}{3} + \psi EI)\bar{\theta}_j^e] \quad (7.59)$$

Combining **Equations 7.56**, **7.57**, **7.58** and **7.59** in conventional matrix form we have the following:

$$\begin{Bmatrix} \bar{V}_i^e \\ \bar{M}_i^e \\ \bar{V}_j^e \\ \bar{M}_j^e \end{Bmatrix} = \begin{bmatrix} \frac{1}{l(\mu+\psi)} & -\frac{1}{2(\mu+\psi)} & -\frac{1}{l(\mu+\psi)} & -\frac{1}{2(\mu+\psi)} \\ -\frac{1}{2(\mu+\psi)} & \frac{l^2+3\psi EI}{3l(\mu+\psi)} & \frac{1}{2(\mu+\psi)} & \frac{l^2-6\psi EI}{6l(\mu+\psi)} \\ -\frac{1}{l(\mu+\psi)} & \frac{1}{2(\mu+\psi)} & \frac{1}{l(\mu+\psi)} & \frac{1}{2(\mu+\psi)} \\ -\frac{1}{2(\mu+\psi)} & \frac{l^2-6\psi EI}{6l(\mu+\psi)} & \frac{1}{2(\mu+\psi)} & \frac{l^2+3\psi EI}{3l(\mu+\psi)} \end{bmatrix} \begin{Bmatrix} \bar{v}_i^e \\ \bar{\theta}_i^e \\ \bar{v}_j^e \\ \bar{\theta}_j^e \end{Bmatrix} \quad (7.60)$$

The differential equation used above in solving for the member end forces was obtained on the assumptions that each cross section of the beam remains parallel, no warping of the cross section occurred, and the deflections of the member are small.

Now taking into account of the effect of shear deformation, the full form of the local member stiffness matrix $[\bar{k}]^{(e)}$ of **Equation 7.2** becomes:

$$[\bar{k}]^{(e)} = \begin{bmatrix} \frac{EA}{l} & 0 & 0 & -\frac{EA}{l} & 0 & 0 \\ 0 & \frac{1}{l(\mu+\psi)} & -\frac{1}{2(\mu+\psi)} & 0 & -\frac{1}{l(\mu+\psi)} & -\frac{1}{2(\mu+\psi)} \\ 0 & -\frac{1}{2(\mu+\psi)} & \frac{l^2+3\psi EI}{3l(\mu+\psi)} & 0 & \frac{1}{2(\mu+\psi)} & \frac{l^2-6\psi EI}{6l(\mu+\psi)} \\ -\frac{EA}{l} & 0 & 0 & \frac{EA}{l} & 0 & 0 \\ 0 & -\frac{1}{l(\mu+\psi)} & \frac{1}{2(\mu+\psi)} & 0 & \frac{1}{l(\mu+\psi)} & \frac{1}{2(\mu+\psi)} \\ 0 & -\frac{1}{2(\mu+\psi)} & \frac{l^2-6\psi EI}{6l(\mu+\psi)} & 0 & \frac{1}{2(\mu+\psi)} & \frac{l^2+3\psi EI}{3l(\mu+\psi)} \end{bmatrix} \quad (7.61)$$

where $\mu = \frac{l^2}{12EI}$ and $\psi = \frac{\alpha_s}{GA}$.

7.5.6 Effect of Semi-rigid connection and Member Shear Deformations

To take into account the effect of shear deformation of the member and semi-rigid connection, the local member stiffness matrix $[\bar{k}]^{(e)}$ remains the same as **Equation 7.61**.

The equivalent joint loads $\{\bar{F}_s\}^{(e)}$ due to the deformations of the semi-rigid connections with the effect of the shear deformation of member can now be written as:

$$\{\bar{F}_s\}^{(e)} = \begin{Bmatrix} 0 \\ -\frac{1}{2(\mu+\psi)}(\bar{\phi}_i^e + \bar{\phi}_j^e) \\ \frac{l^2+3\psi EI}{3l(\mu+\psi)}\bar{\phi}_i^e + \frac{l^2-6\psi EI}{6l(\mu+\psi)}\bar{\phi}_j^e \\ 0 \\ \frac{1}{2(\mu+\psi)}(\bar{\phi}_i^e + \bar{\phi}_j^e) \\ \frac{l^2-6\psi EI}{6l(\mu+\psi)}\bar{\phi}_i^e + \frac{l^2+3\psi EI}{3l(\mu+\psi)}\bar{\phi}_j^e \end{Bmatrix} \quad (7.62)$$

If shear deformation of the member is neglected, we set $\psi = 0$, the element stiffness matrix $[\bar{k}]^{(e)}$ of **Equation 7.61** and the equivalent joint loads of $\{\bar{F}_s\}^{(e)}$ reduce to that in **Equations 7.2** and **7.21**, respectively.

The rotation of semi-rigid connections can be obtained by using the same method given in **Section 7.4.7** and this gives:

$$\bar{\phi}_i^e = \frac{(k_j + C_1)\bar{M}_i^e - C_2\bar{M}_j^e}{C_2 - k_i k_j - C_1(k_i + k_j) - C_1^2} \quad (7.63)$$

where $C_1 = \frac{l^2+3\psi EI}{3l(\mu+\psi)}$ and $C_2 = \frac{l^2-6\psi EI}{6l(\mu+\psi)}$, \bar{M}_i^e and \bar{M}_j^e are member-end moment if connections are rigid.

A similar expression for $\bar{\phi}_j^e$ can also be obtained as:

$$\bar{\phi}_j^e = -\frac{\bar{M}_i^e}{C_2} - \frac{k_i + C_1}{C_2} \bar{\phi}_i^e. \quad (7.64)$$

Member with One End Pinned Connection

For member with left-end rigidly connected and right-end pinned connected, as shown in **Figure 7.9 (a)**, the relationship of the member end-forces and displacements can be obtained by using the same method as above. The details of this analysis are not repeated here, and the results are given as follows.

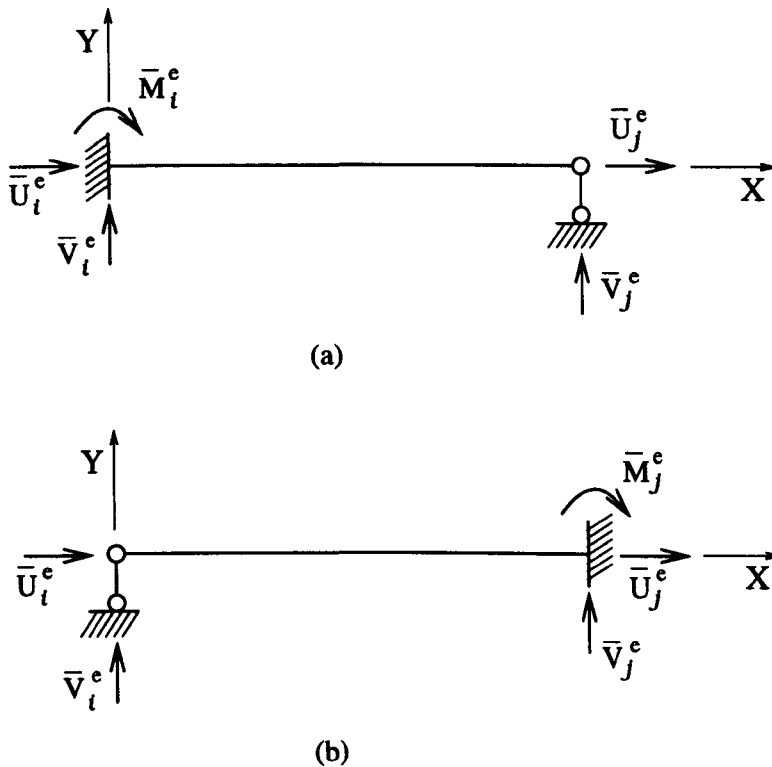


Figure 7.9: Members with pinned connection on one-end.

The general form of the local element stiffness matrix will be as follows:

$$[\bar{k}]^{(e)} = \begin{bmatrix} \frac{EA}{l} & 0 & 0 & -\frac{EA}{l} & 0 & 0 \\ 0 & \frac{1}{l(4\mu+\psi)} & -\frac{1}{4\mu+\psi} & 0 & -\frac{1}{l(4\mu+\psi)} & 0 \\ 0 & -\frac{1}{4\mu+\psi} & \frac{l}{4\mu+\psi} & 0 & \frac{1}{4\mu+\psi} & 0 \\ -\frac{EA}{l} & 0 & 0 & \frac{EA}{l} & 0 & 0 \\ 0 & -\frac{1}{l(4\mu+\psi)} & \frac{1}{4\mu+\psi} & 0 & \frac{1}{l(4\mu+\psi)} & 0 \\ 0 & 0 & 0 & 0 & 0 & 0 \end{bmatrix} \quad (7.65)$$

The equivalent joint loads $\{\bar{F}_s\}^{(e)}$ can be written as:

$$\{\bar{F}_s\}^{(e)} = \begin{Bmatrix} 0 \\ -\frac{1}{4\mu+\psi} \bar{\phi}_i^e \\ \frac{l}{4\mu+\psi} \bar{\phi}_i^e \\ 0 \\ \frac{1}{4\mu+\psi} \bar{\phi}_i^e \\ 0 \end{Bmatrix} \quad (7.66)$$

where $\mu = \frac{l^2}{12EI}$ and $\psi = \frac{\alpha l}{GA}$ as earlier.

The rotation of semi-rigid connection $\bar{\phi}_i^e$ can be obtained as;

$$\bar{\phi}_i^e = -\frac{(4\mu + \psi)\bar{M}_i^e}{l + (4\mu + \psi)k_i} \quad (7.67)$$

where \bar{M}_i^e is the member end moment if connection is rigid.

The member end-rotation $\bar{\theta}_j^e$ at right-end pinned connection due to the member end rotation $\bar{\theta}_i^e$ is given by

$$\bar{\theta}_j^e = \bar{\theta}_i^e - \frac{l^2}{2EI} \bar{V}_j^e. \quad (7.68)$$

To include the sway of the member, the member end-rotation $\bar{\theta}_j^e$ can be written as:

$$\bar{\theta}_j^e = \bar{\theta}_i^e - \frac{l^2}{2EI} \bar{V}_j^e - \frac{\bar{v}_j^e - \bar{v}_i^e}{l}. \quad (7.69)$$

For member with left-end being pinned and right-end rigidly connected, as shown in **Figure 7.9 (b)**, the general form of the local element stiffness matrix can be similarly obtained, and they are given by **Equation 7.70**

$$[\bar{k}]^{(e)} = \begin{bmatrix} \frac{EA}{l} & 0 & 0 & -\frac{EA}{l} & 0 & 0 \\ 0 & \frac{1}{l(4\mu+\psi)} & 0 & 0 & -\frac{1}{l(4\mu+\psi)} & -\frac{1}{4\mu+\psi} \\ 0 & 0 & 0 & 0 & 0 & 0 \\ -\frac{EA}{l} & 0 & 0 & \frac{EA}{l} & 0 & 0 \\ 0 & -\frac{1}{l(4\mu+\psi)} & 0 & 0 & \frac{1}{l(4\mu+\psi)} & \frac{1}{4\mu+\psi} \\ 0 & -\frac{1}{4\mu+\psi} & 0 & 0 & \frac{1}{4\mu+\psi} & \frac{l}{4\mu+\psi} \end{bmatrix} \quad (7.70)$$

The equivalent joint loads $\{F_s\}^{(e)}$ can be written as:

$$\{F_s\}^{(e)} = \begin{Bmatrix} 0 \\ -\frac{1}{4\mu+\psi} \bar{\phi}_j^e \\ 0 \\ 0 \\ \frac{1}{4\mu+\psi} \bar{\phi}_j^e \\ \frac{l}{4\mu+\psi} \bar{\phi}_j^e \end{Bmatrix} \quad (7.71)$$

The rotation of semi-rigid connection $\bar{\phi}_j^e$ can be given as:

$$\bar{\phi}_j^e = -\frac{(4\mu + \psi) \bar{M}_j^e}{l + k_j(4\mu + \psi)} \quad (7.72)$$

where \bar{M}_j^e is the member-end moment for rigid connection.

The member end-rotation $\bar{\theta}_i^e$ at left-end pinned connection due to member end rotation $\bar{\theta}_j^e$ is given by

$$\bar{\theta}_i^e = \bar{\theta}_j^e + \frac{l^2}{2EI} \bar{V}_i^e \quad (7.73)$$

To include the sway of the member, the member end-rotation $\bar{\theta}_i^e$ can be written as:

$$\bar{\theta}_i^e = \bar{\theta}_j^e + \frac{l^2}{2EI} \bar{V}_i^e - \frac{\bar{v}_j^e - \bar{v}_i^e}{l} \quad (7.74)$$

7.6 Stability Functions Used in the Matrix Displacement Method

7.6.1 Stability Functions without Shear

When the lateral displacement of a member under loading changes so does the axial force in the members of a structure vary. Their individual stiffnesses change and so does the overall stiffness of the structure. Majid (1972) indicated that, 'the influence of the axial force in the member is a significant cause of nonlinearity in the behaviour of structures.' Livesley (1975) further explained this as that, 'if any of the individual elements of a structure have \mathbf{K} matrices whose coefficients depend on the element deformation then the structure will behave in a nonlinear manner.'

Majid (1978) explained that 'applying an axial force to a member aggravates its end rotation and thus reduces the member stiffness.' To take into consideration the effect of the axial loads on the stiffness coefficient of the member without shear deformation of member, the stability function s and c can be derived; their derivation can be found elsewhere (Majid, 1972; Coates et al., 1988). Livesley (1956) developed his well-known stability functions by using the various ϕ terms to group the stability function s and c . They are convenient to use in the matrix displacement

method. For a single member, the sub-stiffness matrix are given as follows:

$$[\mathbf{k}_{11}] = \begin{bmatrix} \frac{EA}{l} & 0 & 0 \\ 0 & \frac{12EI}{l^3}\phi_5 & -\frac{6EI}{l^2}\phi_2 \\ 0 & -\frac{6EI}{l^2}\phi_2 & \frac{4EI}{l}\phi_3 \end{bmatrix} \quad (7.75)$$

$$[\mathbf{k}_{12}] = \begin{bmatrix} -\frac{EA}{l} & 0 & 0 \\ 0 & -\frac{12EI}{l^3}\phi_5 & -\frac{6EI}{l^2}\phi_2 \\ 0 & \frac{6EI}{l^2}\phi_2 & \frac{2EI}{l}\phi_4 \end{bmatrix} \quad (7.76)$$

$$[\mathbf{k}_{21}] = \begin{bmatrix} -\frac{EA}{l} & 0 & 0 \\ 0 & -\frac{12EI}{l^3}\phi_5 & \frac{6EI}{l^2}\phi_2 \\ 0 & -\frac{6EI}{l^2}\phi_2 & \frac{2EI}{l}\phi_4 \end{bmatrix} \quad (7.77)$$

$$[\mathbf{k}_{22}] = \begin{bmatrix} \frac{EA}{l} & 0 & 0 \\ 0 & \frac{12EI}{l^3}\phi_5 & \frac{6EI}{l^2}\phi_2 \\ 0 & \frac{6EI}{l^2}\phi_2 & \frac{4EI}{l}\phi_3 \end{bmatrix} \quad (7.78)$$

in which ϕ functions are defined as follows:

$$\phi_1 = \frac{64 - 60\rho + 5\rho^2}{64 - 20\rho + \rho^2} - \sum_{n=1}^7 \frac{a_n \rho^n}{2^{3n}} \quad (7.79)$$

$$\phi_2 = \frac{\pi^2 \rho}{12(1 - \phi_1)} \quad (7.80)$$

$$\phi_3 = \frac{3\phi_2 + \phi_1}{4} \quad (7.81)$$

$$\phi_4 = \frac{3\phi_2 - \phi_1}{2} \quad (7.82)$$

$$\phi_5 = \phi_1 \phi_2 \quad (7.83)$$

where ρ is the ratio of the actual axial load P to the Euler critical load P_E and is

given as follows.

$$\rho = \frac{P}{P_E} = \frac{PL^2}{\pi^2 EI} \quad (7.84)$$

For the ϕ_1 equation derived by Livesley, the constants a_i 's are as follows:

$$\begin{aligned} a_1 &= 1.57973627 & a_2 &= 0.15858587 \\ a_3 &= 0.02748899 & a_4 &= 0.00547540 \\ a_5 &= 0.00115281 & a_6 &= 0.00024908 \\ a_7 &= 0.00005452 \end{aligned}$$

7.6.2 Stability Functions with Shear

Considering that an elastic slender column member buckles laterally, the applied longitudinal force P along the centroidal axis of the member will have a transverse component of load P_y . This transverse load component will produce the moment $m = P_y x$ at distance x from member end and will produce additional deformation due to shear. For practical purposes, this effect is unimportant, amounting to a reduction of a fraction of one percent (Bleich, 1952; Horne & Merchant, 1965). Therefore, this transverse component of axial load and the shear deformation produced by it will be neglected in the following analysis.

If taking into account the effect of shear deformation, the stability functions s (stiffness factor) and c (carry-over factor) will change correspondingly and the ϕ equations developed by Livesley (1956) can no longer be used.

To develop the stability functions which include the influence of axial load on bending stiffness and taking account of the shear deformation, each of the stiffness influence coefficients will be determined separately.

Due to the presence of axial load P , the individual stiffnesses of members change and the deflection of the member is nonlinear. The method described in the previous sections to include shear deformation in linear analysis is no longer valid. In the

following section, the stiffness of member due to the presence of axial force will be studied and the stability functions including shear deformation of member are derived.

Rotation of a member

Consider a member i - j of **Figure 7.10 (a)**, end i rotates at an angle $\bar{\theta}_i^e$, the member carries an axial compressive load P and bending moments \bar{M}_i^e and \bar{M}_j^e . There are uniform shear forces \bar{V}_i^e and \bar{V}_j^e ($\bar{V}_j^e = -\bar{V}_i^e$).

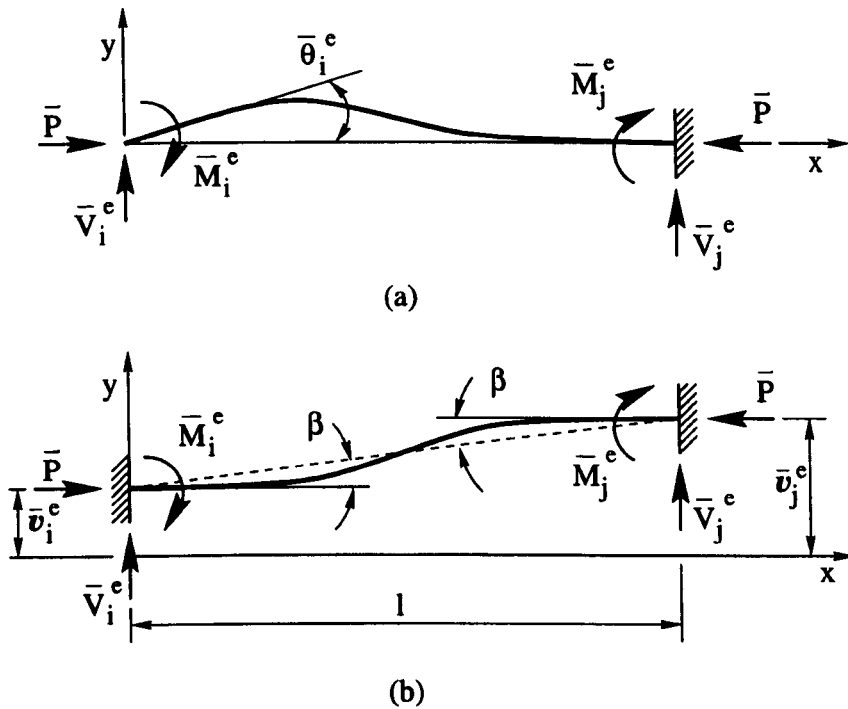


Figure 7.10: Deformation of a member, (a) rotation of end i , (b) a general state of sway.

The equation of flexure can be obtained as:

$$\frac{d^2y}{dx^2} = \frac{1}{EI} [\bar{M}_i^e + \bar{V}_i^e x - Py + P \frac{\alpha_s \bar{V}_i^e}{GA} (l - x)] \quad (7.85)$$

Considering shear deformation due to shear component of the axial force P , the critical load is given by Gaylord and Gaylord (1972) as:

$$P_c = \frac{\pi^2 EI}{l^2} \frac{1}{1 + \frac{\alpha_s \pi^2 EI}{L^2 GA}} \quad (7.86)$$

Substituting for the axial force $P = \rho P_c$ and factor $\alpha^2 = \frac{\pi^2 \rho}{4} \frac{1}{1 + \frac{\alpha_s \pi^2 EI}{L^2 GA}}$ and $k = \frac{EI}{l}$ into **Equation 7.85** the curvature of the member becomes:

$$\frac{d^2y}{dx^2} = \frac{1}{EI} [\bar{M}_i^e + \bar{V}_i^e x - \frac{4\alpha^2 k}{l} y + \frac{4\alpha^2 k}{l} \frac{\alpha_s \bar{V}_i^e}{GA} (l - x)] \quad (7.87)$$

The general solution of **Equation 7.87** is

$$y = C_1 \sin \frac{2\alpha}{l} x + C_2 \cos \frac{2\alpha}{l} x + \frac{l \bar{V}_i^e}{4\alpha^2 k} x + \frac{l \bar{M}_i^e}{4\alpha^2 k} + \frac{\alpha_s \bar{V}_i^e}{GA} (l - x) \quad (7.88)$$

Differentiation of **Equation 7.88** gives the slope:

$$\frac{dy}{dx} = C_1 \frac{2\alpha}{l} \cos \frac{2\alpha}{l} x - C_2 \frac{2\alpha}{l} \sin \frac{2\alpha}{l} x + \frac{l \bar{V}_i^e}{4\alpha^2 k} - \frac{\alpha_s \bar{V}_i^e}{GA} \quad (7.89)$$

The Constants of integration C_1 and C_2 can be found from the boundary conditions, $y = 0$ at $x = 0$, and $y = 0$ at $x = l$.

$$C_1 = \frac{1}{\sin 2\alpha} \left[\frac{l(\cos 2\alpha - 1)}{4\alpha^2 k} \bar{M}_i^e + \left(\frac{l \alpha_s \cos 2\alpha}{GA} - \frac{l^2}{4\alpha^2 k} \right) \bar{V}_i^e \right] \quad (7.90)$$

$$C_2 = -\frac{l}{4\alpha^2 k} \bar{M}_i^e - \frac{\alpha_s \bar{V}_i^e}{GA} l \quad (7.91)$$

The uniform shear force \bar{V}_i^e can be obtained by taking moments about end j:

$$\bar{V}_i^e = -\frac{\bar{M}_i^e + \bar{M}_j^e}{l} \quad (7.92)$$

Substituting the C_1 , C_2 and \bar{V}_i^e in **Equation 7.89**, the boundary condition, $\frac{dy}{dx} = -\frac{\alpha_s \bar{V}_i^e}{GA}$ at $x = l$, provides the carry-over factor c for stability function.

$$c = \frac{\bar{M}_i^e}{\bar{M}_j^e} = \frac{2\alpha - \sin 2\alpha - \frac{8\alpha^3 k\alpha_s}{lGA}}{\sin 2\alpha - 2\alpha \cos 2\alpha + \frac{8\alpha^3 k\alpha_s}{lGA}} \quad (7.93)$$

Finally, the boundary condition, $\frac{dy}{dx} = -\bar{\theta}_i^e - \frac{\alpha_s \bar{V}_i^e}{GA}$ at $x = 0$, provides the stability function s .

$$s = \frac{\bar{M}_i^e}{k\bar{\theta}_i^e} = \frac{\alpha(1 - 2\alpha \cot 2\alpha + \frac{8\alpha^3 k\alpha_s}{lGA \sin 2\alpha})}{\tan \alpha - \alpha + \frac{4\alpha^3 k\alpha_s}{lGA}} \quad (7.94)$$

If let $\phi_1 = \alpha \cot \alpha$, then

$$c = \frac{\alpha^2 - \phi_1 + \phi_1^2 - 4(\alpha^4 + \alpha^2 \phi_1^2) \frac{k\alpha_s}{lGA}}{\phi_1 - \phi_1^2 + \alpha^2 + 4(\alpha^4 + \alpha^2 \phi_1^2) \frac{k\alpha_s}{lGA}} \quad (7.95)$$

$$s = \frac{\alpha^2 + \phi_1 - \phi_1^2 + 4(\alpha^2 \phi_1^2 + \alpha^4) \frac{k\alpha_s}{lGA}}{1 - \phi_1 + 4\alpha^2 \phi_1 \frac{k\alpha_s}{lGA}} \quad (7.96)$$

It can be seen that the value of s and c in **Equations 7.95** and **7.96** depend on the member properties. By taking the length of member (8x8x3/8 inch WF profile) $l = 4m$, section area of member $A = 5.632 \times 10^{-3} m^2$, elastic modulus $E = 1.793 \times 10^7 kN/m^2$, second moment of area $I = 4.128 \times 10^{-5} m^4$, shear modulus $G = 2.930 \times 10^6 kN/m^2$ and shear coefficient $\alpha_s = 3.210$, the stability function s and c with ρ can be shown graphically in **Figure 7.11**, in which cs and ss represent the stability functions by taking account of the effect of the shear deformation of the member.

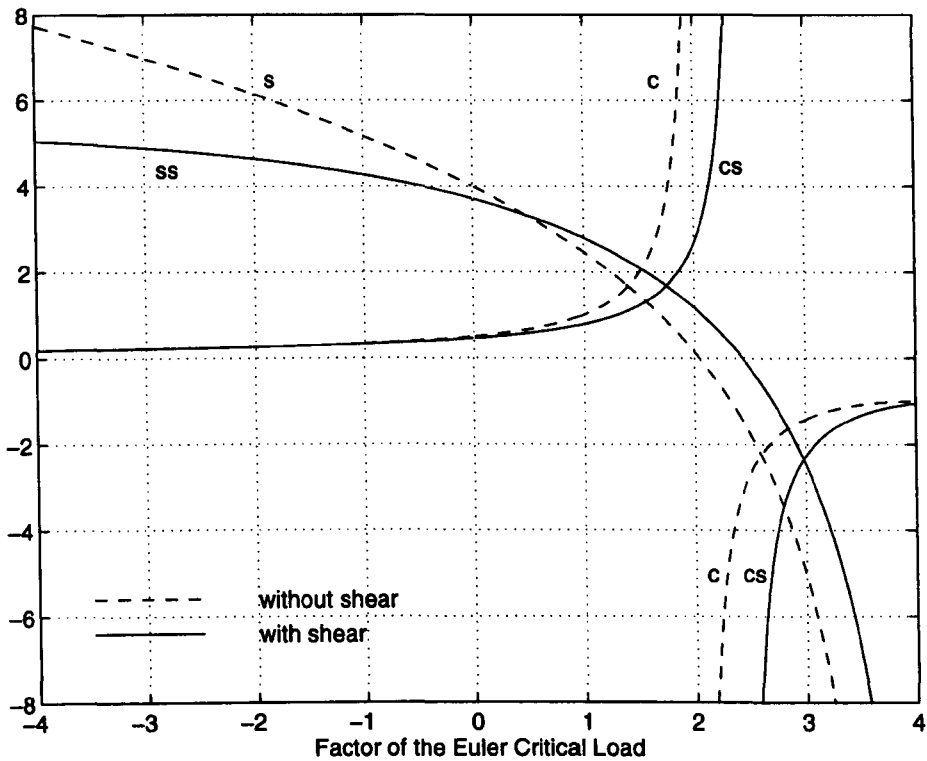


Figure 7.11: The stability functions s and c.

Lateral Deflection

The derivation of the member end forces due to a relative lateral deflection between end i and end j, as shown in **Figure 7.10 (b)**, can be found in text books (Coates et.al, 1988; Majid, 1972) and it is not repeated here. The results are shown as follows:

$$\bar{M}_i^e = \bar{M}_j^e = \frac{s(1+c)k}{l}(\bar{v}_j^e - \bar{v}_i^e) \tag{7.97}$$

$$\bar{V}_i^e = -\bar{V}_j^e = \left(-\frac{2s(1+c)k}{l} + P\right)\frac{\bar{v}_j^e - \bar{v}_i^e}{l} \tag{7.98}$$

ϕ Function

For convenience in the construction of the stiffness matrix of a member, the various ϕ terms used to group the stability function s and c are redefined in **Equations 7.99** to **7.103**, in which the ϕ_1 is defined as the same form as the one defined by Livesley (1956), but $\alpha^2 = \frac{\pi^2 \rho}{4} \frac{1}{1 + \frac{\alpha_4 \pi^2 EI}{l^2 GA}}$.

$$\phi_1 = \alpha \cot \alpha \quad (7.99)$$

$$\phi_2 = \frac{2\phi_3 + \phi_4}{3} \quad (7.100)$$

$$\phi_3 = \frac{s}{4} \quad (7.101)$$

$$\phi_4 = 2c\phi_3 \quad (7.102)$$

$$\phi_5 = \phi_2 - \frac{\alpha^2}{3} \quad (7.103)$$

By using the same member property as that defined earlier in this section the modified ϕ functions can be shown in **Figure 7.12**.

Member with One End Pinned Connection

For member with one end pinned connection as shown in **Figure 7.9** the stiffness matrix can be modified as follows.

If there is a pin at left end, then:

$$[\bar{k}]^{(e)} = \begin{bmatrix} \frac{EA}{l} & 0 & 0 & -\frac{EA}{l} & 0 & 0 \\ 0 & \frac{1}{4l\mu}\phi_5 & 0 & 0 & -\frac{1}{4l\mu}\phi_5 & -\frac{1}{4\mu}\phi_2 \\ 0 & 0 & 0 & 0 & 0 & 0 \\ -\frac{EA}{l} & 0 & 0 & \frac{EA}{l} & 0 & 0 \\ 0 & -\frac{1}{4l\mu}\phi_5 & 0 & 0 & \frac{1}{4l\mu}\phi_5 & \frac{1}{4\mu}\phi_2 \\ 0 & -\frac{1}{4\mu}\phi_2 & 0 & 0 & \frac{1}{4\mu}\phi_2 & \frac{l}{4\mu}\phi_3 \end{bmatrix} \quad (7.104)$$

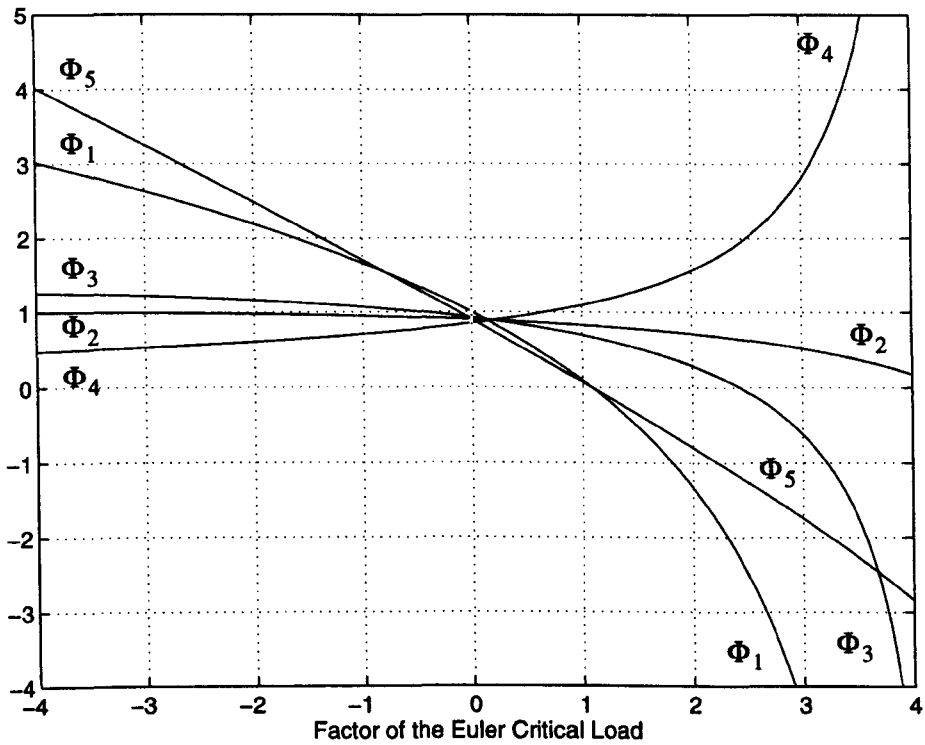


Figure 7.12: Modified Livesley's function with shear deformation.

If there is a pin at right end, then:

$$\left[\bar{k} \right]^{(e)} = \begin{bmatrix} \frac{EA}{l} & 0 & 0 & -\frac{EA}{l} & 0 & 0 \\ 0 & \frac{1}{4l\mu} \phi_5 & -\frac{1}{4\mu} \phi_2 & 0 & -\frac{1}{4l\mu} \phi_5 & 0 \\ 0 & -\frac{1}{4\mu} \phi_2 & \frac{l}{4\mu} \phi_3 & 0 & \frac{1}{4\mu} \phi_2 & 0 \\ -\frac{EA}{l} & 0 & 0 & \frac{EA}{l} & 0 & 0 \\ 0 & -\frac{1}{4l\mu} \phi_5 & \frac{1}{4\mu} \phi_2 & 0 & \frac{1}{4l\mu} \phi_5 & 0 \\ 0 & 0 & 0 & 0 & 0 & 0 \end{bmatrix} \tag{7.105}$$

where $\mu = \frac{l^2}{12EI}$, ϕ_2 , ϕ_3 and ϕ_5 redefined as:

$$\phi_2 = \frac{s}{3}(1 - c^2) \quad (7.106)$$

$$\phi_3 = \frac{s}{3}(1 - c^2) \quad (7.107)$$

$$\phi_5 = \frac{1}{3} \left[s(1 - c^2) - \rho\pi^2 \frac{1}{1 + \frac{\alpha_4 \pi^2 EI}{l^2 GA}} \right]. \quad (7.108)$$

7.7 Sum of Effect of Axial loading, Shearing and Semi-rigid

7.7.1 Member without Pinned Connection

To analyse frame, if the effect of axial load, shear deformation and the semi-rigid connection properties need to be combined, the local member stiffness matrix will now be as follows:

$$[\bar{k}]^{(e)} = \begin{bmatrix} \frac{EA}{l} & 0 & 0 & -\frac{EA}{l} & 0 & 0 \\ 0 & \frac{1}{l\mu}\phi_5 & -\frac{1}{2\mu}\phi_2 & 0 & -\frac{1}{l\mu}\phi_5 & -\frac{1}{2\mu}\phi_2 \\ 0 & -\frac{1}{2\mu}\phi_2 & \frac{l}{3\mu}\phi_3 & 0 & \frac{1}{2\mu}\phi_2 & \frac{l}{6\mu}\phi_4 \\ -\frac{EA}{l} & 0 & 0 & \frac{EA}{l} & 0 & 0 \\ 0 & -\frac{1}{l\mu}\phi_5 & \frac{1}{2\mu}\phi_2 & 0 & \frac{1}{l\mu}\phi_5 & \frac{1}{2\mu}\phi_2 \\ 0 & -\frac{1}{2\mu}\phi_2 & \frac{l}{6\mu}\phi_4 & 0 & \frac{1}{2\mu}\phi_2 & \frac{l}{3\mu}\phi_3 \end{bmatrix} \quad (7.109)$$

where parameter $\mu = \frac{l^2}{12EI}$ and all other terms have been defined earlier. The equivalent joint loads $\{\bar{F}_s\}^{(e)}$ due to the deformations of the semi-rigid connections

can be written as:

$$\{\bar{F}_s\}^{(e)} = \begin{Bmatrix} 0 \\ -\frac{1}{2\mu}\phi_2(\bar{\phi}_i^e + \bar{\phi}_j^e) \\ \frac{1}{3\mu}\phi_3\bar{\phi}_i^e + \frac{1}{6\mu}\phi_4\bar{\phi}_j^e \\ 0 \\ \frac{1}{2\mu}\phi_2(\bar{\phi}_i^e + \bar{\phi}_j^e) \\ \frac{1}{6\mu}\phi_4\bar{\phi}_i^e + \frac{1}{3\mu}\phi_3\bar{\phi}_j^e \end{Bmatrix} \quad (7.110)$$

The foregoing equations are general forms of local member stiffness matrix $\{\bar{k}\}^{(e)}$ and equivalent joint loads $\{\bar{F}_s\}^{(e)}$ when joints are not pinned.

In **Equations 7.109** and **7.110**, if shear deformation of member are neglected, Livesley's ϕ functions (**Equations 7.79** to **7.83**) will be used, otherwise the modified functions are used (**Equations 7.99** to **7.103**). If the effects of axial load and shear deformation of member are not being considered, the ϕ functions are set to those in **Equations 7.109** and **7.110** ($\phi_{1-5} = 1$); the above equations become these when the element has semi-rigid connections only.

The rotations of the semi-rigid connections at end i and j can be obtained from ϕ_i and ϕ_j ,

$$\bar{\phi}_i^e = \frac{(C_1 + k_j)\bar{M}_i^e - B\bar{M}_j^e}{C_2^2 - (C_1 + k_i)(C_1 + k_j)} \quad (7.111)$$

and

$$\bar{\phi}_j^e = -\frac{\bar{M}_i^e + (C_1 + k_i)\bar{\phi}_i^e}{C_2} \quad (7.112)$$

where: $C_1 = \frac{1}{3\mu}\phi_3$ and $C_2 = \frac{1}{6\mu}\phi_4$ and \bar{M}_i^e and \bar{M}_j^e are the member-end moments for the rigid connections.

7.7.2 Member with One End Pinned Connection

For member with left-end rigidly or semi-rigidly connected and right-end pinned connected, as shown in **Figure 7.9 (a)**, the general form of the local element stiffness matrix will be as follows:

$$[\bar{k}]^{(e)} = \begin{bmatrix} \frac{EA}{l} & 0 & 0 & -\frac{EA}{l} & 0 & 0 \\ 0 & \frac{1}{4l\mu}\phi_5 & -\frac{1}{4\mu}\phi_2 & 0 & -\frac{1}{4l\mu}\phi_5 & 0 \\ 0 & -\frac{1}{4\mu}\phi_2 & \frac{l}{4\mu}\phi_3 & 0 & \frac{1}{4\mu}\phi_2 & 0 \\ -\frac{EA}{l} & 0 & 0 & \frac{EA}{l} & 0 & 0 \\ 0 & -\frac{1}{4l\mu}\phi_5 & \frac{1}{4\mu}\phi_2 & 0 & \frac{1}{4l\mu}\phi_5 & 0 \\ 0 & 0 & 0 & 0 & 0 & 0 \end{bmatrix} \quad (7.113)$$

The equivalent joint loads $\{\bar{F}_s\}^{(e)}$ can be written as:

$$\{\bar{F}_s\}^{(e)} = \begin{Bmatrix} 0 \\ -\frac{1}{4\mu}\phi_2\bar{\phi}_i^e \\ \frac{l}{4\mu}\phi_3\bar{\phi}_i^e \\ 0 \\ \frac{1}{4\mu}\phi_2\bar{\phi}_i^e \\ 0 \end{Bmatrix} \quad (7.114)$$

The rotation of semi-rigid connection ϕ_i can be obtained as;

$$\bar{\phi}_i^e = -\frac{4\mu\bar{M}_i^e}{l\phi_3 + 4\mu k_i} \quad (7.115)$$

where \bar{M}_i^e is the member-end moment for the rigid connection.

The member end-rotation $\bar{\theta}_j^e$ at right-end pinned connection due to member end

rotation $\bar{\theta}_i^e$ is given by

$$\bar{\theta}_j^e = -c\bar{\theta}_i^e \quad (7.116)$$

where c is carry-over factor. To include the sway of the member, the member end-rotation $\bar{\theta}_j^e$ can be written as:

$$\bar{\theta}_j^e = -c(\bar{\theta}_i^e + \frac{\bar{v}_j^e - \bar{v}_i^e}{l}). \quad (7.117)$$

For member with right-end rigidly or semi-rigidly connected and left-end pinned connected, as shown in **Figure 7.9 (b)**, the general form of local element stiffness matrix will be as follows:

$$[\bar{k}]^{(e)} = \begin{bmatrix} \frac{EA}{l} & 0 & 0 & -\frac{EA}{l} & 0 & 0 \\ 0 & \frac{1}{4l\mu}\phi_5 & 0 & 0 & -\frac{1}{4l\mu}\phi_5 & -\frac{1}{4\mu}\phi_2 \\ 0 & 0 & 0 & 0 & 0 & 0 \\ -\frac{EA}{l} & 0 & 0 & \frac{EA}{l} & 0 & 0 \\ 0 & -\frac{1}{4l\mu}\phi_5 & 0 & 0 & \frac{1}{4l\mu}\phi_5 & \frac{1}{4\mu}\phi_2 \\ 0 & -\frac{1}{4\mu}\phi_2 & 0 & 0 & \frac{1}{4\mu}\phi_2 & \frac{l}{4\mu}\phi_3 \end{bmatrix} \quad (7.118)$$

The equivalent joint loads $\{F_s\}^{(e)}$ can be written as:

$$\{F_s\}^{(e)} = \begin{Bmatrix} 0 \\ -\frac{1}{4\mu}\phi_2\bar{\phi}_j^e \\ 0 \\ 0 \\ \frac{1}{4\mu}\phi_2\bar{\phi}_j^e \\ \frac{l}{4\mu}\phi_3\bar{\phi}_j^e \end{Bmatrix} \quad (7.119)$$

The rotation of semi-rigid connection ϕ_j can be given as:

$$\bar{\phi}_j^e = -\frac{4\mu\bar{M}_j^e}{l\phi_3 + 4\mu k_j} \quad (7.120)$$

where \bar{M}_j^e is the member-end rotation for the rigid connection.

The member end-rotation $\bar{\theta}_i^e$ at left-end pinned connection due to member end rotation $\bar{\theta}_j^e$ is given by

$$\bar{\theta}_i^e = -c\bar{\theta}_j^e \quad (7.121)$$

where c is carry-over factor. To include the sway of the member, the member end-rotation $\bar{\theta}_i^e$ can be written as:

$$\bar{\theta}_i^e = -c\left(\bar{\theta}_j^e + \frac{\bar{v}_j^e - \bar{v}_i^e}{l}\right). \quad (7.122)$$

7.8 Load between Joints

In the matrix method of analysis, the load applied on the member between the joints are transformed to equivalent joint loads. These equivalent joint loads are then used to form the total loads with loads applied on the joints. The equivalent joint loads can be obtained by using the method of virtual work. For the member with or without pinned connection, the equivalent joint loads of a partial distributed load, vertical concentrated load and horizontal concentrated load are given in the following sections.

7.8.1 Partial Distributed Load

For partial distributed uniform load, ω , between the joints, as shown in **Figure 7.13** (a), the equivalent joint loads when both ends are rigidly fixed are

$$\bar{Q}_i = -\frac{\omega c}{2} \left(2 - 2\frac{c^2}{l^2} + \frac{c^3}{l^3} \right) \quad (7.123)$$

$$\bar{Q}_j = -\omega c - \bar{V}_i \quad (7.124)$$

$$\bar{M}_i = \frac{\omega c^2}{12} \left(6 - 8\frac{c}{l} + 3\frac{c^2}{l^2} \right) \quad (7.125)$$

$$\bar{M}_j = -\frac{\omega c^3}{12l} \left(4 - 3\frac{c}{l} \right) \quad (7.126)$$

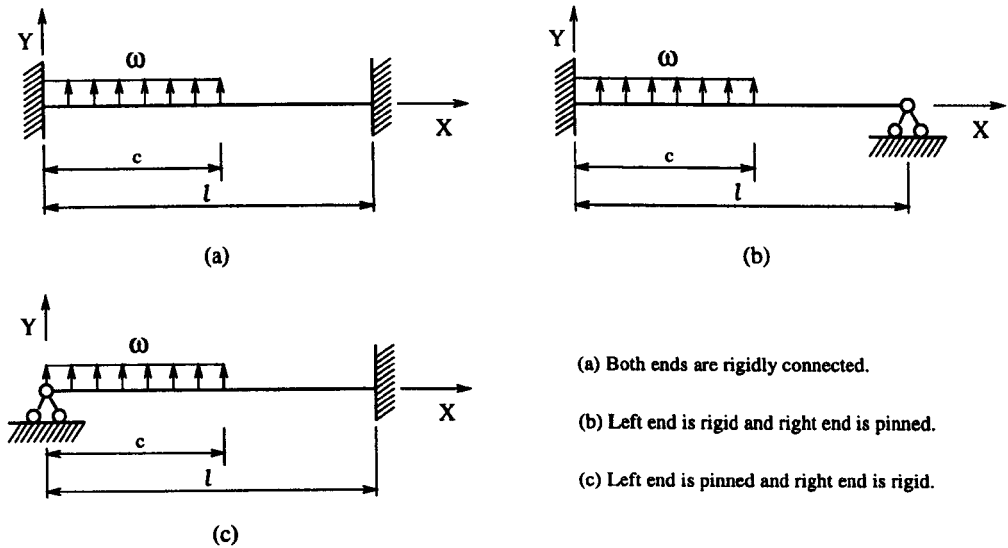


Figure 7.13: Partial distributed load between the joints.

For the member with right-end pinned, as shown in **Figure 7.13** (b), the equivalent joint loads are

$$\bar{Q}_i = -\frac{8l^3 - (4l - c)c^2}{8l^3} \omega c \quad (7.127)$$

$$\bar{Q}_j = -\omega c - \bar{V}_i \quad (7.128)$$

$$\bar{M}_i = \frac{4l^2 - 4lc + c^2}{8l^2} \omega c^2 \quad (7.129)$$

$$\bar{M}_j = 0 \quad (7.130)$$

For the member with left-end pinned, as shown in **Figure 7.13 (c)**, the equivalent joint loads are

$$\bar{Q}_i = -\frac{\omega c}{8l^3}(c^3 - 6cl^2 + 8l^3) \quad (7.131)$$

$$\bar{Q}_j = -qc - \bar{V}_i \quad (7.132)$$

$$\bar{M}_i = 0 \quad (7.133)$$

$$\bar{M}_j = \frac{\omega c}{8l^2}(c^3 - 2cl^2). \quad (7.134)$$

7.8.2 Vertical Concentrated Load

Figure 7.14 (a) shows the vertical concentrated load applied between the joints of a member with fixed ends. The equivalent joint loads are

$$\bar{Q}_i = -P \frac{(l+2c)(l-c)^2}{l^3} \quad (7.135)$$

$$\bar{Q}_j = -P \frac{(3l-2c)c^2}{l^3} \quad (7.136)$$

$$\bar{M}_i = P \frac{c(l-c)^2}{l^2} \quad (7.137)$$

$$\bar{M}_j = -P \frac{c^2(l-c)}{l^2}. \quad (7.138)$$

For the member with right-end pinned and left-end fully clamped (see **Figure 7.14 (b)**), the equivalent joint loads are given as:

$$\bar{Q}_i = -\frac{3PC^2}{2l^3} \left(l - \frac{C}{3} \right) - P \quad (7.139)$$

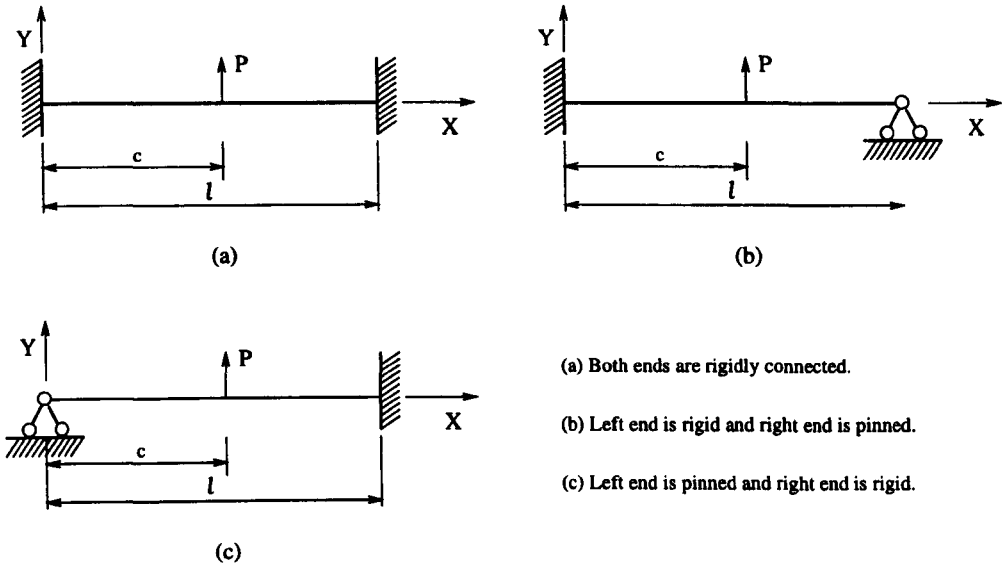


Figure 7.14: Vertical concentrated load between the joints.

$$\bar{Q}_j = -\frac{3PC^2}{2l^3} \left(l - \frac{C}{3} \right) \tag{7.140}$$

$$\bar{M}_i = -\frac{3PC^2}{2l^2} \left(l - \frac{C}{3} \right) + PC \tag{7.141}$$

$$\bar{M}_j = 0. \tag{7.142}$$

The following equations give the equivalent joint loads of a vertical concentrated load applied between the joints for the member with left-end pinned and right-end fully clamped (see **Figure 7.14 (c)**),

$$\bar{Q}_i = -\frac{P}{2l^3} (l - c)^2 (2l + c) \tag{7.143}$$

$$\bar{Q}_j = \frac{P}{2l^3} (c^3 - 3cl^2) \tag{7.144}$$

$$\bar{M}_i = 0 \tag{7.145}$$

$$\bar{M}_j = \frac{P}{2l^2} (c^3 - cl^2). \tag{7.146}$$

7.8.3 Axial Concentrated Load

Figure 7.15 shows the horizontal concentrated load between the joints of a member with fixed end (a) or with one end pinned (b) and (c). For the member with pinned or without pinned connection, the equivalent joint loads are given as follows:

$$\bar{N}_i = -P \frac{l - C}{l} \tag{7.147}$$

$$\bar{N}_j = -P \frac{C}{l} \tag{7.148}$$

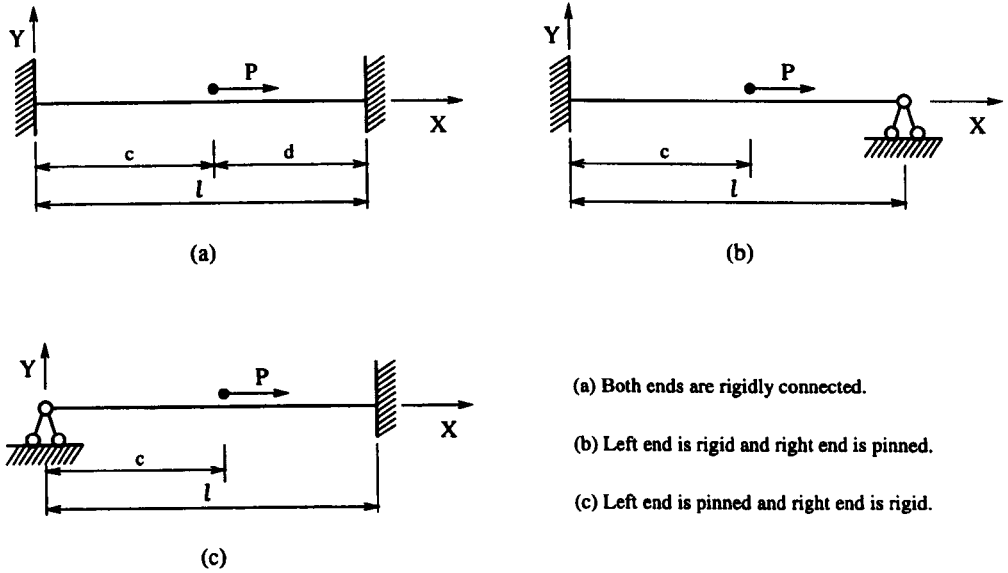


Figure 7.15: Horizontal concentrated load between the joints.

7.9 Computer Program

7.9.1 Program Procedure

The program procedure for determining semi-rigid connection frame behaviour is given in the form of a flowchart in **Figure 7.16**.

The procedure is explained by the following notes:

- To number the joints and the members. Each joint and member is assigned a unique number.
- To calculate the vector of external total loads at joints $\{\mathbf{P}\}$, using **Equation 7.23** (step 7 in flowchart).
- To generate local member stiffness matrix $[\bar{\mathbf{k}}]^{(e)}$ (step 5 in flowchart).
- To transform local member stiffness matrix $[\bar{\mathbf{k}}]^{(e)}$ to member stiffness matrix $[\mathbf{k}]^{(e)}$ in the structure coordinate axes (step 6 in flowchart).
- To construct the structural stiffness matrix $[\mathbf{k}]$ (step 8 in flowchart).
- To modify the structure stiffness matrix $[\mathbf{k}]$, the vector of joint deflections of the structure $\{\delta\}$, and the vector of external loads $\{\mathbf{P}\}$ of the structure by applying load and restraint boundary conditions at the joint of the structure (step 9 in flowchart).
- To calculate $\{\delta\}$ by solving the matrix equation $[\mathbf{k}]^* \{\delta\} = \{\mathbf{P}\}^*$ using Gaussian elimination method (step 10 in flowchart).
- To determine the member forces from:

$$\{\bar{\mathbf{F}}\}^{(e)} = [\bar{\mathbf{k}}]^{(e)} \{\delta\}^{(e)} + \{\bar{\mathbf{F}}_0\}^{(e)} + \{\bar{\mathbf{F}}_s\}^{(e)} \quad (7.149)$$

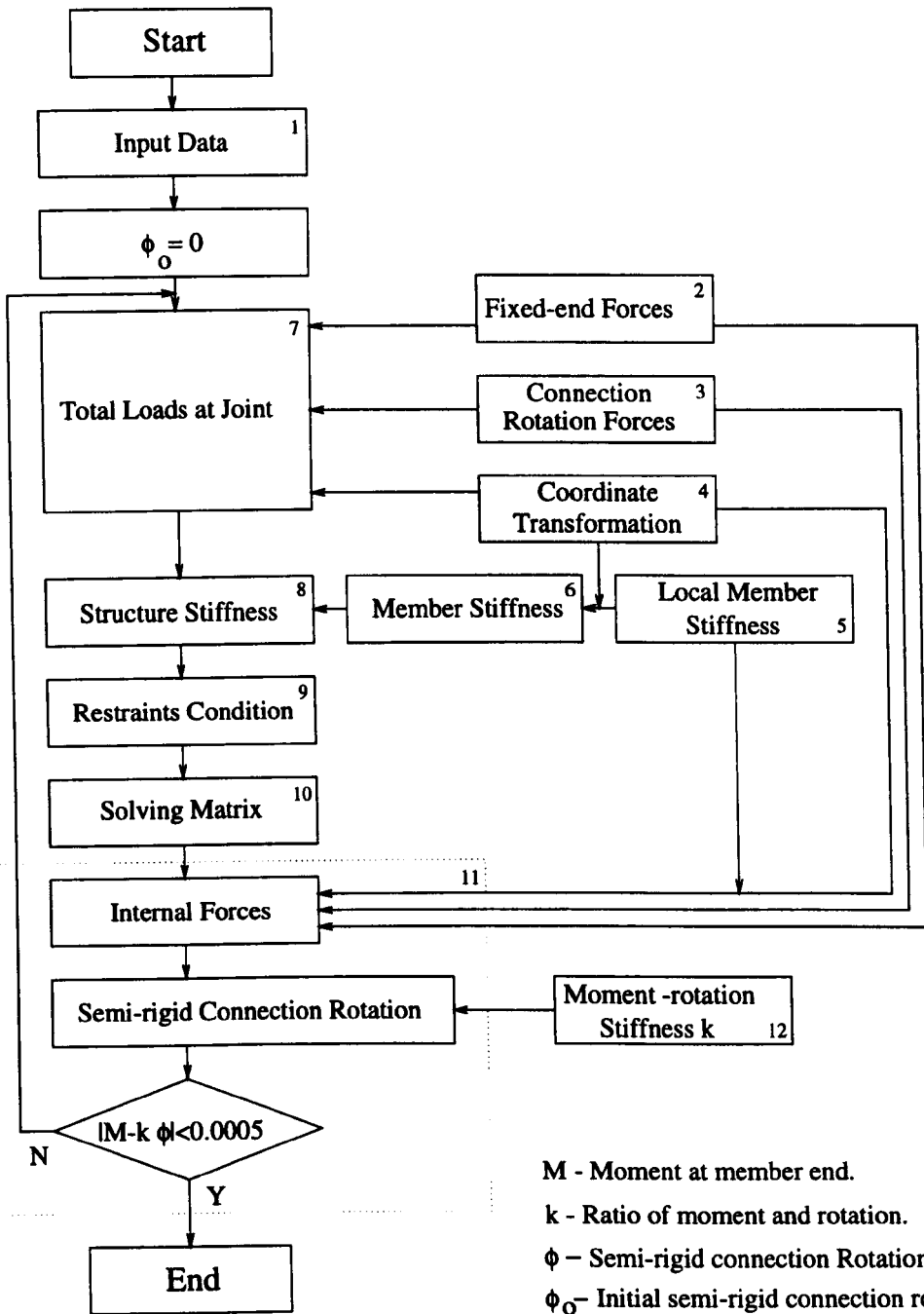


Figure 7.16: Flowchart of programme.

where $\{\bar{\mathbf{F}}_0\}^{(e)}$ is fixed-end force due to loads between joints and $\{\bar{\mathbf{F}}_s\}^{(e)}$ is member fix-end forces due to semi-rigid connection. The calculation of the fixed-end force vector $\{\bar{\mathbf{F}}_0\}^{(e)}$ can be found in Coates et al. (1988) and Ghali and Neville (1989) and therefore is not reproduced here. The fixed-end force vector $\{\bar{\mathbf{F}}_s\}^{(e)}$ is obtained by using the equation defined in this chapter.

- To calculate semi-rigid connection rotations $\bar{\phi}_i^e$ and $\bar{\phi}_j^e$ and the calculated member end moments \bar{M}_i^e and \bar{M}_j^e .
- To compare the obtained member end-moment with the moment obtained by $k\bar{\phi}^e$. If its absolute value is less than the tolerance (0.0005 is used in the programme), the iteration process is terminated, otherwise repeat procedure step 1 to 10 using previous values of $\bar{\phi}_i^e$ and $\bar{\phi}_j^e$ until convergence is achieved.

7.9.2 Moment-rotation Stiffness k

For the nonlinear moment-rotation curve of a semi-rigid connection, a series of straight lines can be used to represent the nonlinear curve in the analysis. The moment-rotation stiffness k used in the program is the gradient of the line which is from the point on the moment-rotation curve to the original point, and this is known as the secant stiffness represented by **Equation 7.150**. For nonlinear moment-rotation curves, the ratio k is not constant, but a function of M and ϕ . To a certain value of the moment M , a corresponding ratio k can be found, and this k is then used to obtain rotation ϕ .

$$M = k\phi \quad (7.150)$$

To obtain the moment-rotation ratio k for the given frame structure under certain load condition, the iteration process is used in the program. The method of iteration

used to obtain each intermediate secant stiffness k is illustrated in **Figure 7.17** and will now be explained.

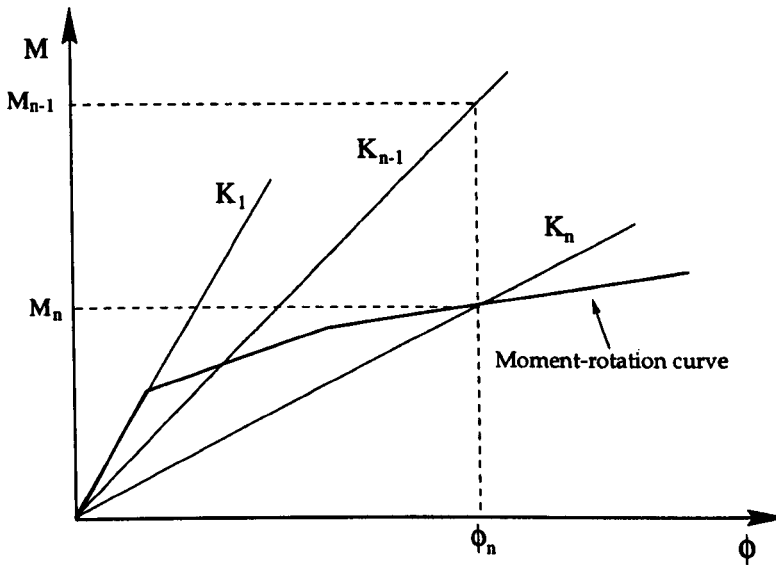


Figure 7.17: The method to obtain moment-rotation ratio k .

With joint moment M_{n-1} calculated from $n-1$ iteration (if it is first iteration, then this moment is from the rigid frame calculation), the value of ϕ_n can be determined by using the previous moment-rotation ratio k_{n-1} . ϕ_n is then used to determine M_n from the moment-rotation curve. The new secant stiffness k_n is obtained from M_n/ϕ_n and so the process can be repeated as many times as is necessary.

7.9.3 Iteration Process and Convergence Problems

In the computer analysis program, the iterative process is used for analysis considering also the effects due to the second-order deflections and of semi-rigid connections.

In the analysis of the second order effect, the axial forces obtained from the previous iteration are used to determine the stability functions ϕ , and these ϕ functions

are then used in the next iteration process.

In the analysis of the effect of semi-rigid connection, the analysis procedure is started by replacing the nonlinear moment-rotation function of the connection with a linear relationship and k used in first iteration is initial tangent stiffness of the moment-rotation curve. From this initial k , a new k is obtained at each iteration.

If both the second order effect and the effect of semi-rigid connections are included in a frame analysis, the program will find it hard converge in some case due to separate determination of ϕ functions and semi-rigid connection rotation. If this happens the program will terminate at the maximum iteration which is defined in a data file by user. Alternatively, the user can change the value of the tolerance in the data file.

7.10 Comparison of Analysis Results with Other Researches

The program has been verified with two recognised steel frame examples of a three-story one-bay frame (frame A) and of a two-story three-bay frame (frame B). They are shown in **Figures 7.18** and **7.19** respectively, and were specified by Zandonini (1986). The elastic modulus for the steel members is 210×10^6 kN/m². The connections used were extended end-plates with backing plates and their moment-rotation curves of the joint of frames A and B are give in **Figure 7.20** by the piece-wise linear relations.

The comparison of the results with other researchers (ECCS) is presented in **Figures 7.21** and **7.22** for frame A and frame B, respectively. As the developed computer analysis program is limited to second-order elastic analysis, the results show a good agreement with other research group before inelastic behaviour occurs

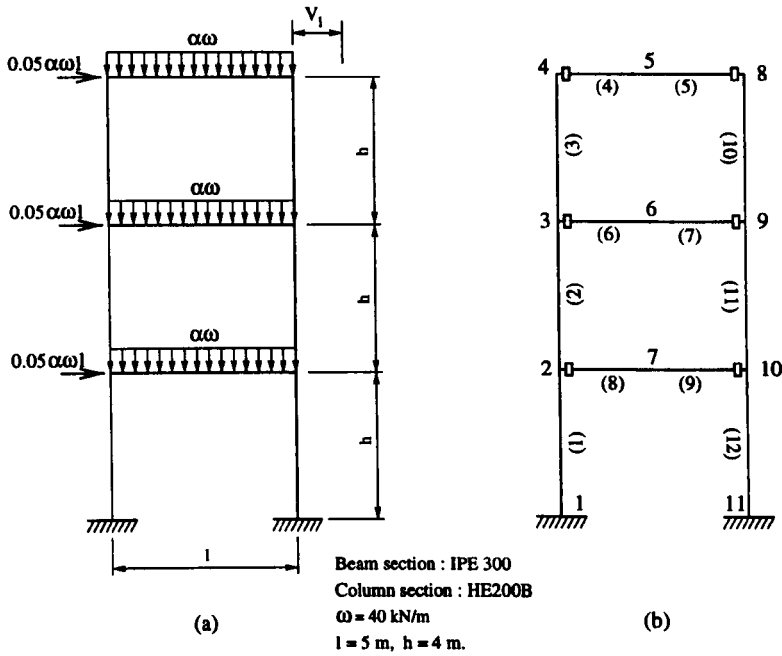


Figure 7.18: Frame A: (a) frame geometries, loading conditions and, (b) the numbering of members and joints.

in the frame. When the load factor *alpha* is over one prescribed for the analysis, deviation in the results will exist.

The resulting behaviour of the frame A, with the comparison with the equivalent rigidly connected frame, the semi-rigid connected frame, the semi-rigid connected frame taking into account of second order effects, and the semi-rigid connected frame taking into account of second order effects and shear is shown in **Figure 7.23**. It is shown that the overall sway of joint 8 is significantly influenced by the connection behaviour and it is also verified that the shear effects can be ignored in the steel frame design.

Verification against the test results of the portal frame (Mosallam and Bank 1992) was carried out according to the frame dimension and loading arrangement

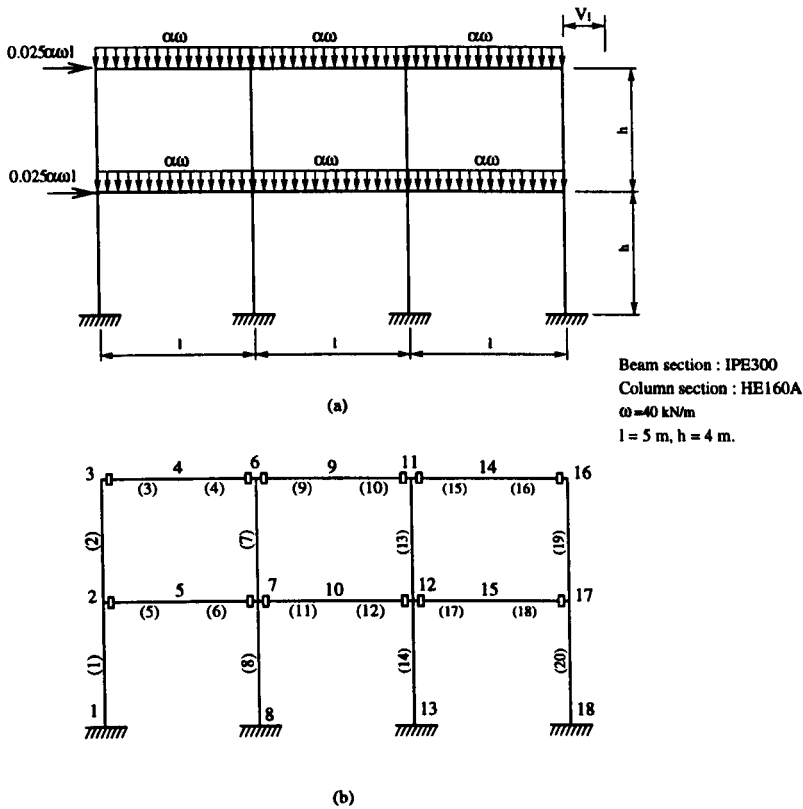


Figure 7.19: Frame B: (a) frame geometries, loading conditions and, (b) the numbering of members and joints.

in **Figure 7.24**

The frame was fabricated from 8x8x3/8 inch (203x203x9.5 mm) WF pultruded section. The moment of inertia and the cross-section area of the section are $I = 4127.8 \text{ cm}^4$ and $A = 56.3 \text{ cm}^2$, respectively. Young's modulus and shear modulus were taken to be $E = 16.2 \text{ kN/mm}^2$ and $G = 3.72 \text{ kN/mm}^2$, as measured experimentally by Mosallam and Bank (1992). Shear coefficient was taken as 3.21 derived from cross-section data given by MMFG (1989). The moment-rotation curve (shown in **Figure 7.25**) is given by Mosallam and Bank (1992). This connection behaviour was used for both beam-to-column and column base connections.

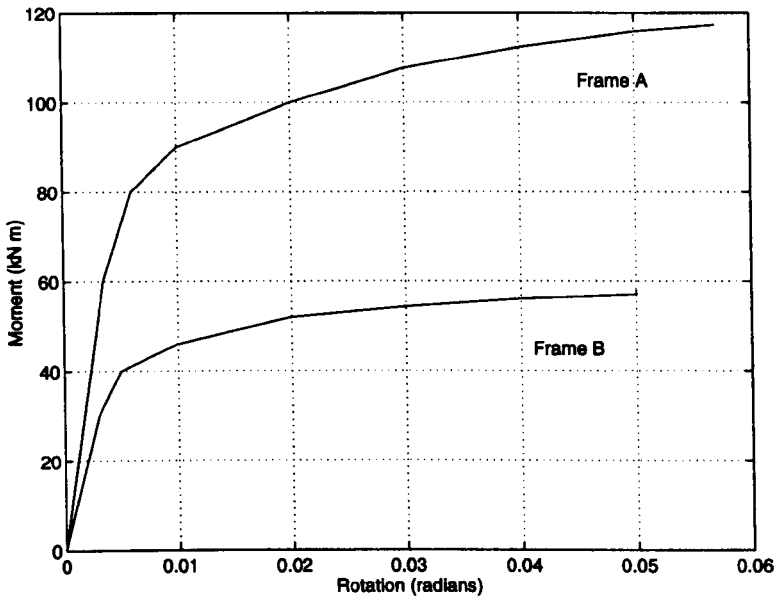


Figure 7.20: Moment-rotation curves of the joint of frames A and B.

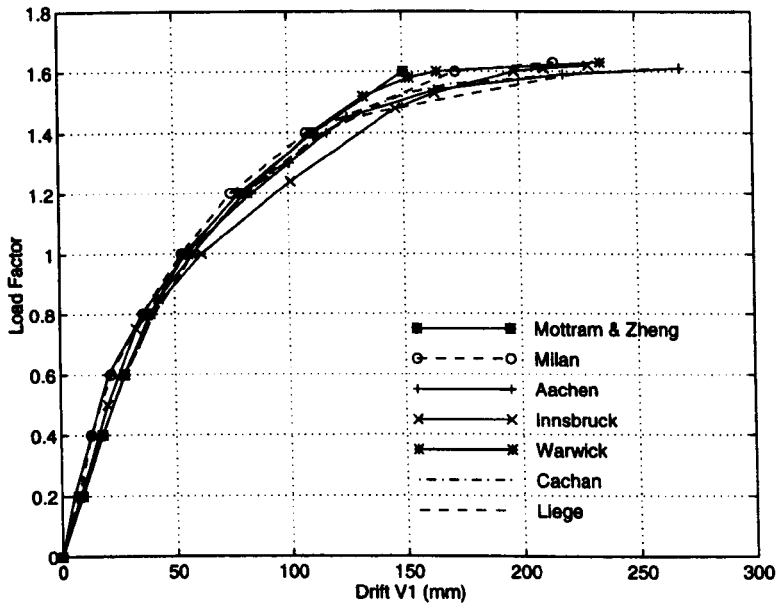


Figure 7.21: Comparison of the results in load-drift for frame A.

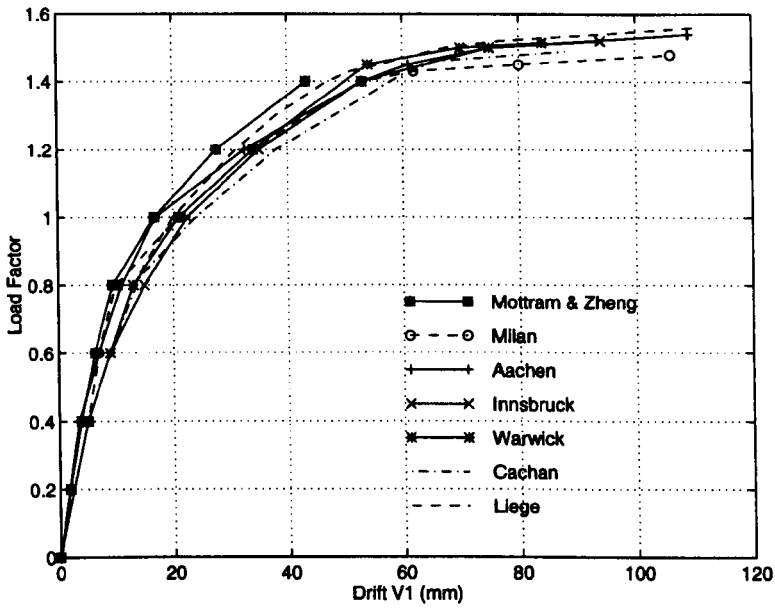


Figure 7.22: Comparison of the results in load-drift for frame B.

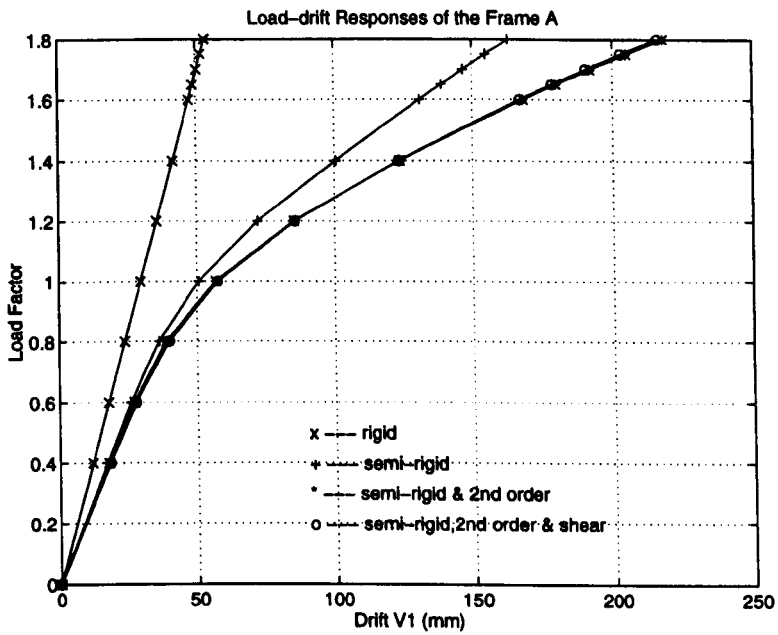


Figure 7.23: Comparison of load-drift behaviour.

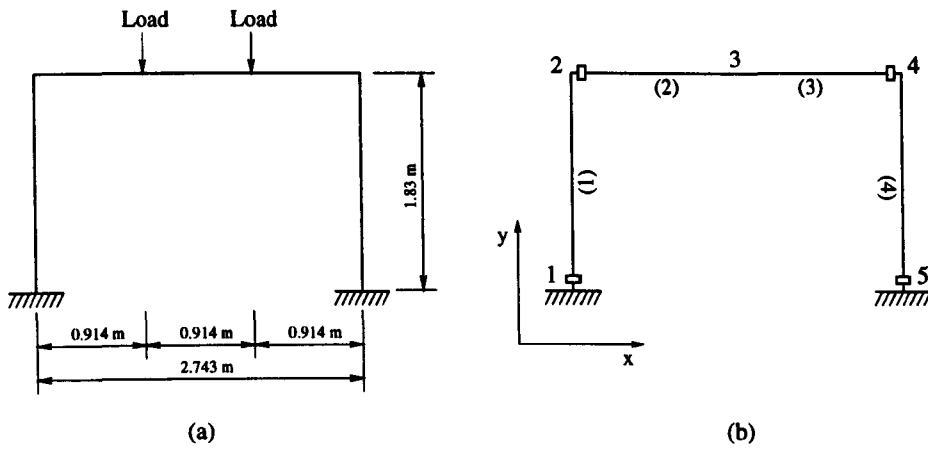


Figure 7.24: Frame dimensions and loading arrange (Mosallam and Bank, 1992).

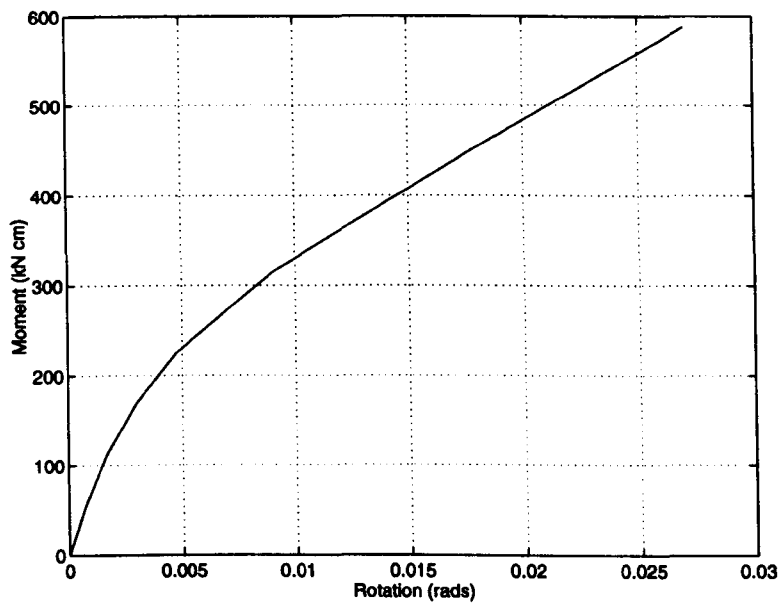


Figure 7.25: Moment-rotation curve for portal frame connections.

The comparison of predictions of the analytical model with the experimental results on load versus midspan deflection of portal frame are plotted in **Figure 7.26**

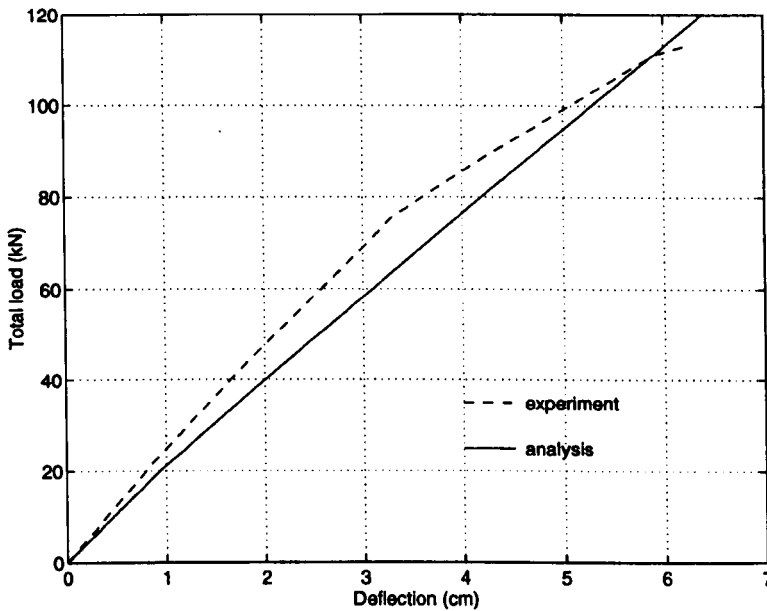


Figure 7.26: Load midspan deflection of portal frame.

It is noticed that at the load of 72 kN, the beam-to-column connection moment is 592 kNcm (the rotation of 0.02735 rad) which exceeded the maximum moment allowed by the $M - \phi$ characteristic of the connection. Further modelling was carried out by using the linearly extended $M - \phi$ curve of the connection.

The model prediction is close to the experimental data and shows good tendency, but slightly underestimates the frame strength before the load over 72 kN. This may be due to the fact that $M - \phi$ curve predicted in the analysis can not exactly represent the connection flexibility of the frame and may underestimate the connection stiffness. Using extended $M - \phi$ curve over the maximum moment allowed resulted in making the model prediction gradually overestimate the frame strength.

It is evident that not just when the experimental data start to show nonlinear

bending the connection moment already exceeds the maximum moment allowed by the $M - \phi$ characteristic of the connection, but the frame collapsed load of 113.03 kN far exceeds the maximum moment allowed by the $M - \phi$ characteristic of the connection.

7.11 Conclusions

A plane frame analysis program included semi-rigid connections, shear deformation of members and stability functions has been developed by using matrix displacement method. In the program, a method of modelling the action of semi-rigid connection is introduced. In this method, the semi-rigid connection is modelled as the part of a member, and its action can be treated as the equivalent joint load acting on the member end, thus the overall stiffness matrix of the frame is reduced.

The stability function s and c , including the shear deformation of the member, are derived and the various ϕ functions to group s and c are obtained, which can be conveniently used in the computing of the matrix stiffness method.

The plane frame analysis program has been verified against the results obtained by other research (ECCS) with two recognised steel frame examples.

The programme is easy to use. The effect of the semi-rigid connection, the shear deformation of member and stability function are treated as options for running the program; thus they can be chosen with the combination of them or each of them alone. Moreover, the load factor as an option can also be changed.

A serviceability beam line is proposed for the beam design under the deflection limit of the serviceability requirement.

Chapter 8

Frame Analysis and Parametric Studies

8.1 Introduction

Why use semi-rigid frame design? Why is the shear deformation included in the frame analysis? Although these questions have been answered to some extent in previous chapters the benefits of semi-rigid frame design and the effect of member shear deformation on frame behaviour will be demonstrated by numerical analyses using three different plane frame structures (one braced and two unbraced frames). Reviewing the previous developments of semi-rigid connections (see **Section 3.3.4**) it is seen that a lot of the effort has been placed into increasing the connection stiffness. Some of the connection designs were reported to significantly increase the connection stiffness compared to others. However, it is also found that, with further increase in the connection stiffness the connection itself gets more complicated, and consequently, the cost increases. The economic benefit achieved by cost saving in the beam from a semi-rigid design may be offset by the increased cost of the

connection. Therefore, it is author's intention to find out if there is an optimum connection stiffness for a semi-rigid frame design and if so, what it is? Furthermore, the author wants to address the question, what is the ultimate connection moment and rotation required? To seek the answers to these questions a parametric study was carried out, in which, the connection stiffness, the load level and the member stiffness influence on frame behaviour were investigated. A comparison was made in terms of connection stiffness using the sway deflection, the mid-span deflection and the moment distribution of the beam. Following this parametric study it is proposed to use the serviceability beam line to determine the ultimate moment and rotation for the connections. Finally, numerical analyses of pultruded frames are presented to show the frame's performance when the connections have the 'moment equalized' stiffness.

The analysis method and author's software, as detailed in **Chapter 7**, can be used to predict the deformation and the element forces for frame analysis and design. Mottram & Zheng (1996 a, 1998) have reported preliminary results using the frame analysis, but the analyses to follow are new.

8.2 Effect of Connection Stiffness and Member Shear Deformation

This analysis is to study the effects of the connection stiffness and the shear deformation of the members on the behaviour of the braced and the un-braced frames and to investigate the extent of their influence on the frame deformation and the moment distribution. Three plane FRP pultruded frame structures were involved in this numerical analysis.

8.2.1 Frame Data

Three plane frame structures evolved from frame A, frame B and frame C devised by Zandonini (1986) for ECCS steel frame structures. They are shown in **Figures 8.1 (a)**, **8.2 (a)** and **8.3 (a)** and are named frame 1, frame 2 and frame 3, respectively. The beam and the column members of the three frames are of 8x8x3/8 inch wide flange pultruded profile. Due to the much less stiffness of the pultruded profile than the steel member given by Zandonini (1986) the lengths of the beam and the column members were reduced to four and three meters, respectively. The loading pattern for each frame remained unchanged, but the value of the distributed load ω was determined by a serviceability requirement of mid-span deflection limited to $l/250$.

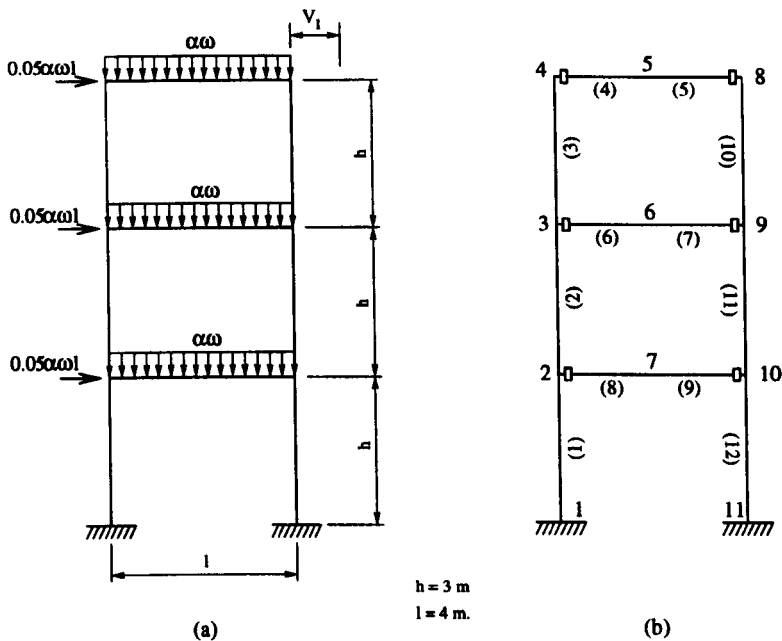


Figure 8.1: Frame 1 (a) geometry, loading conditions and, (b) the numbering of members and joints.

The frame geometries and the loading conditions are given in **Figures 8.1 (a)**,

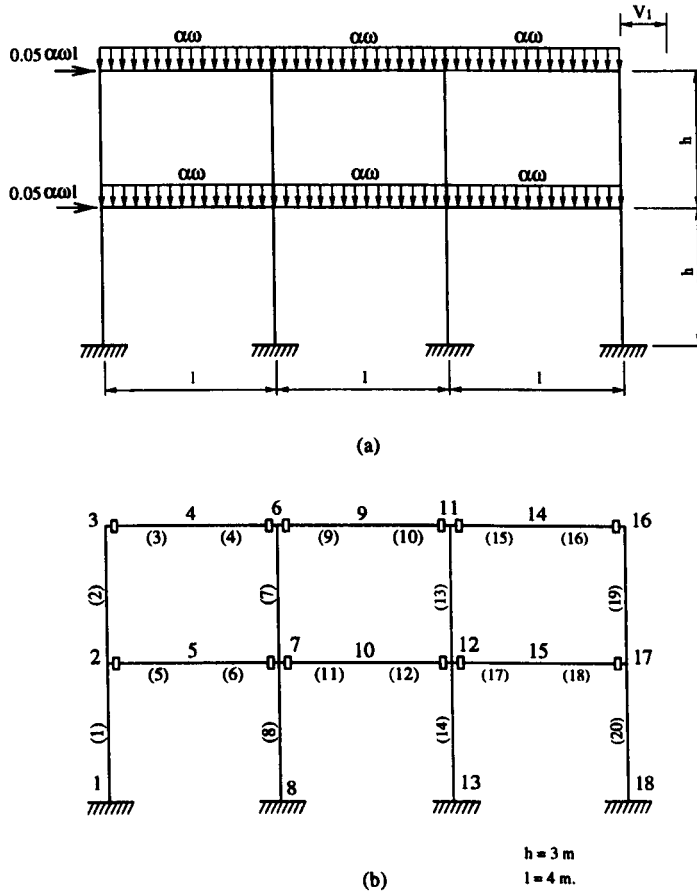


Figure 8.2: Frame 2 (a) geometry, loading conditions and, (b) the numbering of members and joints.

8.2 (a) and 8.3 (a).

Frame 1 and frame 2 are unbraced frames and they are different only in geometry. Frame 1 has three storeys and one bay while frame 2 has two storeys and three bays. The column bases of frame 1 and frame 2 were assumed to be rigid. Frame 3 is a three storey and two bay braced frame, the horizontal movements of the left column and beam joints are restrained, and the column bases are assumed to have pinned supports. The frames are subjected to both distributed and concentrated

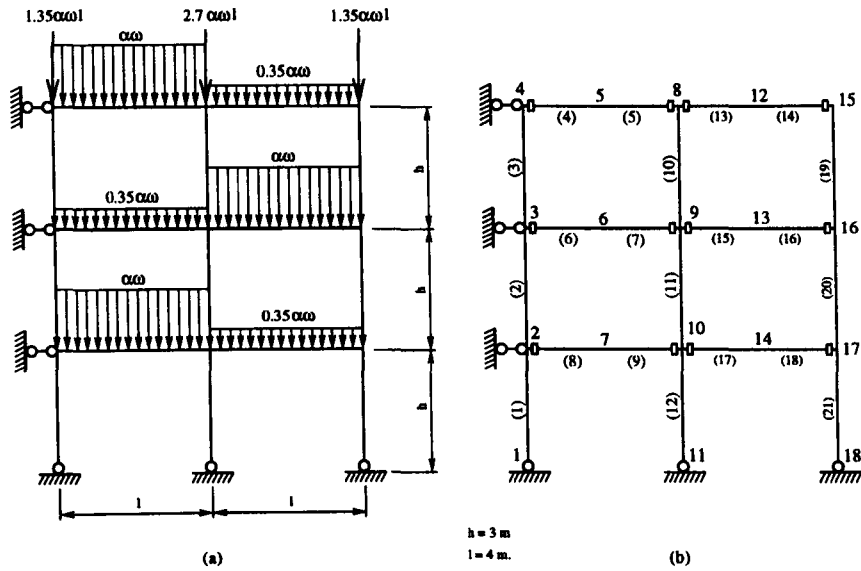


Figure 8.3: Frame 3 (a) geometry, loading conditions and, (b) the numbering of members and joints.

proportional loading and the load level is denoted by the load factor multiplier α .

The numbering of the members and the joints for each frame is presented in Figures 8.1 (b), 8.2 (b) and 8.3 (b), respectively. The numbers of the members are between the brackets, whereas the numbers of the joints are without. The open square symbol shows the location for the connections that can be either pinned, fully-rigid, or have any non-linear $M - \phi$ characteristic.

The properties of the 8x8x3/8 inch wide flange pultruded profile are those given by MMFG (1989) and are reproduced in Table 8.1.

8.2.2 Determination of Distributed Load ω

Let's assume that the beam is simply supported and the maximum mid-span deflection of the beam allowed by the serviceability requirement is $l/250$. From Timoshenko's beam theory (Timoshenko, 1972) the mid-span deflection of the beam can

Table 8.1: Properties of member.

Property	Units	Value
Section area A	m^2	5.632×10^{-3}
Moment of inertia I	m^4	4.128×10^{-5}
Elasticity modulus E	kN/m^2	1.793×10^7
Shear modulus G	kN/m^2	2.930×10^6
Shear coefficient α_s		3.21

be written as:

$$\begin{aligned}\delta &= \frac{5\omega l^4}{384EI} + \frac{\alpha_s \omega l^2}{8GA} \\ &= \omega \left(\frac{5l^4}{384EI} + \frac{\alpha_s l^2}{8GA} \right) = \frac{l}{250}.\end{aligned}\quad (8.1)$$

By substituting the member properties into **Equation 8.1**, the maximum uniform distributed load ω for the simply supported beam under the serviceability condition can be obtained as:

$$\omega = \frac{l}{250} \frac{1}{\frac{5l^4}{384EI} + \frac{\alpha_s l^2}{8GA}} = 3.27 \text{ kN/m}.$$

Hence the distributed load was defined as 3.27 kN/m when α is 1.

8.2.3 Lateral Deflection of the Frame

To demonstrate the effects of the semi-rigid connection and the shear deformation of members on the lateral deflection of the frame, a comparison analysis was made using the three frames with the connections modelled as pinned, fully rigid and semi-rigid. It was assumed that the semi-rigid beam-to-column connections possess the nonlinear $M - \phi$ behaviour of connection **TLMj** (see **Sections 5.2.4** and **5.6.4**).

The stiffness of the MEC (see Section 7.4.8) is 1110 kNm/rad.

The results of the analysis for the load and the corresponding lateral deflection V_1 of the frames are presented in Figures 8.4 and 8.5 for frame 1 and frame 2 respectively. The locations where V_1 was taken for each frame are shown in the Figures 8.1 (a) and 8.2 (a).

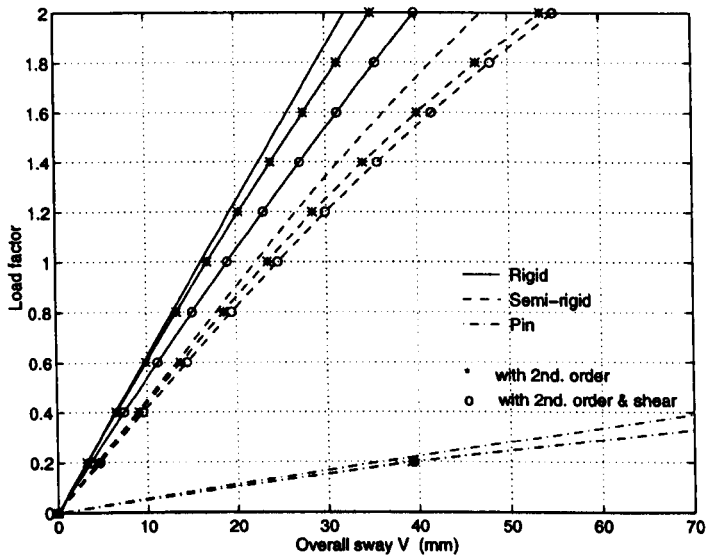


Figure 8.4: Load-overall sway curve of frame 1.

The results show that:

- V_1 is significantly altered for an unbraced frame by changing the connection properties from pinned to semi-rigid.
- There is a distinct influence on the frame's lateral deflection V_1 due to the presence of shear deformation.

For the frames with semi-rigid connection $TLmj$ the percentage increase in V_1 due to taking account of second-order effects, or second-order effects combined with member shear deformation is presented in Figure 8.6.

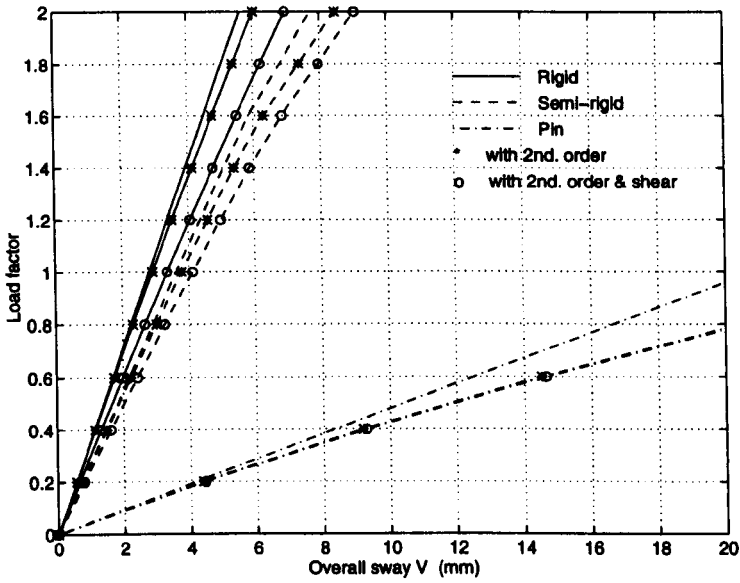


Figure 8.5: Load-overall sway curve of frame 2.

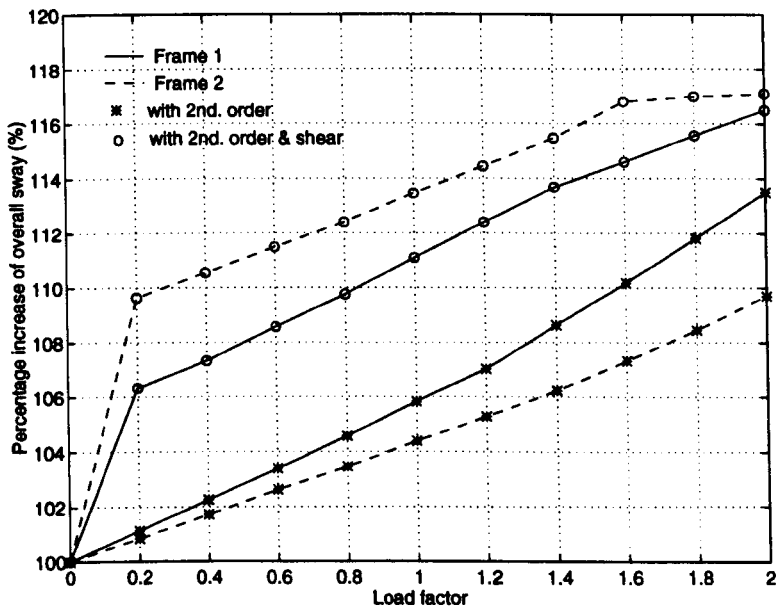


Figure 8.6: Percentage load-sway increment curve for semi-rigid frame 1 and 2 with, and without including, the effects of second-order and shear deformation.

As can be seen from **Figure 8.6**, if only the second-order action is included, the sway v_1 at load factor of 2 is increased by only 13.5% and 9.7% for frame 1 and frame 2, respectively. However, if both the second-order action and the shear deformation effects are included the lateral deflection is increased by 16.5% and 17.1%, respectively. This shows that by ignoring the shear deformation the lateral deflection is underestimated by 3.0% and 7.4% for frame 1 and frame 2.

8.2.4 Mid-span Deflection of the Beam

The maximum mid-span deflection of the three beams in frame 1 is at the top beam. Its mid-span deflection against load factor α is presented in **Figure 8.7** for different connection properties. The maximum mid-span deflection of the beams in frame 2 is at the top beam in the left-side bay and its load-deflection curves are presented in **Figure 8.8**. For frame 3 the maximum beam mid-span deflection is at the top beam in the left-side bay and the load-deflection curves are given in **Figure 8.9**. The mid-span deflections shown in **Figures 8.7 to 8.9** are the absolute values, not the deflections relative to the beam-end supports, therefore the presence of the serviceability limit line ($l/250$) only gives a general impression of how much load can be increased for semi-rigid connection **TLmj** under the deflection limit.

The results of this analysis show that:

- the change on the deflection due to including the second order action is small, and there is virtually no difference between the curves for the modelling situation where the second-order effects are included or not
- the mid-span deflection is increased when shear deformation is included
- the mid-span deflection obtained from the semi-rigid frame analysis is significantly reduced by changing the connection properties from the pinned to

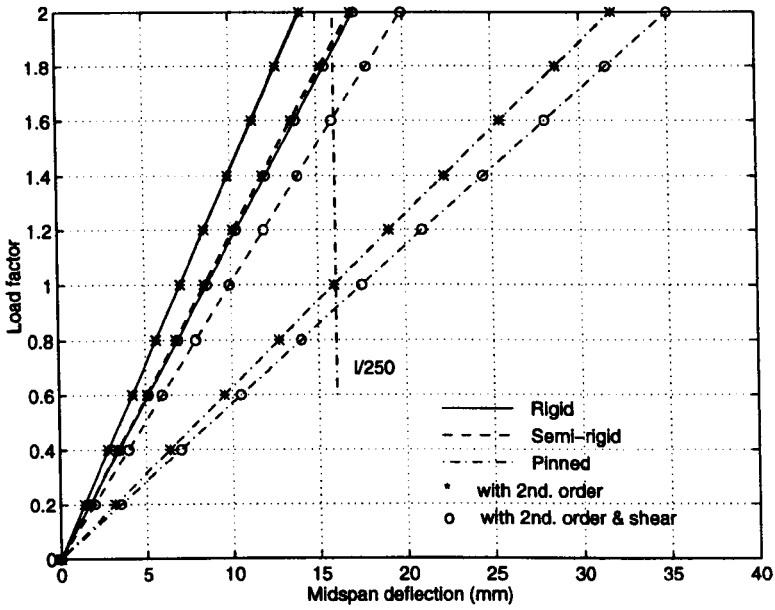


Figure 8.7: Mid-span deflection of the top beam of frame 1.

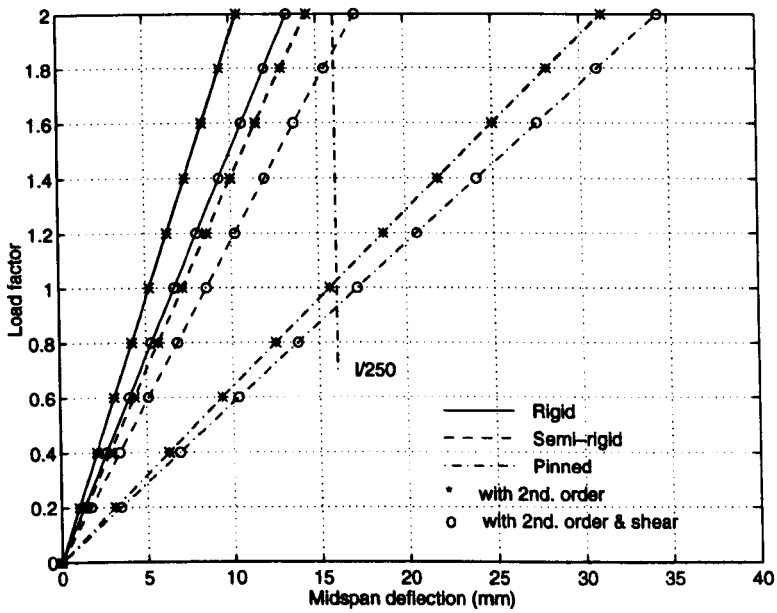


Figure 8.8: Mid-span deflection of the top beam in the left bay of frame 2.

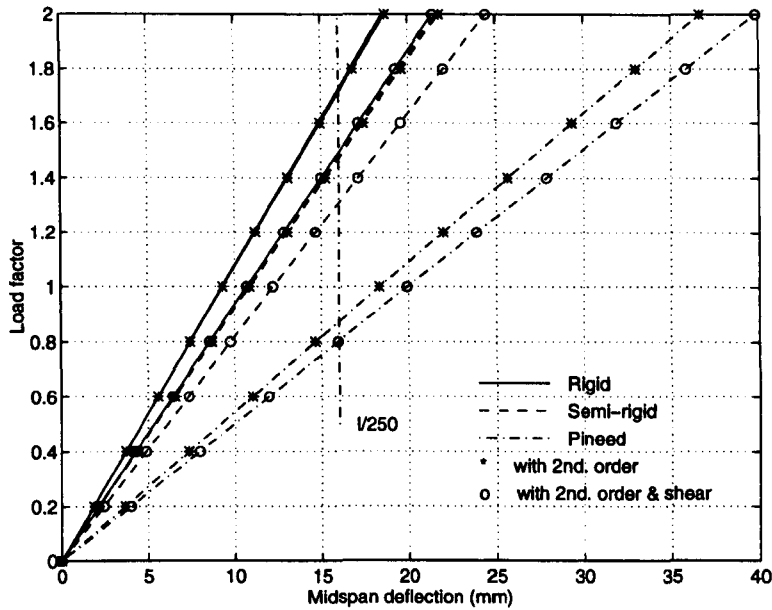


Figure 8.9: Mid-span deflection of the top beam in the left bay of frame 3.

semi-rigid (TLMj). However, by comparing the results obtained from the analyses of rigid frame only a little benefit can be seen as the connection stiffness increases further.

8.3 Sensitivity of Frame Behaviour to Connection Stiffness

Connection stiffness is not a unique factor that affects the overall behaviour of a frame. Member stiffness, load condition and load level also influence the frame behaviour. These factors are interrelated, and it is difficult to isolate any one to discover how it alone affects the overall frame behaviour. However, to make a study of the influence of these factors it is necessary to separate them. It is then possible

to discover how, and to what extent, each of these factors affect the frame behaviour, and how each of them is related to the connection stiffness.

It is the purpose of this analysis to identify the influence of the connection stiffness on the frame behaviour. This investigation is approached by a comparison study on the lateral deflection, the mid-span deflection and the moment distribution.

The three frames used in this parametric study are frames 1 to 3, as defined in **Section 8.2.1**. The connections will be assumed to have a constant stiffness ($k = M/\phi$), which will be taken to vary from 250 to 3000 kNm/rad. The stiffness of the moment equalised connection (MEC) (see **Section 7.4.8**) for the beam members of 4 m span is 1110 kN m/rad. The load conditions that the three frames are subjected to are the same as defined in **Section 8.2.1**. The constant load factor, α , was taken to be 1.5.

The results of the analysis for the lateral deflection V_1 are presented in **Figure 8.10**. They are in the form of the percentage sway deflection increase, in which the sway of the pinned frame relative to that of the rigid frame is defined as 100 per cent.

Using the same definition to present the change in sway the results of the beam mid-span deflections for the three frames are shown in **Figure 8.11**. The mid-span deflection presented in **Figure 8.11** is the relative deflection based on the average deflection at the two beam-ends. The three beams are the top beam in frame 1, the top beams in left-side bay in frames 2 and 3.

The distribution of the bending moments is influenced by the stiffness of the connection. An increase in the connection stiffness results in a moment increase at the beam-ends and a moment decrease at the mid-span. Presented in **Figure 8.12** are the results of the ratio of the mid-span moment to the right-end moment with varying connection stiffness from the three beams as given above.

The comparison on the lateral deflection, the mid-span deflection and the mo-

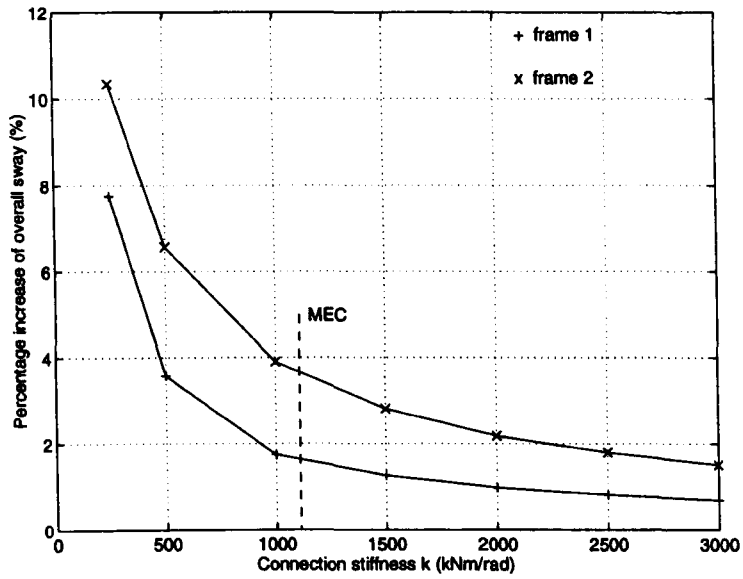


Figure 8.10: Effect of the connection stiffness on the lateral sway of frames.

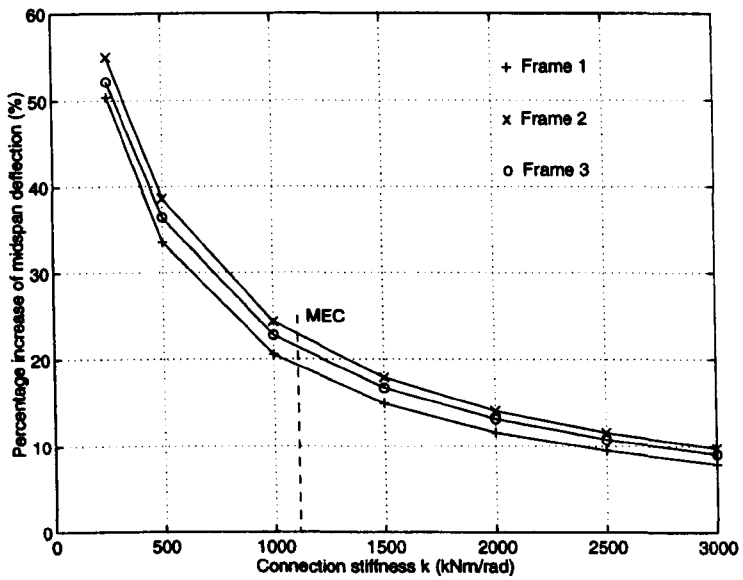


Figure 8.11: Effect of connection stiffness on the mid-span deflection.

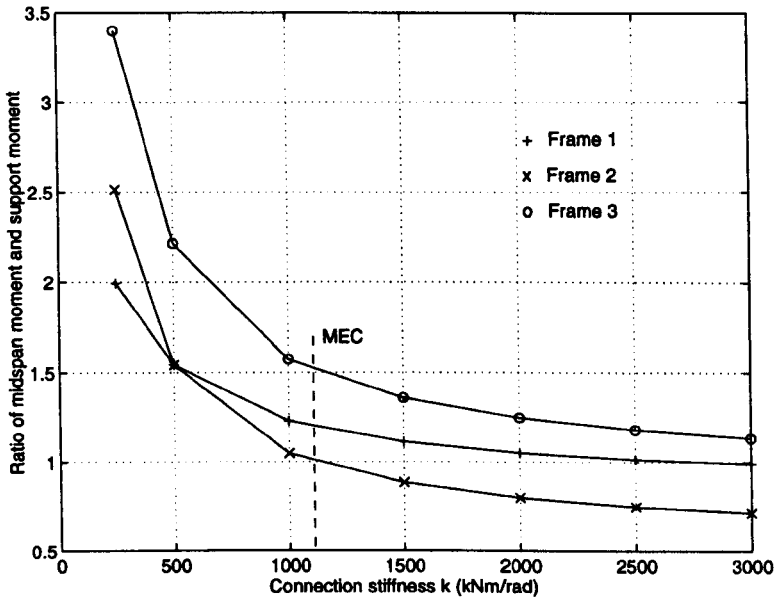


Figure 8.12: Effect of connection stiffness on the moment distribution.

ment distribution ratio shows that the influence of the connection stiffness on them is nonlinear and they are inversely proportional to the connection stiffness. With the increase in the connection stiffness the lateral deflection, the mid-span deflection and the moment distribution ratio all decrease (see **Figures 8.10 to 8.12**). It also shows that these curves decrease rapidly before the connection stiffness reaches the MEC value, and for a stiffness above MEC they asymptotically tend to the value given by the equivalent rigid frame analysis. In the other words, when connection stiffness is less than the MEC value its influence is significant, whereas where the connection stiffness is greater than the MEC stiffness the influence is getting less significant. With the MEC stiffness the lateral sway for frame 1 is less than a 2 % increase. For frame 2 it is less than a 4 % of increase. The mid-span deflections for the three frames are about 20 % of what is presented if the connections are pinned. These comparison results indicate that for the development of a semi-rigid connec-

tion it is more efficient, in terms of benefit in structure performance, to increase the connection stiffness before it reaches the MEC value. The moment distribution ratio at the MEC stiffness is less than 1 for frame 2 but greater than 1 for frames 1 and 3. Although the ratio of the moment distribution at the MEC stiffness is no longer unity (due to the frame deformation under the horizontal loading in frames 1 and 2 and the asymmetrical loading in frame 3), the design moments have been significantly reduced and with further increase of the connection stiffness the shift of the moment distribution will be less efficient.

8.4 Effect of Connection Flexibility, Member Stiffness and Load

Since the connection stiffness, the member stiffness and the loading are interrelated to each other, an attempt is made to study their combined effects. This was carried out by a comparison of the mid-span deflection and of the moment distribution for the top beam in frame 1.

8.4.1 Influence of Connection Stiffness and Load

The investigation in the combined effect of the connection stiffness and the load level on the beam mid-span deflection and the moment distribution was carried out by using the top beam of frame 1. The reason for choosing this beam is that it has the maximum mid-span deflection and the maximum mid-span and support moments. The frame analysis took account of the effects of the second order action and the member shear deformation.

The mid-span deflection with the connection stiffness k at load factors 1, 1.5 and 2 is given in **Figure 8.13**. The ratio of mid-span moment to the beam right-end

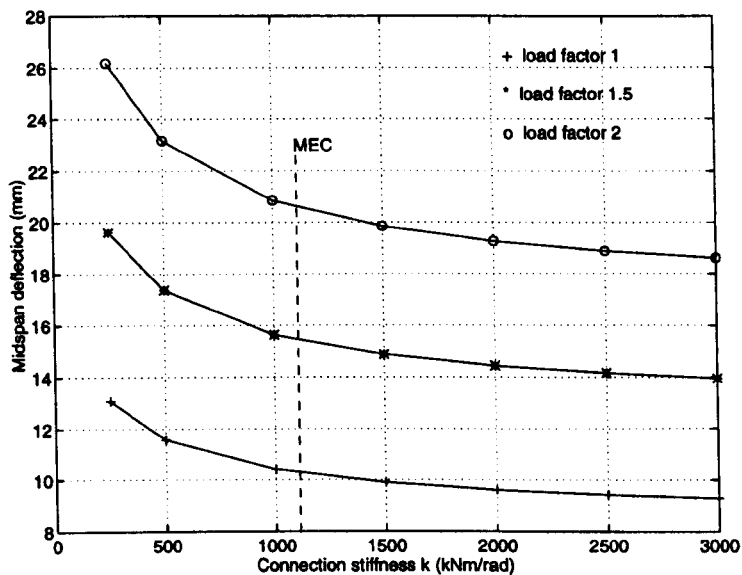


Figure 8.13: Effect of connection stiffness and load on the mid-span deflection.

moment with the connection stiffness at load factors 1, 1.5 and 2 is presented in **Figure 8.14**.

Figure 8.13 and **8.14** show that, since the influence of the load is linear, the shape of the curves of the mid-span deflection and the moment distribution ratio remain the same, no matter what the load level is. Increasing the load the mid-span deflection gives a corresponding linear increase in the **Figure 8.13**, whereas the moment distribution (**Figure 8.14**) remains almost the same. The curves have the same characteristics as those described in **Section 8.3**. The mid-span deflection and the moment distribution are significantly reduced even if the stiffness of the connection is only modest.

This analysis shows that the effect of load on mid-span deflection is linear and there is almost no effect on moment distribution.

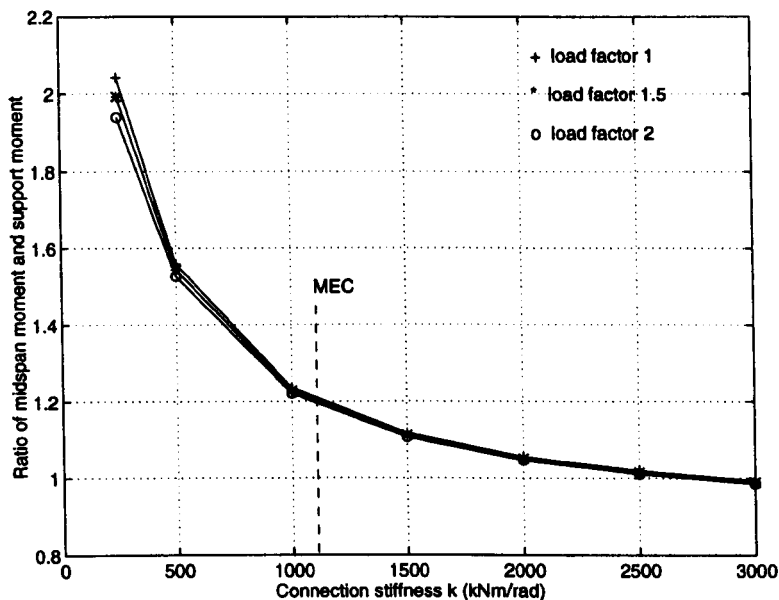


Figure 8.14: Effect of connection stiffness and load on the moment distribution.

8.4.2 Influence of Connection Stiffness and Member Stiffness

The member stiffness not only influences the deformation of the frame but also affects the distribution of the moments. It, therefore, needs to be considered in the study of the influence of the connections flexibility on frame behaviour. For this purpose different member stiffnesses (i.e. EI/l , by considering bending only) are used in the analysis of frame 1. To change the member stiffness, for convenience, instead of changing the member length or the size of the members, the elastic modulus E was taken to be 896.5 kN/cm², 1793 kN/cm², 3586 kN/cm² and 5379 kN/cm² in order to simulate the incremental change in the member stiffness EI/l . The analysis included the second-order action and the member shear deformation. The load factor was 1.5.

Figure 8.15 shows the mid-span deflections at the top beam in frame 1 with the varying connection stiffness and member stiffnesses. In order to show clearly the influence of the member stiffness these results are presented in Figure 8.16 in the form of the mid-span deflection versus the member's elastic modulus E. It can be easily seen that the mid-span deflection and the elastic modulus E curves are nonlinear and are inversely proportional to the connection stiffness and the member stiffness. In other words, the higher the connection stiffness and the member stiffness, the smaller the mid-span deflection is.

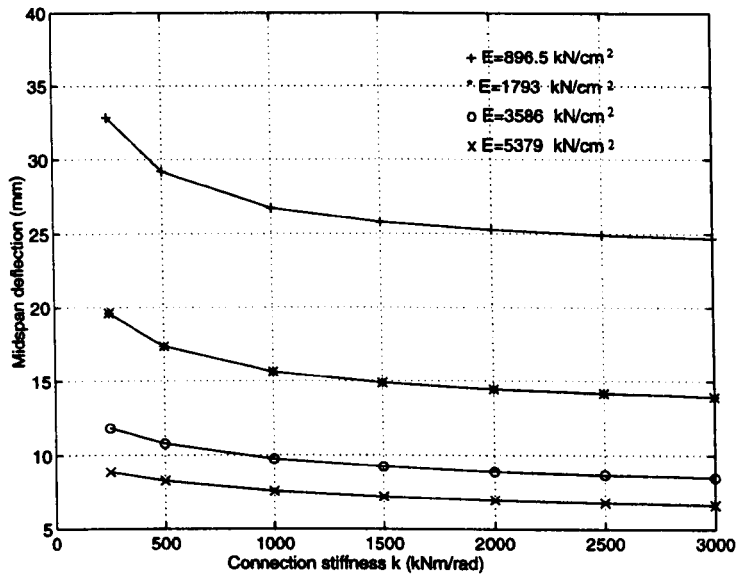


Figure 8.15: Effect of the connection stiffness and the member stiffness on the mid-span deflection.

The ratios of the mid-span moment to the right side beam-end moment for varying connection stiffness and member stiffness are presented in Figure 8.17.

The general shape of the curves in Figures 8.15 and 8.17 are similar to the curves given in Section 8.3, though the slopes of the curves at the same connection stiffness are different for the different member stiffnesses. The slopes of the curves at

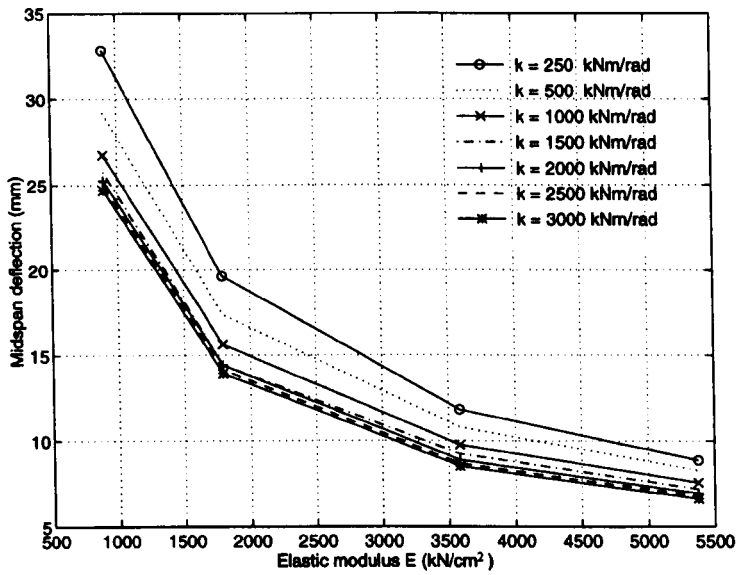


Figure 8.16: Effect of the connection stiffness and the member stiffness on the mid-span deflection.

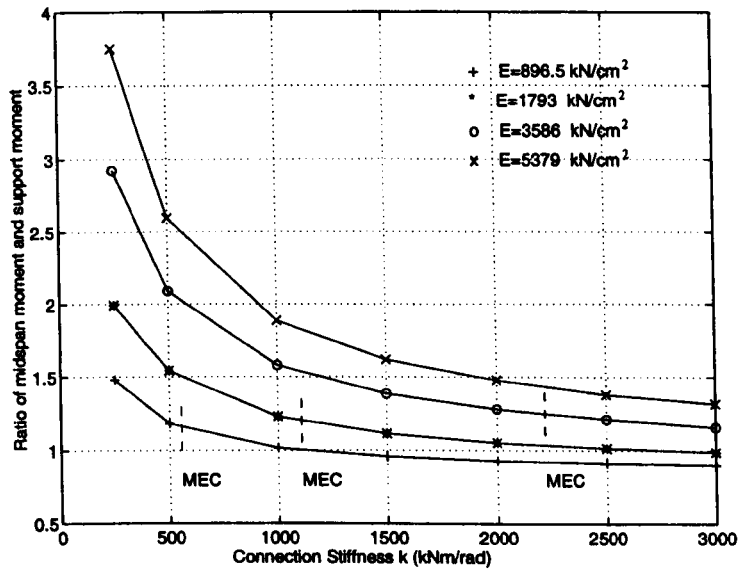


Figure 8.17: Effect of the connection stiffness and the member stiffness on the ratio of mid-span moment and the right side beam-end moment.

the given connection stiffness vary with the member stiffness. However, the curve's slopes for each member stiffness, change rapidly when the connection stiffness is less than its equivalent MEC stiffness (given by $6EI/l$) and tend asymptotically to the value for the rigid frame when the connection stiffness is greater. This evidence confirms for a given member stiffness that the connections used should have a corresponding stiffness in order to obtain the optimum frame design. In other words, for a different member stiffness a different connection stiffness should be considered.

The results presented in **Figures 8.15** and **8.17** also show that the member stiffness and the connection stiffness are related factors to the overall frame behaviour. The influence of the connection stiffness on the mid-span deflection at the lowest member stiffness is greater than at the highest member stiffness, whereas on the moment distribution at the lowest member stiffness is less than at the highest member stiffness.

8.5 Ultimate Connection Moment and Rotation

To examine the required ultimate connection moment and rotation lets start with the serviceability beam-line, as introduced in **Section 7.4.8**. **Figure 8.18** shows a serviceability beam-line for a beam having member properties EI/l and subjected to a distributed load ω . The limit of mid-span deflection for serviceability requirement is given as l/s , where s could be 250. The enclosed area of the serviceability beam-line and the moment and rotation coordinate axes (the shaded area in **Figure 8.18**) is the area that connection acts in, and therefore the $M - \phi$ curve of a connection must be beyond the serviceability beam line and gives a safety reservation. Following this rule $M - \phi$ curve (a) and (c) in **Figure 8.18** are not satisfied, although curve (a) has high moment resistance and curve (c) has high rotation ability. Only connection (b) is acceptable as its $M - \phi$ curve (assuming no failure occurred) ex-

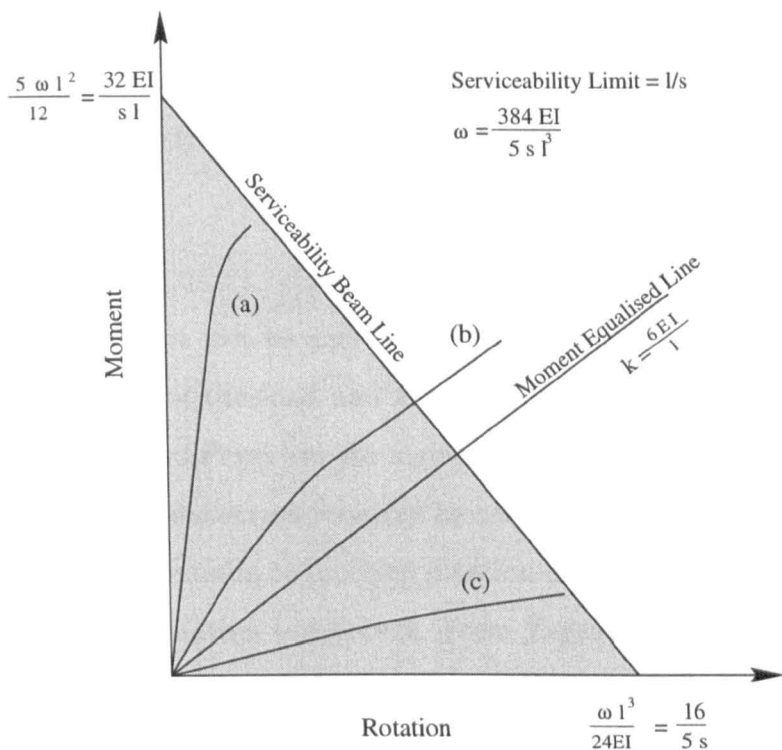


Figure 8.18: Ultimate connection moment and the serviceability beam line.

ceeds the serviceability beam-line. If the extreme values of the rotation ($\omega l^3/24EI$) and the moment ($5\omega l^2/12$) for the serviceability beam-line in **Figure 8.18** can be established, then this extreme serviceability beam-line can be used to examine the connection moment-rotation property.

To establish the extreme values the following analysis is carried out based on a beam subjected to a distributed load. If only the bending deformation is considered the distributed load ω for a simply supported beam can be written as:

$$\omega = \frac{l}{s} \frac{384EI}{5l^4} = \frac{384EI}{5sl^3}. \quad (8.2)$$

By substituting the distributed load ω into the expression for the maximum beam-

end rotation we obtain

$$\frac{\omega l^3}{24EI} = \frac{16}{5s} \quad (8.3)$$

and by substituting ω into the maximum beam-end moment for the rigidly connected beam we obtain

$$\frac{5\omega l^2}{12} = \frac{32EI}{sl}. \quad (8.4)$$

From **Equation 8.3** it can be seen that the maximum beam-end rotation is a function of s , regardless of the load and the member properties. No matter what the load and the member stiffness are, for a given serviceability deflection limit it is a constant. The maximum deflection required by serviceability limit is $l/100$ (MMFG 1989) and this gives a maximum connection rotation of 0.032 rad. For the maximum beam-end moment the situation is different. From **Equation 8.4** it can be seen that it depends on the serviceability deflection limit and the member's stiffness. If the serviceability deflection limit takes its maximum value, then the **Equation 8.4** is now a function of the member stiffness (EI/l). For a specific pultruded profile the EI will be a constant, hence the maximum beam-end moment is now only going to vary due to the member's length l . The smaller is the length, the higher is the beam-end moment. If the minimum beam length is known the extreme limit of the serviceability beam-line can be readily obtained. This extreme serviceability beam-line gives a boundary which a connection $M - \phi$ curve must exceed. It should be borne in mind that for the purpose of safe design a margin of safety should be considered. Since a safety factor has been used for the determination of the design load in the design practice the further connection safety margin may not need to be too high. How high such a safety reservation needs to be investigated.

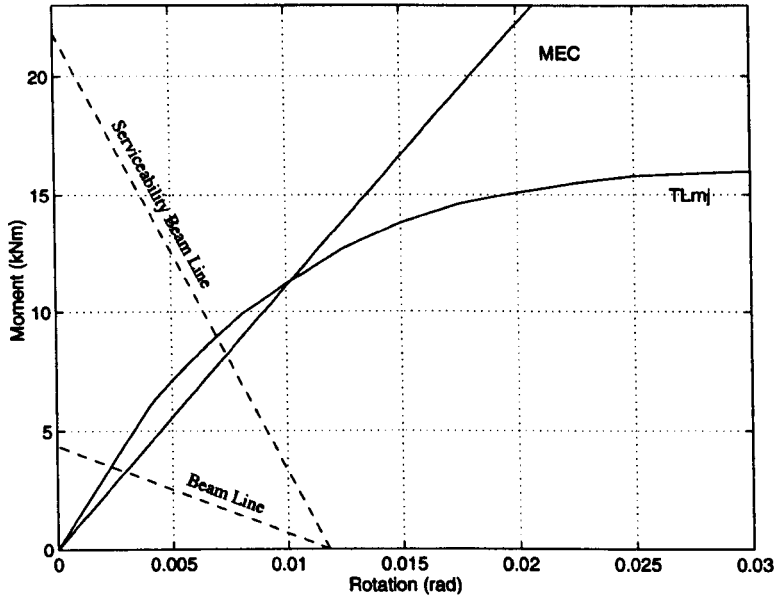


Figure 8.19: Connection $m - \phi$ curves and the serviceability beam line.

8.6 Analysis of Pultruded Frames with Various Connection Properties

The results in **Tables 8.2, 8.3 and 8.4** give the maximum values of: the load factor, the sway deflection V_1 , the axial force and the beam mid-span moment and the beam-end moment in frames 1, 2 and 3, respectively. The frames are with various connection stiffness from pinned, semi-rigid to rigid. The semi-rigid beam-to-column connections are **TLMj** or the **MEC**, and their moment-rotation behaviours are given in **Figure 8.19**. In all cases the highest mid-span deflection has reached 16 mm serviceability limit of $l/250$. Note that the beam deflection takes account of the settlement at the ends by using the average value of the end-deflections to determine the beam's mid-span deflection.

The results show that although the stiffness of connections **TLMj** and **MEC** are

Table 8.2: Results for frame 1.

Connection	Load Factor	Sway V_1	Axial force (kN)	Moment (kNm)	
	α	(mm)	(12) †	5 †	(9) ₁₀ ‡
Rigid	2.15	43.1	46.9	7.3	12.4
TLmj	1.82	48.8	39.5	7.0	9.0
MEC	1.76	48.3	38.2	7.0	8.6
Pinned	0.98	300.7	19.2	6.4	0

† Integer in () is the number of the member, without () is the number of the node.

‡ (9)₁₀ means member 9, at node 10.

Table 8.3: Results for frame 2.

Connection	Load Factor	Sway V_1	Axial force (kN)	Moment (kNm)	
	α	(mm)	(8) †	4 †	(6) ₇ ‡
Rigid	2.76	9.8	74.6	7.7	14.0
TLmj	2.06	9.3	54.9	7.2	8.4
MEC	1.96	8.9	52.1	7.1	7.8
Pinned	0.98	26.6	25.6	6.4	0

† Integer in () is the number of the member, without () is the number of the node.

‡ (6)₇ means member 6, at node 7.

Table 8.4: Results for frame 3.

Connection	Load Factor	Axial force (kN)	Moment (kNm)	
	α	(12) †	5 †	(16) ₁₆ ‡
Rigid	2.25	141.0	7.3	8.7
TLmj	1.85	115.1	7.1	6.1
MEC	1.77	109.9	7.0	5.6
Pinned	0.98	60.6	6.4	0

† Integer in () is the number of the member, without () is the number of the node.

‡ (16)₁₆ means member 16, at node 16.

not very high relative to the fully fixed condition, the increase in load factor and the overall frame stiffness are significantly higher than when the frames are pinned and not much less than when treating the frame as having rigid joints. This evidence means that any further increase in the connection stiffness would not result in a significantly increase in the design load and the frame stiffness. In addition, the maximum beam-end moment for the semi-rigid frame has been reduced by more than one-quarter of the rigid frame. The results show good agreement with the analyses in previous sections that the optimum connection design may not have to have too high a stiffness.

By comparing connections **TLmj** and MEC, the results show that there is not much difference between them since their stiffnesses are quite close. The load factor for **TLmj** is slightly higher than MEC, but the beam-end moment is higher too. Besides this, the ratio of the mid-span moment to the support moment for connection MEC is more close to 1 than connection **TLmj** in frames 1 and 2 and less close in frame 3. However, the design of FRP pultruded frame generally is controlled by the serviceability deflection limit and minimising design moment (by making the moment at the supports equal to the value at mid-span) thus minimising beam depth is not the over-riding concern, therefore, from this point of view the author suggests that the stiffness of connection should be equal to or greater than MEC stiffness.

The results show that the load factor α for a pinned frame reduces from 1 to 0.98. This means that by employing simple frame design procedures under load ($\alpha=1$) will lead to a beam deflection slightly above the serviceability limit. The reason for this is because the standard procedure neglects the second-order action in the determining design load. Since the difference is small the effect can be compensated by the actual stiffness of the 'pinned' connection (see **Section 4.6**).

8.7 Conclusion

A numerical parametric study has been carried out on two unbraced and one braced frame to demonstrate the influence of; connection flexibility, second-order action, and member shear deformation on the frame behaviour. The influence of the connection stiffness, the load and the member stiffness, was also investigated. From the study a theoretical analysis was made to establish what connection properties are needed for joint to be acceptable. From the limited results presented the author is able to conclude the following:

- connection stiffness, second-order action and member shear deformation can have a significant influence on the response of frames. It is therefore recommended that when making calculation part of design process all three effects should be included.
- the frame stiffness has been shown to significantly increase when connections have properties that classify them as semi-rigid.
- the influence of the connection stiffness on the mid-span deflection and the moment distribution is nonlinear. However its influence rapidly decreases with the increase of the connection stiffness and becomes asymptotic to the value given by the equivalent rigid frame when the stiffness is still relatively low. This property shows that the optimum semi-rigid frame design can be achieved with a connection stiffness which is not too high.
- influence of member stiffness on the mid-span deflection is nonlinear. The mid-span deflection decreases as the member stiffness increases. The relative effect of the connection stiffness when member stiffness is low is greater than that when member stiffness is high. This situation is reversed when considering the moment distribution between the mid-span and the end supports.

-
- when establishing overall frame behaviour the member stiffness and the connection stiffness are interrelated factors. To minimize the design moment and to obtain optimum semi-rigid performance it is recommended that the beam-to-column connection stiffness should be six times that of the member stiffness (ie. $\frac{6EI}{l}$ (MEC)), but, since the design of FRP pultruded frame is generally controlled by the serviceability state rather than ultimate strength a higher connection stiffness than MEC stiffness is preferable.
 - the author has developed an extreme serviceability beam-line approach that can be used to establish the minimum requirements of moment and rotation for the connections. By using this approach the boundary on the $M - \phi$ properties can be readily established, thereby providing data which will help to develop optimum connection details.

Chapter 9

Conclusions

9.1 Conclusions

9.1.1 Nominally Pinned Connection

The web cleated beam-to-column connections possess lower connection stiffness, which makes them usually assumed to be the pinned connections in frame design. The very limited previous tests on 8 inch web cleated beam-to-column connections revealed their unsatisfactory performance as pinned connections. To further investigate the behaviour of the web cleated beam-to-column connection three different 10 inch beam-to-column web cleated connection tests were conducted in this laboratory investigation. The result of these tests and the analysis of this laboratory investigation can be concluded as:

- The short-term 10 inch web cleated connection tests showed that this type of connection can not meet the rotation requirement of a pinned connection without any material damage. This result confirmed Mottram's (1994) investigation that the 8 inch pinned beam-to-column connections recommended by

a USA manufacturer may not perform satisfactorily. It has been shown that, if a limited amount of the material damage is acceptable, the web cleated connection can meet the rotation requirement.

- it was found that permanent rotation occurred and that this was associated with a deterioration of the connection pieces as the connection moment was increased. It is, therefore, to be expected that under service condition there might be a reduction in the strength of web cleated connection.
- it is the opinion of the author that when this type of the connection is used in frame construction, a more conservative design needs to be considered because the structure must be reliable and safe. This situation is, however, likely to be relaxed after the effect of this material damage on the long-term connection stability and durability has been investigated and understood.
- combined bonding and bolting prevents the slippage between the beam and the web cleats. In terms of structural behaviour the bonding improves only the initial stiffness of the connection.
- debonding of local mating surfaces could not be prevented from developing where the peel stresses were high. With the debonding developed the stiffness of the connection tended to the stiffness of the bolted only connection. This observation suggests that it is unnecessary to include the practice of adhesive bonding for the purpose of increasing the connection stiffness. Its beneficial function is to prevent the inherent connection slip.

9.1.2 Semi-rigid Connections

The benefit of the semi-rigid connection in the frame design is well-known. The aim to develop the semi-rigid beam-to-column connection for FRP pultruded frame

leads to this laboratory investigation. In this laboratory investigation two steel cleated beam-to-column connections and two pre-preg cleated beam-to-column connections were tested. The steel cleated connection tests showed an alternative choice of the material for connection piece. The pre-preg connection test provided useful information for the semi-rigid connection design of the pultruded frame rather than developing a semi-rigid connection for practical application. Following these laboratory investigations a conceptual design of the connection has been carried out. The results of these laboratory tests, and the test analysis can be summarised thus:

- to develop a semi-rigid beam-to-column connection a connection with standard steel angle top and bottom cleats was tested and the results showed that the connection details gave an acceptable moment-rotation behaviour.
- to increase the stiffness of a semi-rigid connection it is recommended that, not only do the cleats themselves need to be stiffened, but also the beam and the column member sections. Such stiffening of the members was achieved by using the connection bolts between the flanges.
- slip is a main problem of the bolted only connections tested, and to minimise this problem there is a need to provide a solution that could be bonding. Elimination of the connection slip was achieved by adhesively bonding appropriate mating surfaces in connection **TLmj**.
- development of the pre-preg cleated piece showed that the resistance of the strength of the cleat itself was improved due to the bidirectional fibre arrangement, and that there was not a 'brittle' mode of failure; this was often found with the pultruded angle cleat pieces (see Bass, 1994).
- it is the author's opinion, based on the behaviour of the two connections tested having pre-preg cleat pieces, that the stiffness of such pieces cannot be

significantly increased by only increasing the thickness of the legs. To make better use of the material and to efficiently increase the connection stiffness the cleat pieces need to be of a more complex shape design, such as to include ribbing or shell curvature.

The current connection designs mainly mimic steel work and the aim of the present laboratory investigation is to develop a connection design which can make best use the FRP material. For this purpose all information obtained in this thesis can be used to assist in the development of the next generation of connections and their members.

A number of conceptual designs for futuristic connections are presented, and these include; cleated connections, connection components from which connections assembled from parts that are interlocked and will be bonded, and a new structural system based on standard structural profile. The conceptual designs carried out in this thesis can be summarized thus:

- to develop the new cleat connector, solid thin shell cleat geometry is proposed. It can be used in connections between a majority of the available structural profiles.
- to make best use of the properties and the processing technology for FRP materials six different pieces of assembly connection components have been conceived. A number of futuristic connection details which are assembled from these six connection components are presented.
- a new structural system, using the pultruded box section and flat sheet materials is proposed for the pultruded frame structure. It does not mimic what we see in steel frame structure practice. Consideration for its buildability is given.

9.1.3 Analytical Modelling

To gain a better understanding of the connection in terms of the overall frame behaviour, a numerical analysis was carried out. In this study, some novel developments have been made and they are summarised as follows:

- for the theoretical analysis of FRP frame, and to predict the deformation and the element forces, a computer analysis programme of plane frame, in C language, has been developed. Its option included semi-rigid connection, second-order effects and shear deformation of member. It uses the conventional matrix stiffness method.
- in the program, the semi-rigid connection is successfully modelled as the part of a member, its action is treated as the equivalent joint load acting on the member-end. By using this method to model the semi-rigid connection the overall stiffness matrix of the frame is reduced, thus minimising computing resources.
- the true non-linear moment-rotation ($M-\phi$) curve of the semi-rigid connection can be used in the computer analysis by means of a idealised piece-wise linear curve.
- new stability functions s and c have been developed which include the effect of shear deformation of the element. The various ϕ functions are derived to group stability function s and c , which can be conveniently used in the computing of matrix stiffness method.
- the analysis method and the computer program successfully benchmarked against known examples of steelwork (Mottram & Zheng, 1996 a).

- a serviceability beam line is given, which can be used for the beam design in the case that the design is controlled by the deflection.
- the stiffness of the moment equalized connection (MEC) is obtained by graphical method, which answered the question of ‘what connection stiffness of a semi-rigid connection should be?’. This stiffness can be used as guidance in choosing connection in the frame design and in connection design.
- from the results given in **Chapter 8** it can be seen that; the connection properties, the second order effects, the shear deformation of the members, all have significant effects on behaviour of pultruded frames with practical dimensions. For realistic predictions of frame deformation and forces they should be included in analysis and design.
- the analysis of the effects of the connection stiffness on the overall behaviour of the frame shows that the influence of the connection stiffness on the overall sway, the midspan deflection and the moment distributions is nonlinear and to efficiently increase the connection stiffness for the semi-rigid frame design is before it reaches $\frac{6EI}{l}(MEC)$.
- the author has developed an extreme serviceability beam-line approach that can be used to establish the minimum requirements of moment and rotation for the connections. By using this approach the boundary on the $M - \phi$ properties can be readily established, thereby providing data which will help to develop optimum connection details.

9.2 Future Work

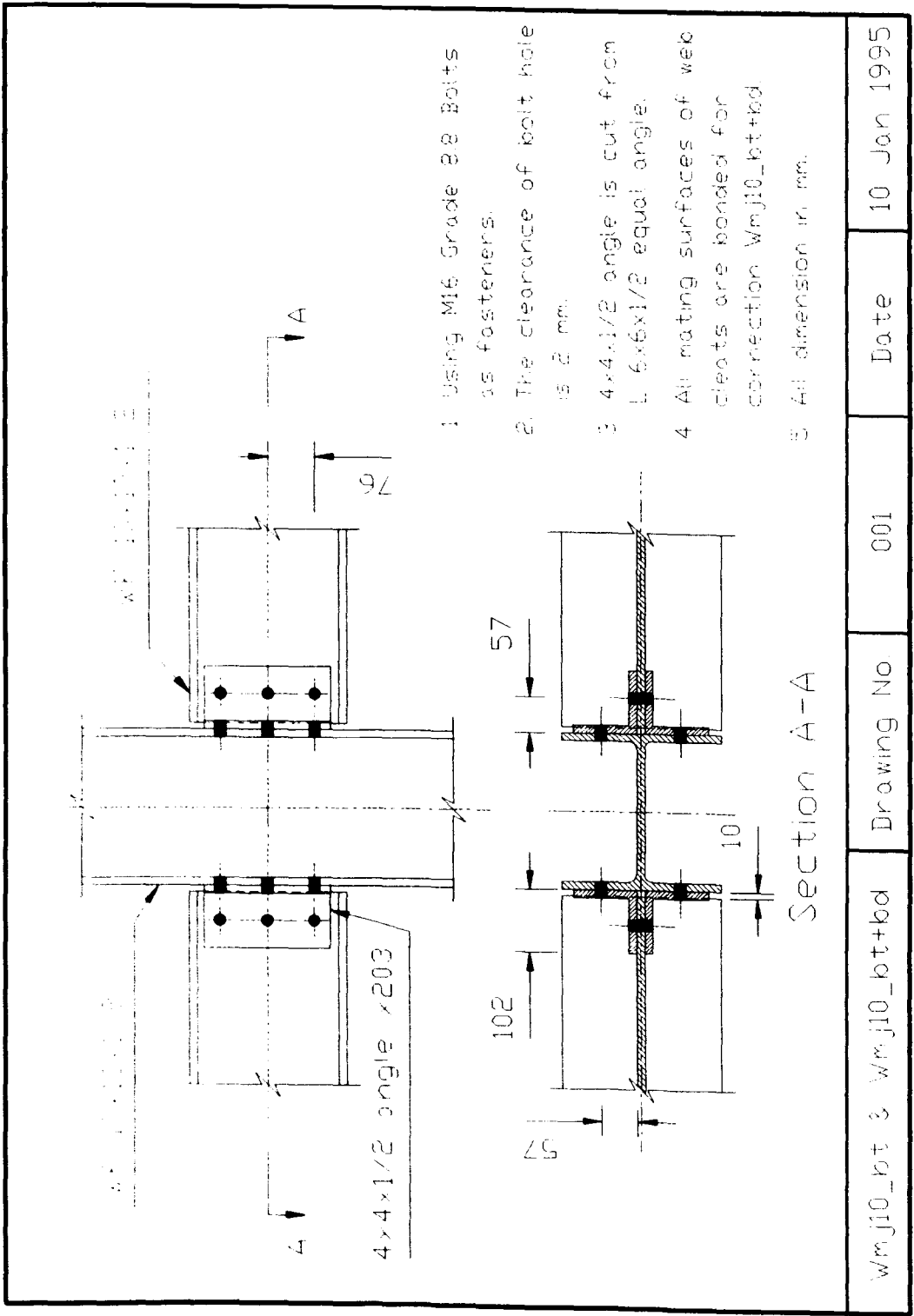
From the laboratory investigation, the design and analysis, the following works are recognised as needing to be continued for the further development on the beam-to-column connection:

- for reasons of safety and the efficient use of material, as stated above, the long term behaviour of web cleated connection needs to be investigated.
- if the permanent connection rotation in the long-term or the connection under dynamic loading is to be developed, this needs to be further investigated.
- the effect of creep and fatigue on the connection stability in long-term needs to be investigated, and the information obtained will benefit future connection design.
- the finite element modelling analysis and the experiment test on the thin shell cleat connector designed in this thesis need to be carried out.
- for the practical application and the further development of the concepts of connections and structural system proposed, full size laboratory experimental tests will be needed.

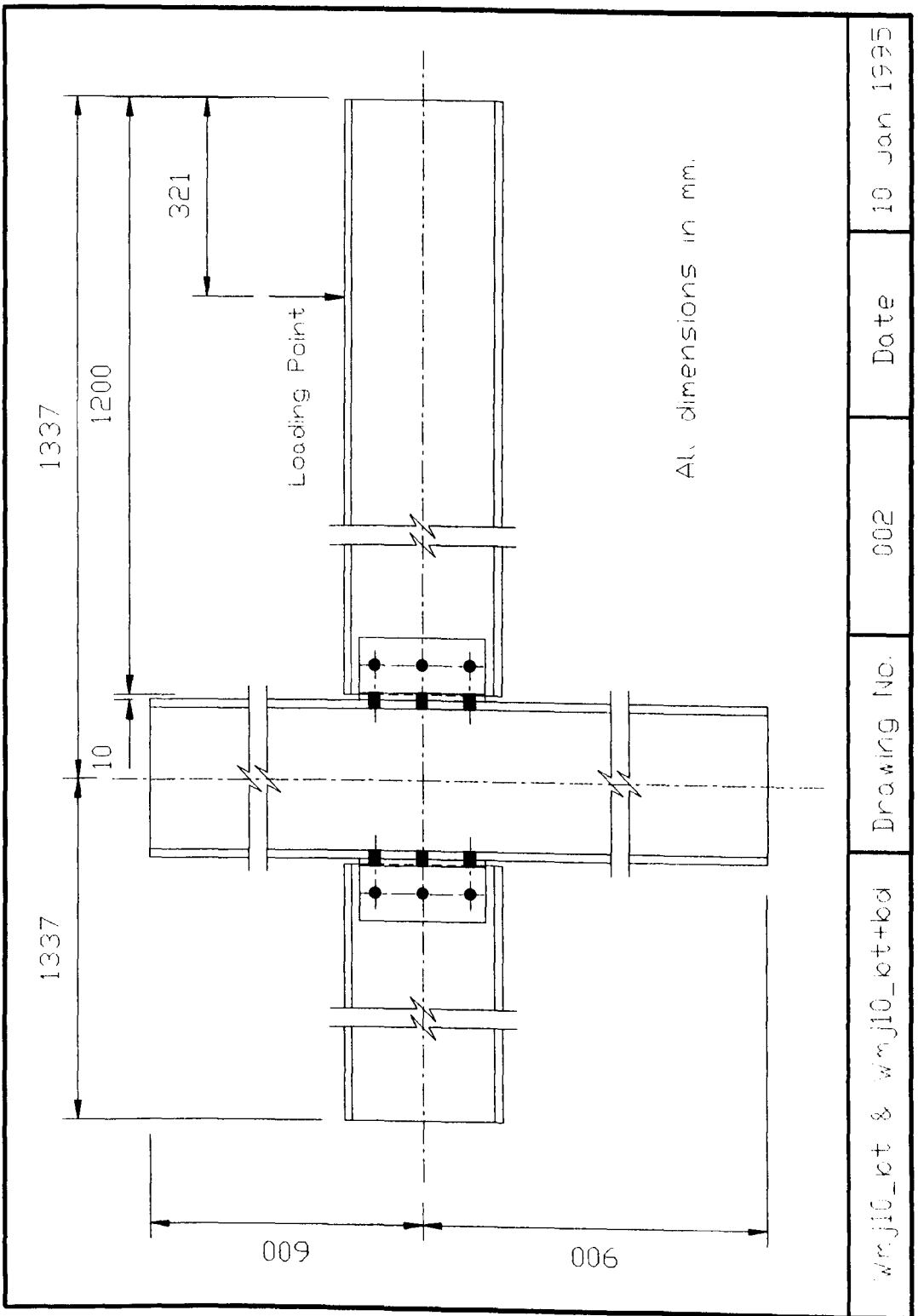
Appendix A

The Detail of Pinned

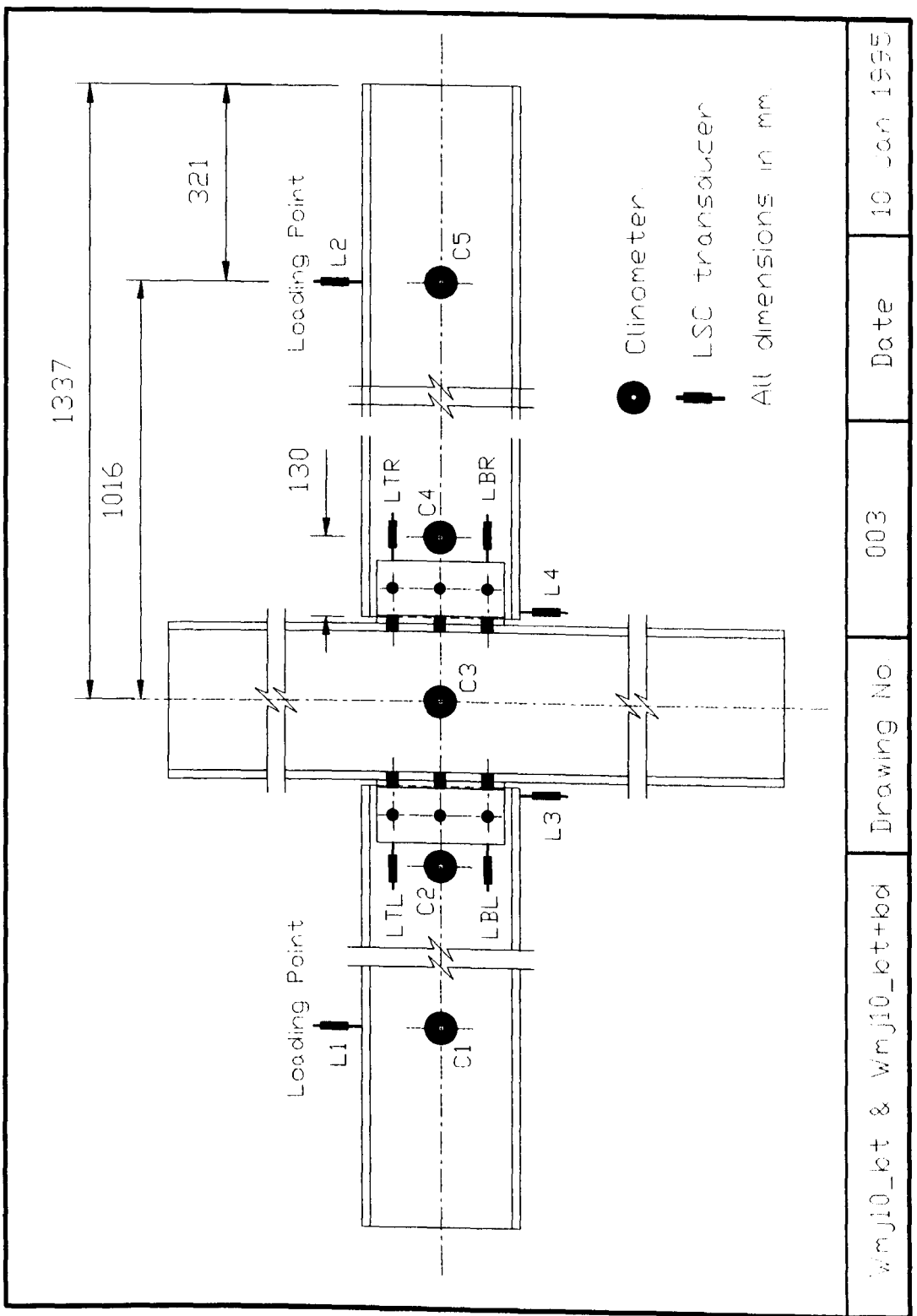
Beam-to-column Connections



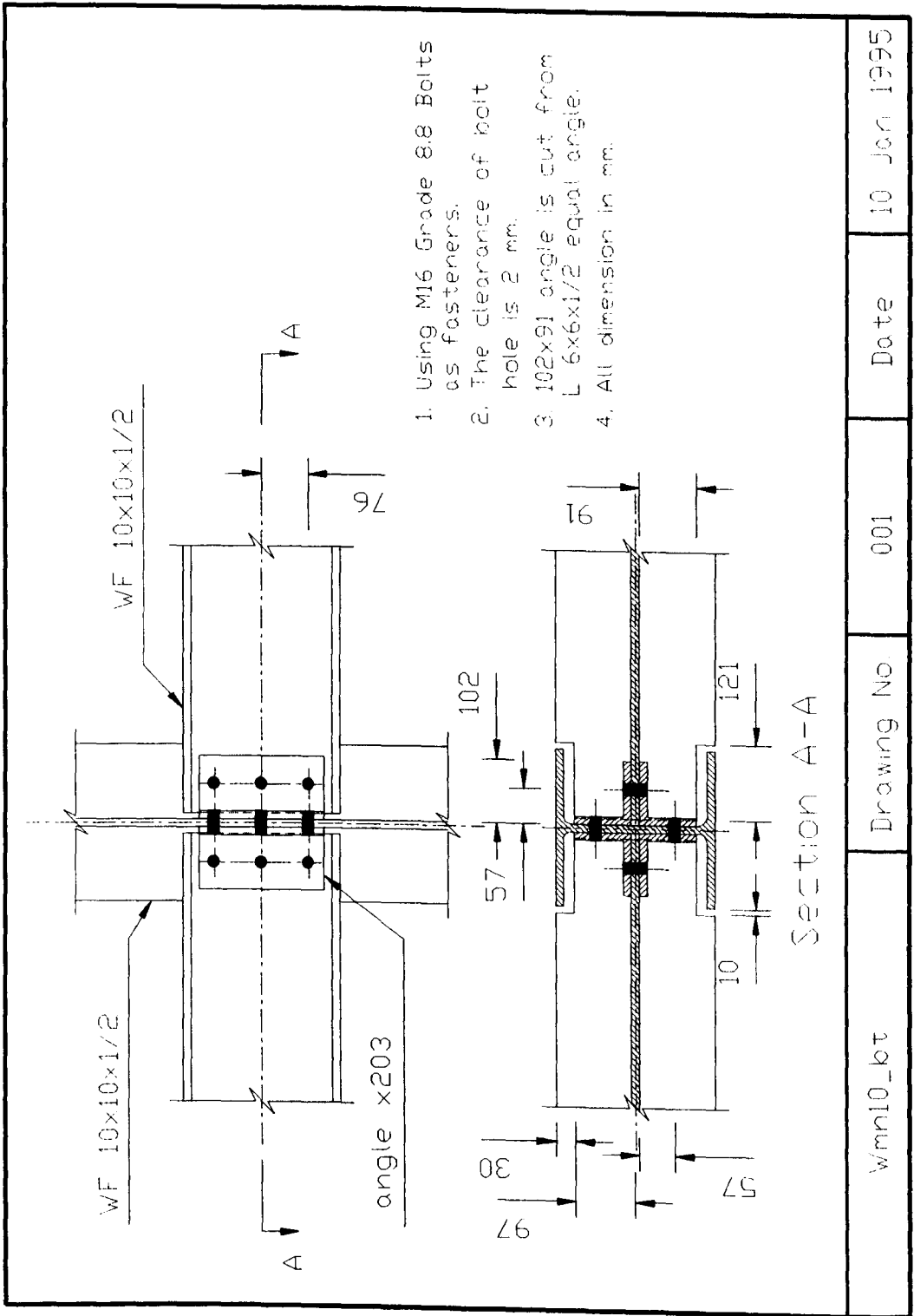
APPENDIX A. THE DETAIL OF PINNED BEAM-TO-COLUMN CONNECTIONS



APPENDIX A. THE DETAIL OF PINNED BEAM-TO-COLUMN CONNECTIONS



wmj10_ket & wmj10_ket+kd	Drawing No	003	Date	10 Jan 1995
--------------------------	------------	-----	------	-------------



wmn10_bot

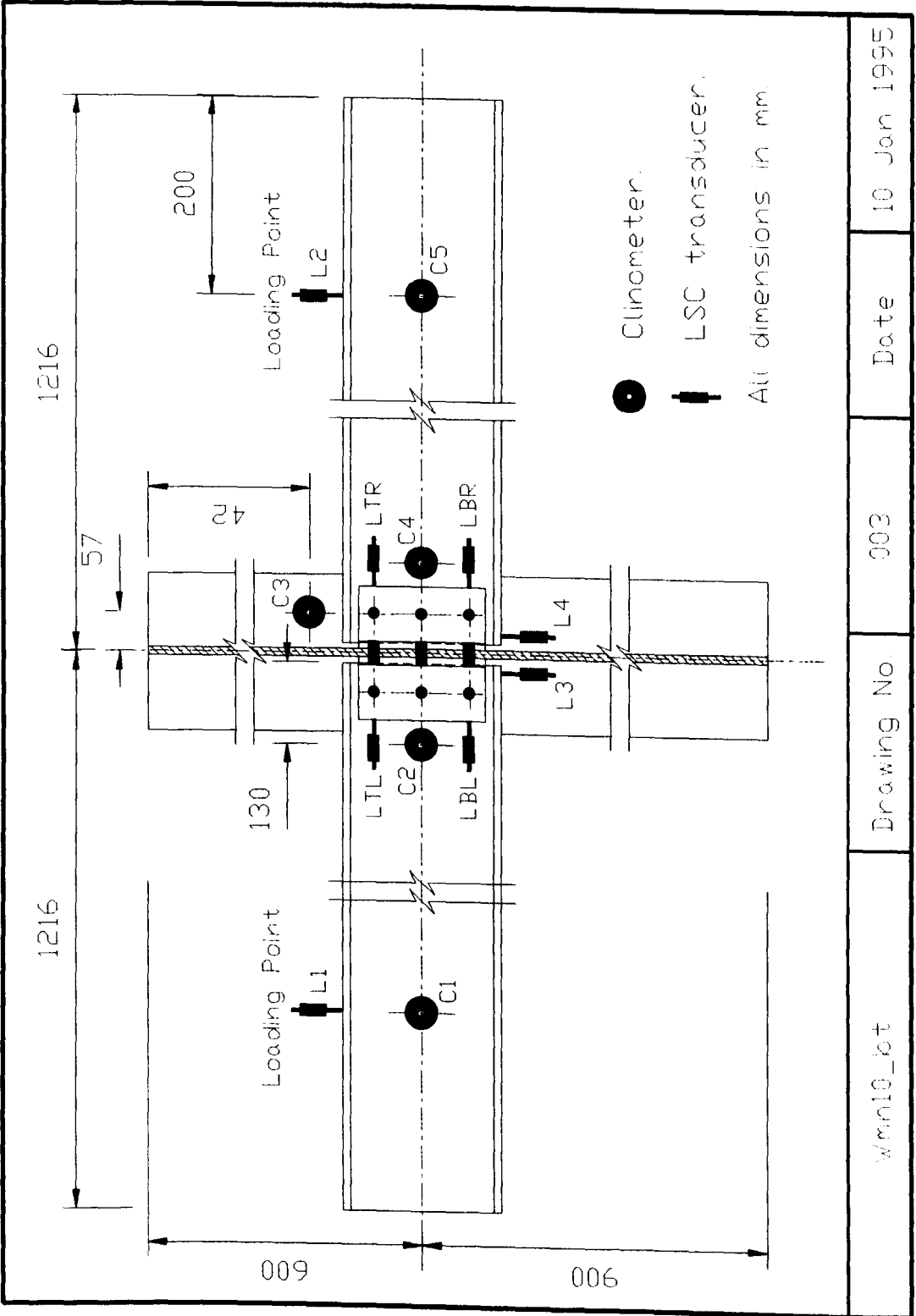
Drawing No.

001

Date

10 Jan 1995

APPENDIX A. THE DETAIL OF PINNED BEAM-TO-COLUMN CONNECTIONS

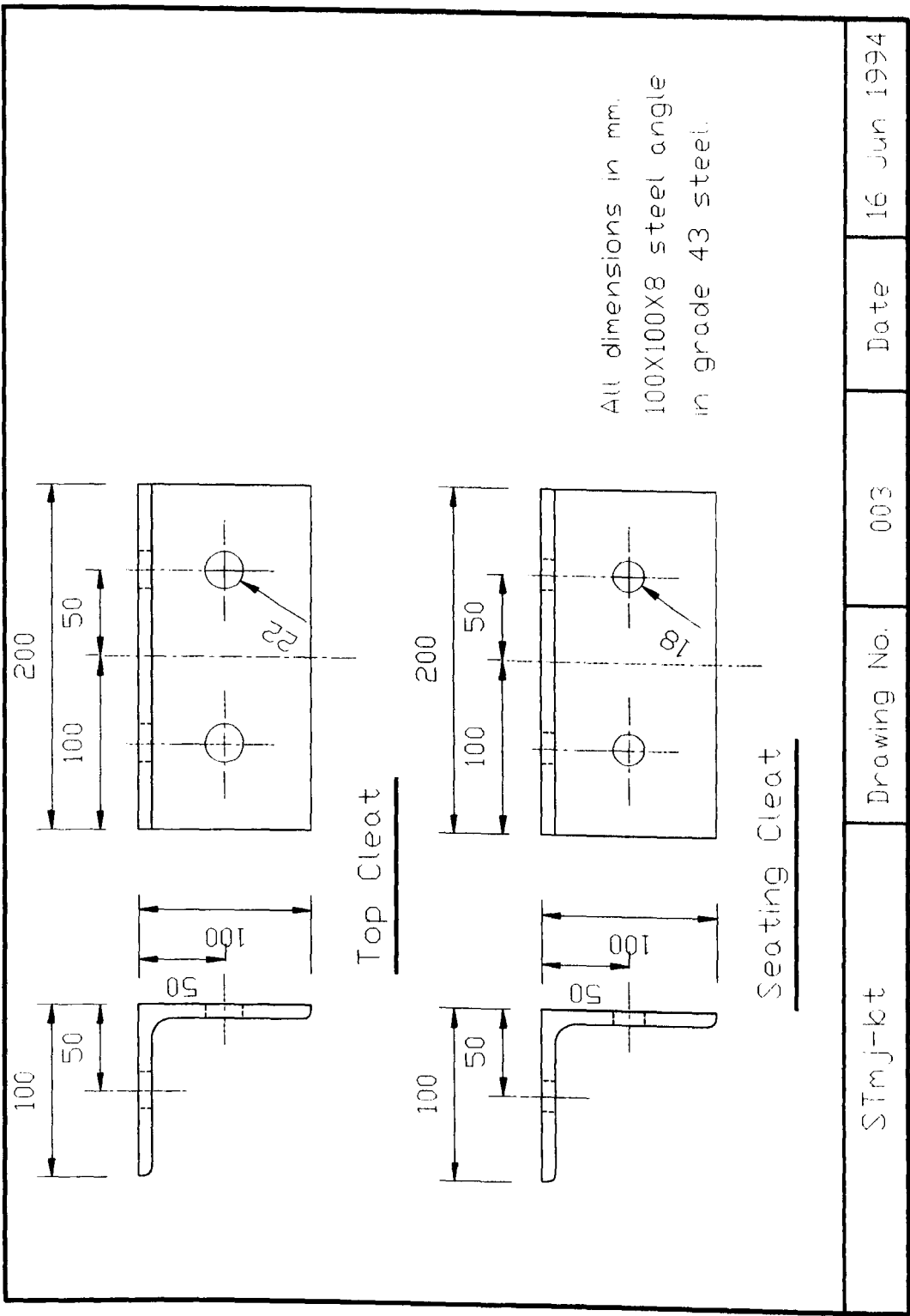


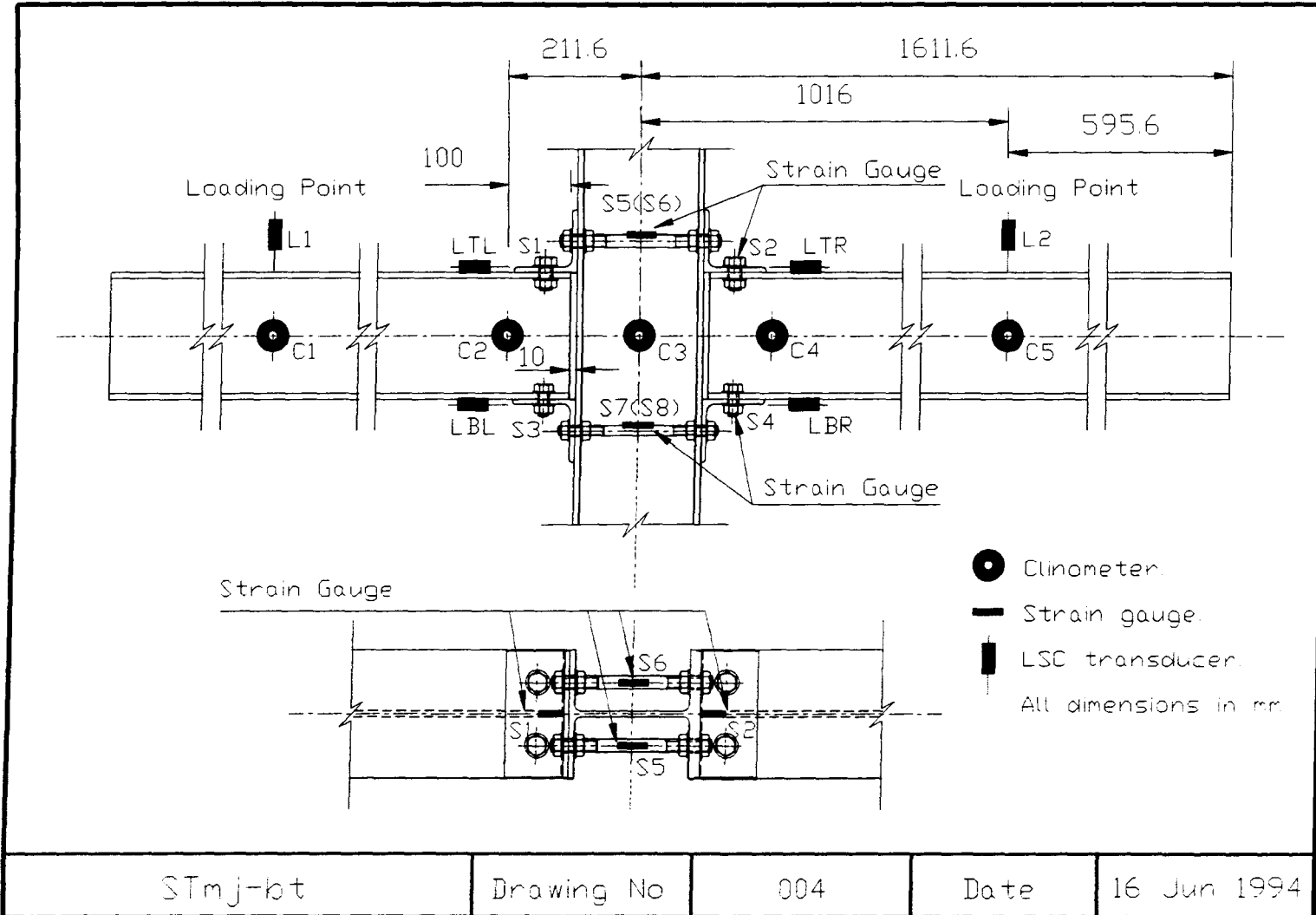
wm10_bot	Drawing No.	003	Date	10 Jan 1995
----------	-------------	-----	------	-------------

Appendix B

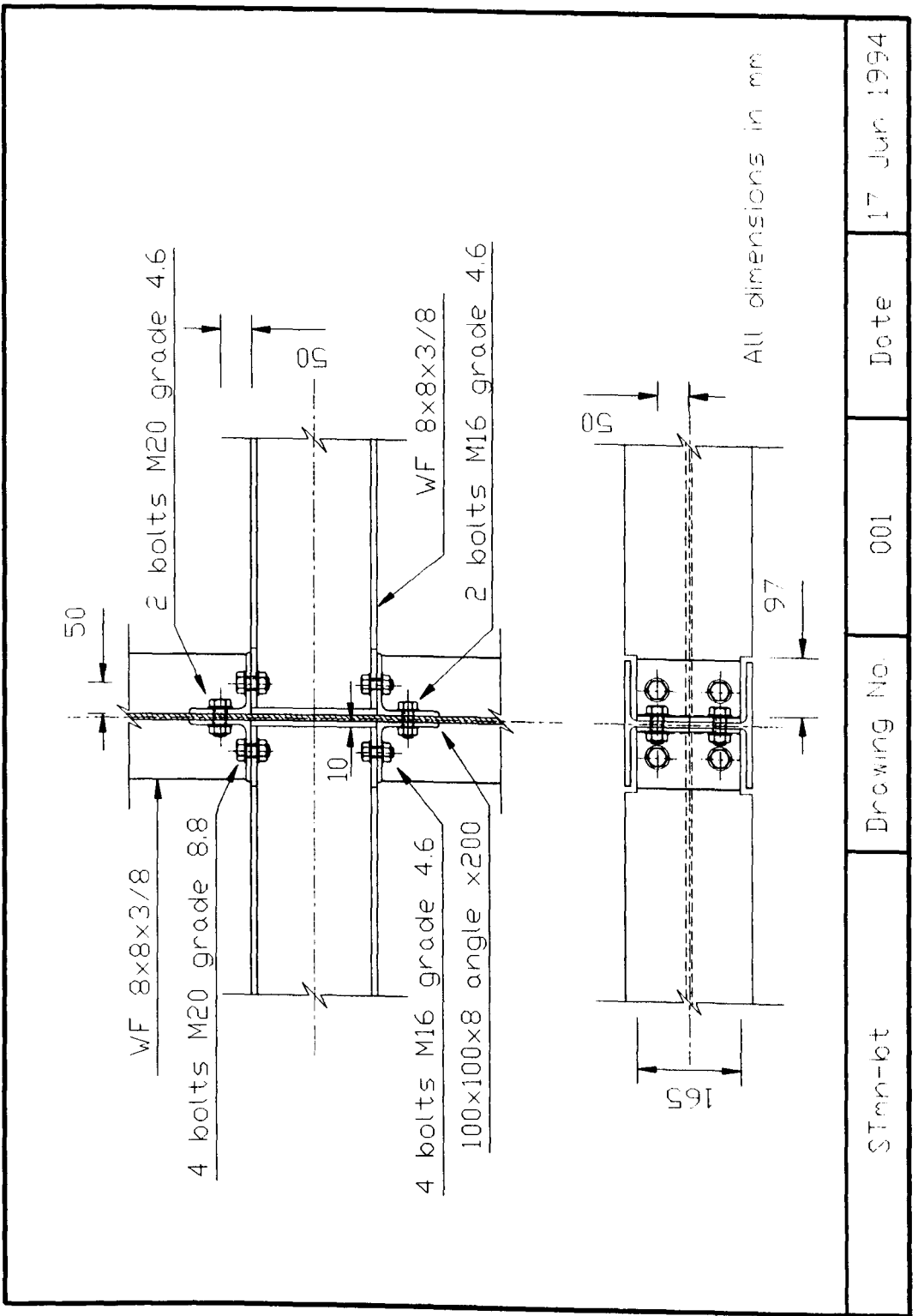
The Detail of Semi-rigid Beam-to-column Connections

APPENDIX B. THE DETAIL OF SEMI-RIGID BEAM-TO-COLUMN CONNECTIONS

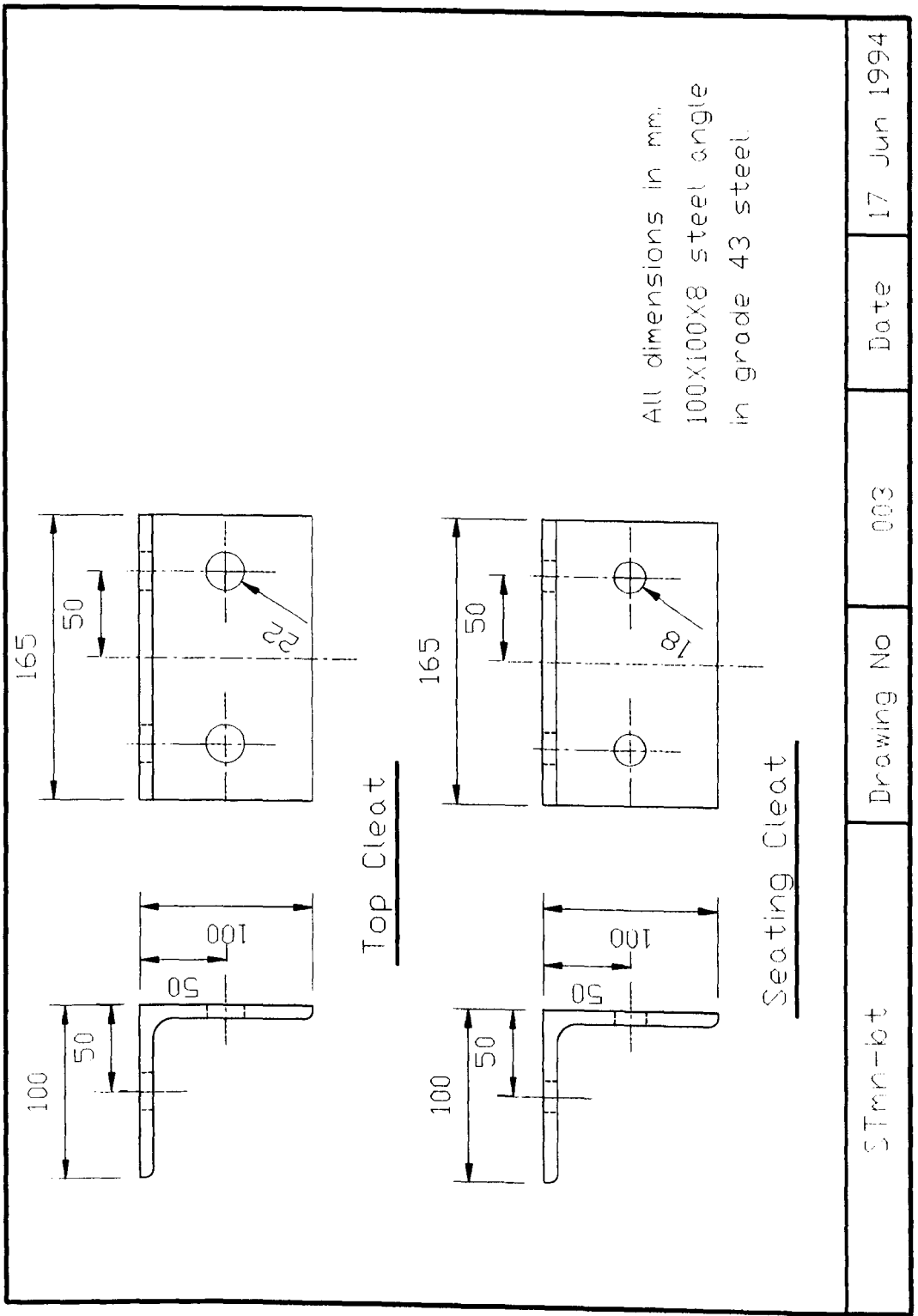




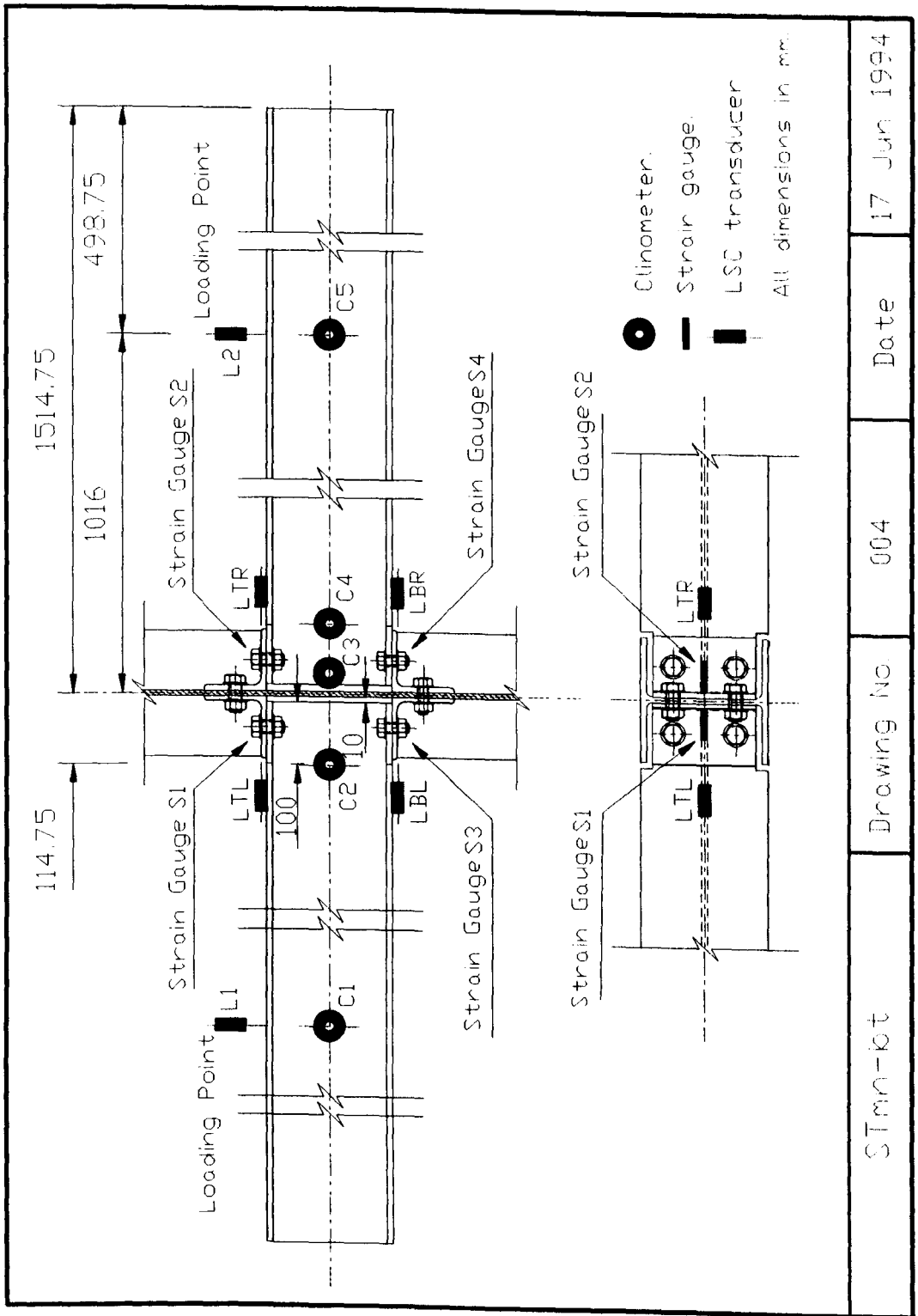
APPENDIX B. THE DETAIL OF SEMI-RIGID BEAM-TO-COLUMN CONNECTIONS



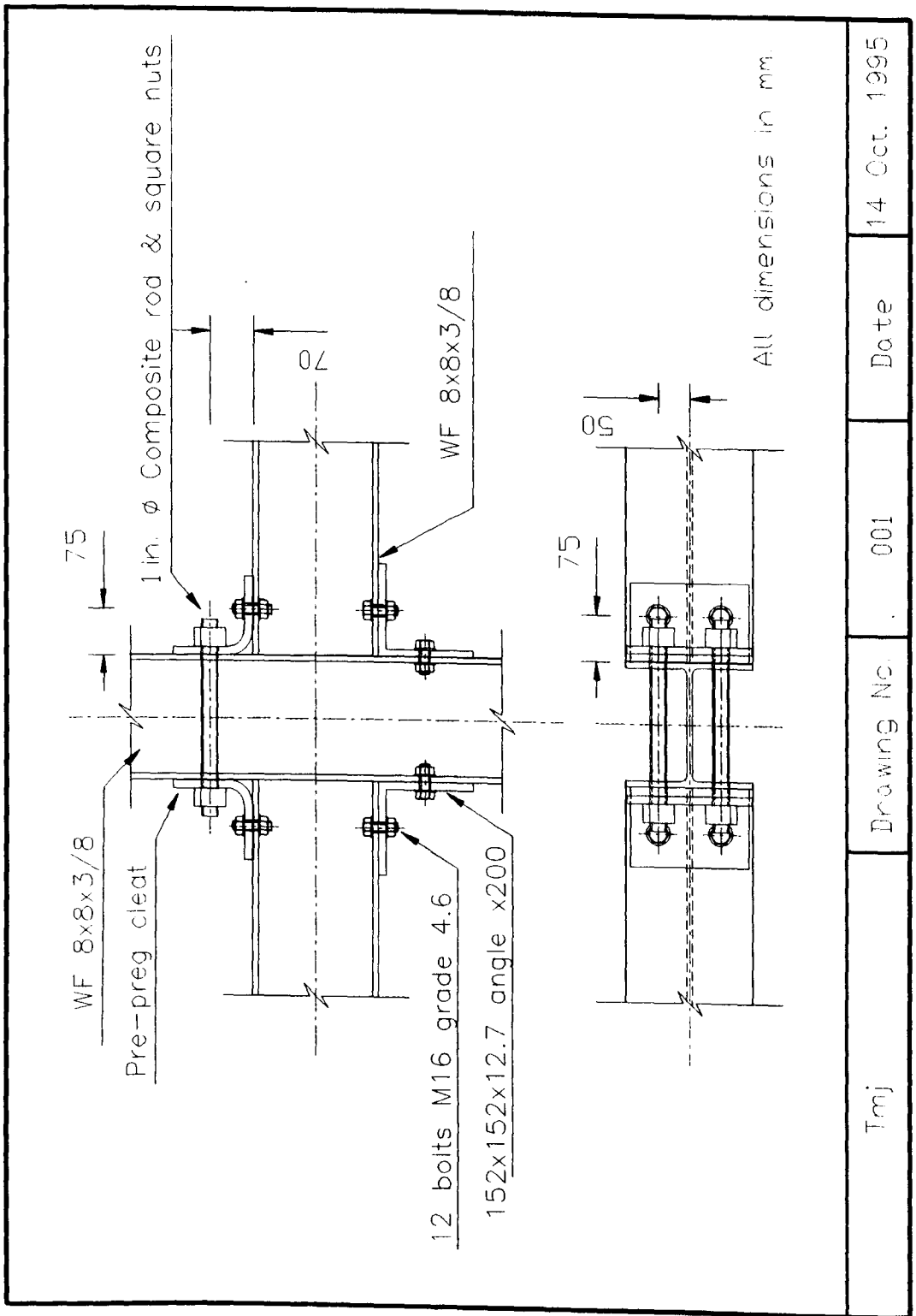
APPENDIX B. THE DETAIL OF SEMI-RIGID BEAM-TO-COLUMN CONNECTIONS



APPENDIX B. THE DETAIL OF SEMI-RIGID BEAM-TO-COLUMN CONNECTIONS

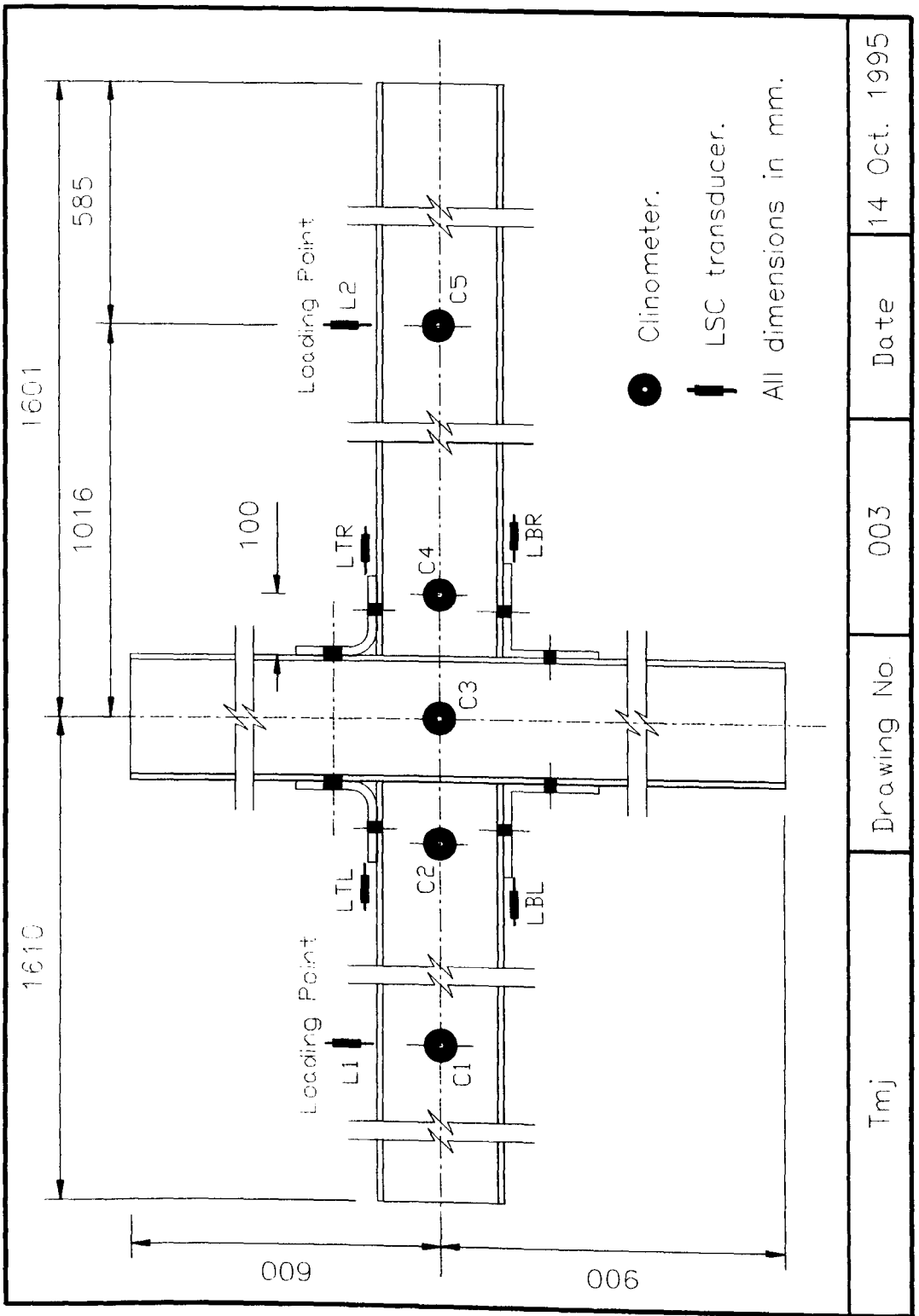


APPENDIX B. THE DETAIL OF SEMI-RIGID BEAM-TO-COLUMN CONNECTIONS

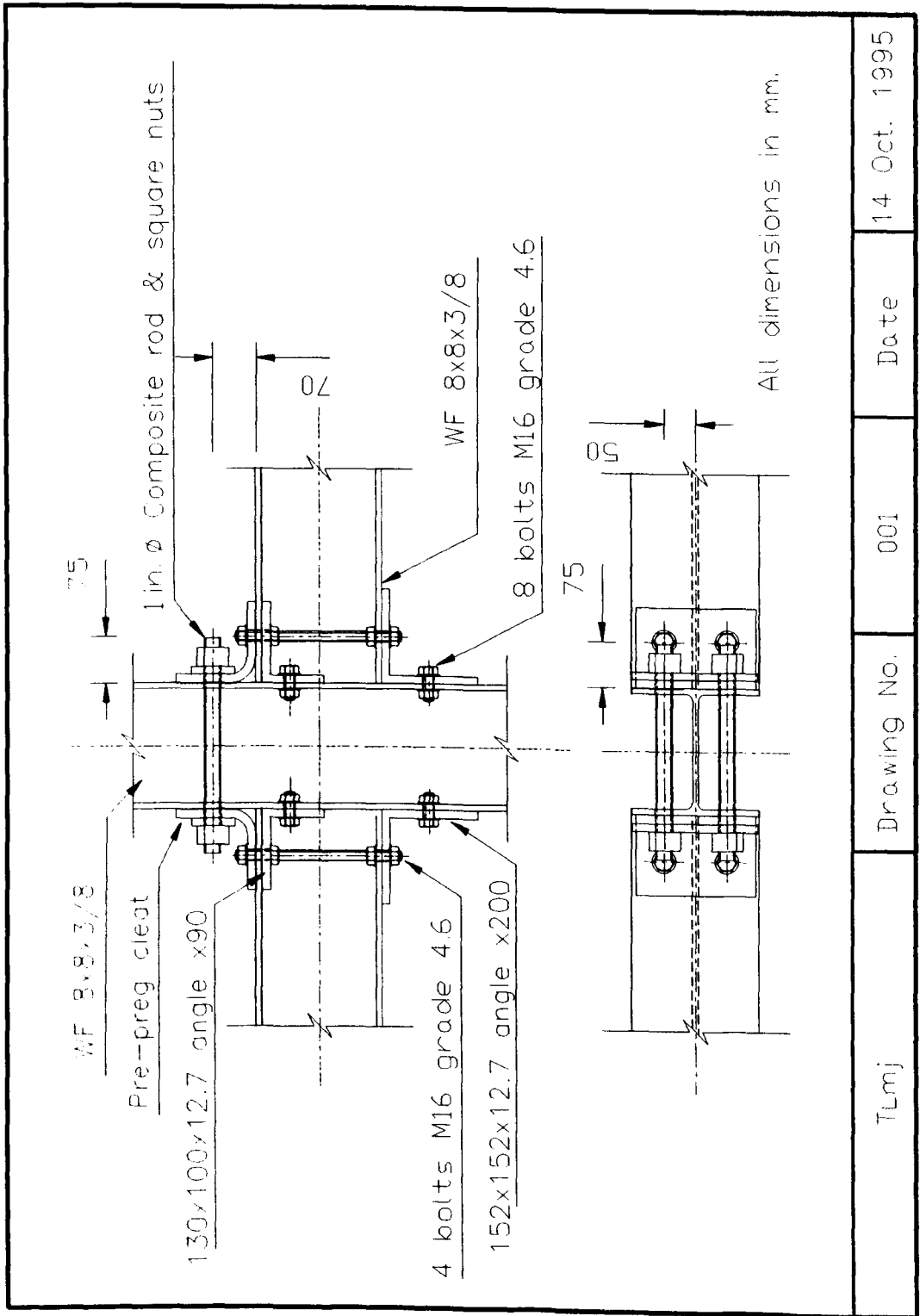


Tmj	Drawing No.	001	Date	14 Oct. 1995
-----	-------------	-----	------	--------------

APPENDIX B. THE DETAIL OF SEMI-RIGID BEAM-TO-COLUMN CONNECTIONS



APPENDIX B. THE DETAIL OF SEMI-RIGID BEAM-TO-COLUMN CONNECTIONS



Tlmj

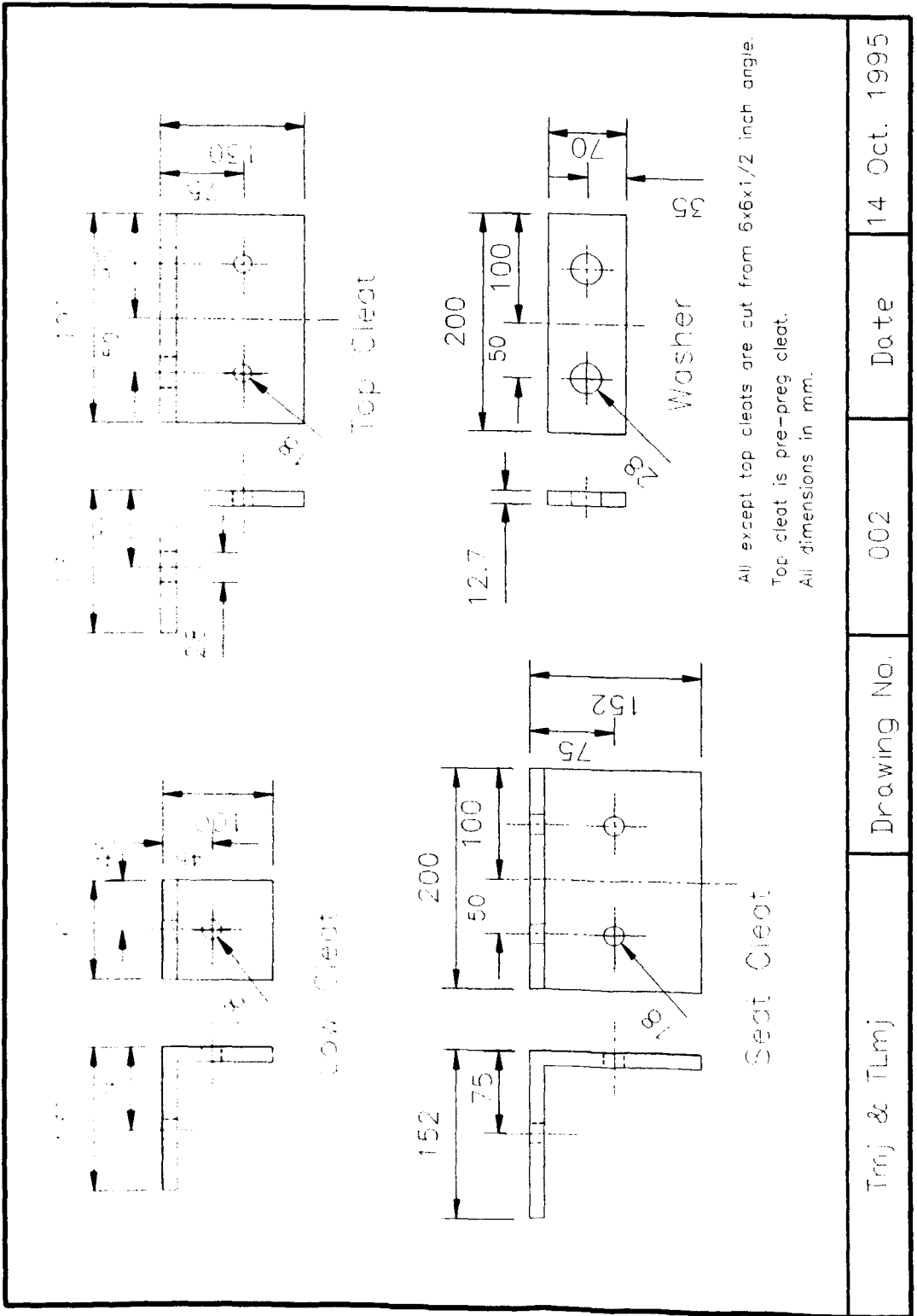
Drawing No.

001

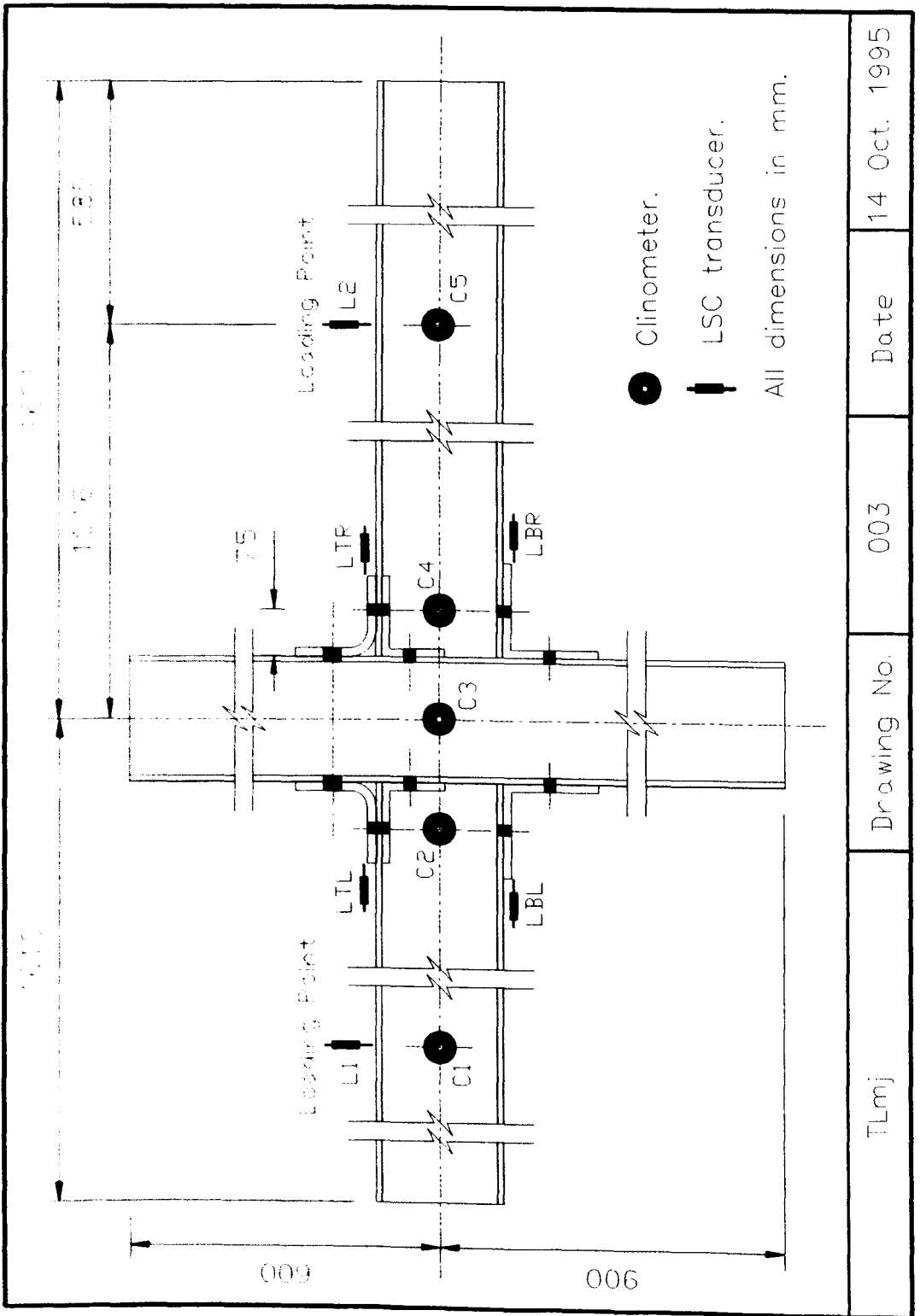
Date

14 Oct. 1995

APPENDIX B. THE DETAIL OF SEMI-RIGID BEAM-TO-COLUMN CONNECTIONS



APPENDIX B. THE DETAIL OF SEMI-RIGID BEAM-TO-COLUMN CONNECTIONS



FLmj

Drawing No.

003

Date

14 Oct. 1995

Appendix C

A Guide for Using Frame Structure Analysis Programme `sframe`

The programme `sframe.c` uses the matrix stiffness method to analyse a plane frame structure. The programme is written in the C programme language. The algorithms used in this programme are illustrated in the flowchart in **Fig. 7.16**. To run the programme a data file is required. How to use the programme, the preparation of the data file and the sign convention for analyse of general plane frame structures are described in the following sections. Five example data files are given with explanation.

C.1 How to Use the Programme

Before running the programme, it is required to compile the source code file `sframe.c` to an executable file. This can be done by using the following command:

```
cc -o sframe sframe.c -lm
```

After compiling the source file **sframe.c**, the executable file is saved in the name of **sframe**. To run **sframe**, a data file is required. You can name your data file with any name, but it is recommended that the extension name (wildcard) of your data file is **.dat**, for example a data file could be **example.dat**. To run **sframe** with the data file enter the following UNIX command:

```
sframe [-s] [-n] [-q] [-l{f}] [-d{na}] [example.dat]
```

The options are **-s**, to include effect of having semi-rigid connections, **-n** to include stability functions that allow for second order deflections, **-q** to include shear deformation of the elements in the frame, **-l{f}**, for the load factor which will multiply all loads applied by **f**, **-d{na}** is for displaying the **n** iterative results, in which **n** is an integer number and **a** is to display results of all iterations. In default of these options, output is the results of the rigid frame analysis with load factor being unit.

Using the above command, the results will be displayed on the terminal. If you want to store the results in an output file, for example, file named **examp.out**, you can run your **sframe** with the following command:

```
sframe example.dat > examp.out
```

C.2 Assumptions and Sign Convention

It is assumed that the x-y plane for each vertical or horizontal element coincides with the plane of the structure. As two-dimensional frames are being considered here there are just three degrees of freedom at each end of a element, and to each degree there is a corresponding force component.

For element, forces and displacements, the sign convention is as follows.

The two ends of a element are given the local numbers 1 and 2. This is shown

in Fig. C.1. The direction from 1 to 2 is stipulated as the positive direction.

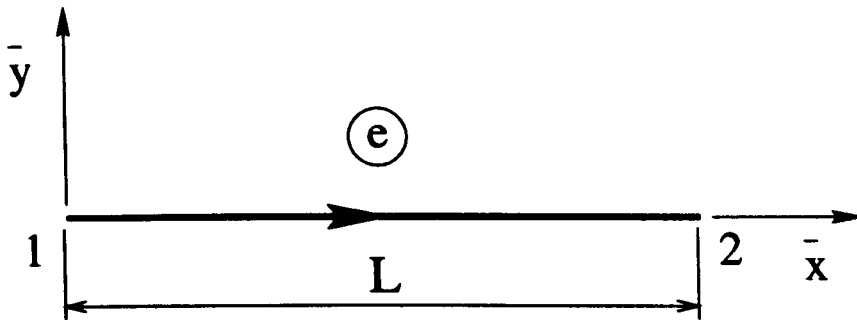


Figure C.1: Member local coordinate system.

For each force component \bar{U} , \bar{V} and \bar{M} and displacement component \bar{u} , \bar{v} and $\bar{\theta}$ at the ends of a element, their positive direction is shown in Fig. C.2.

In the structure's global coordinate system, the positive direction of each force and displacement component is consistent with this coordinate system; the moment and rotation components are clockwise positive.

C.3 Units

There are no 'built-in' units in **sframe** program. The user must prepare the input in a consistent set of units. The output produced by the program will conform to the same set of units. For example, if the units of the load is kN and the units of the element length is cm, then the units of the section area of the element and the units of the elastic modulus must be cm^2 and kN/cm^2 respectively. The output units will then be in kN and cm, so that the frame member axial force will be in kN, bending moments will be in kN-cm, and displacements will be in cm. Joint and connection rotations, however, are in radians, irrespective of units.

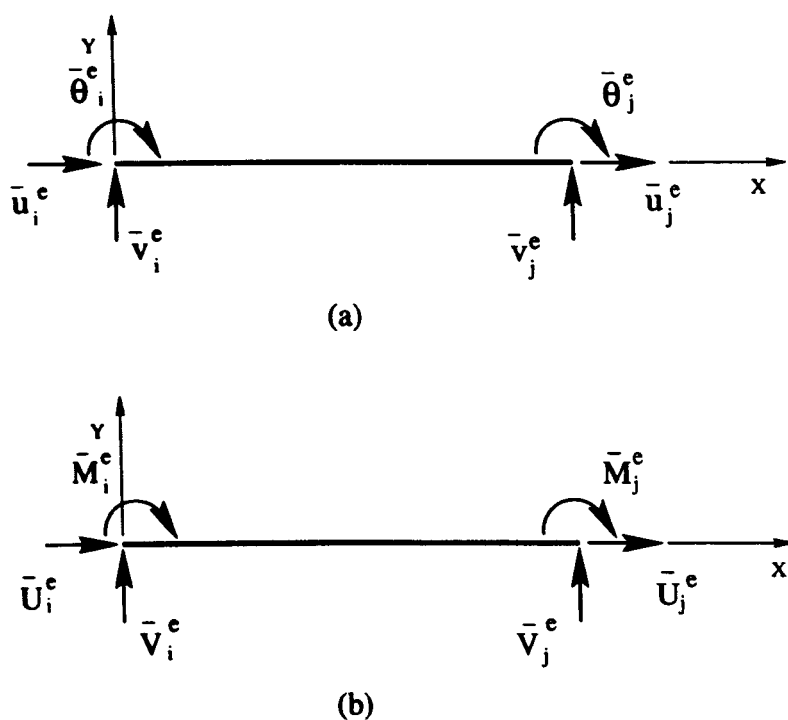


Figure C.2: Sign convention for member end displacements (a) and forces (b).

C.4 Preparation of Data File

The data file consists of six parts, and these are; basic frame specification data (C.4.1), element properties (C.4.2), restraint conditions (C.4.3), applied loads (C.4.4), tolerance for moment and maximum number of iterations (C.4.5), and the semi-rigid connection $M - \phi$ data (C.4.6). The preparation of the data in each part is given in the following sub-sections, respectively.

C.4.1 Basic Frame Specification Data

The basic frame specification data gives general information on the frame structure. It includes the number of elements, of joints, of restraints, of loads at joints and of

loads between joints. For example 1 in Section C.6, the data and the format are:

No. of elements	No. of joints	No. of restrains	No. of loads at joint	No. of load between joint
4	5	6	0	2

All the data given in this section should be integer. Note that the column headers are given here to aid the reader and are not part of the data file format.

C.4.2 Element Properties

The information of elements required is given as follows (see Section C.6, example 4):

Joint No.		Pin Joint		Length of	Inclination	Area of	2nd Moment	Elastic	Shear	Shear
end 1	end 2	end 1	end 2	elements	of elements	section	of area	moduli	moduli	coefficient
1	2	0	0	5	0	0.5	0.0416667	30000000	0	0
3	1	0	0	5	90	0.5	0.0416667	30000000	0	0

Each line of the data is for one element. The number assigned to the element will be automatically assigned from the first line to the end line. The list should be compiled in the corresponding order consistent with the numbering of the frame elements.

If a pinned joint is at the end of a element, the corresponding column of Pin Joint should be filled with 1, otherwise 0, see example 2 and 5.

Shear coefficient α_s is a numerical factor by which the average shear stress must be multiplied to obtain the shear stress at the centroid of the cross section. For an I beam, α_s is approximately equal to $\frac{A}{A_w}$, where A_w is the area of the web of the beam. In this example the shearing effect is not considered and therefore both the shear moduli and the shear coefficient are set to 0.

C.4.3 Boundary Condition

For each joint, there are three displacement components corresponding to three degrees of freedom. They are numbered for a frame in the order of X, Y and θ in structure's coordinate system. For example, restraints of joint one are 1, 2, 3 and joint two are 4, 5, 6 and so on.

In example 4 (Section C.6), joint numbers two and three have fully fixed ends. All three degrees of freedom at these joint are zero. The corresponding numbers for these displacement vectors are 4, 5, 6 for joint two and 7, 8, 9 for joint three. The entry in the data file is

Joint 2			Joint 3		
X	Y	θ	X	Y	θ
4	5	6	7	8	9

Note that these, X Y θ , are in the structure's global coordinate system, they are not necessarily consistent with the element's local coordinate system.

C.4.4 Loads

The data of loads have two parts, loads at joints and loads between joints. They are given in the following sub-sections respectively.

Loads at Joints

The load values and their displacement direction for Example 4 (Section C.6) are as follows.

Loads	Displacement
value	code
6 (horizontal load)	1 (X)
2 (vertical load)	2 (Y)
5 (moment)	3 (θ)

Note that the displacement direction of load are in structure's global coordinate.

Loads Between Joints

In this part, distributed load is assumed to apply on the element starting from end 1 of the element. Type of load is assigned as 1 for a distributed load, 2 for a vertical concentrated load and 3 for a horizontal concentrated load. The data of loads between joints for Example 4 (in Section C.6) are given as follows:

Loads value	Distances from end 1	No. of element applied	Type of loads
4.8	5	1	1
-8	2.5	2	2

C.4.5 Tolerance of Moment and Maximum Number of Iterations

The tolerance of moment at each element end is the accuracy required in the frame analysis when account is made of the effects of the second-order deflection and/or of the semi-rigid connections. After each iteration is completed, the results of moments for each element end are compared with the results in the previous iteration. If the difference is smaller than the tolerance value, the analysis terminates, otherwise the iterative process is repeated.

In example 4, the tolerance of moment is set to 0.005. If the analysis does not include the second-order deflections or/and semi-rigid connections the value of the tolerance can be set to any value without affecting the results.

The maximum number of iterations is used to limit the programme running times for the situation where convergence is not readily achieved. If this happens, the tolerance value can be increased in an attempt to help the analysis to produce a convergent solution.

The tolerance and the maximum number of iterations for example 4 (in Section C.6) are given as follows:

0.005 300

C.4.6 Semi-rigid Connection Data

The semi-rigid connection data starts with a caption line, followed by the number of different semi-rigid connection types, and their moment-rotation curves. Finally, the connection type (pinned, semi-rigid, fixed) at each element end is given.

Caption Line

The caption line is a one line message. It can be changed, but it must be no more than one line in length. The following example is the caption line used in example 1 (in Section C.6).

semi-rigid yes

The caption line goes at the beginning of the semi-rigid connection data entry and it simply states that the following data are for the semi-rigid connections of a frame.

Number of Semi-rigid Connection Types

This is the number of different semi-rigid connections in the frame. In Example 1 (Section C.6), there are the two types of semi-rigid connections which are beam-to-column and column-to-base connections, and they possess different moment-rotation behaviour. The number of semi-rigid connection types in this example is 2.

Moment-rotation Curve

In the programme **sframe** the continuous smooth $M - \phi$ curve is defined in terms of a piecewise linear discretisation. For each type of semi-rigid connection, its $M - \phi$ curve needs to be defined. This can be done by giving the number of discrete points

along the $M - \phi$ curve, followed by moment and rotation value at each point. The data is given in the order that the first $M - \phi$ curve for type 1 connection and so on. The the units of moment should be in a consistent set of units used for the element properties and the load, the rotation ϕ must be in units of radian.

```

5
0      0
136    0.0017
362.6  0.009
589.2  0.028
623.2  0.038

```

```

5
0      0
48     0.005
107    0.015
133    0.020
160    0.0258

```

Connection Type at Each Member End

The connection types for each element are given in the order end 1 and end 2. In example 1 (Section C.6), the data for each element end are in order:

```

2  0
1  0
0  1
0  2

```

Note that for the fixed or pinned end, the connection type should be set to 0 here (the pinned connection is defined earlier in the section of element properties).

C.5 Output Results

For each element-end, its end displacements \bar{u} , \bar{v} and $\bar{\theta}$ and relevant internal forces \bar{U} , \bar{V} and \bar{M} are given with label X[i], Y[i] and R[i] and N[i], Q[i] and M[i] respectively (i is the element end number). For a semi-rigid connection, the end displacement R[i] is the joint rotation, and the element-end rotation is given by Rotation[n][i] and is equal to R[i]+Phi[n][i], Phi[n][i] is the semi-rigid connection rotation and n is the element number.

kratio[i] is the semi-rigid connection stiffness given by moment/rotation ($M[i]/R[i]$).

The results of example 1 (in Section C.6) are given below. The displacements X[i], Y[i] and R[i] are in the local coordinate system. They are actually the joint displacements. The actual rotation displacement of the element-end with a semi-rigid connection at the end is the sum of the joint rotation R[i] and the semi-rigid connection rotation Phi[n][i], which is given as Rotation[n][i] (n is No. of the element, and i is end of the element).

***** iterative 86 ***** ---- number of iterations

Element No.	1		
X[1]=	0.000e+00	N[1]=	50.000 ---- axial force.
Y[1]=	0.000e+00	Q[1]=	-3.428 ---- shear force.
R[1]=	0.000e+00	M[1]=	13.066 ---- moment.
kratio[1][1]=	9.600e+03		
Phi[1][1]=	-1.36098e-03		---- connection rotation (rad).
Rotation[1][1]=	-1.36098e-03		---- element end rotation (rad).
X[2]=	-8.125e-02	N[2]=	-50.000
Y[2]=	-4.175e-03	Q[2]=	3.428
R[2]=	5.365e-03	M[2]=	613.419

```

Element No.      2
X[1]=  4.175e-03      N[1]=   3.428
Y[1]= -8.125e-02      Q[1]=  50.000
R[1]=  5.365e-03      M[1]= -613.419
kratio[2][1]=  1.746e+04
Phi[2][1]=  3.51242e-02
Rotation[2][1]=  4.04889e-02      ---- element 2, end 1 rotation.
X[2]=  1.792e-06      N[2]=  -3.428
Y[2]= -5.029e+00      Q[2]=  -0.000
R[2]= -1.431e-09      M[2]= -3964.641

```

```

Element No.      3
X[1]=  1.792e-06      N[1]=   3.428
Y[1]= -5.029e+00      Q[1]=   0.000
R[1]= -1.431e-09      M[1]= 3964.641
X[2]= -4.172e-03      N[2]=  -3.428
Y[2]= -8.125e-02      Q[2]=  50.000
R[2]= -5.365e-03      M[2]=  613.419
kratio[3][2]=  1.746e+04
Phi[3][2]= -3.51242e-02
Rotation[3][2]= -4.04889e-02      ---- element 3, end 2 rotation.

```

```

Element No.      4
X[1]=  8.125e-02      N[1]=  50.000
Y[1]= -4.172e-03      Q[1]=   3.428
R[1]= -5.365e-03      M[1]= -613.420
X[2]=  0.000e+00      N[2]= -50.000
Y[2]=  0.000e+00      Q[2]=  -3.428
R[2]=  0.000e+00      M[2]= -13.066
kratio[4][2]=  9.600e+03
Phi[4][2]=  1.36100e-03
Rotation[4][2]=  1.36100e-03

```

C.6 Examples

C.6.1 Example 1

For this U-frame example, all joints and elements are numbered as shown in Fig. C.3 (b). For each element, numbered with (1) to (4), its ends 1 and 2 are numbered using small 1 and 2, respectively. The semi-rigid connections are at element (1) end 1, element (2) end 1, element (3) end 2 and element (4) end 2. The joints are numbered with large 1 to 5. Fig. C.3 (a) gives the loading and the dimensions of the frame.

The section area of the element is 56.31 cm^2 , the 2nd moment of area is 4127.8 cm^4 , and the elastic modulus is 2000 kN/cm^2 , the shear modulus is 230 kN/cm^2 and the shear coefficient is 3.0745.

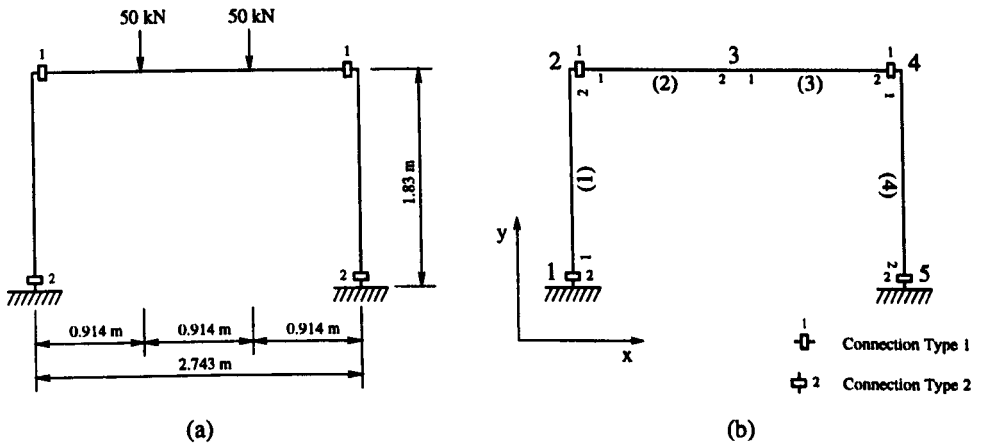


Figure C.3: Example frame 1: (a) frame geometry, loading conditions and, (b) the numbering of elements and joints.

4	5	6	0	2						
1	2	0	0	183	90	56.31	4127.8	2000	230	3.0745

2	3	0	0	137.1	0	56.31	4127.8	2000	230	3.0745
3	4	0	0	137.1	0	56.31	4127.8	2000	230	3.0745
4	5	0	0	183	270	56.31	4127.8	2000	230	3.0745

1	2	3	13	14	15
---	---	---	----	----	----

-50	91.4	2	2
-----	------	---	---

-50	45.7	3	2
-----	------	---	---

0.01	300
------	-----

semi-rigid yes

2

5

0	0
---	---

136	0.0017
-----	--------

362.6	0.0099
-------	--------

589.2	0.028
-------	-------

623.2	0.038
-------	-------

5

0	0
---	---

48	0.005
----	-------

107	0.015
-----	-------

133	0.020
-----	-------

160	0.0258
-----	--------

2	0
---	---

1	0
---	---

0	1
---	---

0 2

C.6.2 Example 2

Fig. C.4 shows the sample of the U frame with pinned column-to-base connection.

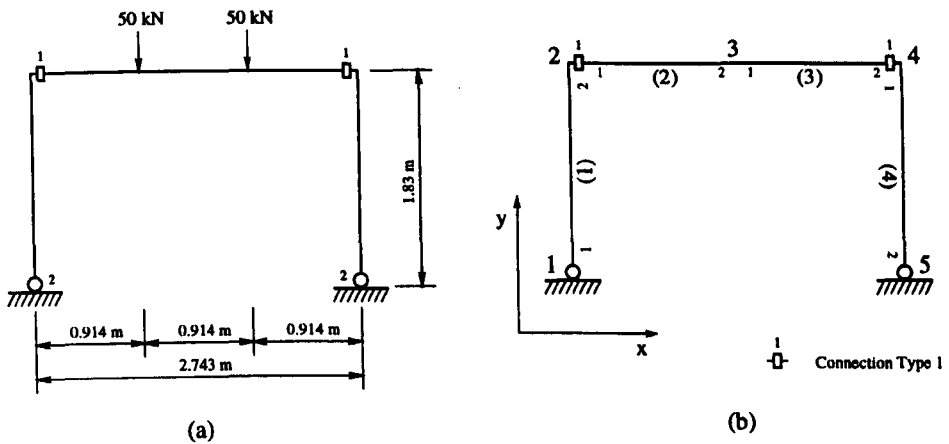


Figure C.4: Example frame 2: (a) frame geometry, loading conditions and, (b) the numbering of elements and joints.

The units used here are the same as example 1 and the data file is given as follows:

4	5	6	0	2						
1	2	1	0	183	90	56.31	4127.8	1620	230	3.0745
2	3	0	0	137.1	0	56.31	4127.8	1620	230	3.0745
3	4	0	0	137.1	0	56.31	4127.8	1620	230	3.0745
4	5	0	1	183	270	56.31	4127.8	1620	230	3.0745
1	2	3	13	14	15					
-50	91.4	2	2							

-50 45.7 3 2

0.001 300

semi-rigid yes

1

5

0 0

136 0.0017

362.6 0.0099

589.2 0.028

623.2 0.038

0 0

1 0

0 1

0 0

C.6.3 Example 3

For this example frame, all joints and elements are numbered as showing in **Fig. C.5**. For each element, the end 1 and end 2 are numbered by small 1 and 2 respectively. In this example, element 2 end 1 and element 3 end 2 are semi-rigid connection.

4 5 6 0 2

1	2	0	0	183	90	56.31	4127.8	1620	230	1
2	3	0	0	137.1	0	56.31	4127.8	1620	230	1
3	4	0	0	137.1	0	56.31	4127.8	1620	230	1
4	5	0	0	183	270	56.31	4127.8	1620	230	1

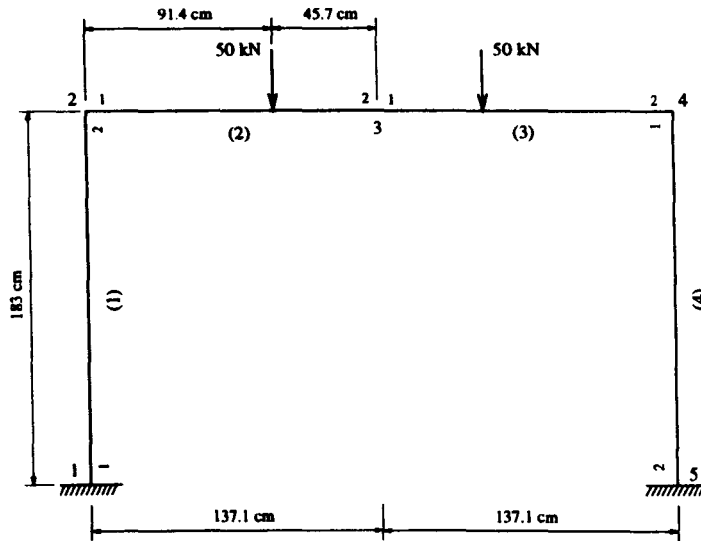


Figure C.5: Example frame 3.

1 2 3 13 14 15

-50 91.4 2 2

-50 45.7 3 2

0.001 300

semi-rigid

1

5

0 0

136 0.0017

362.6 0.0099

589.2 0.028

623.2 0.038

0 0
 1 0
 0 1
 0 0

C.6.4 Example 4

Fig. C.6 shows a plane frame structure, which consists of two elements and three joints. The frame structure undergoes distributed load, horizontal and vertical load and moment load. The load values and dimension of frame structure is as showing in Fig. C.6.

The coordinate of the frame structure is set up as showing in Fig. C.6. For this example frame, all joints and elements are numbered as showing in Fig. C.6. For each element, the end 1 and end 2 are numbered by small 1 and 2 respectively.

The section area of the element is 0.5 m^2 , the second moment of area is 0.0416667 m^4 and elastic modulus is 30000000 kN/m^2 .

2	3	6	3	2						
1	2	0	0	5	0	0.5	0.0416667	30000000	0	0
3	1	0	0	5	90	0.5	0.0416667	30000000	0	0
4	5	6	7	8	9					
6	1									
2	2									
5	3									
4.8	5	1	1							

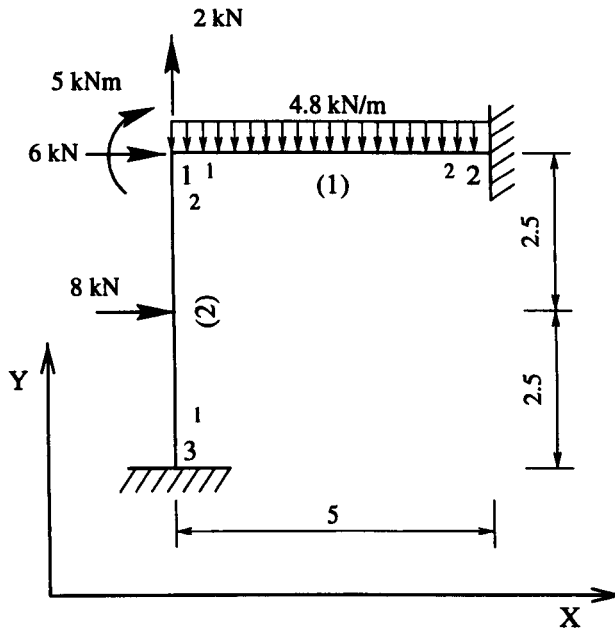


Figure C.6: Example frame 4.

-8 2.5 2 2

0.005 300

C.6.5 Example 5

This example is a plane truss. Since the rotation displacement for each joint is zero, the corresponding displacements need to be restricted. The corresponding numbers for these displacement vectors are 3, 6, 9, 12, 15 and 18.

The section area of the element is 1 m^2 , the second moment of area is 1 m^4 and elastic modulus is 1 kN/m^2 .

10 6 9 2 0

1 3 1 1 1.25 36.8699 1 1 1 700 1

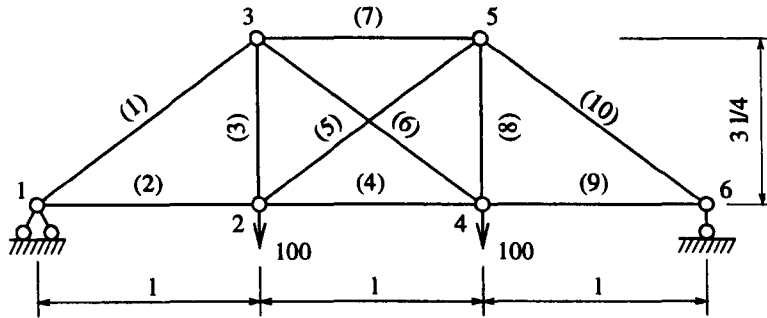


Figure C.7: Example frame 5.

1	2	1	1	1.00	0	1	1	1	700	1
2	3	1	1	0.75	90	1	1	1	700	1
2	4	1	1	1.00	0	1	1	1	700	1
2	5	1	1	1.25	36.8699	1	1	1	700	1
3	4	1	1	1.25	-36.8699	1	1	1	700	1
3	5	1	1	1.00	0	1	1	1	700	1
4	5	1	1	0.75	90	1	1	1	700	1
4	6	1	1	1.00	0	1	1	1	700	1
5	6	1	1	1.25	-36.8699	1	1	1	700	1

1 2 3 6 9 12 15 17 18

-100 5

-100 11

0.001 300

C.7 Computer Programme of Frame Analysis

The computer programme of the frame structural analysis in C programme language is given as follows:

```

/* sframe.c (version 2, sframe6: different of version 1 & 2 is display )
*****
NAME          sframe

SYNOPSIS      sframe [-nsq] [-dn] filename.

DESCRIPTION   sframe.c (version 7) is frame structrue analysis program.
It is capable for analysing plane frames with or without
semi-rigid connection and pinned connection. The programme
is also capable of counting statibility function and the
effect of shearing. It can be used to analyse the frame by
counting semi-rigid connection, statibility function and the
effect of shearing individually or by combining any of them.
It is also can be used to analyse the truss frame.

OPTIONS       -n include stability function.
              -q include shear deformation of members.
              -s include effec of semi-rigid connection.
              -ln load factor, n is a number.
              -dn display the n iterative results. If 'a' instead number
                  (-da), it will display all iterative results.
              default: without stability function, semi-rigid and shear.

COMPILE      cc -o sframe sframe.c -lm

```

Matrix Stiffness Method

copyright (c) 1997 Written by Y. Zheng
e-mail address: es258@eng.warwick.ac.uk

```

#include <stdio.h>
#include <math.h>

```

```

#define MAXMEMB 30          /* maximum elements (members) */
#define MAXRESTR 20        /* maximum restraints */
#define MAXLAJ 20          /* maximum numbers of loads at joint */
#define MAXLBJ 20          /* maximum numbers of loads between joint */
#define MAXELE 90          /* maximum matrix elements = 3*No. of Joint */
#define MAXNTSRC 10        /* maximum No. of type of Semi-Rigid Connection */
#define MAXNP 10           /* maximum No. of points in connection M-Phi curve */
#define MAXLINE 1000       /* maximum lines of displaying in function ll */
#define Pi 3.14159265358979

```

```

#define MSTARS *****
#define PR(X) printf("\n%s X %s\n", MSTARS, MSTARS)

```

```

#define L memb[e].gc        /* Length */
#define A memb[e].mj        /* Area of cross section */
#define I memb[e].gx        /* 2nd moment of area */
#define E memb[e].e0        /* Elastic moduli */
#define G memb[e].g0        /* Modulus of elasticity in shear */

```

```

int c, stabilit=0, semi=0, shear=0; /* command-line arguments */
float load_factor=1;
int ndisp;
float tolerance; /* tolerance for moment */
int max_iterative; /* maximum iterative time */

```

```

struct element {
    int jm[2]; /* Joint No of member end. */
    int jp[2]; /* Pined joint of member end */
    float gc; /* Length */
    float gj; /* Inclination */
    float mj; /* Area of cross section */
    float gx; /* 2nd moment of area */
    float e0; /* Elastic moduli */
    float g0; /* Modulus of elasticity in shear */
    float gs; /* Shear coefficient */
};
struct element memb[MAXMEMB];

struct load_at_joint {
    float load; /* value of load */
    int code; /* vector No. of load applied */
} laj[MAXLAJ];

struct load_between_joint {
    float load; /* value of load */
    float dist; /* distances to start end */
    int memb; /* No. of member applied */
    int type; /* type of loads, 1 distributed, 2 vertical, 3 horizontal */
} lbj[MAXLBJ];

main(argc, argv)
int argc;
char *argv[];
{
    FILE *in; /* declare FILE pointers */
    int ne, nj, nz; /* No of member, joint and Restrains */
    int nlj, nlb; /* No of load at joint and load between joint */
    int nj3; /* 3*No of joint */
    int zc[MAXRESTR]; /* Restrains */

    float **kz; /* Stiffness matrix pointers */
    float p[MAXELE]; /* Total Loads at Joint */
    int i;

    int ntsrc; /* No. of type of Semi-Rigid Connection */
    int np[MAXNTSRC]; /* No. of points in connection M-Phi curve */
    int sctp[MAXMEMB][2]; /* connection type of member end */
    float moment[MAXNTSRC][MAXNP], rotation[MAXNTSRC][MAXNP]; /* M-Phi curve */
    int iterative, converge; /* No. of iterative time, converge sign */
    float phi[MAXMEMB][2]; /* connection rotation */
    float kratio[MAXMEMB][2]; /* ratio of moment-rotation */
    float m[MAXMEMB][2], n[MAXMEMB][2]; /* moment and axial load of member end */

    void data_input1(), data_input2(), data_input3(), data_input4(), freematrix();
    void gdn12(), crf3(), ctm4(), lsmat5(), esmat6(), tlaj7(), ssmat8();
    void boundary9(), solve_matrix10(), inte_force11();
    void phi_function();
    float **mkmatrix();
    float k_ratio();

    int ndot=0, dot=0;
    char *name;

    name=argv[0];
    while (--argc > 0 && (++argv)[0] == '-') {
        while (c=++argv[0])
            switch (c) {
                case 'n': /* -n: stability function */

```

```

    stabilit=1;
    break;
    case 's':      /* -s: semi-rigid connection */
        semi=1;
        break;
    case 'q':      /* -s: effect of shearing */
        shear=1;
        break;
    case 'l':      /* -l: load factor */
        load_factor=0;
        while ( c==++argv[0] )
            if(c>='0' && c<='9' && dot==0)
                load_factor=load_factor*10+(c-'0');
            else if (c>='0' && c<='9' && dot==1) {
                load_factor=load_factor+(c-'0')/(pow(10.0,(float)++ndot));
            } else if (c=='.' ) {
                dot=1;
            }
            else {
                fprintf(stderr, "%s: illegal option %c\n", name, c);
                argc=0;
            }
        *--argv[0];
        break;
    case 'd':      /* -d: display */
        ndisp=0;
        while ( c==++argv[0] )
            if(c>='0' && c<='9')
                ndisp=ndisp*10+(c-'0');
            else if (c=='a')
                ndisp=10000;
            else {
                fprintf(stderr, "%s: illegal option %c\n", name, c);
                argc=0;
            }
        *--argv[0];
        break;
    default:
        fprintf(stderr, "%s: illegal option %c\n", name, c);
        argc=0;
        break;
}

if ( argc != 1 ) {
    /* check if there is an input file */
    printf("Usage: %s [-n -s -q -ln -dn] datafile.\n", name);
    printf("  -n count stability function.\n");
    printf("  -s count effec of semi-rigid connection.\n");
    printf("  -q count shear deformation.\n");
    printf("  -ln load factor, n is a number.\n");
    printf("  -dn display the n iterative results.\n");
    printf("  n can be a number or a (for all).\n");
    printf("  default: rigid frame.\n");
} else {
    if ( (in=fopen(*argv,"r")) != NULL ) {
        data_input1(in, &ne, &nj, &nz, &nlj, &nlb);
        data_input2(in, ne);
        data_input3(in, nz, nlj, nlb, zc);
        display_in_data(ne, nj, nz, nlj, nlb, zc);
        if ( semi == 1 ) {
            data_input4(in, ne, &ntsrc, np, sctp, moment, rotation);
            display_semi_rigid(ne, ntsrc, np, sctp, moment, rotation);
        }
    }
    nj3=3*nj;

```

```

    kz=mkmatrix(nj3, nj3);
    for (i=1; i<ne; i++) {
        phi[i][0]=0;
        phi[i][1]=0;
    }
    iterative=1;
    converge=0;

    while (iterative <= max_iterative && converge == 0) {
        tlaj7(nj, nlj, nlb, p, phi, ne, sctp, n);
        ssmat8(ne, nj3, kz, n);
        boundary9(kz, p, nj3, nz, zc);
        solve_matrix10(nj3, kz, p);
        freematrix(kz, nj3);
        inte_forcell(ne, nlb, p, phi, moment, rotation, np, sctp, kratio, &converge, iterative,
        m,n);
        iterative++;
    }
    } else
        printf("I can not open file %s.\n", *argv);
}

/* Display Input Data */
display_in_data(ne, nj, nz, nlj, nlb, zc)
int ne, nj, nz, nlj, nlb, zc[];
{
    int i, e;

    PR(Input Data);
    printf(" Number of elements ..... %2d\n", ne);
    printf(" Number of joints ..... %2d\n", nj);
    printf(" Number of degrees of freedom restrained at supports ..... %2d\n", nz);
    printf(" Number of loads at joint ..... %2d\n", nlj);
    printf(" Number of loads between joints ..... %2d\n", nlb);

    printf(" Element Joint No. Joint No. Pin Joint Pin Joint\n");
    printf(" number      end 1      end 2      end 1      end 2 \n");

    for (i=0; i<ne; i++) {
        printf("%5d %6d %7d %6d %7d\n", i+1, memb[i].jm[0], memb[i].jm[1], memb[i].jp[0], memb[i].jp[1]);
    }
    printf("\n");

    printf(" Element Length of Orientation Area of ");
    printf(" 2nd Moment Young's Shear Shear\n");
    printf(" number element of Member element ");
    printf(" of Area moduli modulus coefficient\n");

    for (e=0; e<ne; e++) {
        printf("%5d %9.3f %9.3f %5.3e", e+1, L, memb[e].gj, A);
        printf(" %5.3e %5.3e %5.3e %5.3e\n", I, E, G, memb[e].gs);
    }
    printf("\n");

    printf(" --- Number of restraint that is fully-fixed ---\n");
    /* printf(" X Y Thate\n"); */
    for (i=0; i<nz; i++)
        printf("%3d\t", zc[i]);
    printf("\n");

```

```

if (nlj != 0) {
    printf("-----* Load at joint *-----\n");
    printf(" Load values          Displacment code\n");
    for(i=0; i<nlj; i++)
        printf("%8.3f\t%15d\n",laj[i].load/load_factor, laj[i].code);
    printf("\n");
}

if (nlb != 0){
    printf("-----* Load between joint *-----\n");
    printf(" Loads          Distances to No. of element Type of\n");
    printf("          start end          applied loads \n");
    for(i=0; i<nlb; i++)
        printf("%8.3f\t%8.3f\t%8d\t%8d\n",lbj[i].load/load_factor,lbj[i].dist,lbj[i].memb,lbj[i].type);
    printf("\n");
}

printf("Load factor\t%f\n", load_factor);
printf("Tolerance of moments\t%f\n", tolerance);

if ( semi == 1 )
    return;

PR(End of Input Data);
return;
}

/* Display Semi-rigid Input Data */

display_semi_rigid(ne, ntsrc, np, sctp, moment, rotation)
int ne, ntsrc, np[], sctp[][2];
float moment[][MAXNP], rotation[][MAXNP];
{
    int i, j;

    printf("\n -----* Semi-rigid connection *-----\n");

    printf(" No. of types of semi-rigid connection %d\n", ntsrc);
    for (i=0; i<ntsrc; i++) {
        printf("\n Type %d\n", i+1);
        printf(" No. of points in connection M-Phi characteristic %d\n", np[i]);
        printf(" Moment          Rotation\n");
        for (j=0; j<np[i]; j++)
            printf(" %10f \t%10f\n", moment[i][j], rotation[i][j]);
    }
    printf("\n\n Connection type at element ends\n");
    printf(" Element      End 1      End 2\n");
    for (i=0; i<ne; i++)
        printf("%5d      %6d      %7d\n", i+1, sctp[i][0], sctp[i][1]);

    PR(End of Data);
    return;
}

/* Data input (Basic data) 1-1 */

void data_input1(in, ne, nj, nz, nlj, nlb)
FILE *in;
int *ne, *nj, *nz, *nlj, *nlb;

```

```

{
    int i, temp[5];

    for (i=0; i<5; i++)
        fscanf(in,"%d", &temp[i]);

    *ne=temp[0];
    *nj=temp[1];
    *nz=temp[2];
    *nlj=temp[3];
    *nlb=temp[4];

    return;
}

/*Data input (Members) 1-2 */

void data_input2(in, ne)
FILE *in;
int ne;
{
    int i;
    struct element *dt;

    dt=memb;

    for (i=0; i<ne; i++) {
        fscanf(in,"%d%d", &(dt+i)->jm[0], &(dt+i)->jm[1]);
        fscanf(in,"%d%d", &(dt+i)->jp[0], &(dt+i)->jp[1]);
        fscanf(in,"%f", &(dt+i)->gc);
        fscanf(in,"%f", &(dt+i)->gj);
        fscanf(in,"%f", &(dt+i)->mj);
        fscanf(in,"%f", &(dt+i)->gx);
        fscanf(in,"%f", &(dt+i)->e0);
        fscanf(in,"%f", &(dt+i)->g0);
        fscanf(in,"%f", &(dt+i)->gs);
    }

    return;
}

/* Data input (Restrains, Loads at joint and between joint) 1-3 */

void data_input3(in, nz, nlj, nlb, zc)
FILE *in;
int nz, nlj, nlb, zc[];
{
    int i;

    for (i=0; i<nz; i++)
        fscanf(in,"%d", &zc[i]);
    for (i=0; i<nlj; i++) {
        fscanf(in,"%f%d", &laj[i].load, &laj[i].code);
        laj[i].load=load_factor*laj[i].load;
    }
    for (i=0; i<nlb; i++) {
        fscanf(in,"%f%f%d%d", &lbj[i].load, &lbj[i].dist, &lbj[i].memb, &lbj[i].type);
        lbj[i].load=load_factor*lbj[i].load;
    }
}

```

```

fscanf(in, "%f", &tolerance);
fscanf(in, "%d", &max_iterative);
return;
)

/* Data input (Semi-rigid connection) 1-4 */
void data_input4(in, ne, ntsrc, np, sctp, moment, rotation)
FILE *in;
int ne, *ntsrc, np[], sctp[][2];
float moment[][MAXNP], rotation[][MAXNP];
{
    int i, j;
    char *s[60];

    fscanf(in, "%s", s);
    fgets(s, 60, in);

    if (semi == 1) {
        fscanf(in, "%d", ntsrc);
        for (i=0; i<*ntsrc; i++) {
            fscanf(in, "%d", &np[i]);
            for (j=0; j<np[i]; j++) /* read in the points in M-Phi curve */
                fscanf(in, "%f %f", &moment[i][j], &rotation[i][j]);
        }
        for (i=0; i<ne; i++)
            fscanf(in, "%d%d", &sctp[i][0], &sctp[i][1]);
    }

    for (i=0; i<ne; i++) { /* check the connection defining */
        if (sctp[i][0]>0 && memb[i].jp[0]>0) {
            printf("\n\n !$ Multi-defined Element %d end 1 connection.\n", i+1);
            exit(1);
        } else if (sctp[i][1]>0 && memb[i].jp[1]>0) {
            printf("\n\n !$ Multi-defined Element %d end 2 connection.\n", i+1);
            exit(1);
        }
    }
}

/* 2 Fixed-End Forces Vector {Fo}(6*1) */
void gdn12(hz, fo)
int hz;
float fo[];
{
    int e, ind;
    float g, d;
    float c;

    g=lbj[hz].load;
    c=lbj[hz].dist;
    e=lbj[hz].memb-1;
    ind=lbj[hz].type;
    d=L-c;

    if (ind==1) { /* *** distributed load *** */
        if (memb[e].jp[0]<1 && memb[e].jp[1]<1) { /* no pinned joint */
            fo[1]=-g*c/2*(2-2*c*c/L/L+c*c*c/(L*L*L));
            fo[2]=g*c*c/12*(6-8*c/L+3*c*c/L/L);

```

```

            fo[4]=-g*c-fo[1];
            fo[5]=-g*c*c*c/12/L*(4-3*c/L);
        } else if (memb[e].jp[0]==1 && memb[e].jp[1]==1) { /* both ends pin-joint */
            fo[1]=-g*c*(1-c/(2*L));
            fo[2]=0;
            fo[4]=-g*c*c/(2*L);
            fo[5]=0;
        } else if (memb[e].jp[0]==1 && memb[e].jp[1]<1) { /* left-end is pin-joint */
            fo[1]=-g*c*(c*c*c-6*c*L+8*L*L)/(8*L*L*L);
            fo[2]=0;
            fo[4]=-(fo[1]+g*c);
            fo[5]=-(fo[1]*L+g*c*(L-c/2));
        } else { /* right-end is pin-joint */
            fo[1]=g*c*(c*c*(4*L-c)/(8*L*L*L)-1);
            fo[2]=g*c*c*(4*L*L-4*L*c+c*c)/(8*L*L);
            fo[4]=-g*c*c*c*(4*L-c)/(8*L*L*L);
            fo[5]=0;
        }
        fo[0]=0;
        fo[3]=0;
    } else if (ind==2) { /* *** vertical concentrated load *** */
        if (memb[e].jp[0]<1 && memb[e].jp[1]<1) { /* no pinned joint */
            fo[1]=-g*d*d*(L+2*c)/(L*L*L);
            fo[2]=g*c*d*d/L/L;
            fo[4]=-g*c*c*(L+2*d)/(L*L*L);
            fo[5]=-g*c*c*d/L/L;
        } else if (memb[e].jp[0]==1 && memb[e].jp[1]==1) { /* both ends pin-joint */
            fo[1]=-g*(1-c/L);
            fo[2]=0;
            fo[4]=-g*c/L;
            fo[5]=0;
        } else if (memb[e].jp[0]==1 && memb[e].jp[1]<1) { /* left-end is pin-joint */
            fo[1]=-g*(1-3*c/(2*L)+c*c*c/(2*L*L*L));
            fo[2]=0;
            fo[4]=-(fo[1]+g);
            fo[5]=-fo[1]*L-g*(L-c);
        } else { /* right-end is pin-joint */
            fo[1]=3*g*c*c*(L-c/3)/(2*L*L*L)-g;
            fo[2]=-(fo[1]+g)*L-g*c;
            fo[4]=-(fo[1]+g);
            fo[5]=0;
        }
    }
    fo[0]=0;
    fo[3]=0;
} else { /* *** horizontal concentrated load *** */
    fo[0]=-g*d/L;
    fo[1]=0;
    fo[2]=0;
    fo[3]=-g*c/L;
    fo[4]=0;
    fo[5]=0;
}

return;
}

/* 3 Connection Rotation Force {fs}(6*1) in local member coordinate */
void crf3(fo, phi, e, n)
int e;
float phi[][2], fo[], n[][2];
{
    register int i;

```

```

float a, a1, a2, a3, u;
float q1, q2, q3, q4, q5;

if(shear!=1)
    a=0; /* no shearing */
else
    a=memb[e].gs/G/A; /* effect of shearing */
u=L*L/12/E/I;

if ( stabilit != 1 || n[e][0] <= 0 ) { /* No Stability Function or with */
    /* Stability Function but Axial Force <= 0 */
    if(shear!=1)
        a=0; /* no shearing */
    else
        a=memb[e].gs/G/A; /* effect of shearing */
    if (memb[e].jp[0]< 1 && memb[e].jp[1]< 1) { /* no pinned joint */

        a1=(L*L+3*a*E*I)/3/L/(u+a);
        a2=(L*L-6*a*E*I)/6/L/(u+a);

        for (i=0; i<2; i++) {
            fo[3*i]=0;
            fo[3*i+1]=(2*i-1)/(2*(u+a))*(phi[e][0]+phi[e][1]);
            fo[3*i+2]= a1*phi[e][i]+a2*phi[e][1-i];
        }
    } else if (memb[e].jp[0]==1 && memb[e].jp[1]==1) { /* pins at both ends */

        for (i=0; i<6; i++)
            fo[i]=0;
    } else { /* pin at one end */

        for (i=0; i<2; i++) {
            fo[3*i]=0;
            fo[3*i+1]=(2*i-1)/(4*u+a)*(phi[e][0]+phi[e][1]);
            fo[3*i+2]= L/(4*u+a)*((1-i)*phi[e][0]+i*phi[e][1]);
        }
    }
} else { /* With Stability Function but Axial Force != 0*/
    if ( stabilit == 1 )
        phi_function(e,&q1,&q2,&q3,&q4,&q5,n); /* stability function */
    if (memb[e].jp[0]< 1 && memb[e].jp[1]< 1) { /* no pinned joint */

        for (i=0; i<2; i++) {
            fo[3*i]=0;
            fo[3*i+1]=(2*i-1)/(2*u)*q2 *(phi[e][0]+phi[e][1]);
            fo[3*i+2]= L/(3*u)*q3*phi[e][i]+L/(6*u)*q4*phi[e][1-i];
        }
    } else if (memb[e].jp[0]==1 && memb[e].jp[1]==1) { /* pins at both ends */

        for (i=0; i<6; i++)
            fo[i]=0;
    } else { /* pin at one end */

        for (i=0; i<2; i++) {
            fo[3*i]=0;

```

```

        fo[3*i+1]=(2*i-1)/(4*u)*q2*(phi[e][0]+phi[e][1]);
        fo[3*i+2]= L/(4*u)*((1-i)*phi[e][0]+i*phi[e][1]);
    }
}
return;
}

/* 4 Coordinate Transformation Matrix [T](6*6) */
void ctm4(e, t)
int e;
float t[][6];
{
    register int i, j;
    float co, si;
    double ceta;

    ceta=memb[e].gj*Pi/180;
    co=(float)cos(ceta);
    si=(float)sin(ceta);

    for (i=0; i<6; i++)
        for (j=0; j<6; j++)
            t[i][j]=0;

    t[0][0]=co;
    t[0][1]=si;
    t[1][1]=co;
    t[1][0]=-si;
    t[2][2]=1;

    for (i=0; i<3; i++)
        for (j=0; j<3; j++)
            t[i+3][j+3]=t[i][j];
}

return;
}

/* 5 Local Element Stiffness Matrix [Kd](6*6)*/
void lsmat5(e, kd, n)
int e;
float kd[][6], n[][2];
{
    register int i, j;
    float a, u, q1, q2, q3, q4, q5;

    for (i=0; i<6; i++) /* initiate the matrix kd[6][6] */
        for (j=0; j<6; j++)
            kd[i][j]=0;

    u=L*L/12/E/I;

    if ( stabilit != 1 || n[e][0] <= 0 ) { /* No Stability Function or with */
        /* Stability Function but Axial Force <= 0 */
        if(shear!=1)

```

```

a=0; /* no shearing */
else
a=memb[e].gs/G/A; /* effect of shearing */

if (memb[e].jp[0]< 1 && memb[e].jp[1]< 1) { /* no pinned joint */
kd[0][0]=E*A/L;
kd[1][1]= 1/L/(u+a);
kd[2][1]=-1/(2*(u+a));
kd[2][2]=(L*L+3*a*E*I)/3/L/(u+a);
kd[3][0]=-kd[0][0];
kd[3][3]=kd[0][0];
kd[4][1]=-kd[1][1];
kd[4][2]=-kd[2][1];
kd[4][4]=kd[1][1];
kd[5][1]=kd[2][1];
kd[5][2]=(L*L-6*a*E*I)/6/L/(u+a);
kd[5][4]=-kd[2][1];
kd[5][5]=kd[2][2];
} else if (memb[e].jp[0]==1 && memb[e].jp[1]==1) { /* pins at both ends */
kd[0][0]=E*A/L;
kd[3][0]=-kd[0][0];
kd[3][3]=kd[0][0];
} else { /* pin at one end */
kd[0][0]=E*A/L;
kd[1][1]= 1/L/(4*u+a);
kd[3][0]=-kd[0][0];
kd[3][3]=kd[0][0];
kd[4][1]=-kd[1][1];
kd[4][4]=kd[1][1];
if (memb[e].jp[0] == 1) { /* pin at left-end */
kd[5][1]=-1/(4*u+a);
kd[5][4]=-kd[5][1];
kd[5][5]=L/(4*u+a);
} else { /* pin at right-end */
kd[2][1]=-1/(4*u+a);
kd[2][2]=L/(4*u+a);
}
kd[4][2]=-kd[2][1];
}

) else { /* With Stability Function but Axial Force != 0 */
if ( stabilit == 1 )
phi_function(e,&q1,&q2,&q3,&q4,&q5,n); /* stability function */

if (memb[e].jp[0]< 1 && memb[e].jp[1]< 1) { /* no pinned joint */
kd[0][0]=E*A/L;
kd[1][1]= 1/L/u*q5;
kd[2][1]=-1/(2*u)*q2;
kd[2][2]=L/(3*u)*q3;
kd[3][0]=-kd[0][0];
kd[3][3]=kd[0][0];
kd[4][1]=-kd[1][1];
kd[4][2]=-kd[2][1];
kd[4][4]=kd[1][1];
kd[5][1]=kd[2][1];
kd[5][2]=L/(6*u)*q4;
kd[5][4]=-kd[2][1];
kd[5][5]=kd[2][2];
} else if (memb[e].jp[0]==1 && memb[e].jp[1]==1) { /* pins at both ends */
kd[0][0]=E*A/L;
kd[3][0]=-kd[0][0];
kd[3][3]=kd[0][0];
} else { /* pin at one end */
kd[0][0]=E*A/L;
kd[1][1]= 1/L/u/4*q5;

```

```

kd[3][0]=-kd[0][0];
kd[3][3]=kd[0][0];
kd[4][1]=-kd[1][1];
kd[4][4]=kd[1][1];
if (memb[e].jp[0] == 1) { /* pin at left-end */
kd[5][1]=-1/(4*u)*q2;
kd[5][4]=-kd[5][1];
kd[5][5]=L/(4*u)*q3;
} else { /* pin at right-end */
kd[2][1]=-1/(4*u)*q2;
kd[2][2]=L/(4*u)*q3;
}
kd[4][2]=-kd[2][1];
}
}

for (i=0; i<6; i++)
for (j=0; j<=i; j++)
kd[j][i]=kd[i][j];

return;
}

/* 6 Element Stiffness Matrix [Ke](6*6) */

void esmat6(e, ke, n)
int e;
float ke[][6], n[][2];
{
register int i, j, k;
int m;
float kd[6][6], t[6][6];

lsmat5(e, kd, n); /* 5 Local Stiffness Matrix [Kd] */
ctm4(e, t); /* 4 Coordinate Transformation Matrix [T] */

for (i=0; i<6; i++)
for (j=0; j<6; j++) {
ke[i][j]=0;
for (k=0; k<6; k++)
for (m=0; m<6; m++)
ke[i][j]=ke[i][j]+t[k][i]*kd[k][m]*t[m][j];
}

return;
}

/* 7 Total Loads at Joint {P}(3*nj) */

void tlaj7(nj, nlj, nlb, p, phi, ne, sctp, n)
int nj, nlj, nlb, ne, sctp[][2];
float p[], phi[][2], n[][2];
{
int i, j, k, e, a1, b1, nj3;
float fo[6], t[6][6], pe[6];

nj3=3*nj;

for (i=0; i<nj3; i++)
p[i]=0;

```

```

if (nlj>0)
  for (i=0; i<nlj; i++) {
    j=la[j][i].code;
    p[j-1]=la[j][i].load;
  }

if (nlb>0) {
  for (i=0; i<nlb; i++) {
    gdn12(i, fo); /* 2 Fixed-End Forces Vector {Fo} */
    e=lbj[i].memb-1;
    ctm4(e, t); /* 4 Coordinate Transformation Matrix [T] */
    for (j=0; j<6; j++) {
      pe[j]=0;
      for (k=0; k<6; k++)
        pe[j]=pe[j]-t[k][j]*fo[k];
    }
    a1=memb[e].jm[0];
    b1=memb[e].jm[1];

    p[3*a1-3]=p[3*a1-3]+pe[0];
    p[3*a1-2]=p[3*a1-2]+pe[1];
    p[3*a1-1]=p[3*a1-1]+pe[2];
    p[3*b1-3]=p[3*b1-3]+pe[3];
    p[3*b1-2]=p[3*b1-2]+pe[4];
    p[3*b1-1]=p[3*b1-1]+pe[5];
  }
}

if (semi == 1) { /* semi-rigid joint */
  for (e=0; e<ne; e++) {
    if (sctp[e][0]>0 || sctp[e][1]>0) {
      crf3(fo, phi, e, n); /* 3 Connection Rotation Force {fs} */
      ctm4(e, t); /* 4 Coordinate Transformation Matrix [T] */

      for (j=0; j<6; j++) {
        pe[j]=0;
        for (k=0; k<6; k++)
          pe[j]=pe[j]-t[k][j]*fo[k];
      }

      a1=memb[e].jm[0];
      b1=memb[e].jm[1];

      p[3*a1-3]=p[3*a1-3]+pe[0];
      p[3*a1-2]=p[3*a1-2]+pe[1];
      p[3*a1-1]=p[3*a1-1]+pe[2];
      p[3*b1-3]=p[3*b1-3]+pe[3];
      p[3*b1-2]=p[3*b1-2]+pe[4];
      p[3*b1-1]=p[3*b1-1]+pe[5];
    }
  }
}

return;
}

/* 8 Structure Stiffness Matrix [Kz](nj3*nj3) */
void ssmat8(ne, nj3, kz, n)
int ne, nj3;
float kz[][MAXELE], n[][2];

```

```

{
  register int i, j;
  int e, h, l, hh, ii, jj, ll;
  float ke[6][6];

  for (i=0; i<nj3; i++)
    for (j=0; j<nj3; j++)
      kz[i][j]=0;

  for (e=0; e<ne; e++) {
    esmat6(e, ke, n); /* 6 Element Stiffness Matrix [Ke] */
    for (i=0; i<2; i++)
      for (ii=0; ii<3; ii++) {
        h=3*(i)+ii;
        hh=3*(memb[e].jm[i]-1)+ii;
        for (j=0; j<2; j++)
          for (jj=0; jj<3; jj++) {
            l=3*(j)+jj;
            ll=3*(memb[e].jm[j]-1)+jj;
            kz[hh][ll]=kz[hh][ll]+ke[h][l];
          }
      }
  }

  return;
}

/* 9 Modify [Kz] and {P} by considering Boundary Condition */
void boundary9(kz, p, nj3, nz, zc)
int nz, nj3, zc[];
float p[], kz[][MAXELE];
{
  register int i, k;
  int j;

  for (i=0; i<nz; i++) {
    j=zc[i]-1;

    for (k=0; k < nj3; k++)
      if (k==j)
        kz[j][j]=1;
      else {
        kz[j][k]=0;
        kz[k][j]=0;
      }
    p[j]=0;
  }

  return;
}

/* 10 Solving Matrix by Using Gaussian Elimination Method */
void solve_matrix10(nj3, kz, p)
int nj3;
float p[], kz[][MAXELE];
{
  register int i, j, k;
  float c;

```

```

for (k=0; k<nj3-1; k++)
  for (i=k+1; i<nj3; i++) {
    c=kz[i][k]/kz[k][k];
    for (j=k; j<nj3; j++)
      kz[i][j]=kz[i][j]-c*kz[k][j];
    p[i]=p[i]-c*p[k];
  }

p[nj3-1]=p[nj3-1]/kz[nj3-1][nj3-1];

for (i=nj3-2; i>=0; i--) {
  for (j=i+1; j<nj3; j++)
    p[i]=p[i]-kz[i][j]*p[j];
  p[i]=p[i]/kz[i][i]; /* p[i] here to store displacement in common coordinate */
}

return;
}

/* 11 Internal Force */

void inte_force11(ne,nlb,p,phi,moment,rotation,np,sctp,kratio,converge,iterative,m,n)
int ne, nlb, np[], sctp[][2], *converge, iterative;
float moment[1][MAXNP], rotation[][MAXNP], phi[][2], m[][2], n[][2];
float p[], kratio[][2];
{
  int e, i, ii, h, hh, j, k, nn;
  float wy[6], we[6], f[6], fo[6], t[6][6], kd[6][6], theta[2];
  float k1, k2, a, a1, a2, a3, u, q1, q2, q3, q4, q5;
  float c, g;
  int ind;

  int semi_flag, stabi_flag;
  char s[MAXLINE][110];

  semi_flag=0;
  stabi_flag=0;

  nn=0;
  sprintf(s[nn++], "\n\n***** Iterative %d **", iterative);
  printf(s[nn++], "          X          Y          R          N          Q");
  printf(s[nn++], "          M          Phi          Rotation");

  for (e=0; e<ne; e++) {
    ind=0;

    lsmat5(e, kd, n); /* 5 Local Stiffness Matrix [Kd] */
    ctm4(e, t); /* 4 Coordinate Transformation Matrix [T] */

    for (i=1; i<=2; i++)
      for (ii=1; ii<=3; ii++){
        h=3*(i-1)+ii-1;
        hh=3*(memb[e].jm[i-1]-1)+ii-1;
        wy[h]=p[hh]; /* wy[i], member displacement in common coordinate */
      }

    for (i=0; i<6; i++){
      f[i]=0;
      for (j=0; j<6; j++)
        for (k=0; k<6; k++)

```

```

      f[i]=f[i]+kd[i][j]*t[j][k]*wy[k];
    }

    if (nlb > 0)
      for (i=0; i<nlb; i++)
        if (lbj[i].memb-1==e) { /* 2 Fixed-End Forces Vector (Fo) */
          gdnl2(i, fo);
          for (j=0; j<6; j++) {
            f[j]=f[j]+fo[j];
          }
        }

    if (semi == 1) { /* for semi-rigid connection */
      if (sctp[e][0]>0 || sctp[e][1]>0) { /* 3 Connection Rotation Force (fs) */
        crf3(fo, phi, e, n);
        for (j=0; j<6; j++)
          f[j]=f[j]+fo[j];
      }

      for (i=0; i<2; i++) /* moment rotation ratio k */
        if (sctp[e][i]>0)
          kratio[e][i]=k_ratio(f[3*i+2],kratio[e][i],sctp[e][i],moment,rotation,np,iterative);
      else
        kratio[e][i]=0;
      k1=kratio[e][0];
      k2=kratio[e][1];

      if (shear!=1) /* no shearing */
        a=0;
      else
        a=memb[e].gs/G/A; /* effect of shearing */
      u=L*L/12/E/I;

      if (stabilit == 1 && n[e][0] > 0) /* Stability Function */
        phi_function(e,&q1,&q2,&q3,&q4,&q5,n);
      else /* no Stability Function */
        q1=q2=q3=q4=q5=1;

      if (shear == 1 && stabilit == 1) /* stability function with shear */
        a1=4*E*I/L*q3;
        a2=2*E*I/L*q4;
        a3=3*E*I/L*q3;
      ) else { /* stability function without shear */
        a1=(L*L+3*a*E*I)/3/L/(u+a)*q3; /* or no stability function */
        a2=(L*L-6*a*E*I)/6/L/(u+a)*q4;
        a3=L/(L*L/(3*E*I)+a)*q3;
      }

      if (iterative==1)
        fo[2]=fo[5]=0;
      if (sctp[e][0]>0 && sctp[e][1]>0) {
        phi[e][0]=((a1+k2)*(f[2]-fo[2])-a2*(f[5]-fo[5]))/(a2*a2-(a1+k1)*(a1+k2));
        phi[e][1]=-(f[2]-fo[2]+(a1+k1)*phi[e][0])/a2;
      } else if (sctp[e][0]>0 && sctp[e][1]<=0) { /* semi-rigid connection at left */
        if (memb[e].jp[0]<1 && memb[e].jp[1]==1)
          phi[e][0]=-(f[2]-fo[2])/(a3+k1); /* right-end is pin-joint */
        else
          phi[e][0]=-(f[2]-fo[2])/(a1+k1); /* right-end is rigid */
        phi[e][1]=0;
      } else if (sctp[e][0]<=0 && sctp[e][1]>0) { /* semi-rigid connection at right */
        if (memb[e].jp[0]==1 && memb[e].jp[1]<1)
          phi[e][1]=-(f[5]-fo[5])/(a3+k2); /* left-end is pin-joint */

```

```

else
  phi[e][1]=-(f[5]-fo[5])/(a1+k2);          /* left-end is rigid */
  phi[e][0]=0;
) else {
  phi[e][0]=0;
  phi[e][1]=0;
}

for (i=0; i<2; i++)
  if (sctp[e][i]>0 )
    if ( fabs((double)(f[3*i+2]-(-kratio[e][i]*phi[e][i]))) >= tolerance )
      semi_flag=semi_flag+1;
}

if ( stabilit == 1 )
  for (i=0; i<2; i++) {
    if ( f[3*i+2]-m[e][i] >= tolerance )
      stabi_flag=stabi_flag+1;
    m[e][i]=f[3*i+2];
    n[e][i]=f[3*i];
  }

for (i=0; i<6; i++){          /* we[i], member displacement in Lcal coordinate */
  we[i]=0;
  for (j=0; j<6; j++)
    we[i]=we[i]+t[i][j]*wy[j];
}

if ( nlb>0 ) {
  for (i=0; i<nlb; i++)
    if (lbj[i].memb-1==e){
      g=lbj[i].load;
      c=lbj[i].dist;
      ind=lbj[i].type;
    }
} else
  ind=0;

if ( memb[e].jp[0]==1 && memb[e].jp[1]<1 ) {          /* left-end is pin-joint */
  theta[0]=(we[5]+phi[e][1]) + f[1]*L*L/(2*E*I);
  if (ind== 1)
    theta[0]=theta[0]+g*c*c/(6*E*I)+g*c*L*(L-c)/(2*E*I);
  if (ind== 2)
    theta[0]=theta[0]+g*(L-c)*(L-c)/(2*E*I);
}

if ( memb[e].jp[0]<1 && memb[e].jp[1]==1 ) {          /* right-end is pin-joint */
  theta[1]=(we[2]+phi[e][0]) - f[4]*L*L/(2*E*I);
  if (ind== 1)
    theta[1]=theta[1] - g*c*c/(6*E*I);
  if (ind== 2)
    theta[1]=theta[1] - g*c*c/(2*E*I);
}

sprintf(s[nn++], "\nElement No.  %d", e+1);
for(i=0; i<2; i++) {
  if ( memb[e].jp[i]==1 && memb[e].jp[1-i]<1 ) /* one end is pinned joint */
    sprintf(s[nn++], "%d%12.3e%12.3e%12.3e %11.3f%11.3f%11.3f %11.3e", i+1, we[3*i],
  we[3*i+1], we[3*i+2], f[3*i], f[3*i+1], f[3*i+2], theta[i]);
  else if (semi == 1 && sctp[e][i]>0 )
    sprintf(s[nn++], "%d%12.3e%12.3e %11.3f%11.3f%11.3f %22.3e %11.3e", i+1, w
  e[3*i], we[3*i+1], we[3*i+2], f[3*i], f[3*i+1], f[3*i+2], phi[e][i], we[3*i+2]+phi[e][i]);
  else
    sprintf(s[nn++], "%d%12.3e%12.3e %11.3f%11.3f%11.3f", i+1, we[3*i], we[3*i+
  1], we[3*i+2], f[3*i], f[3*i+1], f[3*i+2]);
}

```

```

)
}

if( ndisp==iterative || ndisp==10000 || iterative==max_iterative)
  for (i=0; i<nn; i++)
    puts(s[i]);
if (iterative==max_iterative && (semi_flag>0 || stabi_flag > 0))
  printf("out of maximum iterative time (%d)\n", max_iterative);

if ( semi_flag==0 && stabi_flag == 0 ){
  *converge=1;
  for (i=0; i<nn; i++)
    puts(s[i]);
}

return;
}

/* Moment-Rotation Ratio k */

float k_ratio(moment, ko, ctp, m, r, np, iterative)
int ctp, np[], iterative;
float moment, ko, m[][MAXNP], r[][MAXNP];
{
  int i, npoint;
  float m1, m2, m3, r1, r2, phi, k;

  npoint=np[ctp-1];

  if (iterative==1)
    ko= (m[ctp-1][1]-m[ctp-1][0])/(r[ctp-1][1]-r[ctp-1][0]);

  phi= fabs((double) (moment/ko));

  if ( phi > r[ctp-1][npoint-1] ) {
    m2= m[ctp-1][npoint-1];
    m1= m[ctp-1][npoint-2];
    r2= r[ctp-1][npoint-1];
    r1= r[ctp-1][npoint-2];
  } else
    for (i=0; i< npoint-1; i++ )
      if(phi > r[ctp-1][i] && phi <= r[ctp-1][i+1]) {
        m2= m[ctp-1][i+1];
        m1= m[ctp-1][i];
        r2= r[ctp-1][i+1];
        r1= r[ctp-1][i];
      }

  m3=(phi-r1)*(m2-m1)/(r2-r1)+m1;
  k=m3/phi;

  return k;
}

/* Free 1-d and 2-d Matrix Function */

void freematrix(matrix, ydir)
float **matrix;
int ydir;

```

```

(
    int i;

    for (i = 0; i < ydir; i++)
        free(matrix[i]);
    free(matrix);
)

/* Make 1-d and 2-d Matrix Function */
float **mkmatrix(yrow,xcolumn)
int yrow;
int xcolumn;
{
    float **matrix;
    int i;

    if ( (matrix = (float**) malloc (yrow * sizeof(float*))) == NULL ) {
        printf("Cannot allocate memory \n");
        exit(0); /****** EXIT *****/
    }

    for (i = 0; i < yrow; i++)
        if ( (matrix[i] = (float*) malloc (xcolumn * sizeof(float))) == NULL ) {
            printf("Cannot allocate memory \n");
            exit(0); /****** EXIT *****/
        }

    return matrix;
}

/* Stability Function */
void phi_function(e, q1, q2, q3, q4, q5, n)
int e;
float *q1, *q2, *q3, *q4, *q5, n[[2]];
{
    register int i;
    float t, r, a, s, c, h;
    static float b[]={1.57973627, 0.15858587, 0.02748899, 0.00547540,
                      0.00115281, 0.00024908, 0.00005452};

    if (n[e][0] <= 0) /* axial force <= 0, no stability function considered */
        *q1=*q2=*q3=*q4=*q5=1;
    else {
        if (shear == 1 && stabilit == 1) { /* stability function with shear */
            r=n[e][0]*(L*L/Pi/Pi/E/I+memb[e].gs/G/A); /* Actual load/Critical Load */
            h=Pi*Pi*r/4/(1+memb[e].gs*Pi*Pi*E*I/L/L/G/A); /* square alpha */
            *q1=sqrt(h)*cos(sqrt(h))/sin(sqrt(h));
            a=E*I*memb[e].gs/L/L/G/A;
            s=(h>(*q1)-(*q1)*(*q1)+4*(h>(*q1)*(*q1)+h*h)*a)/(1>(*q1)+4*h>(*q1)*a);
            c=(h>(*q1)+(*q1)*(*q1)-4*h*(h>(*q1)*(*q1)*a)/(((*q1)-(*q1)*(*q1)+h+4*h*(h>(*q1)
            *(*q1)*a);
        } else { /* stability function without shear */
            r=n[e][0]*L*L/Pi/Pi/E/I; /* ratio of the actual load P to the Euler load Pe
*/

```

```

h= Pi*Pi*r/4; /* square alpha */
*q1=(64-60*r+5*r*r)/(64-20*r+r*r);
for(i=1; i<=7; i++) {
    t=3.0*i;
    *q1=*q1-b[i-1]*pow(r,(float)i)/pow(2.0,t); /* Livesley phi functions (1956)
*/
}
s=(h>(*q1)-(*q1)*(*q1))/(1>(*q1)); /* Stability Functions (Majid 1972) */
c=(h>(*q1)+(*q1)*(*q1))/(s*(1>(*q1)));
}

if (memb[e].jip[0]< 1 && memb[e].jip[1]< 1) { /* no pinned joint */
    *q2=s*(1+c)/6;
    *q3=s/4;
    *q4=s*c/2;
    *q5=(*q2)-h/3;
} else if (memb[e].jip[0]==1 && memb[e].jip[1]==1) { /* both ends pin-joint */
    *q1=*q2=*q3=*q4=*q5=1; /* no stability function */
} else { /* pin at one end */
    *q2=s*(1-c*c)/3;
    *q3=*q2;
    *q5=(s*(1-c*c)-4*h)/3;
}
}

return;
}

```

Bibliography

Abd-El-Naby, S.F.M and Hollaway, L. (1993 a) The Experimental Behaviour of Bolted Joints in Pultruded Glass/Polyester Material. Part 1: Single- bolt Joints, *Composites*, Volume 24. Number 7, pp. 531-538.

Abd-El-Naby, S.F.M and Hollaway, L. (1993 b) The Experimental Behaviour of Bolted Joints in Pultruded Glass/Polyester Material. Part 2: Two-bolt Joints, *Composites* Volume 24. Number 7, pp. 539-546.

Anderson, D., Bijlaard, F.S.K., Nethercot, D.A. and Zandonni, R. (1992) *Analysis and Design of Steel Frames with Semi-rigid Connections*, Publ. No. 67, Technical Working Group 8.2, European Convention for Constructional Steelwork (ECCS), Brussels.

Anderson, D., Colson, A. and Jaspart, J. (1993) Connections and Frame Design for Economy, *New Steel Construction*, vol.1, No.6, October 1993, pp. 30-33.

Anderson, D. and Lok, T.S. (1985) *Elastic Analysis of Semi-rigid Frame*, University of Warwick, Research Report CE/17, January 1985.

Anon (1992 a) Airbus A340 Completes Maiden Flight, *Advanced Composites Engineering*, Vol.7, No.1, 2/1992, The Design Council, p. 4.

- Anon (1992 b) Ford Show Car Has Transverse Composite Leaf Spring, *Advanced Composites Engineering*, Vol.7, No.1, 2/1992, The Design Council, p. 8.
- Anon (1993 a) Longest Fiber Bridge in the USA, *FRP International*, Vol.1, Issue 2, Spring 1993, p. 7.
- Anon (1993 b) Reinforced Plastics, Oct. 1993, pp. 26-30.
- Anon (1994 a) GFRP Structures in China, *FRP International*, Vol.2, Issue 1, Winter 1994, p. 6.
- Anon (1994 b) Pioneering Plastic, *New Civil Engineer*, 14 July 1994, p. 6.
- Anon (1995) *Fiberline Design Manual for Structural Profiles in Composite Materials*, Fiberline Composites A/S, Kolding, Denmark.
- Anon (1995 a) Composite Twoers Aid Maritime Safety, *Materials World*, The Journal of the Institute of Materials, 3, 2, 1995, p. 62.
- Anon (1995 b) Structural News, No.173, *The Structural Engineer*, Vol.73, No.5, 1995, p. 5.
- Anon (1996 a) Composite French Minivan, *Advanced Materials & Processes*, 10/1996, p. 9.
- Anon (1996 b) MMFG Profile, Fall 1996.
- Anon (1996 c) Longest Stress-ribbon Footbridge Using FiBRA, *FRP International*, Vol.2, Issue 3, Summer 1996, p. 5.
- Anon (1997) SSC Approach Roads-enclosed Bridges, *The Consulting Engineering*, Issu 8, Summer, 1997, p. 41.
- Bailie, J.A. (1991) Woven Composite Structures, in Lee, S.M. *International Ency-*

lopedia of Composites, Vol. 6, VCH Publishers, Inc. pp. 110-122.

Ballinger, C. (1990) Structural FRP Composites, *Civ. Engrg.*, ASCE, 60 7 ,1990, pp. 63-65.

Ballinger, C. (1992) Advanced Composites in the Construction Industry 37th Inter. SAMPE Symp. and Exh., Araheim CA, Mar. 9-12, V37, SAMPE, 1992, pp. 1-4.

Bank, L.C. (1987) Shear Coefficients for Thin-walled Composite Beams, *Composite Structures*, 8, 1987, pp. 47-61.

Bank, L.C. (1989 a) Flexural and Shear Moduli of Full-section Fiber Reinforced Plastic (FRP) Pultruded Beams, *ASTM J. Testing and Evaluation*, 17 1, 1989, pp. 40-45.

Bank, L.C. (1989 b) Properties of Pultruded Fiber Reinforced Plastic (FRP) Structural Members, *Transportation Research Record 1223, Bridge Design and Performance and Composite Materials*, Transportation Research Board, National Research Council, 1989, pp. 117-124.

Bank, L.C. (1989 c) Flexural and Shear Moduli of FRP Beams, in Orofino, J.F Structural Materials, Proc. ASCE 7th Structures Congress, San Francisco, CA, May 1-5, 1989. pp. 494-503.

Bank, L.C., Gentry, T.R., and Nadipelli M., (1994 a) *Local Buckling of Pultruded FRP Beams - Design and Analysis*. 49th Annual SPI Con., Composite Inst., SPI, Cincinnati, OH, Feb. 7-10, 1994, Session 8-D, p. 6.

Bank, L.C. and Mosallam, A.S. (1990) Creep and Failure of a Full-size Fiber Reinforced Plastic Pultruded Frame, in Hui, D. and Kozik, T. Composite Materials Tech., PD-Vol. 32, ASME Energy-Sources Tech. Conf. and Exh. (ETCE), New

Orleans, LA, Jan. 14-17, 1990, pp. 49-56.

Bank, L.C., Mosallam, A.S. and Gonsior, H.E. (1990) Beam-to-column Connections for Pultruded FRP Structures, in Suprenant, B. Serviceability and Durability of Construction Materials, Proc. ASCE First Material Engineering Congress, Denver, CO., ASCE, 1990, pp. 804-813.

Bank, L.C., Mosallam A.S. and McCoy G.T. (1992) *Design and Performance of Connections for Pultruded Frame Structures*, Proc. 47th Annual SPI Conf., Composite Institute, Society for the Plastics Industry, Cincinnati, OH., Session 2-B, 1992, pp. 1-8.

Bank, L.C., Mosallam, A.S. and McCoy, G.T. (1994 b) Design and Performance of Connections for Pultruded Frame Structures, *Reinforced Plastics and Composites*, 13, 1994, pp. 199-212.

Bank, L.C., Nadipelli, M. and Gentry, T.R. (1993) Local Buckling and Failure of Pultruded Fiber-reinforced Plastic Beams, *Use of Plastics and Plastic Composites: Materials and Mechanics Issues ASME.*, MD-Vol. 46, pp. 499-519.

Bank, L.C., Yin, J., Moore, L., Evans, D.J., and Allison. R.W. (1996) Experimental and Numerical Evaluation of Beam-to-column Connections for Pultruded Structures, *Reinforced Plastics and Composites*, 15, 1996, pp. 1052-1067.

Barbero, E. and Tomblin, J. (1992) Buckling Testing of Composite Columns., *AIAA Journal*, Vol. 30, No. 11, pp. 2798-2880.

Bass, A.J. (1994) *Behaviour of Polymeric Composite Connections in Pultruded Frames*, MSc Thesis, Department of Engineering, University of Warwick.

Bass, A.J. and Mottram, J.T. (1994) Behaviour of Connections in Frames of Fibre-reinforced-polymer Section, *The Structural Engineer*, Vol.72 No. 17, 1994, pp. 280-

285.

Benterkia, Z. (1991) *End-plate Connections and Analysis of Semi-rigid Steel Frames*, PhD thesis, University of Warwick.

Bishop, G.R. & Sheard, P.A. (1992) Fire Resistant Composites for Structural Sections, *Composite Structures*, Vol.21, Issus 2, 1992, pp. 85-89.

Bleich, F. (1952) *Buckling Strength of Metal Structures*, McGraw-Hill.

Bridge Design & Engineering (1996) Now for the Landmark, *Bridge Design & Engineering*, May 1996, p. 25.

Brooks, R.J. and Turvey, G.J. (1995) Lateral Buckling of Pultruded GRP I-section Cantilevers, *Composite Structures* 32, 1-4, 1995, pp. 203-215.

Brown, N.D., Mottram, J.T. and Anderson, D. (1998) The Behaviour of Columns for the Design of Pultruded Frames: Tests on Isolated Centrally Loaded Columns, in Saadatmanesh, H. and Ehsani, M.R. (Eds.), *The Second International Conference on Composites in Infrastructure*, University of Arizona, USA, Vol. II, January 5-7 1998. pp. 248-260.

Bruce, R. (1990) Fiber Reinforced Plastic Bridges in Chongqing, *IABSE Symposium Brussels* Vol. 60, pp. 581-586.

Charrier, J. (1990) *Polymeric Materials and Processing*, Hanser Publishers.

Clarke, J.L. (1996) *Structural Design of Polymer Composites —EUROCOMP Design Code and Handbook*, E & FN Spon.

Coates, R.C., Coutie, M.G. and Kong, F.K (1988) *Structural Analysis*, Van Nostrand Reinhold.

Cooper, C. and Turvey, G.J. (1995) Effects of Joint Geometry and Bolt Torque on the Structural Performance of Single Bolt Tension Joints in Pultruded GRP Sheet

- Material, *Composite Structures*, 32, 1-4, 1995, pp. 217-226.
- COST (1994) Semi Rigid Behaviour of Civil Engineering Structural Connections, *COST Action C1*, Round II, European Cooperation in the Field of Scientific and Technical Research, COST 343/94.
- Creative Pultrusions (1988) *Design Guide*, Creative Pultrusions, INC. Alum Bank, Pennsylvania, USA.
- Erki, M.A. (1995) Bolted Glass-fibre-reinforced Plastic Joints, *Canada Civil Engineering*, 22:736-744.
- EUROCODE 3 (1992) Design of Steel Structures Part 1.1: General Rules and Rules for Buildings, ENV 1993-1-1, London, BSI.
- Fewster, M. (1995) Joints in Steel Construction: Moment Connections, *New Steel Construction*, Vol.3, No.5, October 1995, pp. 10-11.
- GangaRao, H.V.S and Barbero, E. (1991) Construction, Structural Application, in Lee, S.M. *International Encyclopedia of Composites*, Vol. 6, VCH Publishers, Inc.
- Gaylord, E.H. and Gaylord, C.N. (1972) *Design of Steel Structures*, Second Edition, McGraw-Hill Kogakusha, Ltd.
- Ghali, A. and Neville, A.M. (1989) *Structural Analysis: Unified Classical and Matrix Approach*, Chapman and Hall.
- Goldsworthy W.B. (1991) Pultrusion in Lee, S.M. *International Encyclopedia of Composites*, Vol. 6, VCH Publishers, Inc.
- Gordaninejad, F., Sanders, D.H. and Mudri, S. (1997) Behavior of Adhesively Bonded FRP Beam-to-column Connection, *Proceedings of ICCM-10*, Whistler, B.C., Canada, August 1995, pp. III 605-612.
- Hassan, N.K., Mohamedien, M.A. and Rizkalla, S.H. (1997 a) Multibolted Joints

dor GFRP Structural Members, *Journal of Composites for Construction*, Feb. 1997 Vol.1 No.1, pp. 3-9.

Hassan, N.K., Mohamedien, M.A. and Rizkalla, S.H. (1997 b) Rational Model for Multibolted Connections for GFRP Members, *Journal of Composites for Construction*, May 1997 Vol.1 No.2, pp. 71-78.

Head, P. (1995) Composite Materials for Bridges and Structures, in Bank, L.C. and Ben-Bassat, M (Eds.) *Composite Materials for Civil Engineering Construction*, Proc. of the First Israeli Workshop on Composite Materials for Civil Engineering Construction, Technion City, Haifa, Israel, 28-29 May, 1995, pp. 136-144.

Head, P. (1996) *High Performance Structural Materials Advanced Composites*, International Association for Bridge and Structural Engineering, 15th Congress, Copenhagen Jun 16-20, 1996.

Head, P. (1997) Civil Composites, *Materials Word*, February 1997.

Hewson, P.J. (1978) Buckling of Pultruded Glass Fibre-reinforced Channel Sections, *Composite*, 9 1, 1978, pp.56-60.

Hollaway, L. (1978) *Glass Reinforced Plastics in Construction*, Surrey University Press, Glasgow.

Hollaway, L. (1993) *Polymer Composites for Civil and Structural Engineering*. Blackie Academic & Professional.

Horn, M.R. and Merchant, W. (1965) *The Stability of Frame*, Pergamon Press Ltd.

Kedward, K.T. (1981) *Joining of Composite Materials*, American Society for testing and materials.

Lass, H. (1986) At Last, Pultrusion May Be Ready for the Big Time, Chemical

Week April 2, 1986.

Leggatt, A.J. (1984) *GRP and Building*, Butterworths.

Liskey, K. A. (1985) Pultruded Fiberglass-reinforced Plastic (FRP): A Structural Solution for Corrosive Environments, *Chemical Engineering*, November 11,1985, pp. 221-224.

Livesley, R.K. (1956) The Application of an Electronic Digital Computer to Some Problems of Structural Analysis, *The Structural Engineer*, Vol. 54 January 1956.

Livesley, R.K. (1975) *Matrix Methods of Structural Analysis*, Pergamon Press, Oxford.

Majid, K.I. (1972) *Non-Linear Structures*, Butterworth & Co. (Publishers) Ltd.

Majid, K.I. (1978) *Theory of Structures*, NewnesButterworths.

Majid, K.I. and Anderson, D. (1968) The Computer Analysis of Large Multistorey Frames Structures, *The Structural Engineer*, Vol.46, No. 11, November 1968.

Matthews, F.L. (1985) *The Static Strength of Bolted Joints in Fiber Reinforced Plastics*, Department of Aeronautics and Centre for Composite Materials, Imperial College of Science & Technology.

Mayer, R.M. (1993) *Design with Reinforced Plastics, a Guide for Engineers and Designers.*, The Design Council, London.

Meyer, R.W. (1985) *Handbook of Pultrusion Technology*, Chapman and Hall.

MMFG. (1989) *Design Manual*, Morrison Molded Fibre Glass Company, U.S.A.

Mosallam A.S. (1990) *Short and Long-term Behaviour of a Pultruded Fiber Reinforced Plastic frame*, Ph.D Thesis, The Catholic University of America, Washington

DC, Oct.

Mosallam A.S. (1993) Pultruded Composites: Materials for the 21st Century, Proc. Plastics Composites for 21st Century Infrastructure Session, 1993 Annual Convention & Exposition of ASCE) ASCE, NY, Oct. 24-28, Dallas Texas, 1993, pp. 23-55.

Mosallam A.S. (1994) Connection and Reinforcement Design Details for Pultruded Reinforced Plastics (PFRP) Composite Structures, Proc. 49th Annual Conf., Composite Inst., SPI, Feb. 7-9, 1994, Session 8-E, p. 14.

Mosallam, A.S., Abdelhamid, M.K. and Conway, J.H. (1994 a) Performance of pultruded PFRP frame connections under static and dynamic loads, *J. of Reinforced Plastics and Composites*, 13, 1994, pp. 386-407.

Mosallam, A.S. and Bank, L.C. (1991) Creep and Recovery of a Pultruded FRP frame, in Iyer, S.L., and Sen, R., (Eds.) *Advanced Composite Materials in Civil Engrg. Structures*, Materials Engrg. Division ASCE, Proc. ASCE Specialty Conf., Las Vegas, Nev, Jan. 31 - Feb. 1, 1991, pp. 288-301.

Mosallam, A.S, and Bank, L.C. (1992) Short-Term Behavior of Pultruded Fiber-Reinforced Plastic Frame, *Journal of Structural Engineering*, Vol. 118, No. 7, July, 1992, pp. 1937-1954.

Mosallam, A.S., Bedewi, N.E. and Goldstein, E. (1994 b) *Design optimization of FRP universal connectors*, Proc. 49th Annual Conf., Composite Inst., SPI, Feb. 7-9, 1994, Session 2-D, p. 7.

Mottram J.T. (1991) Structural Properties of a Pultruded E-glass Fibre-reinforced Polymeric I-beam, in Marshall, I.H. (Ed.) *Composite Structures 6, Inter. Conf. on Comp. Struct.*, (9-11 Sept. 1991), Paisley College of Tech., Elsevier Applied

Science, 1991, pp. 1-28.

Mottram J.T. (1992) Lateral-Torsional Buckling of a Pultruded I-Beam, *Composites*, Vol. 23 No.2, pp. 81-92.

Mottram, J.T. (1994) *Connections Tests for Pultruded Frames as Part EUREKA EU468:EUROCOMP*, Research Report CE47, University of Warwick.

Mottram J.T. (1996) Nominally Pinned Connections for Pultruded Frames, In Clarke, J.L., (Ed.) *Structural Design of Polymer Composites - EUROCOMP Design Code and Handbook*, E & FN Spon. pp. 703-718.

Mottram, J.T. and Zheng, Y. (1996 a) Analysis of Pultruded Frames with Semi-rigid Connection, *2nd International Conference on Advanced Composite Materials in Bridges and Structures*, Montréal (Québec) Canada, 11-14 August 1996, Canadian Society of Civil Engineers, Montreal, (1996), pp. 919-926.

Mottram, J.T. and Zheng, Y. (1996 b) State-of-the-Art Review on the Design of Beam-to-column Connections for Pultruded Frames, *Composite Structures* 35 (1996), pp. 387-401.

Mottram, J.T. and Zheng, Y. (1998) Analysis of a Pultruded Frame with Various Connection Properties, in Saadatmanesh, H. and Ehsani, M.R. (Eds.), *The Second International Conference on Composites in Infrastructure*, University of Arizona, USA, January 5-7 1998. pp. 261-274.

Nethercot, D.A (1985) Joint Action and the Design of Steel Frame, *The Structural Engineering*, Vol. 63A, No. 12, December 1985.

Robbins, J. (1992) Plastic Surgery, *NEC Consultants File*, 1992, pp. 24-25.

Rosner C.N. and Rizkalla S.H. (1995) Bolted Connections for Fiber-reinforced Composite Structural Members: Experimental Program, *Journal of Materials in Civil*

Engineering. November 1995 pp. 223-231.

Sims, G.D., Johnson, A.F., and Hill, R.D. (1987) Mechanical and structural properties of GRP pultruded section, *Composite Structures*, 8, 1987, pp. 173-187.

Smith, C. and Stone J. (1990) 6. Continuous Fiber Molding Process B: Pultrusion, in Mallick, P.K. and Newman, S. *Composite materials technology, processes and properties*, Munich, New York, Hanser Publishers.

Stonier, R.A. (1991) Stealth Low Observable Composite Aircraft, in Lee, S.M. *International Encyclopedia of Composites*, Vol. 6, VCH Publishers, Inc.

Timoshenko, S.P. and Gere, J.M (1972) *Mechanics of Materials*, Van Nostrand Reinhold Company.

Turvey, G.J. (1996) Lateral Buckling Tests on Rectangular Cross-section Pultruded GRP Cantilever Beams, *Composites Part B: Engineering*, 27B, pp. 35-42.

Turvey, G.J. (1996) Testing of a Pultruded GRP Pinned Base Rectangular Portal Frame for the EUROCOMP Project, in Clarke, J.L. (Ed.) *Structural Design of Polymer Composites - EUROCOMP Design Code and Handbook*, E & FN Spon, pp. 719-741.

Turvey, G.J. (1998) Frame Connection, in Mottram, J.T and Turvey, G.J. (Eds.) *Behaviour of Civil Engineering Structural Connections (State-of-the-art review on Design, Testing, Analysis and Applications of Polymeric Composite Connections)* Brussels Luxembourg.

Turvey, G.J. and Cooper, C. (1996 a) Semi-rigid pultruded GRP frame connections: tests to determine static moment-rotation characteristics, *Proceedings ECCM-7 (Seventh European Conference on Composite Materials) - Realising their commer-*

- cial potential*, Woodhead Publishing Limited, Cambridge, Vol. 2 1996, pp. 295-300.
- Turvey, G.J. and Cooper, C. (1996 b) Characterization of the Short Term Static Moment-rotation Response of Bolted Connections between Pultruded GRP Beam and Column WF-sections, in El-Badry, M.M., (Ed.) *2nd International Conference on Advanced Composite Materials in Bridges and Structures*, Montréal (Québec) Canada, 11-14 August 1996, Canadian Society of Civil Engineers, Montreal, (1996), pp. 927-934.
- Yuan, R.L. and Liu, C.J (1996) Study of Mechanical Connection for GFRP Laminated Structures, *2nd International Conference on Advanced Composite Materials in Bridges and Structures*, Montréal (Québec) Canada, 11-14 August 1996, Canadian Society of Civil Engineers, Montreal, (1996), pp. 951-958.
- Zandonini, R. (1986) *Private Communication*, Politechnico di Milano, Dipartimento di Ingegneria Strutturale, Milan, Italy.